SAND2021-8886PE

Nonlinear Characterization of a Joint Exhibiting a Reduction in Damping at High Energy

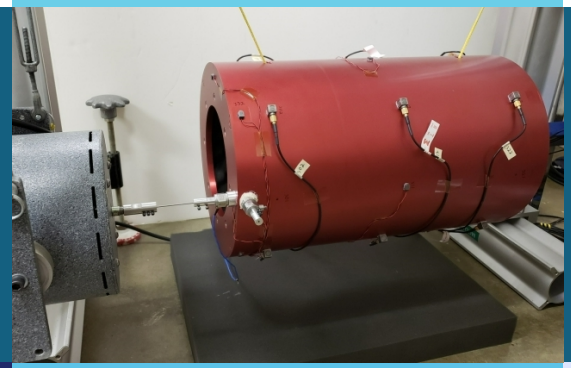

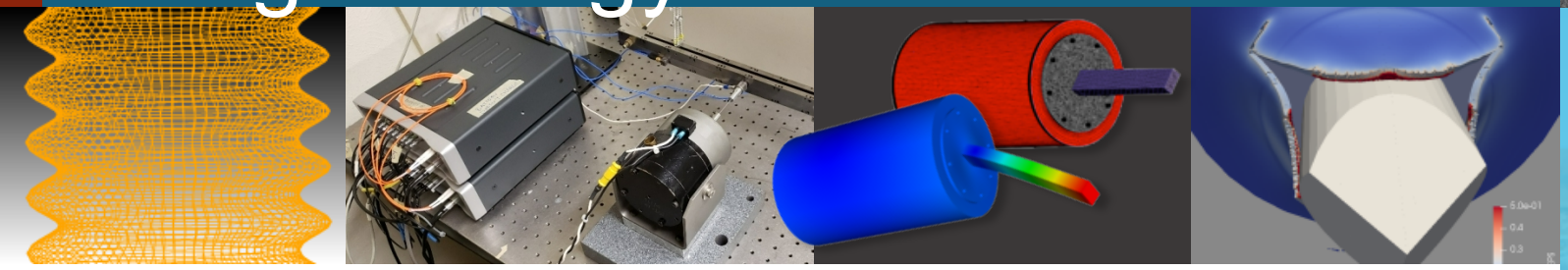

STUDENTS

Daniel Agramonte, Gabrielle Graves, Kenneth Meyer

MENTORS

Ben Pacini, Matt Allen, Mo Khan, David Najera, Dan Roettgen

Sandia National Laboratories is a multimission laboratory managed and operated by National Technology & Engineering Solutions of Sandia, LLC, a wholly owned subsidiary of Honeywell International Inc., for the U.S. Department of Energy's National Nuclear Security Administration under contract DE-NA0003525.

Sandia National Laboratories is a multimission laboratory managed and operated by National Technology & Engineering Solutions of Sandia, LLC, a wholly owned subsidiary of Honeywell International Inc., for the U.S. Department of Energy's National Nuclear Security Administration under contract DE-NA0003525.

Meet the Interns!

Fig 0a. Daniel Agramonte
University of Georgia

Fig 0b. Gabrielle Graves
New Mexico State University

Fig 0c. Kenneth Meyer
University of Texas at Austin

Background And Motivation

- Bolted joints are heavily used in simple and complex structures due to the ease of assembly and disassembly.
- They are also a source of nonlinearities and energy dissipation, making a jointed interface difficult to model
  - Dynamics of structure difficult to predict
  - Response can be very different than a monolithic structure with out interfaces
- Main source of nonlinearities occur from the stick-slip behavior of the interface
  - Typically cause nonlinear softening and damping

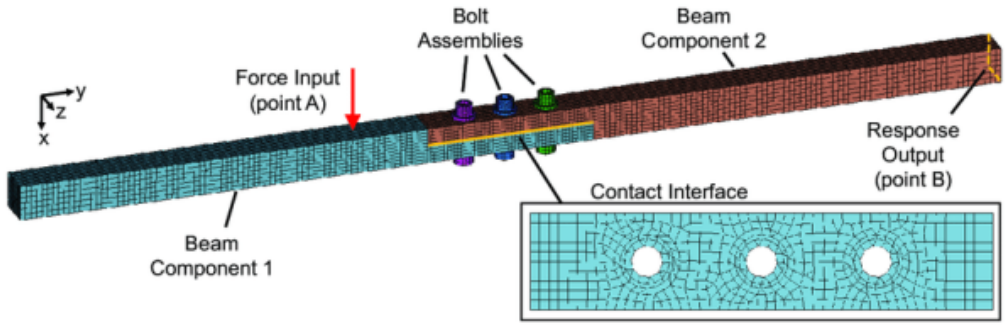

Fig 1. Representative Joint

Fig 2. Large bolted structure

Background And Motivation – Previous Experiment

- During tension/compression fatigue testing of the bolt connecting a kettlebell to a fixture, a decrease in damping was observed with increased excitation amplitude.
- Damping generally increases as excitation amplitude increases – this was unexpected

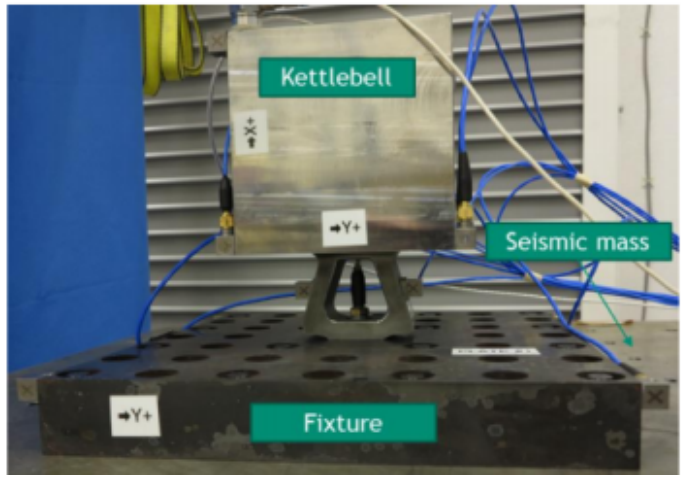

Fig 3. Test setup

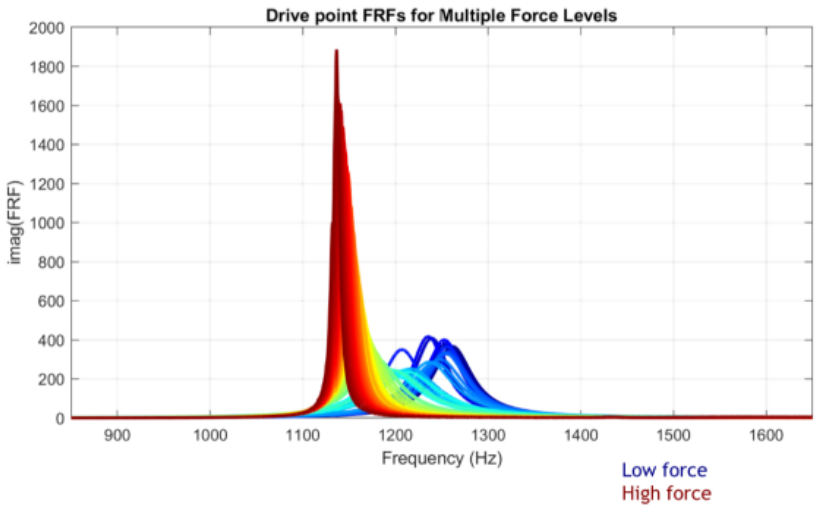

Fig 4. FRFs for various forcing levels

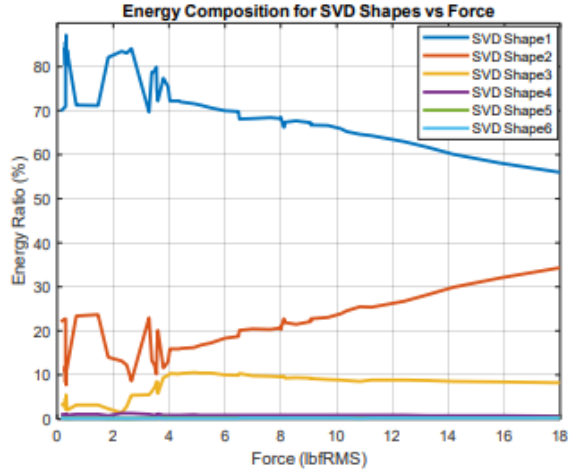

Fig 5. SVD Shapes

- Motivating question: is the decrease in damping due to modal coupling, or a nonlinear characteristic of one of the modes in question (the 2nd bending mode in Y (4), and the axial mode in X (5))?
- The SVD shapes in figure 5 represent the modal deflection shapes and is derived from the columns of the FRF matrix
  - Presence of 2 modes indicates that coupling could be occurring

Objectives

Project Goal: Determine if the decrease in damping is caused by modal coupling of the axial and 2nd bending mode in Y

Tasks:

1. Perform linear modal and nonlinear testing
   - Nonlinear identification of the axial and 2nd bending mode in Y
2. Create nonlinear finite element model
3. Create a nonlinear Hurty-Craig-Bampton (HCB) reduced order model
   - Capture nonlinearities with Iwan elements
4. Conduct MM-QSMA on the full fidelity finite element model
   - QSMA has only been used to examine weakly coupled structures

Experimental Setup

- Kettlebell-plate system is similar to the setup used for tension/compression failure testing
- 4340 Steel Kettlebell
- Boundary Conditions: Fixed base – Free end

Fig 6. Close-up of contact between the kettlebell and plate

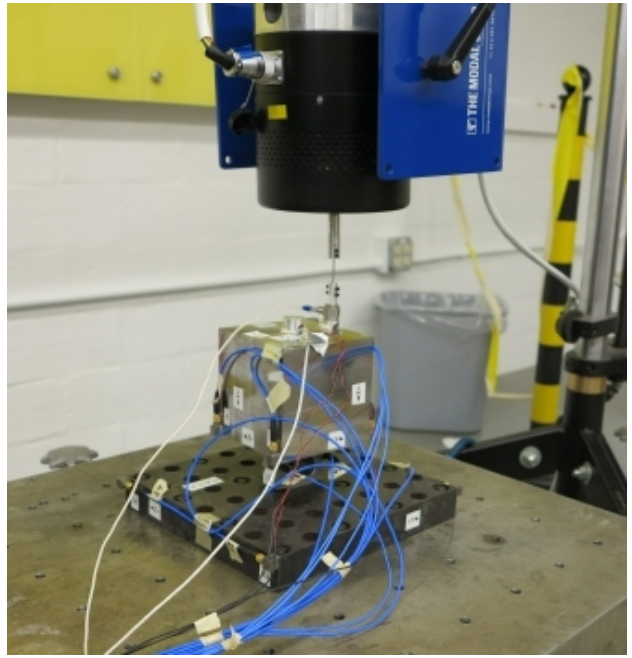

Fig 7. Full setup for a shaker test

Location of Hammer Impacts

- Node 1001: excites axial mode (mode 4)
- Node 1002: excites both modes
- Node 1003: excites 2nd bending mode (mode 5)

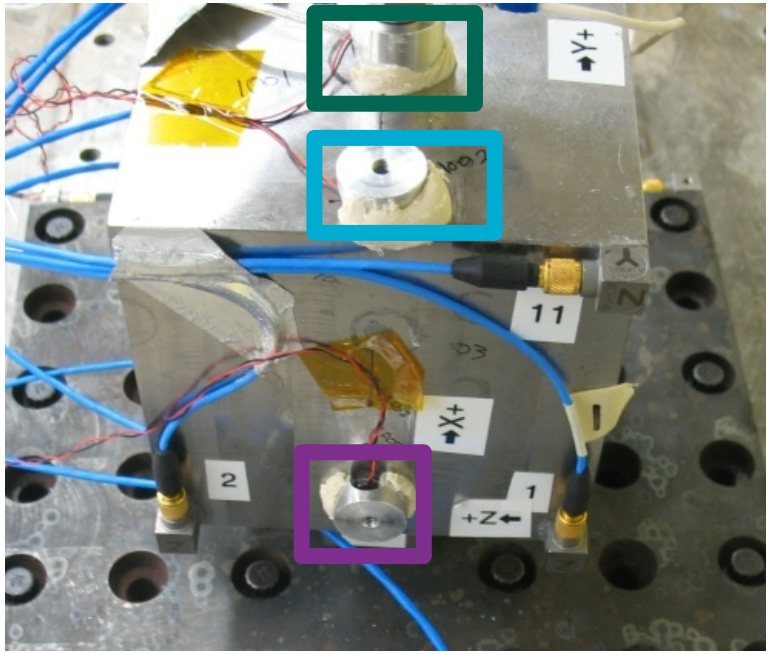

Fig 8. Close-up of kettlebell with reference node/drive point locations

Governing Equations and Linear Results

- We model the physical system using a system of equations

$$M\ddot{x} + C\dot{x} + Kx = f \quad \text{Eqn. 1}$$

$$\ddot{q} + 2\zeta_n\omega_n\dot{q} + \omega_n^2 q = \phi^t f \quad \text{Eqn. 2}$$

- Given an excitation force f and known natural frequencies and damping ω_n and ζ_n, we can solve for the modal and physical response of the system, q and x
- Extraction of modes for low-level input data – response is effectively linear at low force levels
- Bending and Axial modes are fit well with the extraction
- Equation for FRF (Frequency Response Function) used to extract the mode shapes:

$$H_{ij}(\omega) = \sum \frac{-\omega^2 \phi_{ik}\phi_{jk}}{\omega_k^2 - \omega^2 + i2\zeta_k\omega\omega_k} \quad \text{Eqn. 3}$$

- Each column of the FRF matrix (H) corresponds to the individual FRF for each mode

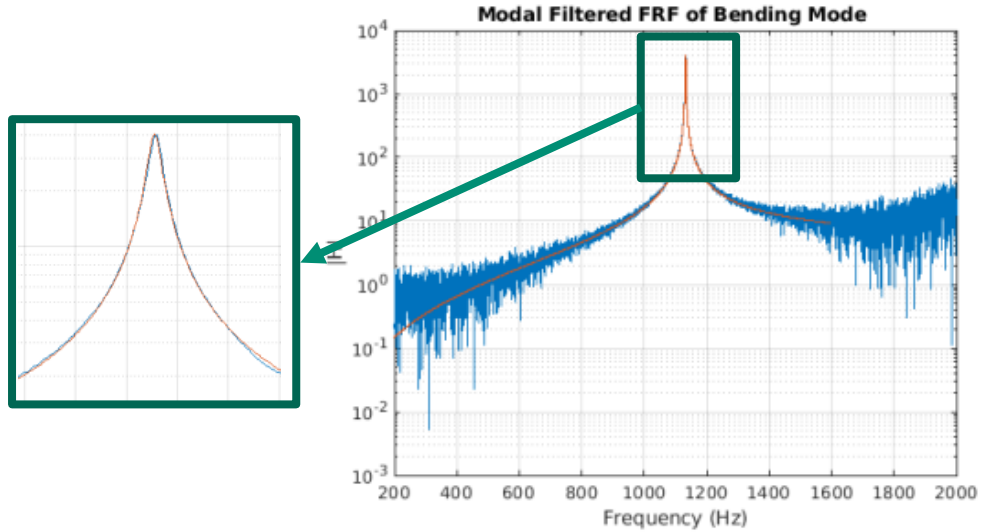

Fig 9. Bending Mode Extraction

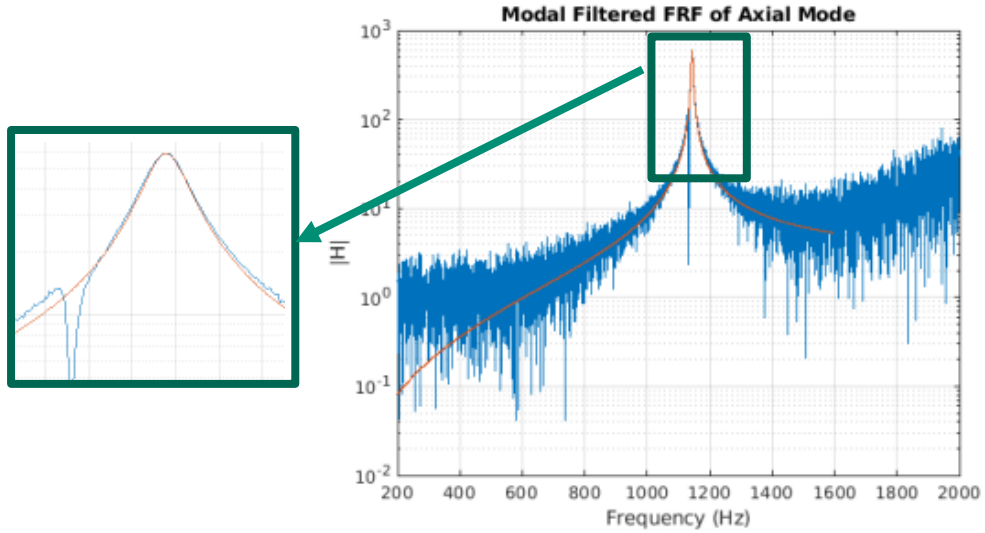

Fig 10. Axial Mode Extraction

Nonlinear Identification

- Using acceleration data and known mode shapes, we can compute the nonlinear natural frequency and damping of the structure (flow chart from Ben Pacini)

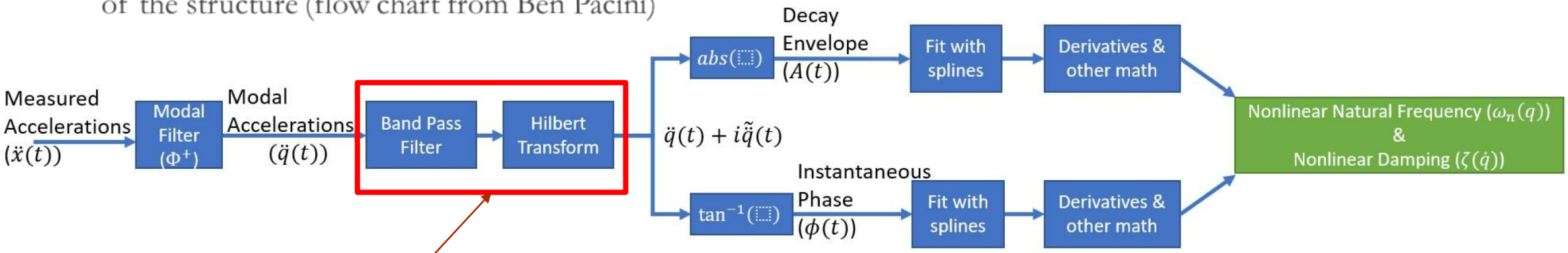

Fig 11. Nonlinear Amplitude Dependent Natural Frequency and Damping Workflow

- Standard Hilbert Transform did not filter the bending and axial modes well due to closeness of modes
- Other filters (Butterworth and Chebyshev2) and transformation methods (Short Time Fourier Transform) were attempted, but also do not properly filter response
- A new method must be used – nonlinear optimization is used to curve fit the oscillation
  - This method was discovered too late in NOMAD 2021 to be properly used/implemented in the reduced order modeling of the system
  - $\tilde{y}(t) = e^{\beta(t)}\cos(\alpha(t))$ (Ben Moldenhauer)

Structure Rotation

- The Kettlebell-Fixture structure rotated slightly in the z direction a Force Appropriation test!
- Linear natural frequency and damping shifted in each mode as a result

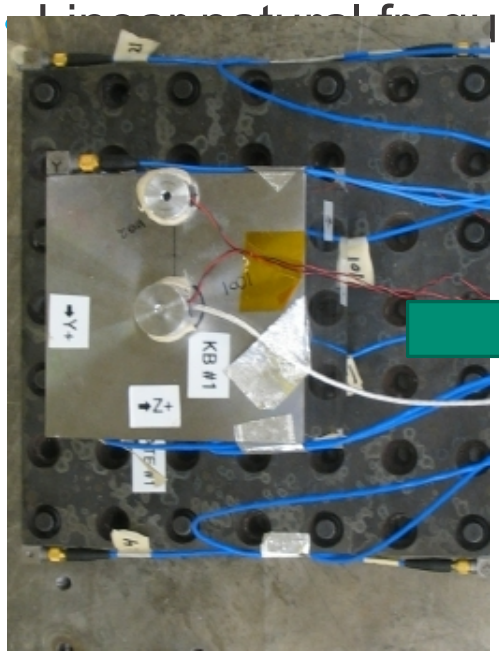

Fig 12. Original Structure

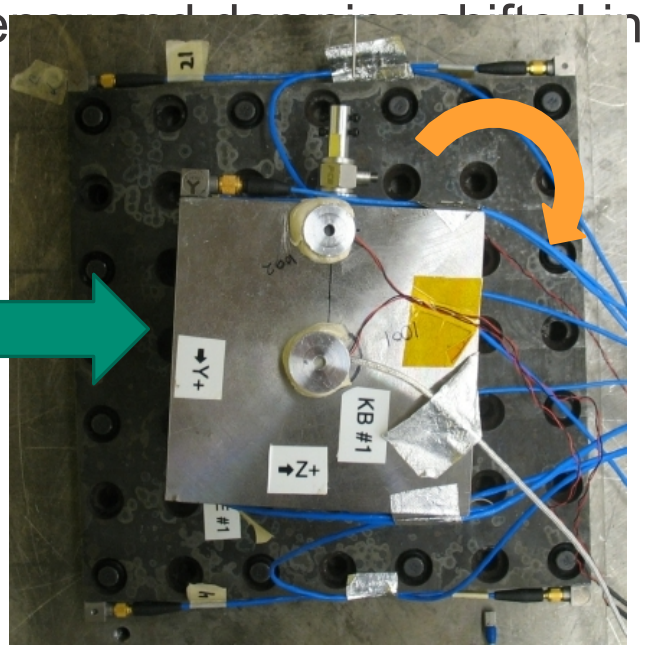

Fig 13. Rotated Structure

Table 1. Frequency Shift

Mode			Change
1	84.9	101.5	19.55%
2	166.8	178.9	7.25%
3	328.7	348.1	5.90%
4	1132.1	1137.3	0.46%
5	1145.4	1182.3	3.22%
6	1429.6	1469.0	2.76%

- Separation between mode 4 and 5 increased!
  - Previously separated by ~13 Hz, now separated by 45 Hz

Structure Rotation – New Frequency And Damping

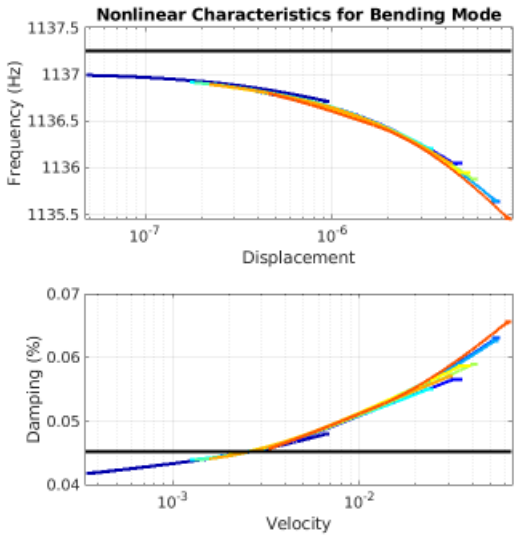

Fig 14a. Individual ω_n and ζ_n - bending

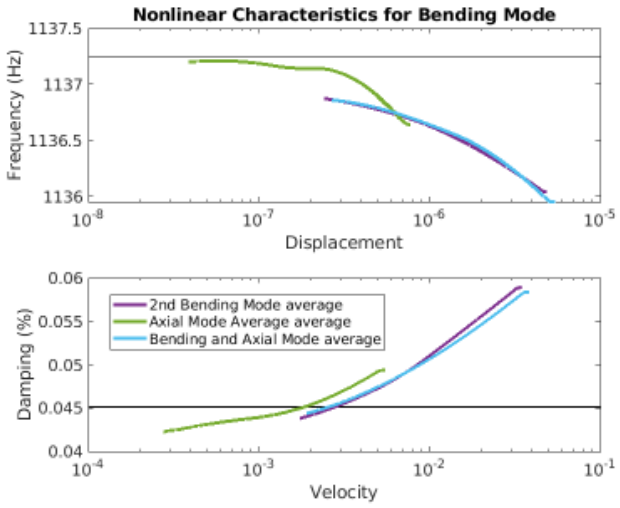

Fig 14b. Averaged ω_n and ζ_n - bending

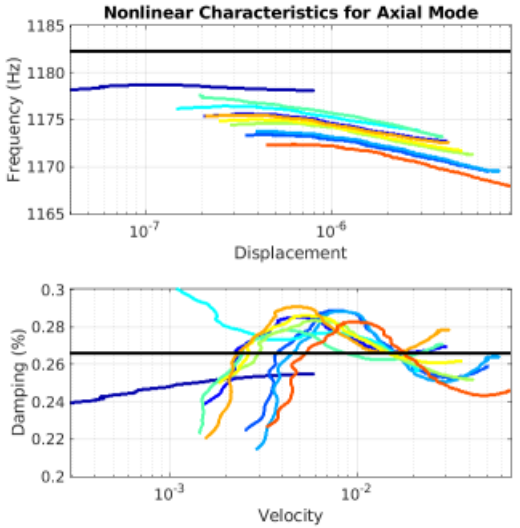

Fig 14c. Individual ω_n and ζ_n - axial

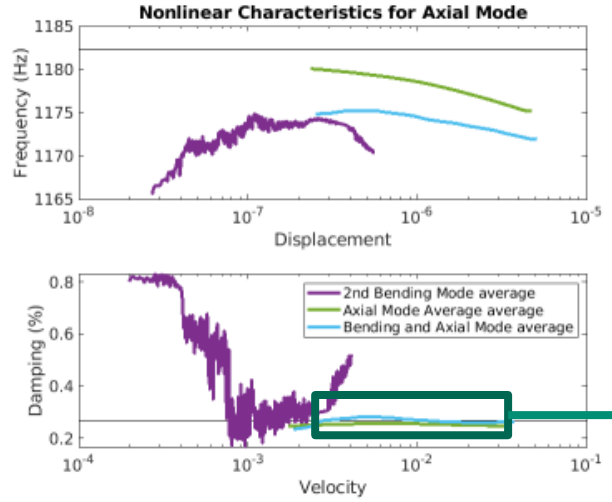

Fig 14d. Averaged ω_n and ζ_n - axial

- Isolated axial mode damping curve is concave down; previously concave up
- Behavior of bending mode is constant during isolation and joint excitation with axial mode
  - This indicates that there is less coupling occurring between the axial and bending modes
- Axial mode is non-monotonic
  - This presents problems with using an Iwan spring for the nonlinear model

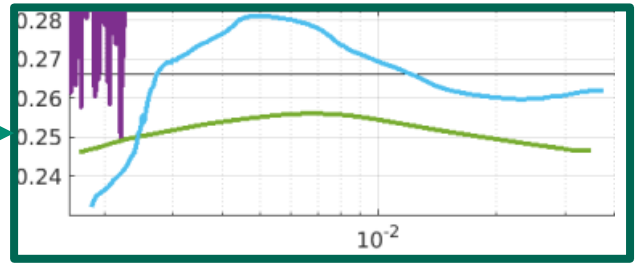

Modal Filtering - FRFs

- Influence of the 2nd Bending mode is still present in the FRF for the axial model – there are two peaks
- The increased separation of the bending and axial modes appears to have decreased the peak, but the bending mode is clearly still present
- Other filtering methods must be correctly extract the axial mode

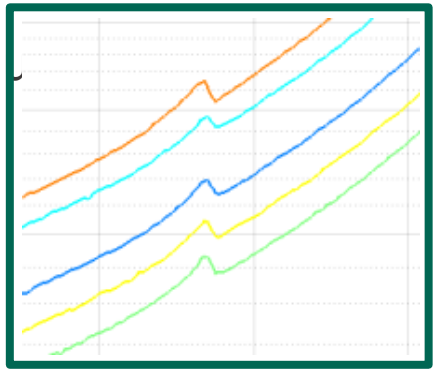

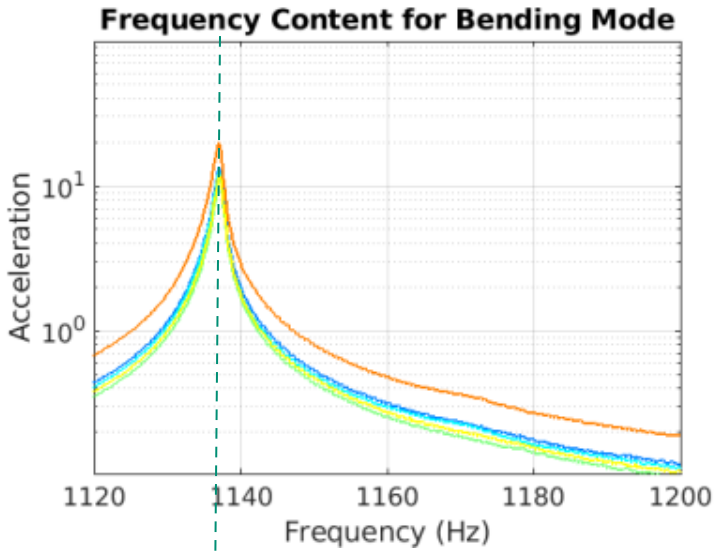

Fig 15a. FRFs for Bending mode

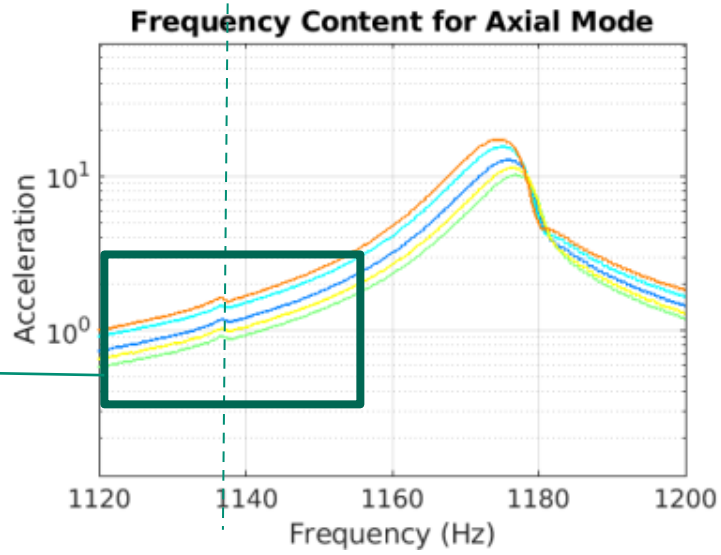

Fig 15b. FRFs for Bending mode

Picking the Right Band Pass filter

- When using a bandpass filter to obtain the individual FRFs for the bending and axial mode, the shoulder is only eliminated with a very narrow filter. The filter extracts frequency content between the lower and upper ratio of the natural frequency of the mode in question
  - FRF is not a good fit for the axial mode with the narrowest filters ([0.99 1.01] and [0.99 1.03])
- Thus, we need an alternative method to filter the data

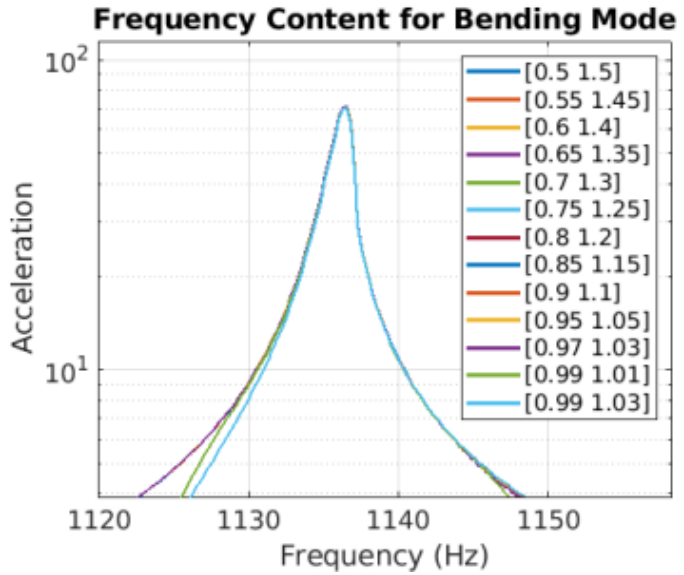

Fig 16a. FRFs for various bandpass filters

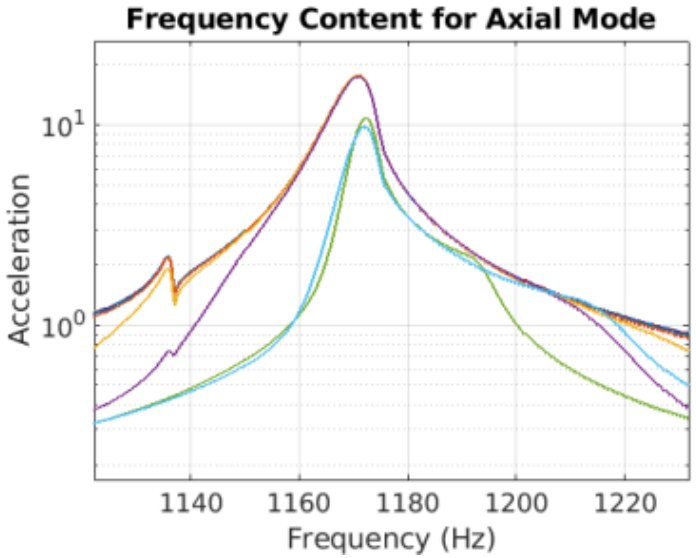

Fig 16b. Roll-off Effects of Different filters

Other Filtration Methods

- **Butterworth**: designed to have a flat frequency response in the passband
- **Chebyshev2**: has a steeper roll-off than the Butterworth filter, but has a stopband ripple (oscillations after the roll-off)
- Both filters were tested on our data; no noticeable difference was observed

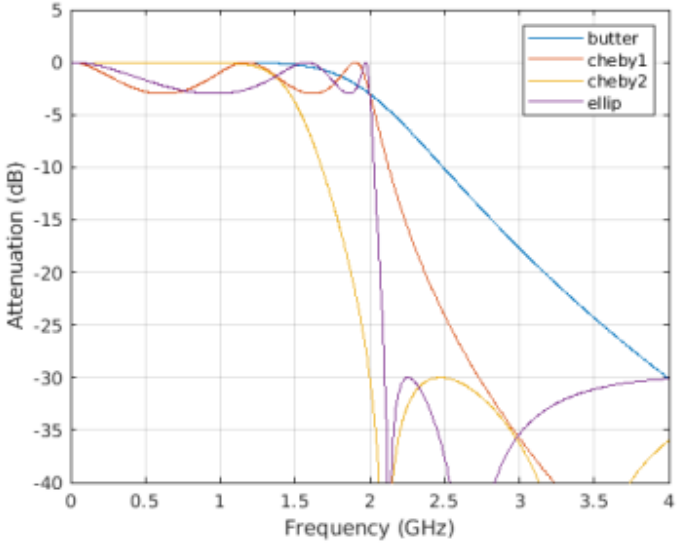

Fig 17a. Roll-off Effects of Different filters

STFT (Short Time Fourier Transform)

- Fourier transform of evenly spaced band pass filters
- Hoped to capture individual modes because we were processing subsets of the data, hence the drop between the bending and axial mode could be targeted
- Nonlinear frequency and damping curves calculated using instantaneous amplitude of FRFs

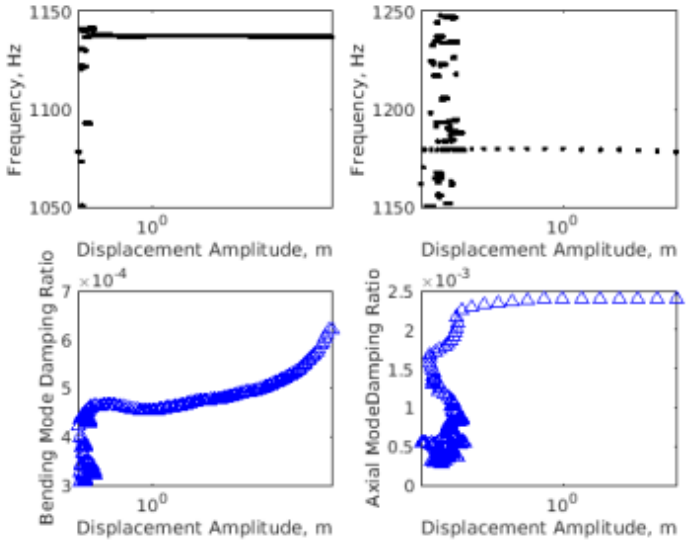

Fig 17b. STFT Frequency and Damping

Quasi Static Modal Analysis (QSMA)

- Determines the quasi-static response of a structure when a force in the shape of a mode of interest is applied
  - Determines nonlinear natural frequencies and damping ratios (amplitude dependent)
  - Allows modes shapes to change with amplitude
  - Not conventionally used to determine modal coupling
  - Modal coupling can be assessed by the skew of each mode when only one activated

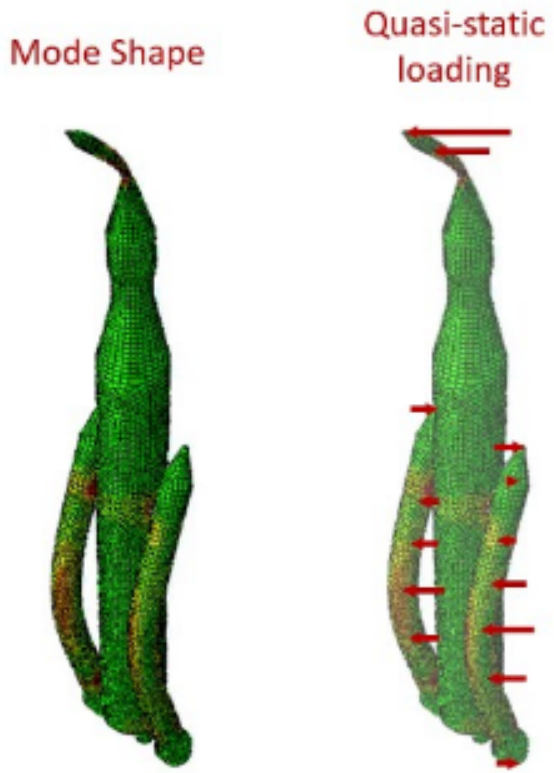

$$\omega_r(\alpha) = \sqrt{\frac{\alpha}{q_r(\alpha)}} \qquad \text{Eqn. 4}$$

Amplitude dependent frequency

$$\zeta_r(\alpha) = \frac{D(\alpha)}{2\pi(q_r(\alpha)\omega_r(\alpha))^2} \qquad \text{Eqn. 5}$$

Nonlinear Damping

$$\mathbf{f}_{ext} = \mathbf{M}\,\boldsymbol{\phi}_r$$

QSMA: Modal Coupling

- QSMA used on simple bolted structures with weak/negligible modal coupling
  - 2D and 3D bolted cantilever beam models
  - Test hardware for Orion Multipurpose Crew Vehicle
- Modal coupling can be examined by plotting the displacement ratio of each mode vs the peak velocity or the displacement vs the modal amplitude
- Other method of quantifying modal coupling is through an SVD energy based method

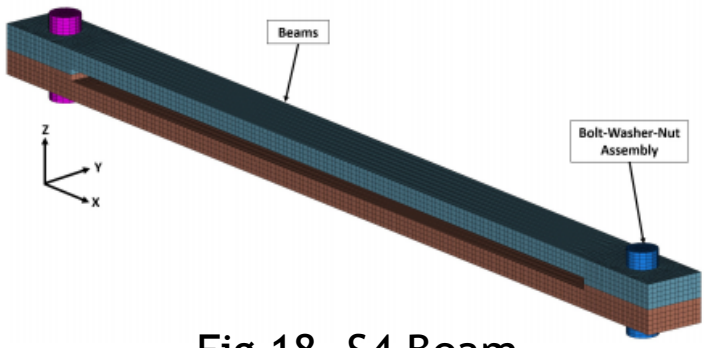

Fig 18. S4 Beam

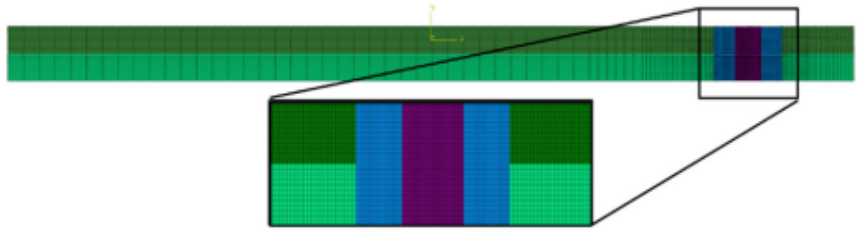

Fig 19. 2D Bolted Cantilever Beam

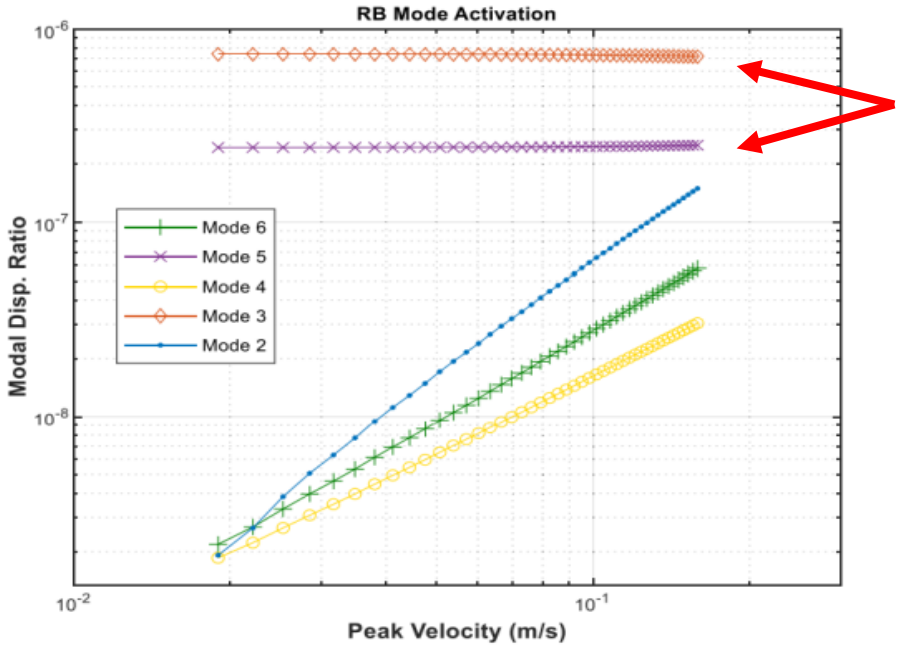

Weak modal coupling with mode 1

Fig 20. 2D Beam Mode 1 activation

Nonlinear FEM: Linearized Modes

- High fidelity of model of Kettlebell structure with nonlinear joint interface contact to examine linear modes of vibration
  - Bolt is vital part of QSMA so the nonlinearities of joint can be assessed
  - 163173 tetrahedral elements
  - Bolt preload: 2025 lbf

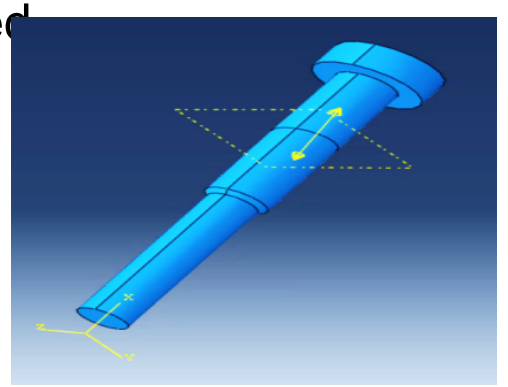

Fig 21. Bolt

Table 2. Linear Mode Preliminary Data

Mode	*Model*	*Experimental*	*Error*
1st Bending in Z	117.93	101.5	16%
1st Bending in Y	169.43	178.9	5.3%
Torsion about X	364.35	348.1	4.67%
2nd Bending in Y	1114.9	1137.3	1.97%
Axial in X	1183.2	1182.3	0.1%
2nd Bending in Z	1485.6	1469.0	1.42%

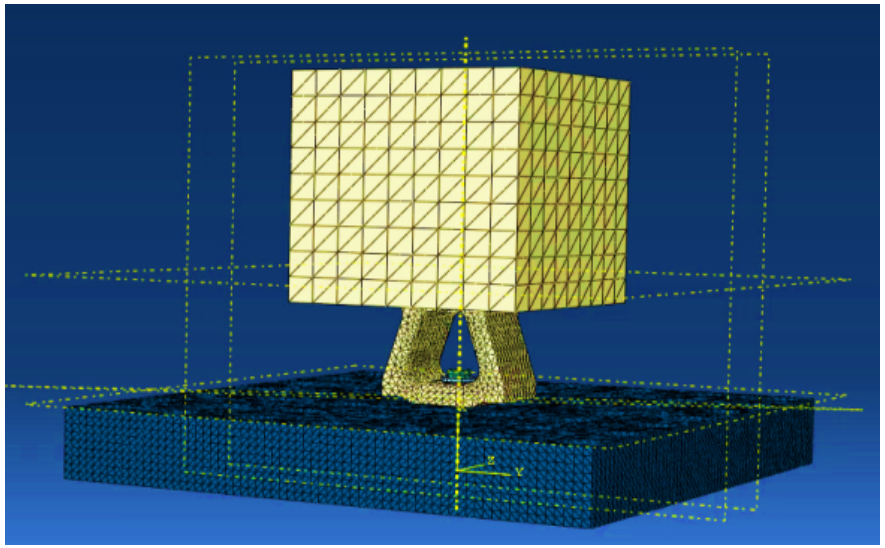

Fig 22. Pic of Model

Nonlinear FEM: Mode Shapes & Modal Assurance Criterion

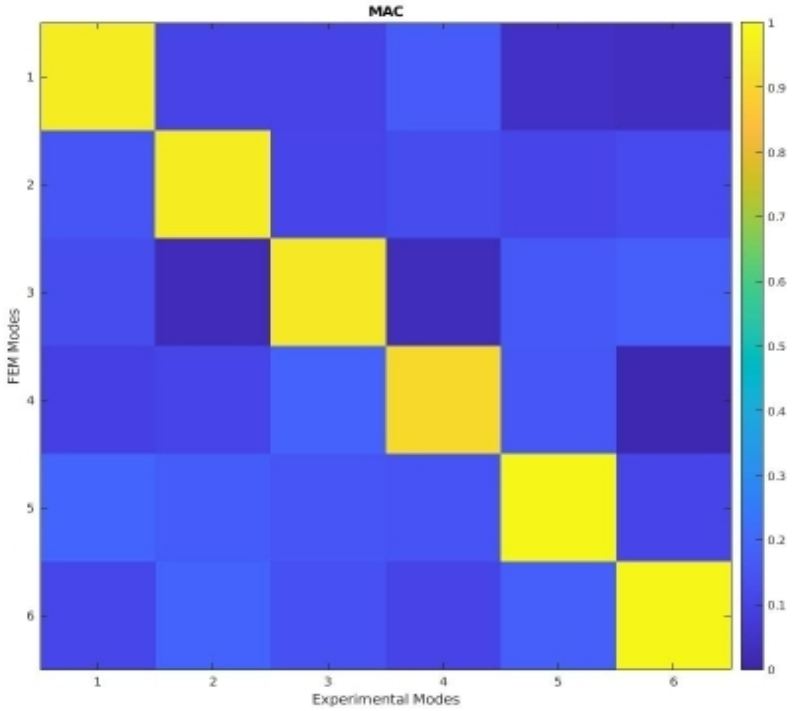

Fig 23. MAC (rep. data)

$$MAC(r,q) = \frac{\left|\{\varphi_A\}_r^T \{\varphi_X\}_q\right|^2}{\left(\{\varphi_A\}_r^T \{\varphi_A\}_r\right)\left(\{\varphi_X\}_q^T \{\varphi_X\}_q\right)}$$

Eqn. 6

- Correlates the simulated mode shapes with the experimental mode shapes.
  - > 90%, simulated has good agreement with experimental
  - Modes #-# have the appropriate correlation between exp. and sim.
  - Experimental mode shape data is collected form 11 tri-axial accelerometers

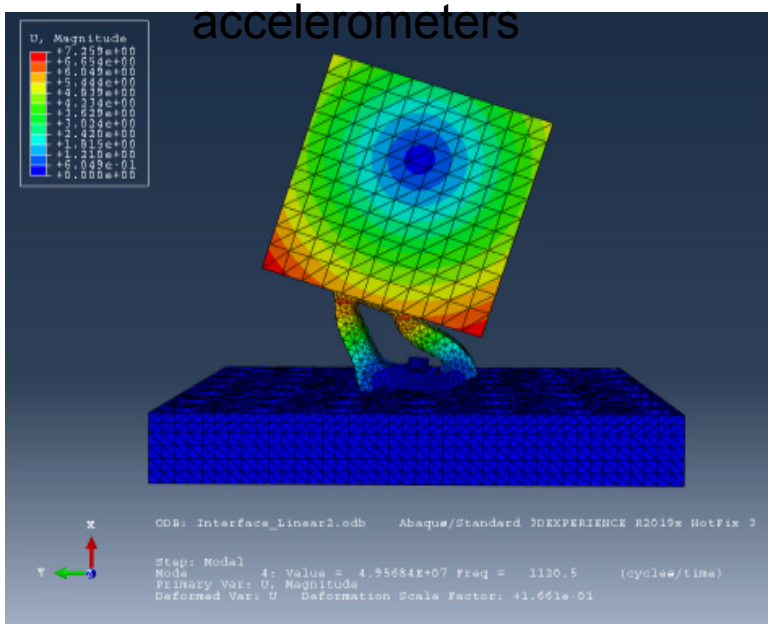

Fig 24. Pic of 2nd Y Bending mode

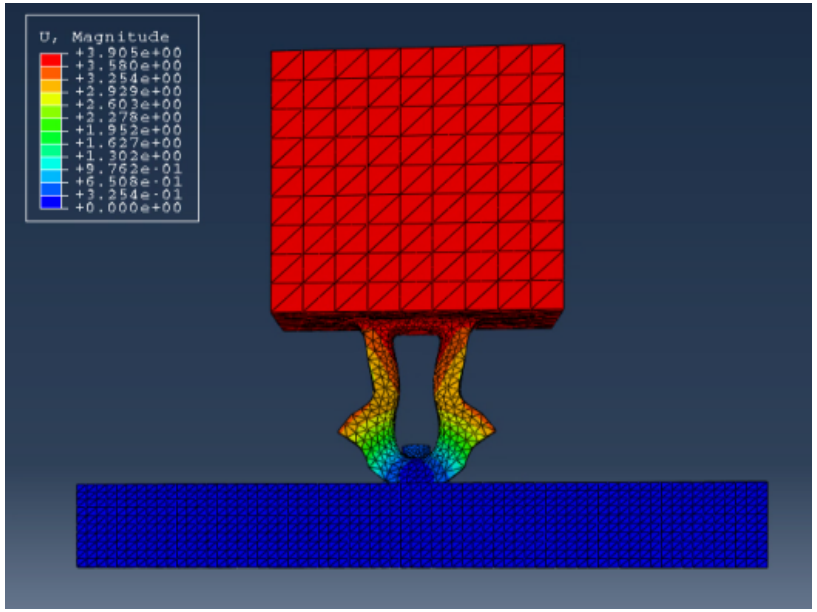

Fig 25. Pic of axial mode

Nonlinear FEM: QSMA Results

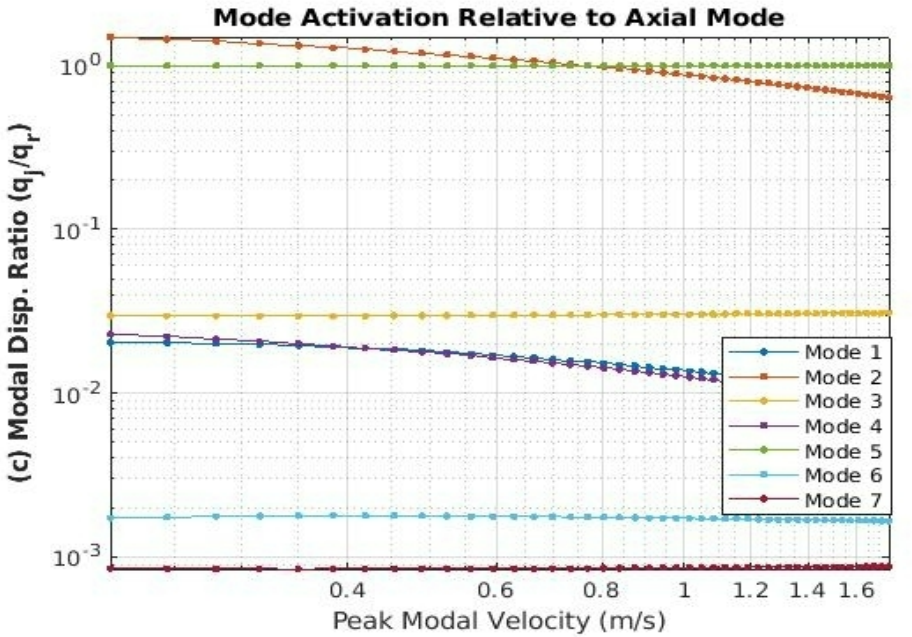

Fig 26. Modal coupling w/ axial as mode of interest (rep)

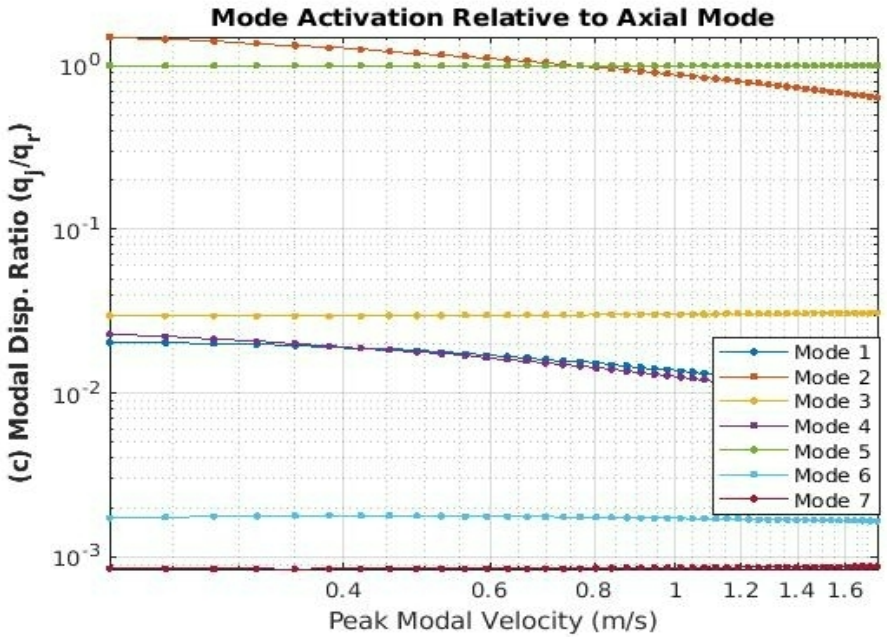

Fig 27. Modal coupling w/ bending- y as mode of interest (rep)

- Displacement of modes at amplitudes indicates activation and coupling
- Axial mode has considerable coupling with mode #-#
- 2nd bending mode in Y has considerable coupling with modes #-#

Axial & Bending-Y Mode Results

- The Axial mode damping ratio changes non-monotonically/monotonically
  - Inconsistent/consistent with FRF plot, show initial increase in damping followed by sudden decrease
  - The initial QSMA-derived natural frequency has a #% error from FEM
- The 2nd bending in y mode shows hardening/softening effect and a decrease/increase in the damping ratio
  - Damping ratio behaves non-monotonically/monotonically
- Results are consistent/inconsistent with the experimental results

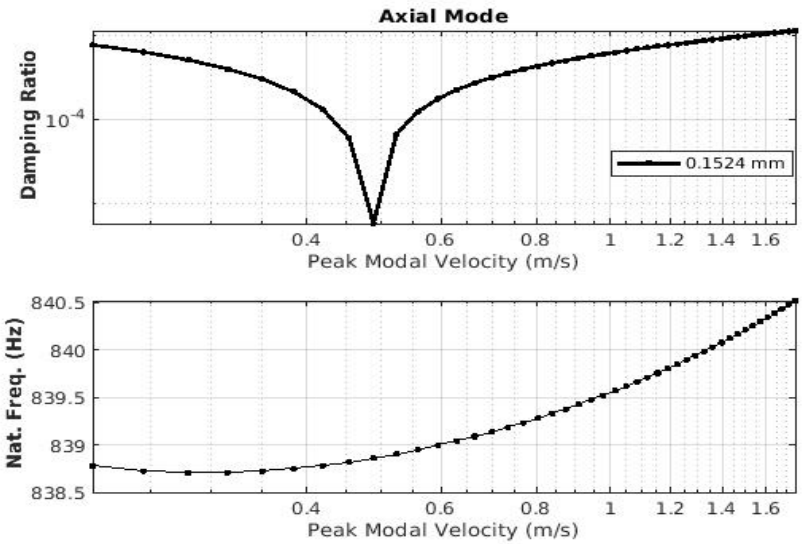

Fig 28. Axial Mode amplitude dependent data (rep)

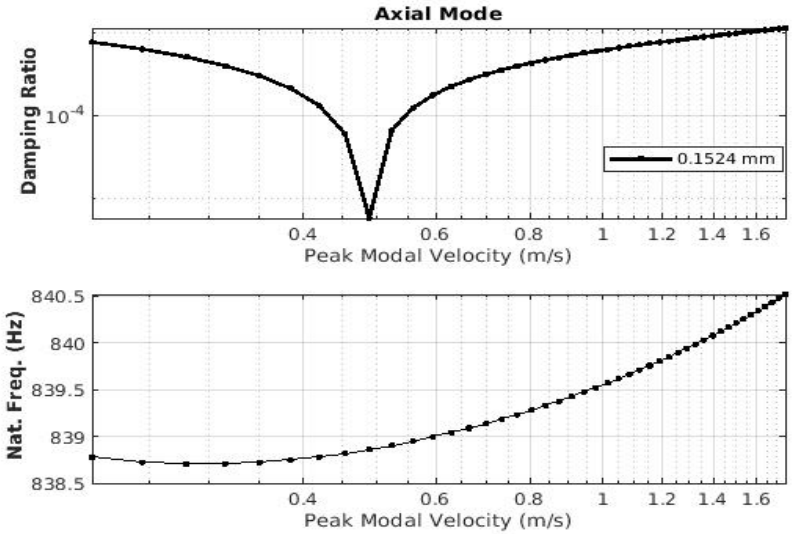

Fig 29. Bending in Y amplitude dependent data (rep)

Interface Static Analysis: *2nd Y bending mode*

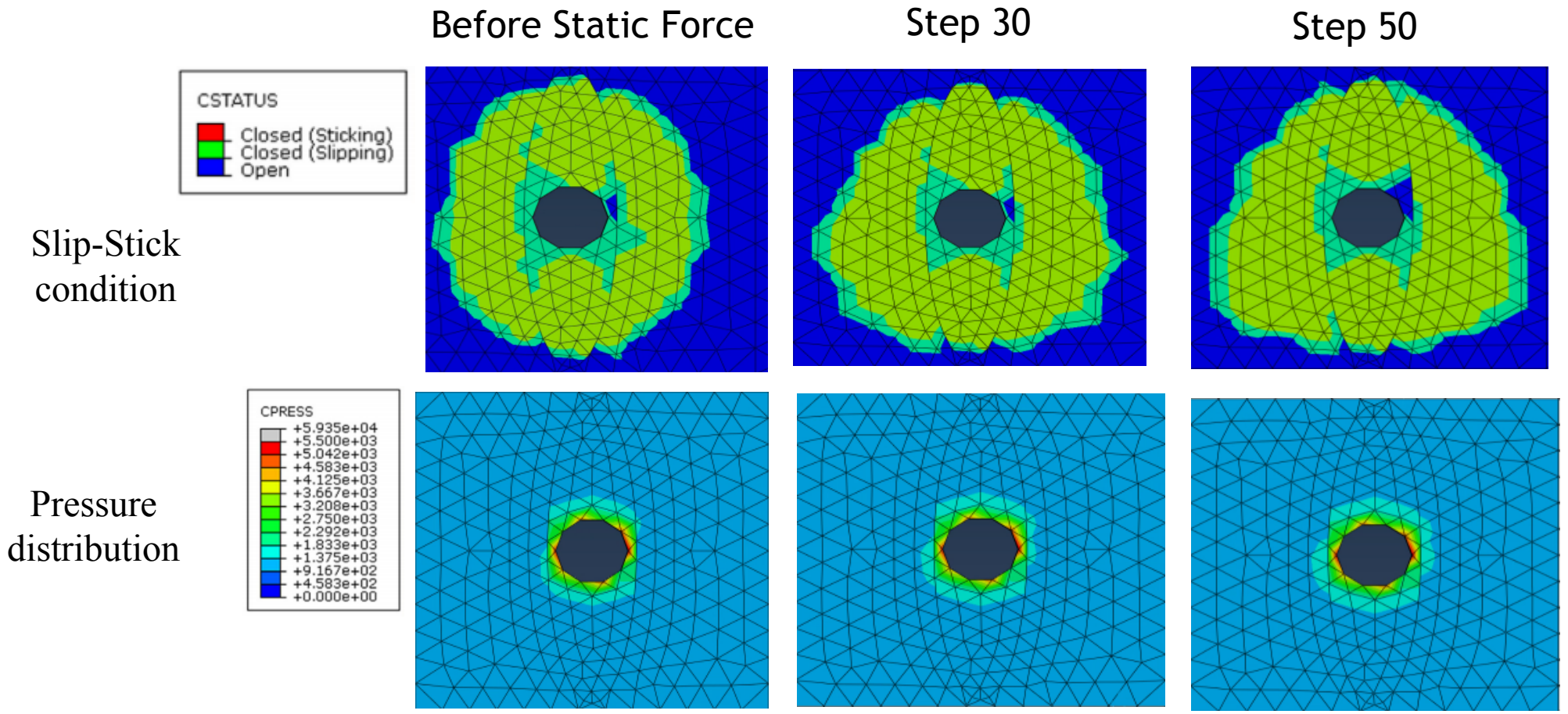

Fig 30a-f. Pressure distribution and Slip-Stick conditions (rep)

- Slipping region is **increasing**/decreasing with amplitude while stick region is **decreasing**/increasing
  - This causes **decrease**/increase of stiffness as amplitude increases (nonlinear

Interface Static Analysis: *Axial Mode*

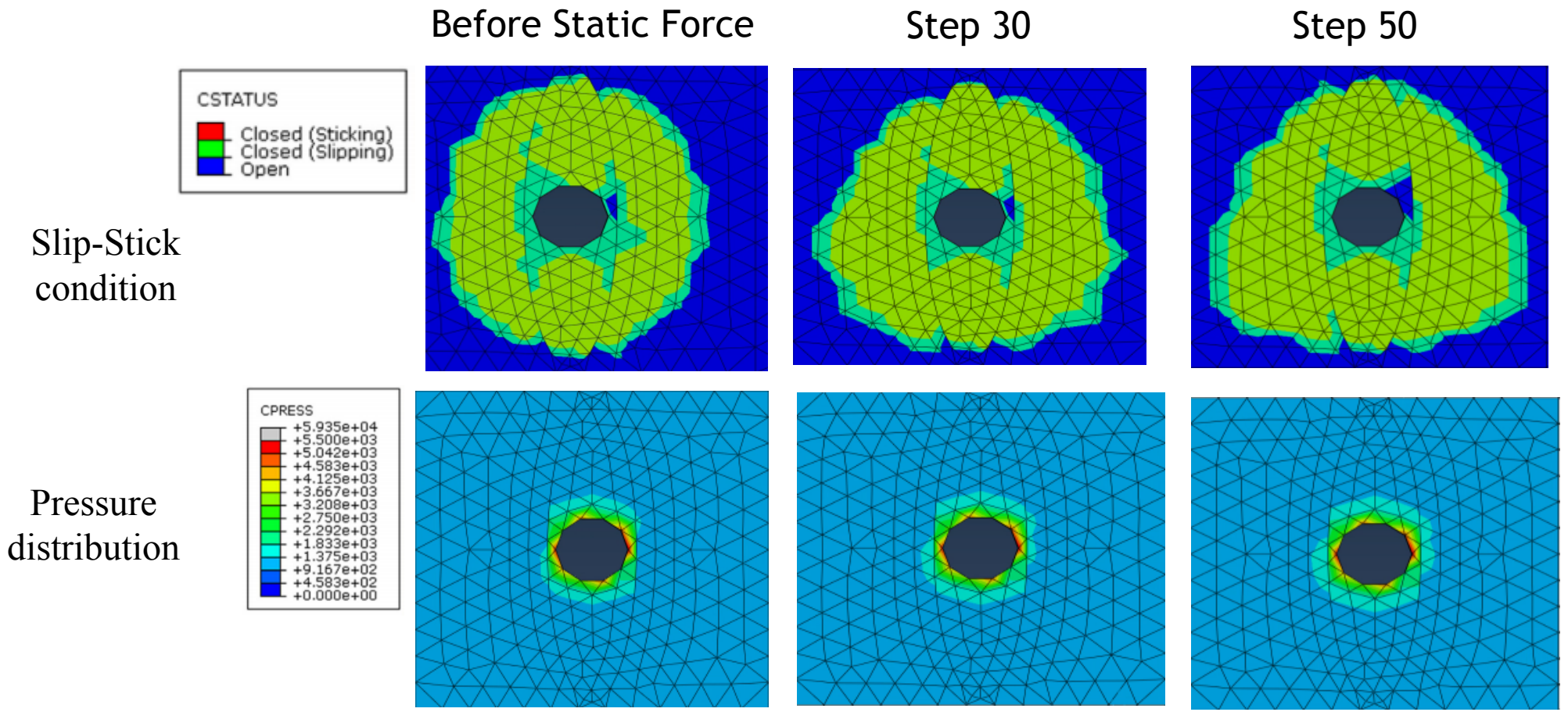

Fig 31a-f. Pressure distribution and Slip-Stick conditions (rep)

- Slipping region is increasing/decreasing with amplitude while stick region is decreasing/increasing
  - This causes decrease/increase of stiffness as amplitude increases (nonlinear

Variation of Nonlinear FEM

- Implements an asymmetric stick region with different frictional properties through out the jointed interfaces
  - Elliptical Stick region allowing finite slip
  - Friction Coefficients: 0.1 and 0.05 for two halves of slip region

Table 3. Adjusted Linear Modes

Mode	*Model*	*Experimental*	*Error*
1st Bending in Z	103.58	101.5	2.05%
1st Bending in Y	168.36	178.9	5.89%
Torsion about X	358.98	348.1	3.13%
2nd Bending in Y	1101.9	1137.3	3.11%
Axial in X	1200.9	1182.3	1.5%
2nd Bending in Z	1486.9	1469.0	1.21%

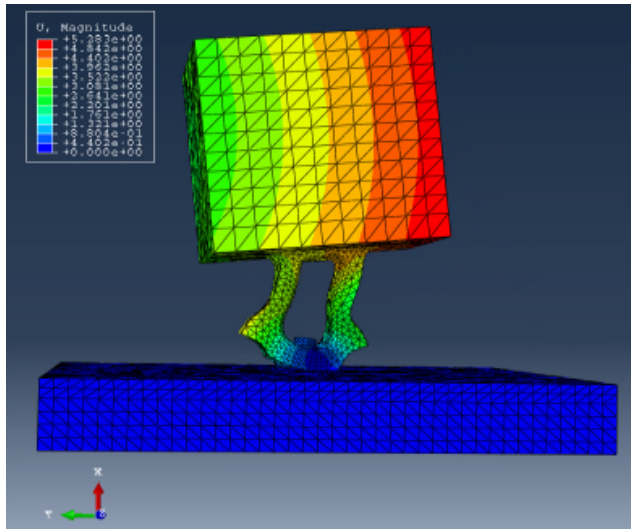

Fig 32. Axial mode with tilt in y-direction

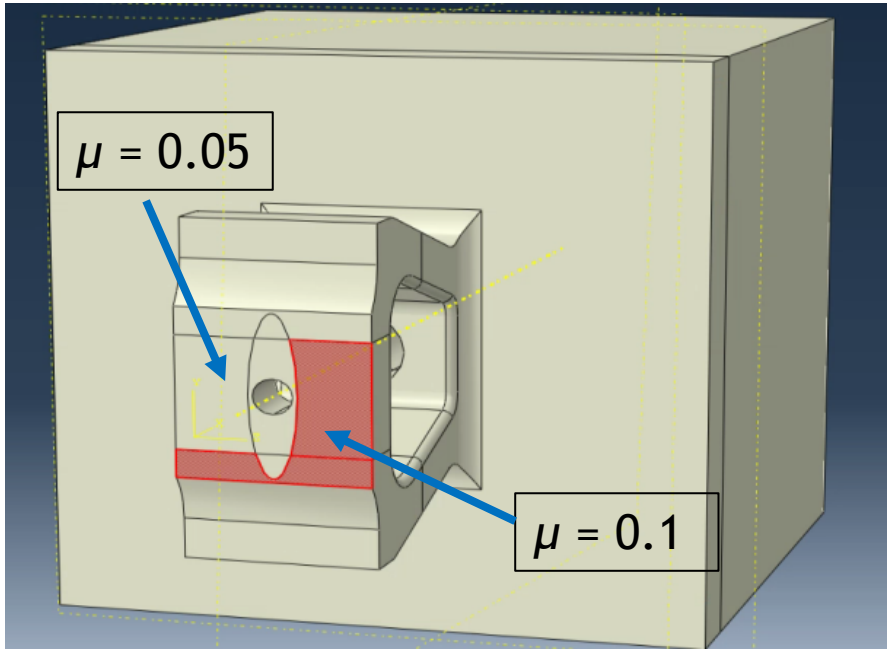

Fig 33. Model joint

The Hurty-Craig-Bampton (HCB) Method

- The Hurty-Craig-Bampton (HCB) method is a dynamic sub-structuring technique which allows the modeler to significantly reduce the size of models
- For an HCB model with 2 super-elements: Size of HCB model = 2*(number of fixed interface modes + 6*boundary nodes)
- MDOF EOM with DOF's partitioned into boundary and interior DOF's

$$\begin{bmatrix} \mathbf{M}_{ii} & \mathbf{M}_{ib} \\ \mathbf{M}_{bi} & \mathbf{M}_{bb} \end{bmatrix} \begin{bmatrix} \ddot{x}_i \\ \ddot{x}_b \end{bmatrix} + \begin{bmatrix} \mathbf{K}_{ii} & \mathbf{K}_{ib} \\ \mathbf{K}_{bi} & \mathbf{K}_{bb} \end{bmatrix} \begin{bmatrix} x_i \\ x_b \end{bmatrix} = \begin{bmatrix} F_i \\ F_b \end{bmatrix} \qquad \text{Eqn. 7}$$

- Definition of the HCB transformation

$$\begin{bmatrix} x_i \\ x_b \end{bmatrix} = \begin{bmatrix} \mathbf{\Phi}_{ik} & \mathbf{\Psi}_{ib} \\ \mathbf{0} & \mathbf{I}_{bb} \end{bmatrix} \begin{bmatrix} q_k \\ x_b \end{bmatrix} = \mathbf{\Phi}_{CB} \begin{bmatrix} q_k \\ x_b \end{bmatrix} \qquad \text{Eqn. 8}$$

- Applying the HCB transformation and $\mathbf{\Phi}_{CB}^T$ we now define premultiplying by

$$\mathbf{\Phi}_{CB}^T \begin{bmatrix} \mathbf{K}_{ii} & \mathbf{K}_{ib} \\ \mathbf{K}_{bi} & \mathbf{K}_{bb} \end{bmatrix} \mathbf{\Phi}_{CB} = \begin{bmatrix} \omega_k^2 & \mathbf{0} \\ \mathbf{0} & \mathbf{K}_{bb} \end{bmatrix} \qquad \mathbf{\Phi}_{CB}^T \begin{bmatrix} \mathbf{M}_{ii} & \mathbf{M}_{ib} \\ \mathbf{M}_{bi} & \mathbf{M}_{bb} \end{bmatrix} \mathbf{\Phi}_{CB} = \begin{bmatrix} \mathbf{I} & \mathbf{M}_{kb} \\ \mathbf{M}_{bk} & \mathbf{M}_{bb} \end{bmatrix} \qquad \text{Eqn. 9}$$

- EOM in HCB space

$$\begin{bmatrix} \mathbf{I} & \mathbf{M}_{kb} \\ \mathbf{M}_{bk} & \mathbf{M}_{bb} \end{bmatrix} \begin{bmatrix} \ddot{q}_k \\ \ddot{x}_b \end{bmatrix} + \begin{bmatrix} 2\zeta_k\omega_k & \mathbf{0} \\ \mathbf{0} & \mathbf{0} \end{bmatrix} \begin{bmatrix} \dot{q}_k \\ \dot{x}_b \end{bmatrix} + \begin{bmatrix} \omega_k^2 & \mathbf{0} \\ \mathbf{0} & \mathbf{K}_{bb} \end{bmatrix} \begin{bmatrix} q_k \\ x_b \end{bmatrix} = \begin{bmatrix} 0 \\ F_b \end{bmatrix} \qquad \text{Eqn. 10}$$

Contact Interface Determination

- The contact interface between the adaptor plate and kettlebell was determined using Mo Khan's Sierra/SM simulation with a bolt preload of 2000lbf
- From this simulation, the contact patch size was estimated to be a circle with a diameter of 1.1"

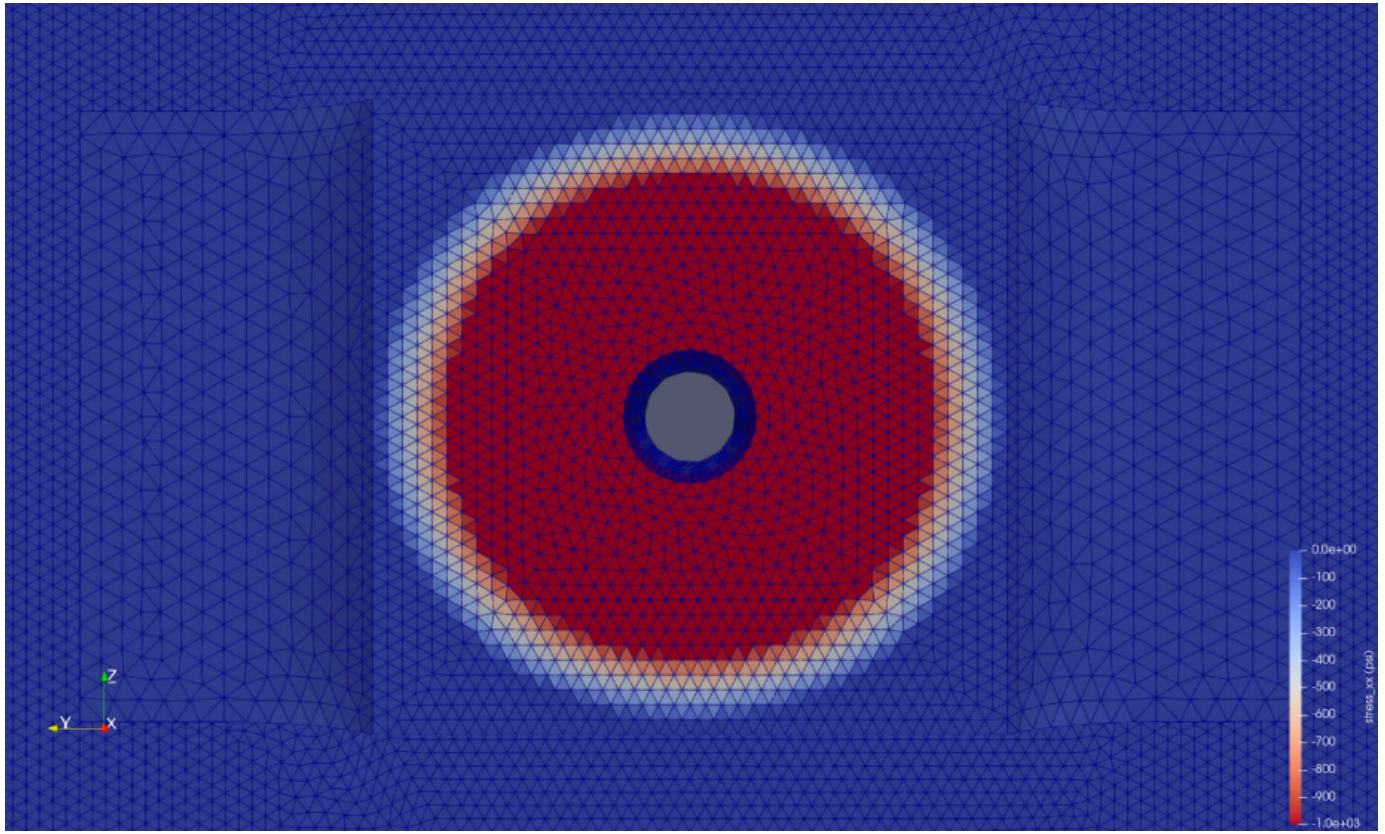

Fig 34. Contact Interface Pressure Distribution

Mesh Generation within Cubit

- Mesh was generated within Cubit with 923,662 nodes
- Mesh only failed the general guideline for the Scaled Jacobian on 3 elements, and given the size of the model, this level of failure was deemed acceptable

Table 4. Mesh Quality Summary

Function Name	*Average*	*Standard Deviation*	*Minimum*	*Maximum*	*General Guideline*
Shape	0.8508	0.077	0.4293	0.9996	>0.4
Normalized In-radius	0.7735	0.1026	0.2219	0.9985	>0.2
Scaled Jacobian	0.6471	0.1221	0.1846	0.9951	>0.2
Aspect Ratio	1.239	0.1594	1.000	3.467	<4.000

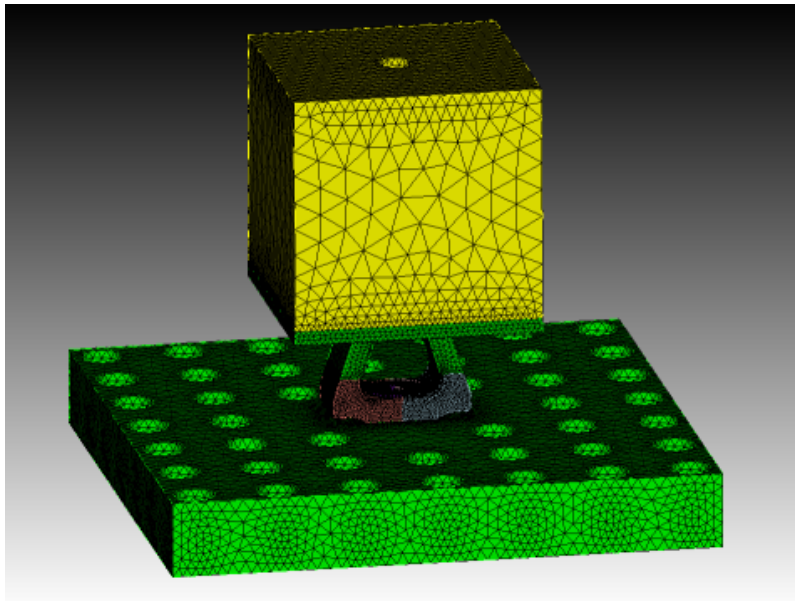

Fig 35. Kettlebell Meshed Geometry

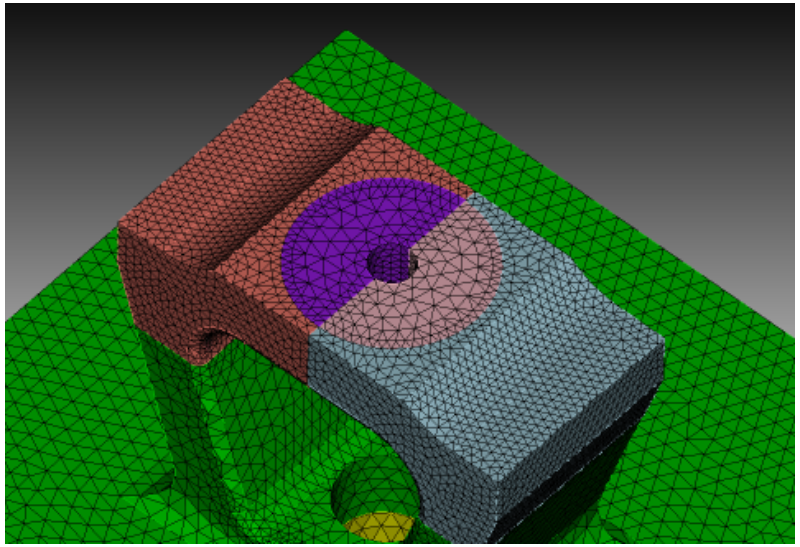

Fig 36. Contact Interface Mesh

Dynamic Sub-structuring with the HCB Approach

- The model was dynamically sub-structured into two super-elements: the adaptor plate and the kettlebell
- This was done to focus the analysis on the joint between the two parts
- Joint is initially modeled as a spring with stiffness in all 6 DOF's (3 linear + 3 rotational) with RBAR links tying contact nodes to a single interface node
- Computation speed was decreased by a factor of ≈54,000 and model size was reduced to 72 DOF's

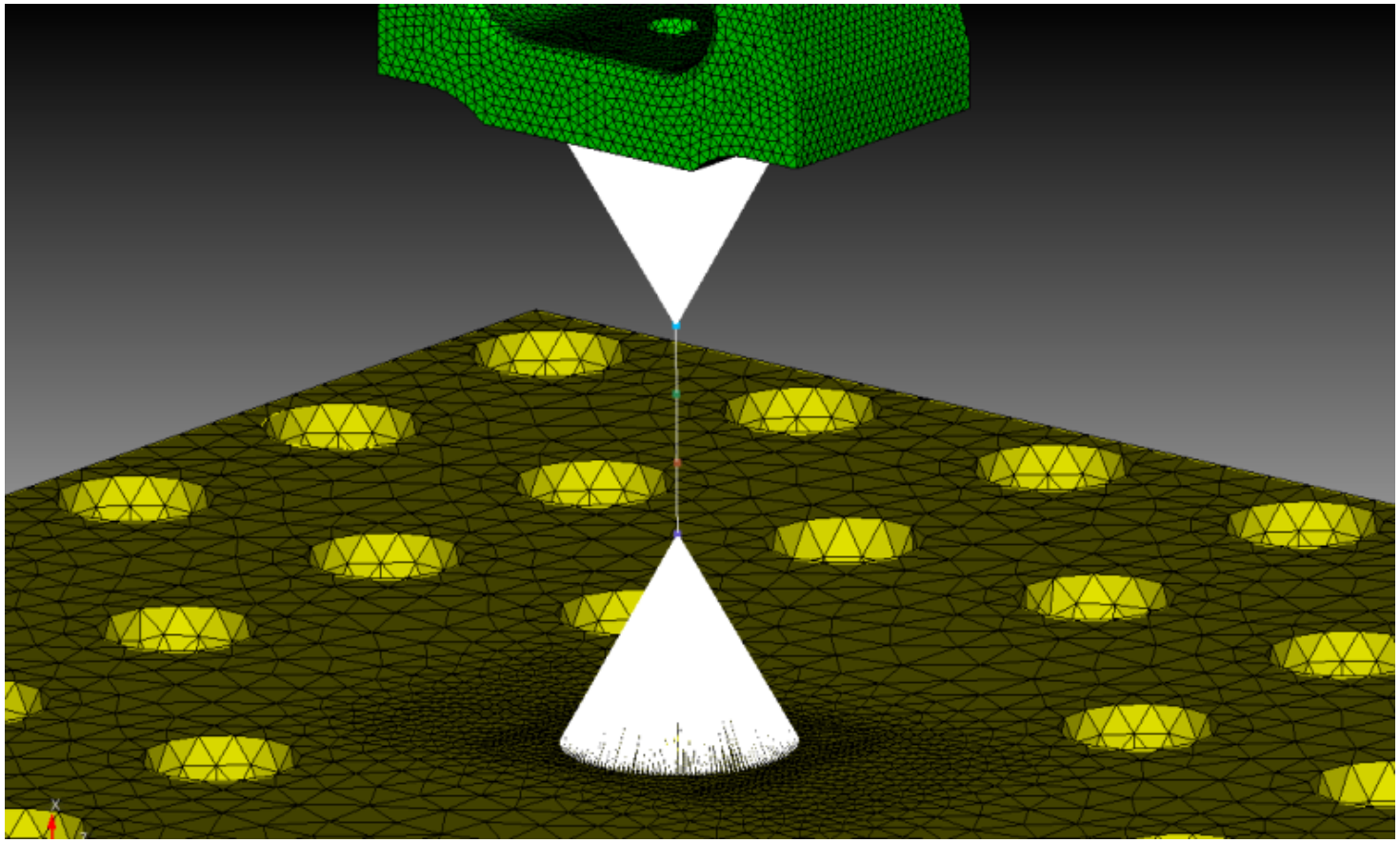

Fig 37. Contact Interface Modelling Approach

Linear Model Updating

- An inverse problem was formulated and solved by Sandia's Rapid Optimization Library (ROL) in order to tune the HCB model with experimental natural frequency truth data
- Poor fit of experimental axial mode due to slight bending in y-direction

Table 5. Linear Model Updating in Sierra

Mode	*Model*	*Experimental (Truth)*	*Error*
1st Bending in Z	101.614	101.5	0.112%
1st Bending in Y	178.890	178.9	0.006%
Torsion about X	348.076	348.1	0.007%
2nd Bending in Y	1137.250	1137.3	0.004%
Axial in X	1182.250	1182.3	0.004%
2nd Bending in Z	1458.200	1469.0	0.735%

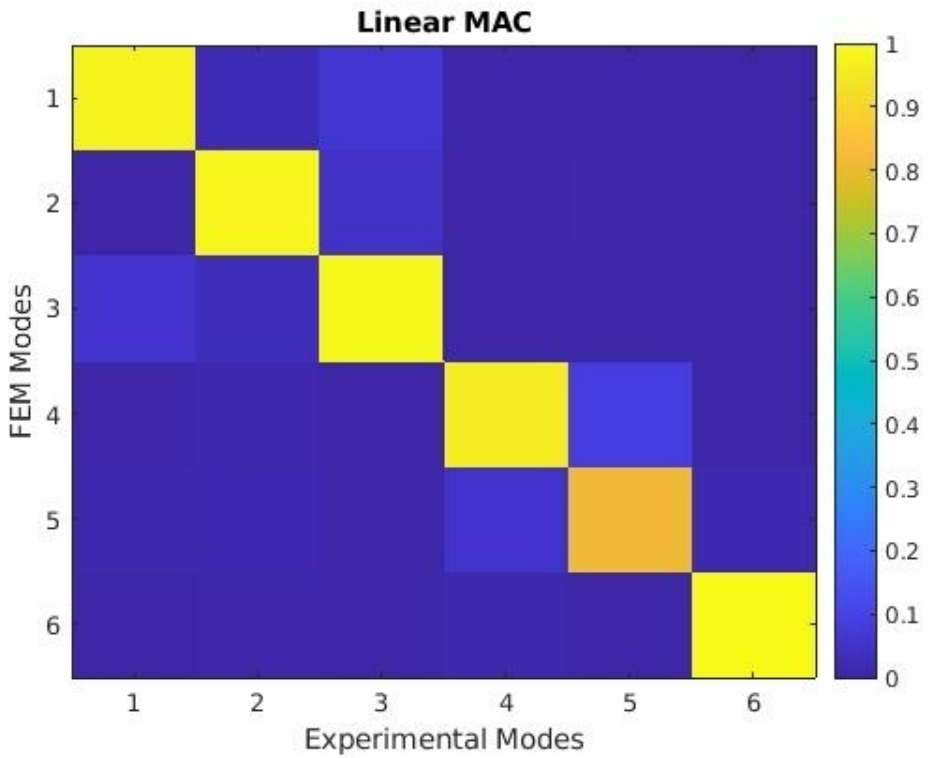

Fig 38. MAC for Linear Model

Nonlinear Model Formulation

- The frequencies of the 2nd bending mode in Y and the axial mode are highly dependent on the joint stiffness in the rot-Z and linear-X directions, respectively
- Iwan joints were placed in these directions to simulate slipping in these directions

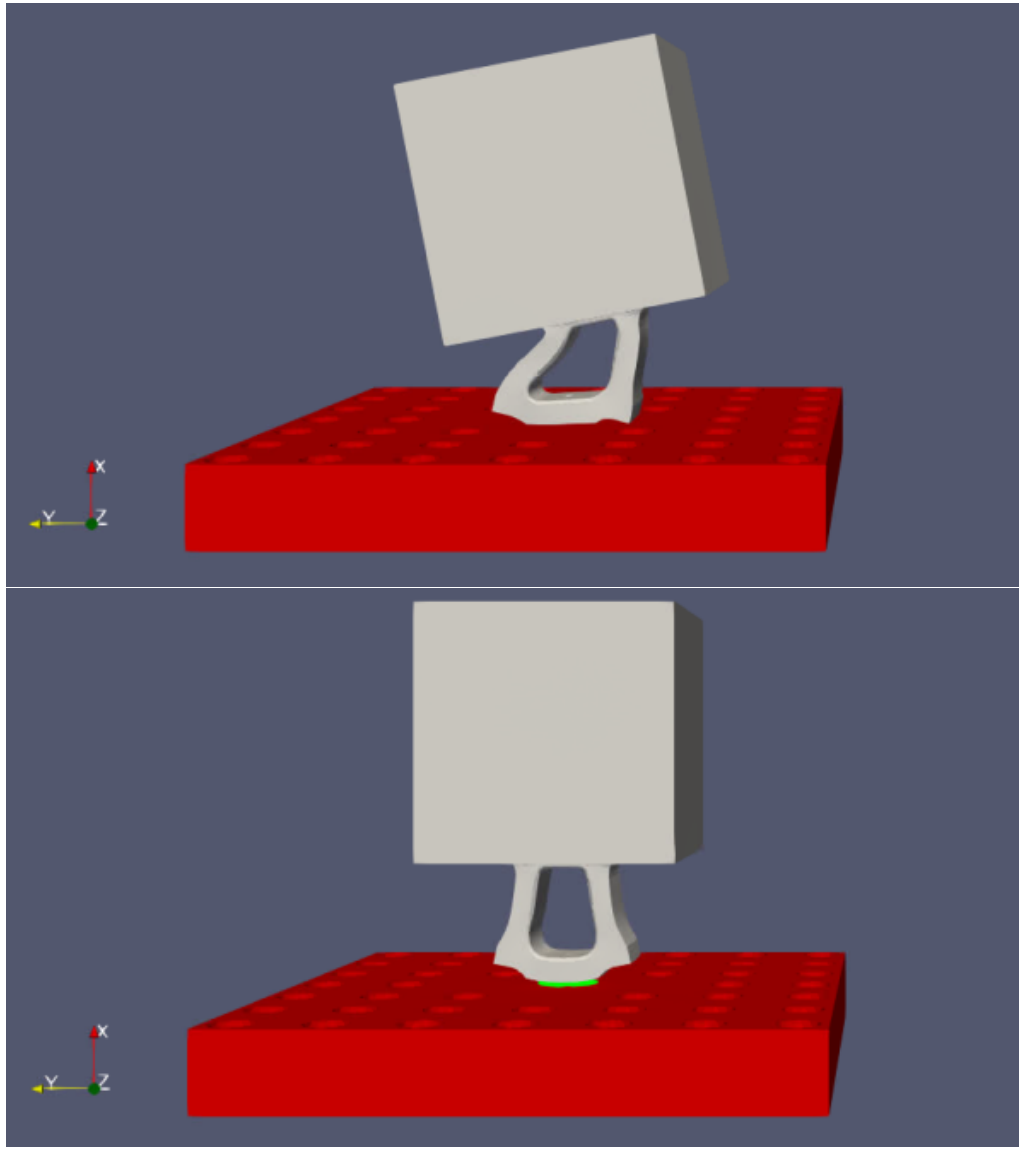

Fig 39a-b. Axial and 2nd bending in Y mode shapes

Iwan Spring Theory

- An Iwan spring consists of multiple Jenkins sliders (i.e., frictional sliders with springs) attached in parallel
- A typical hysteretic cycle for an Iwan spring is shown below

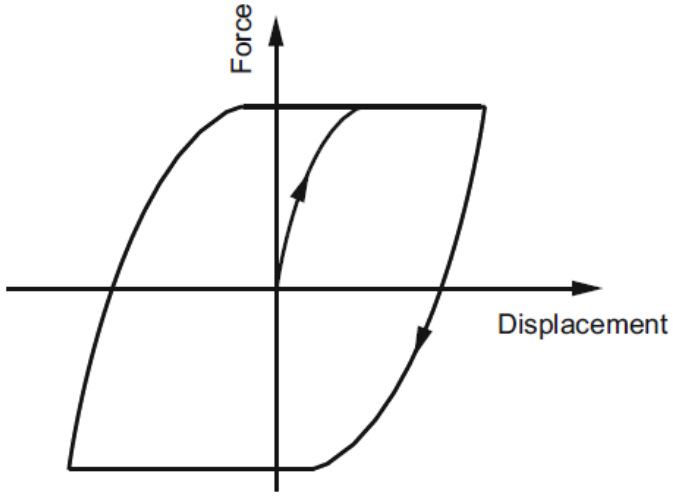

Fig #. Iwan Spring Hysteretic Cycle

$$F_{IWAN} = \frac{F_S(\chi+1)}{\phi_{MAX}^{\chi+2}\left(\beta+\frac{\chi+1}{\chi+2}\right)}\left(\left(\frac{1}{\chi+2}-\frac{1}{\chi+1}\right)u^{\chi+2}+\frac{\phi_{MAX}^{\chi+1}}{\chi+1}u\right)+\frac{F_s}{\phi_{MAX}}\frac{\beta}{\beta+\frac{\chi+1}{\chi+2}}\Gamma(u,\phi_{MAX}) \quad \text{Eqn. 11}$$

$$\Gamma(u,\phi)=\begin{cases} u & u<\phi \\ \phi & u\geq\phi \end{cases} \quad \text{Eqn. 12}$$

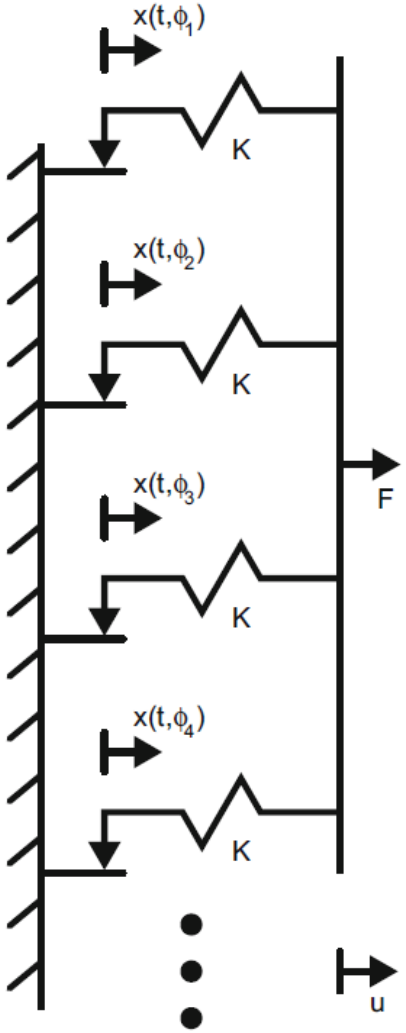

Fig 40. Iwan Spring Schematic

Nonlinear Model Updating

- A nonlinear optimizer was used to tune Iwan parameters within MATLAB
- Poor agreement with damping of axial mode
  - Physics of systems cannot be captured by Iwan spring

Table 6. Tuned Iwan Parameters

Linear-X	0.004889 lbf	26672231 lb/in	0.1858	3.4742
Rot-Z	3.2581e-5 lbf	12485674 lb/in	0.2194	0.01434

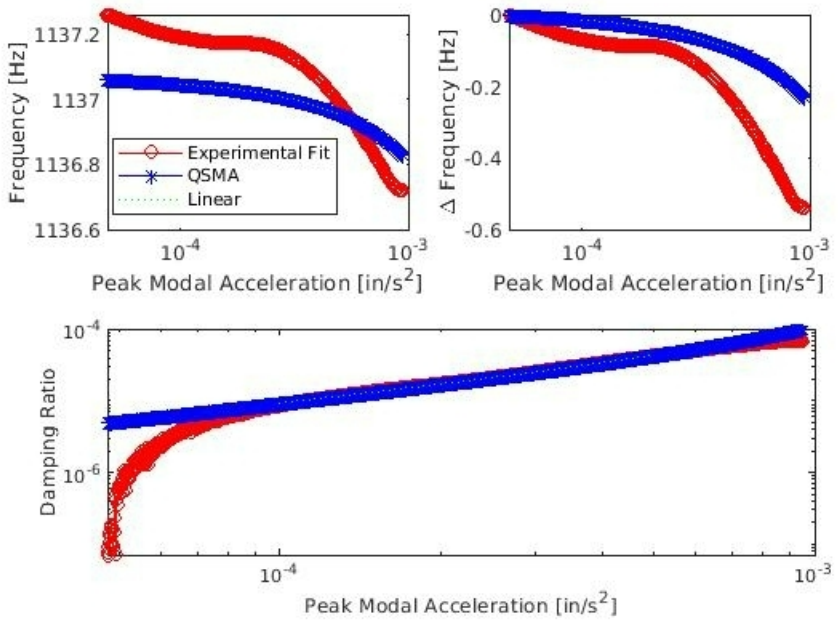

Fig 41. Iwan Spring Tuning for Second Bending Mode

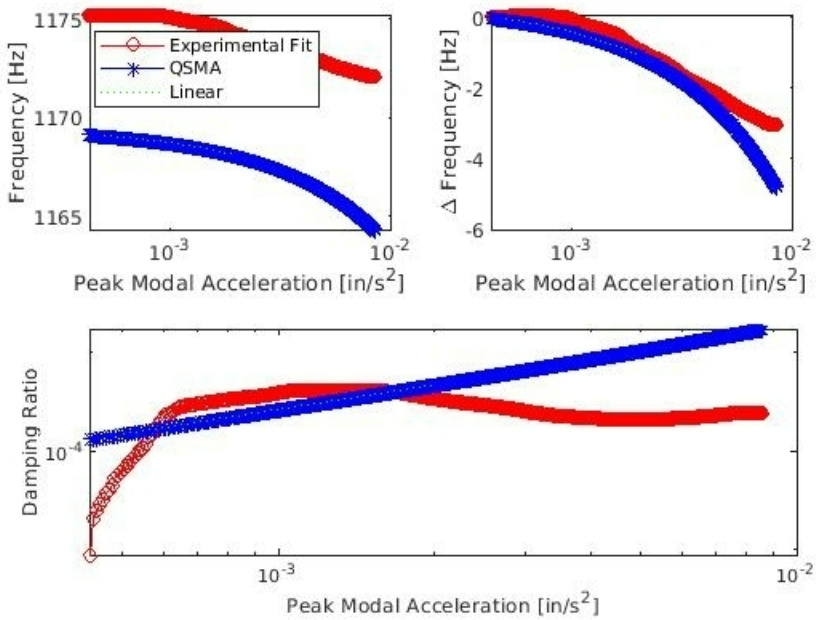

Fig 42. Iwan Spring Tuning for Axial Mode

Potential Constitutive Model and Physical Mechanisms

- A number of physical mechanisms and models have been proposed to explain the behavior of the joint in question:
  1. Constitutive model which assumes linear damping of joint but nonlinear stiffness dependent on integral average of linear stiffness at a given bolt force and loading amplitude
     - Affect of reduced contact area on material damping
  2. Modal coupling through Poisson's effect
  3. Multiple Asperity Contact
  4. Asymmetry of contact pressure distribution
  5. Mix of the aforementioned effects (1-4)

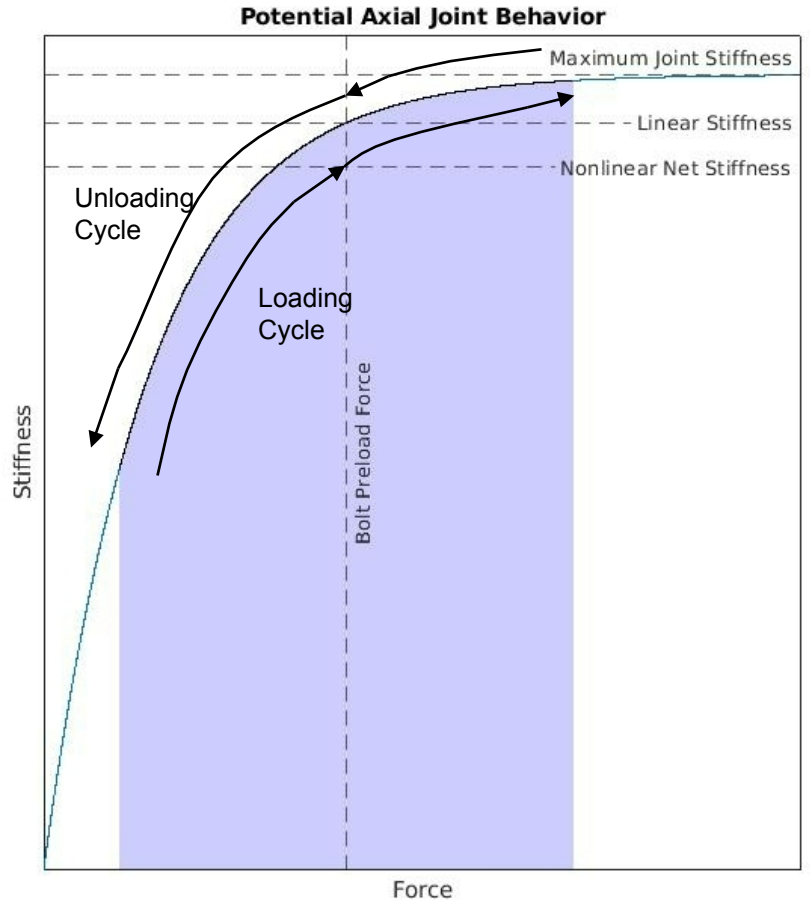

Fig 43. Potential Constitutive Model for Axial Mode

Conclusions and Future Work

Conclusions

- QSMA can be an effective method for quantifying modal coupling
- Additional research and work will be required to understand how to modally filter data well when there is modal coupling and tightly spaced mode shapes
- Additional research and work will be required in order to effectively model axial modes in joints

Future Work:

- Explore different constitutive models and physical mechanisms
- Explore application of ML to joint modeling
- Mode shape shifting with higher force levels

Appendix

* don’t need to make this an official appendix section until after this goes through R&A

Nonlinear Damping And Frequency

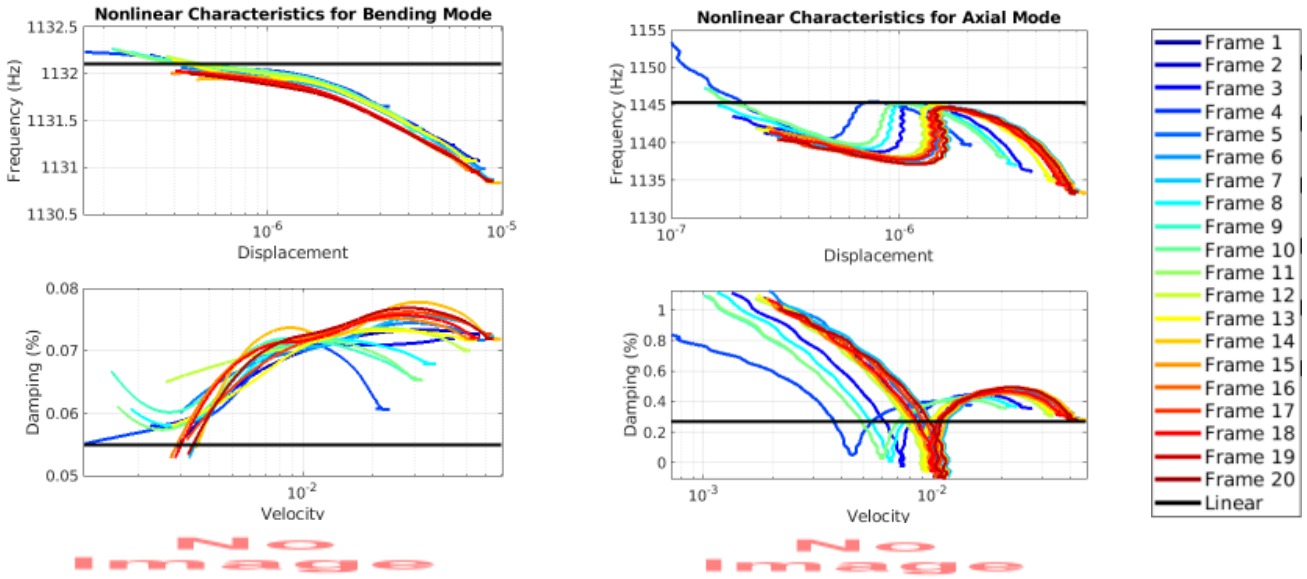

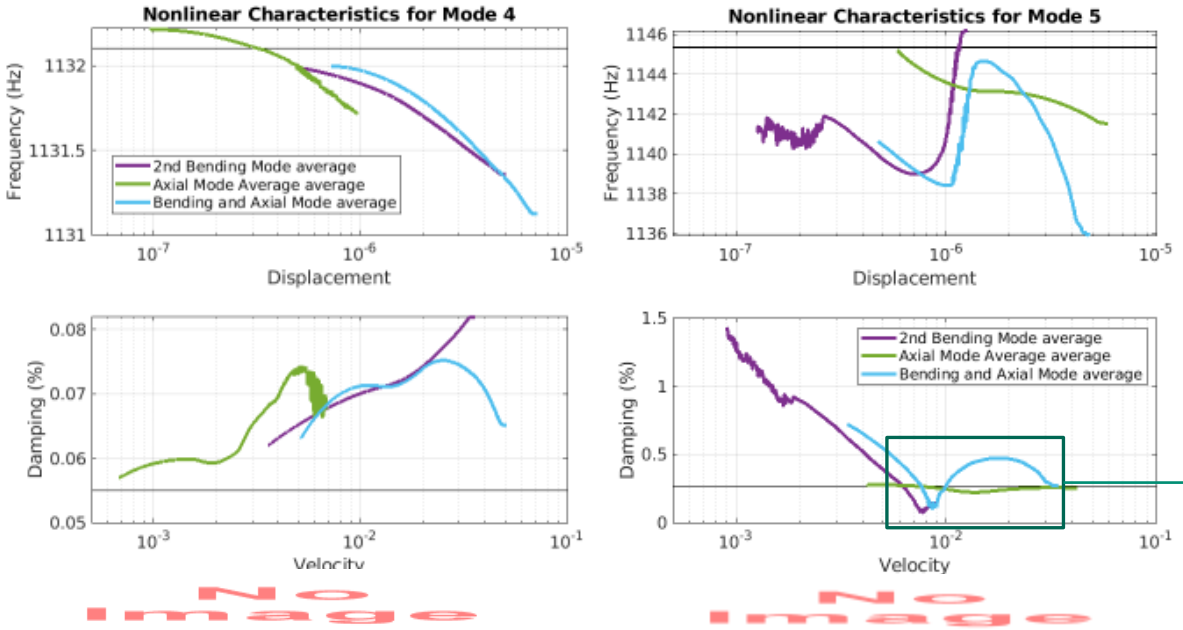

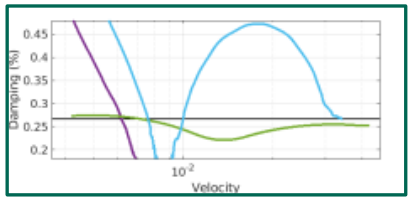

- Behavior for the axial mode is non-monotonic, which presents issues when using Iwan elements to model this system
- With a reasonable bandpass filter, significant noise exists in data for the axial mode

- Behavior of axial mode changes drastically when excited with bending mode vs. when excited alone
- Suggests that the bending mode is still captured in this response

Modal Filtering - FRFs

- Influence of the 2nd Bending mode is still present in the FRF for the axial model – there are two peaks!
  - Modes also increased in separation
- This indicates that modal coupling is occurring between the Bending mode in y and Axial mode in x

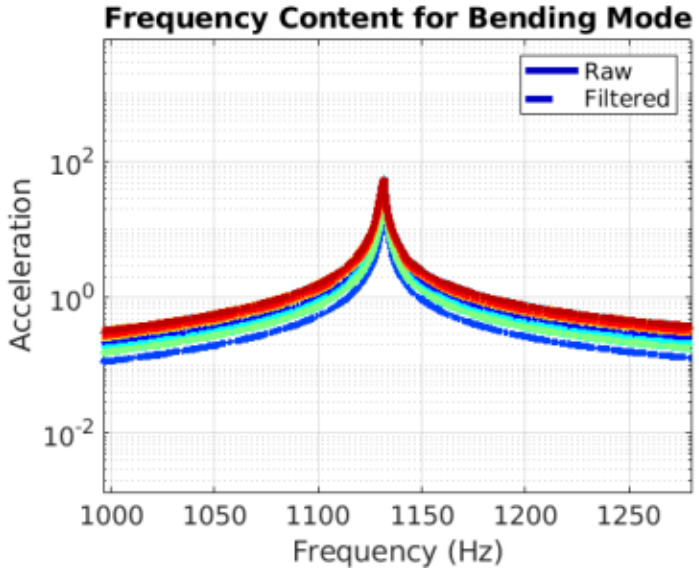

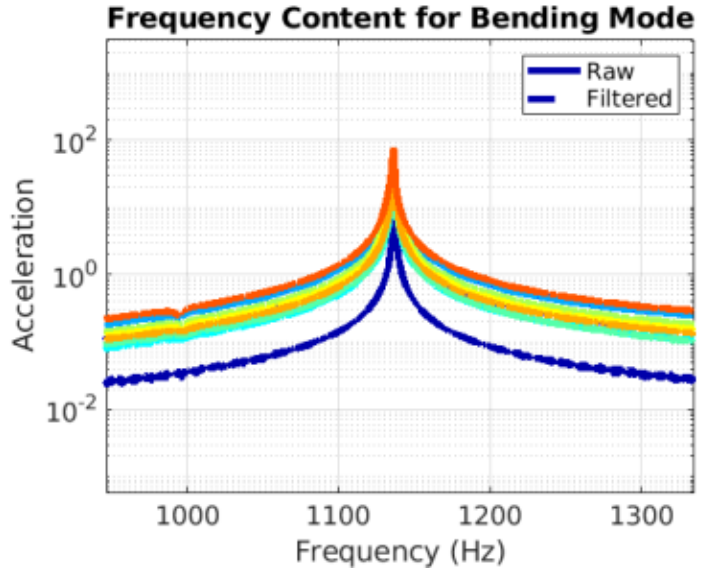

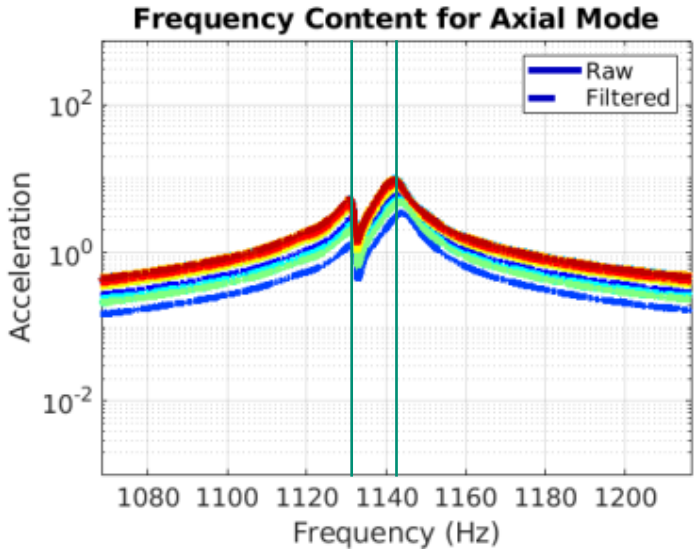

FRFs of response from original structure

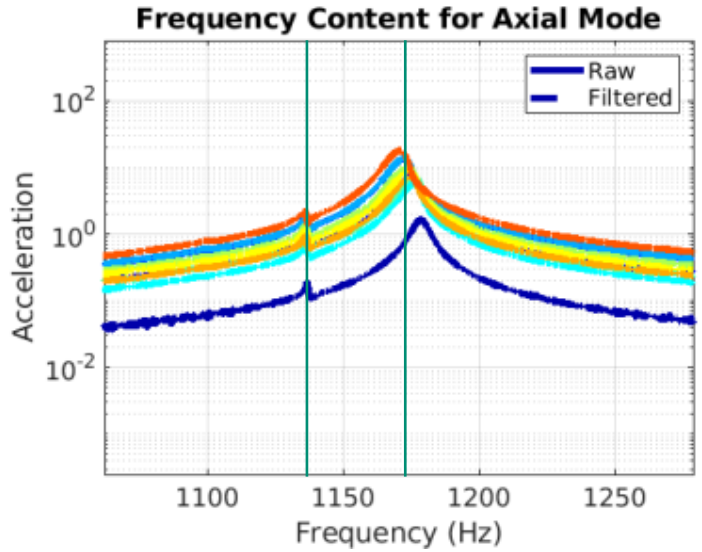

FRFs of response from rotated structure

Acknowledgements

This research was conducted at the 2021 Nonlinear Mechanics and Dynamics Research Institute hosted by Sandia National Laboratories and the University of New Mexico.

Sandia National Laboratories is a multimission laboratory managed and operated by National Technology and Engineering Solutions of Sandia, LLC, a wholly owned subsidiary of Honeywell International, Inc., for the U.S. Department of Energy's National Nuclear Security Administration under contract DE-NA-0003525.

Empirical Model of Puncture Energy for Metals

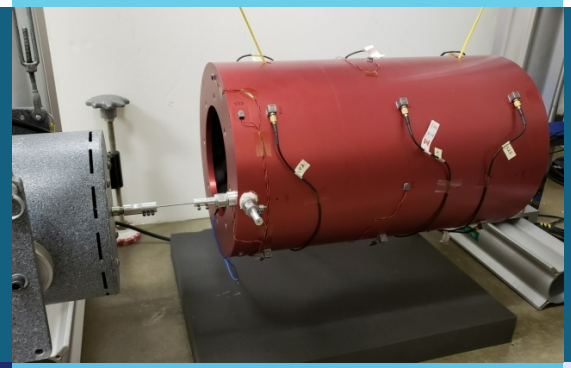

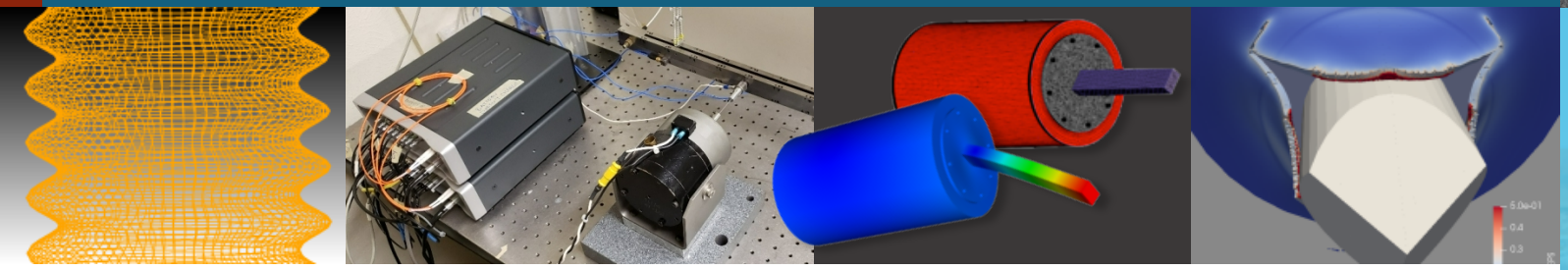

Students:

J. Albelo-Cortes (UTD), L. Alqawasmi (UNM), J. Jacobowitz (CU)

Mentors:

N. Hubbard, Dr. R. Kuether, Dr. T. Khraishi (UNM)

Sandia National Laboratories is a multimission laboratory managed and operated by National Technology & Engineering Solutions of Sandia, LLC, a wholly owned subsidiary of Honeywell International Inc., for the U.S. Department of Energy's National Nuclear Security Administration under contract DE-NA0003525.

Motivation and Background

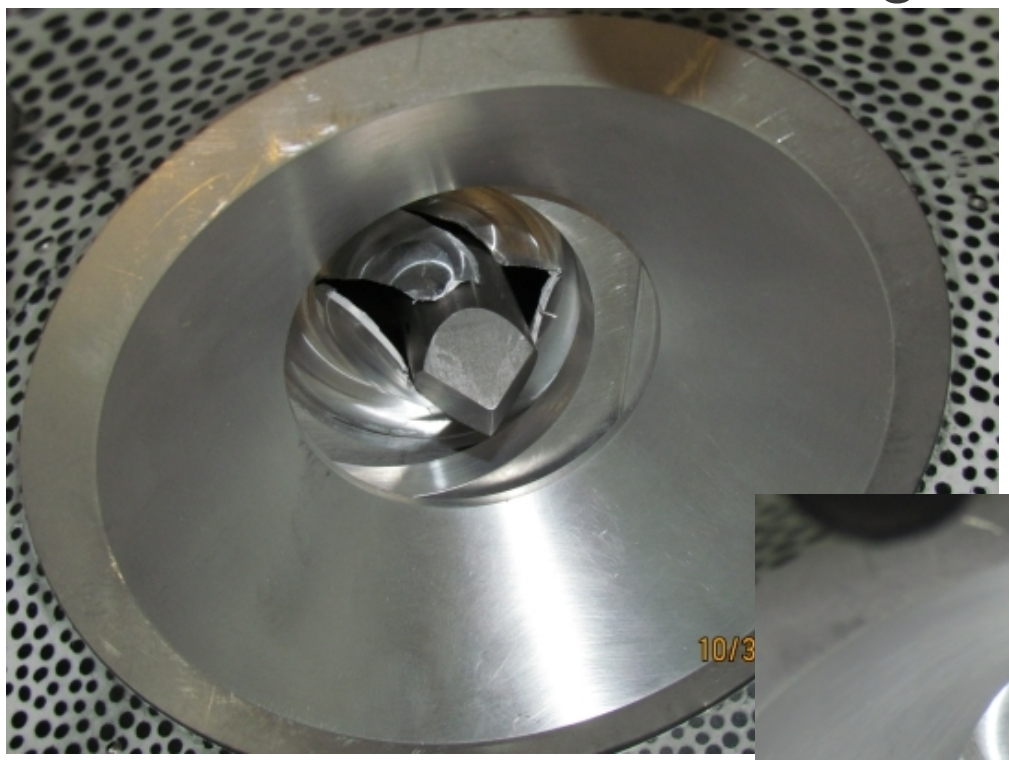

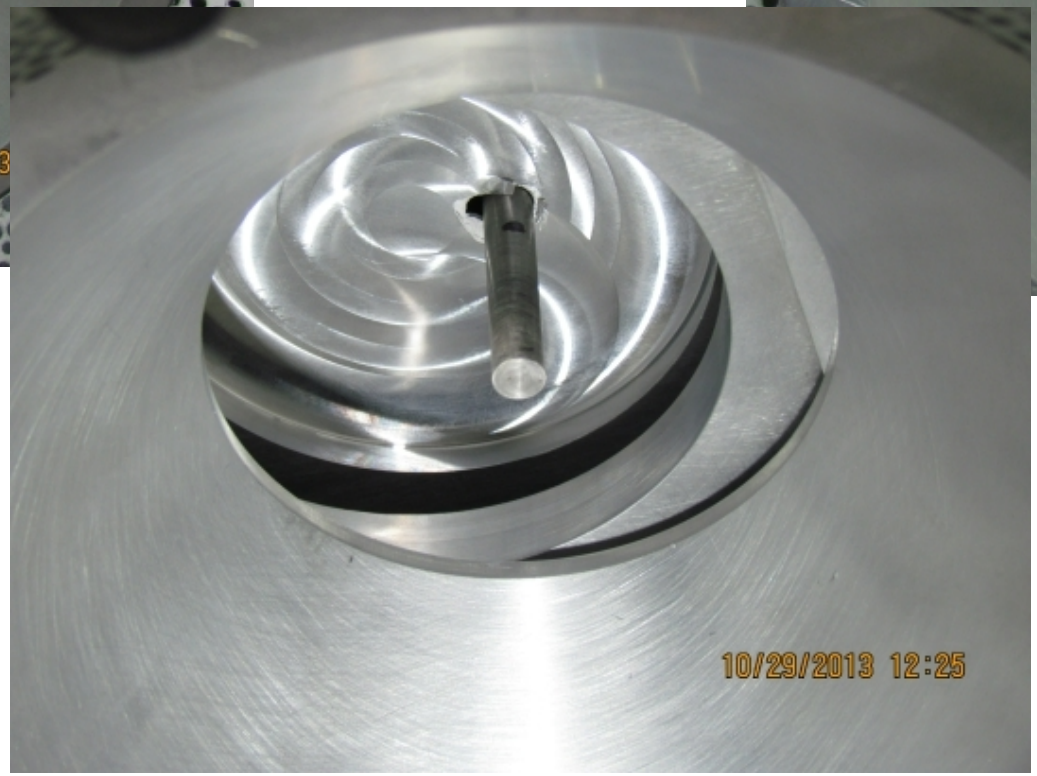

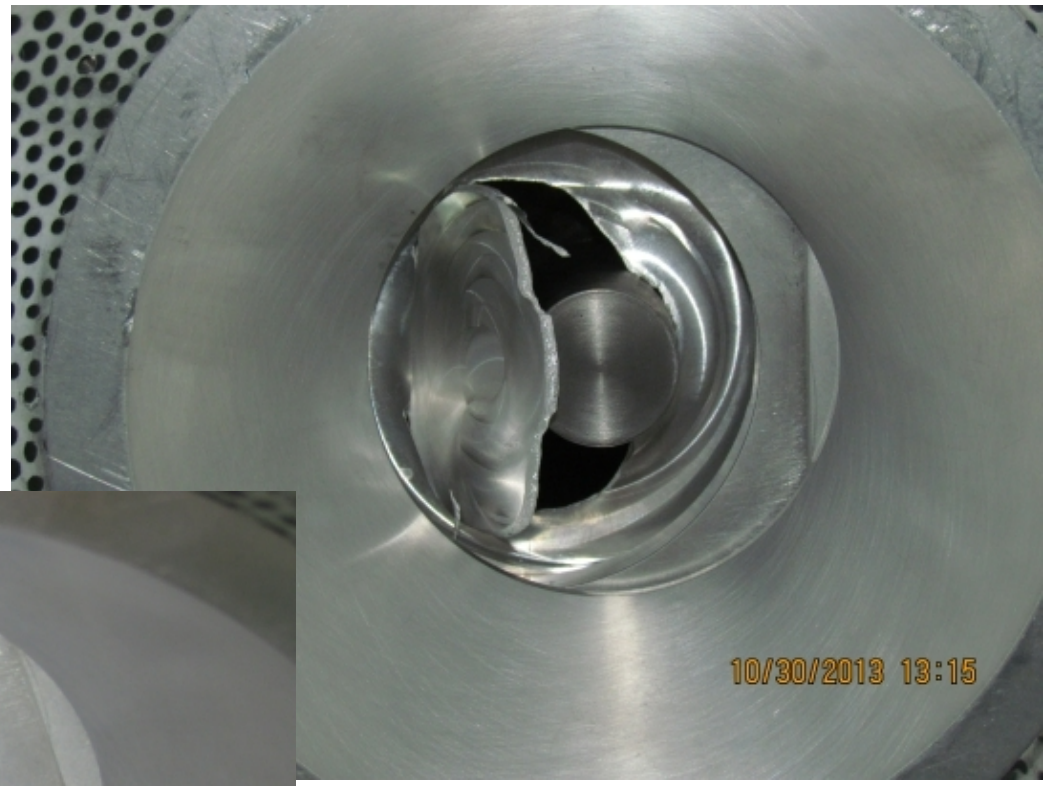

Multiple Probe Shapes and Coupon Thickness & Materials were Simulated

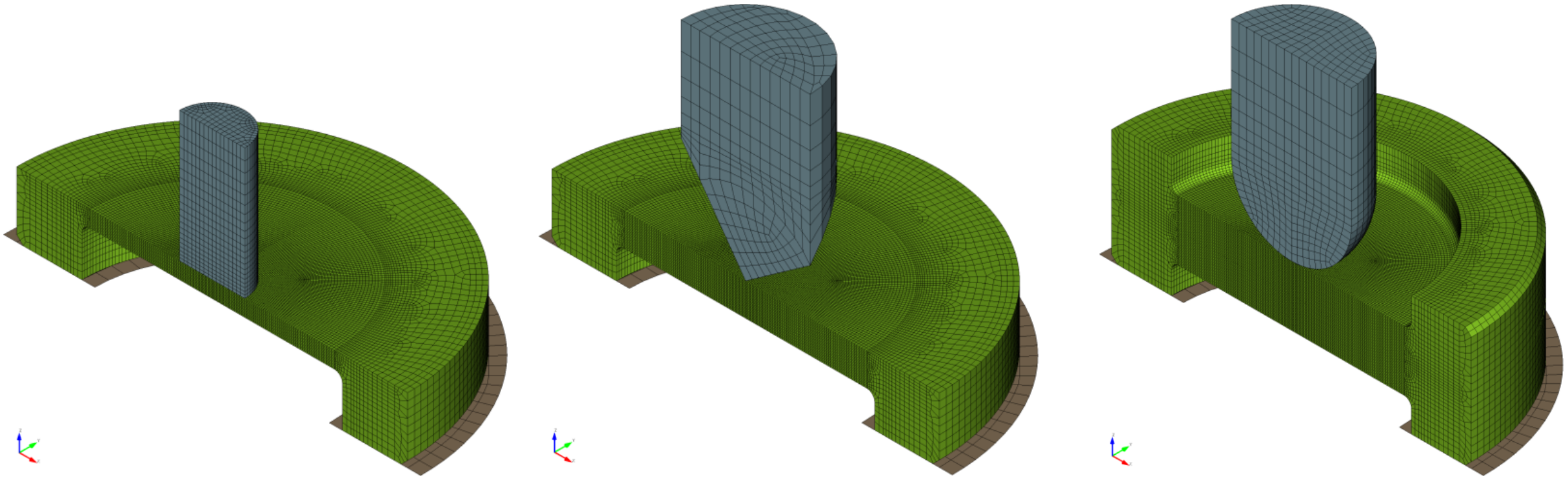

Flat : 0.25in Probe Through 0.125in 7075 Al

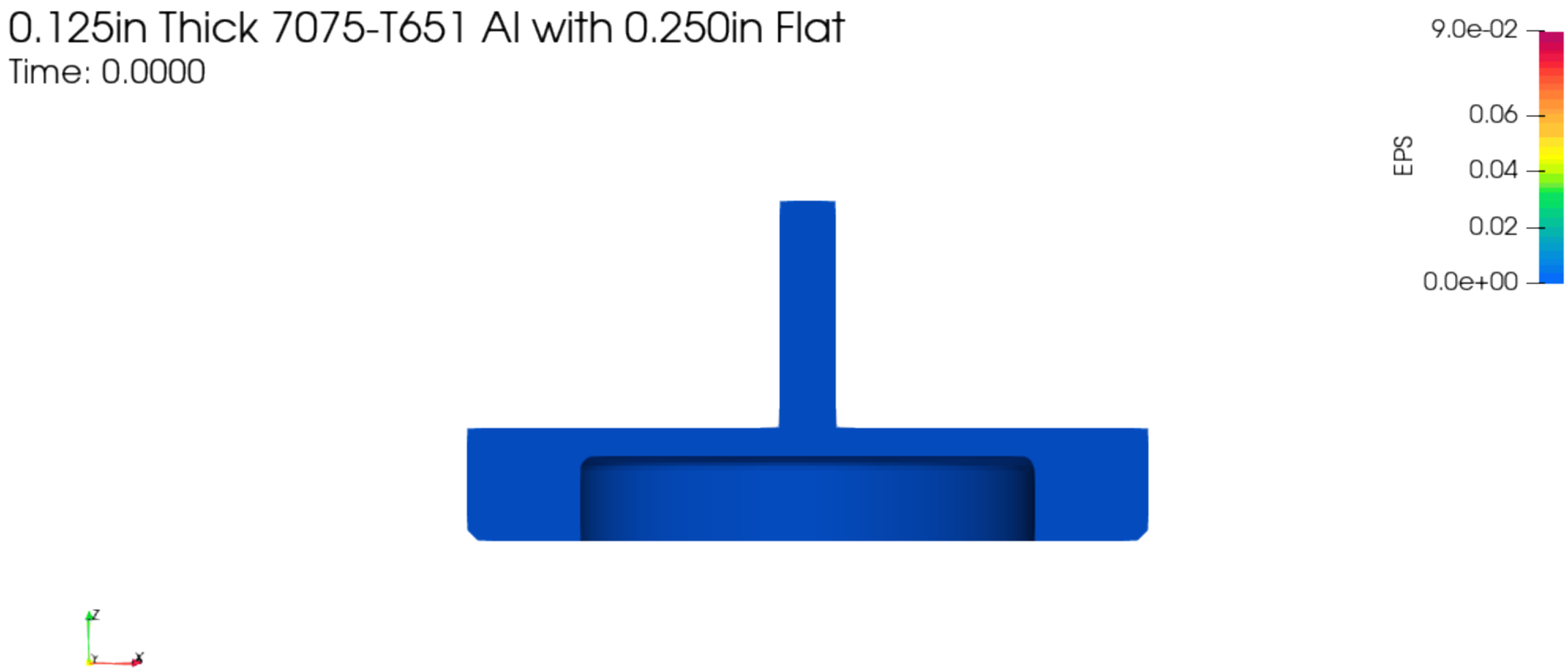

Corner : 0.25in Probe Through 0.125in 7075 Al

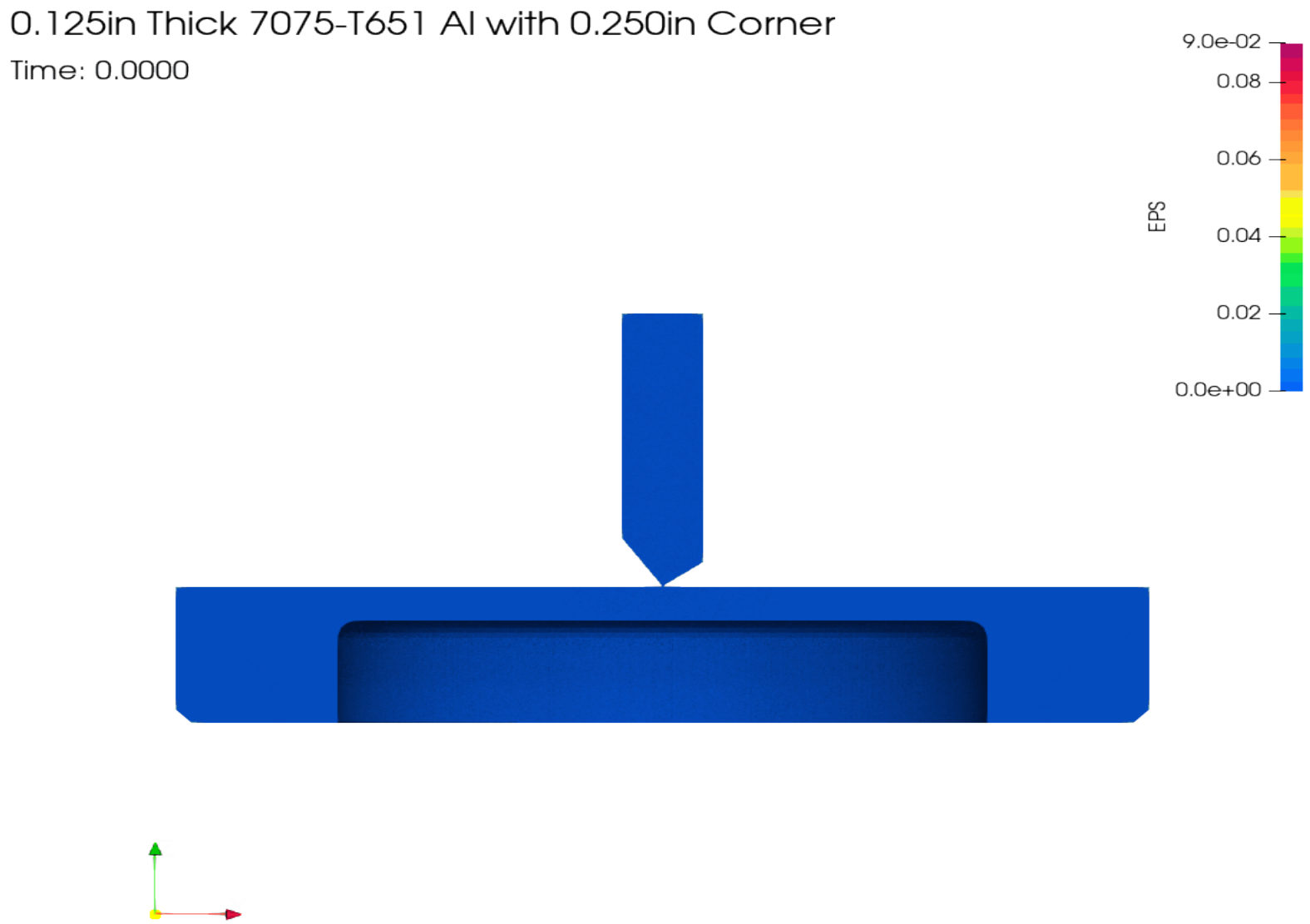

Hemisphere : 0.25in Probe Through 0.125in 7075 Al

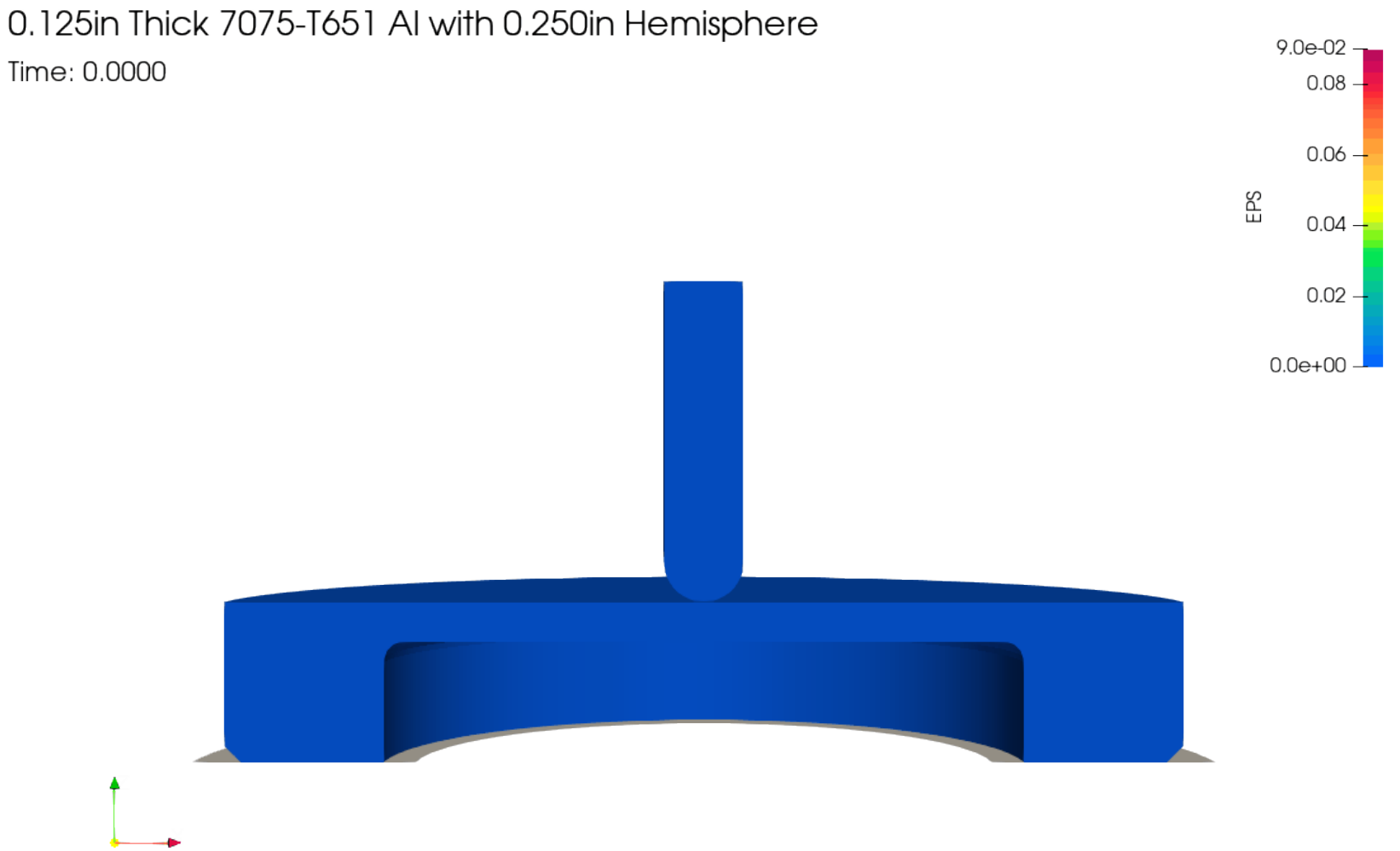

Flat : 0.50in Probe Through 0.50in 304L SS

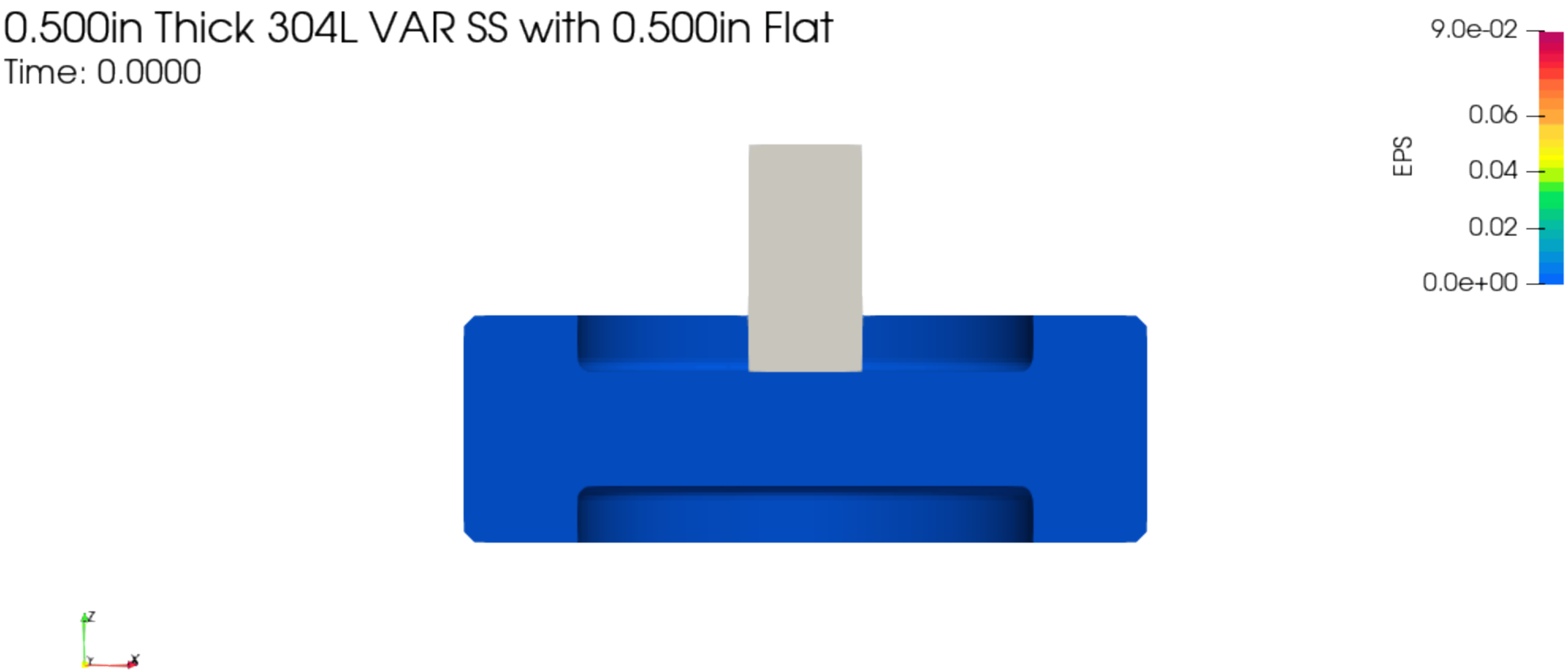

Note: The probe model was set to elastic and therefore does not show elastic plastic strain (EPS).

Corner : 0.50in Probe Through 0.50in 304L SS

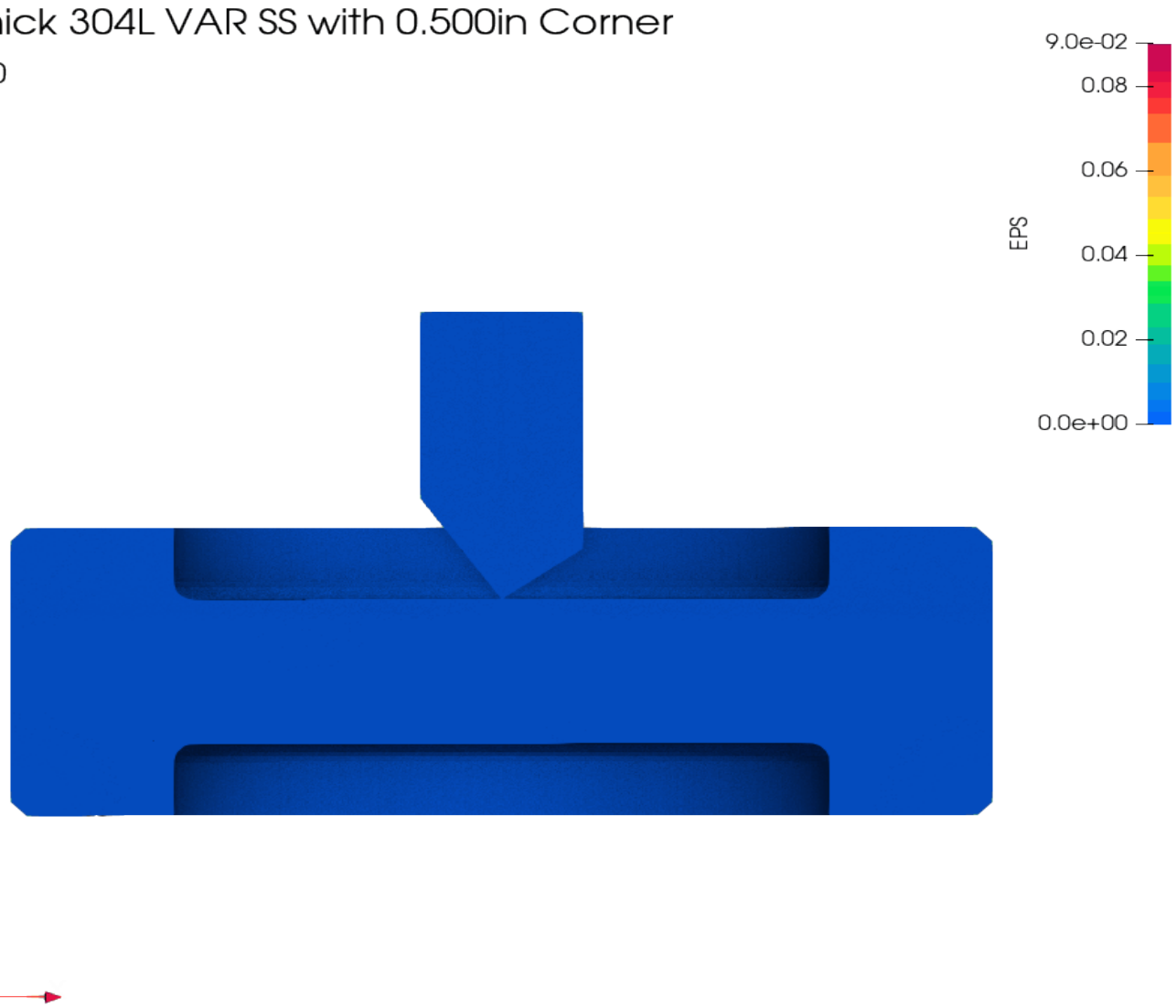

Hemisphere : 0.50in Probe Through 0.50in 304L SS

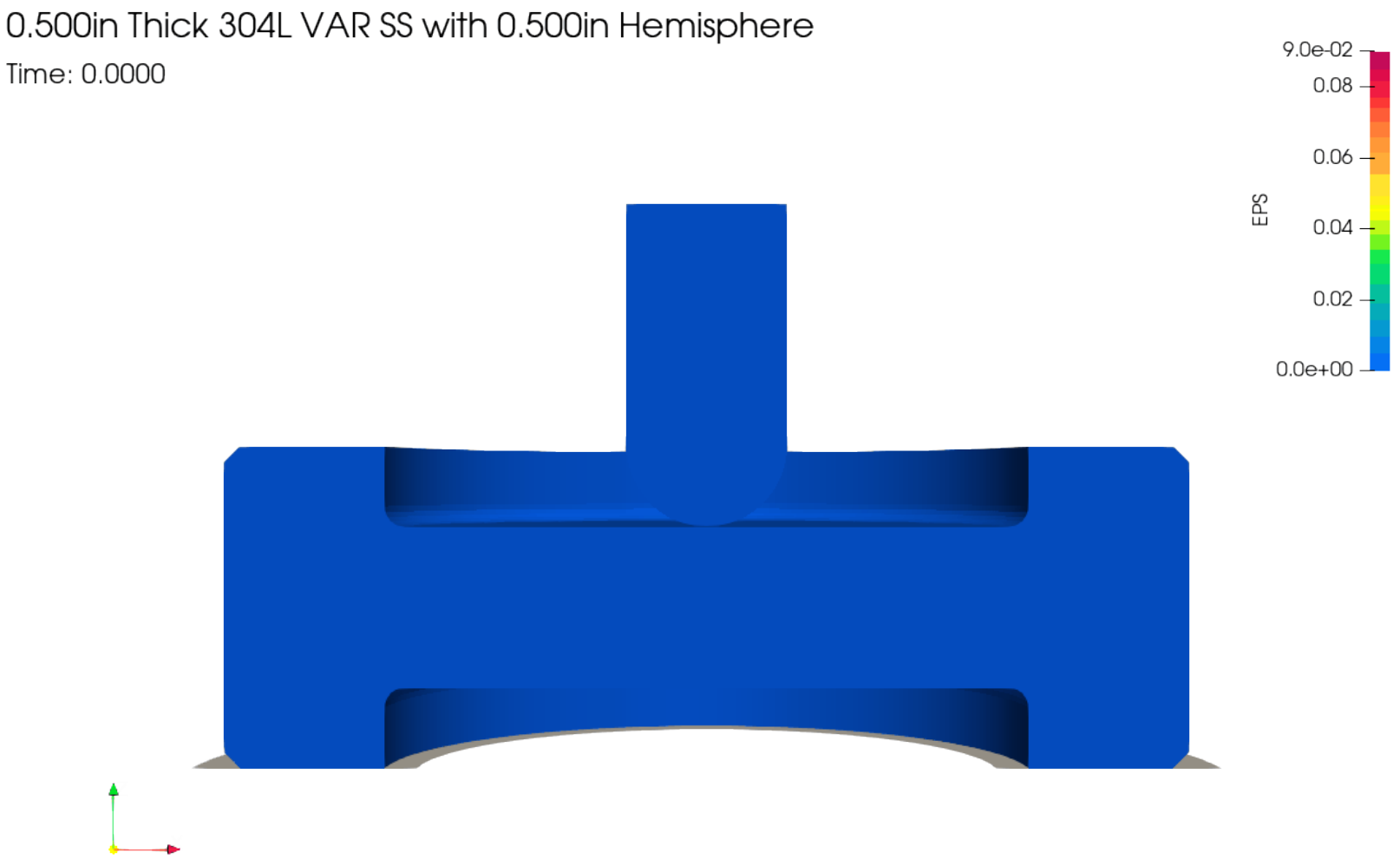

The 6061 Material Model Can Fail Easily

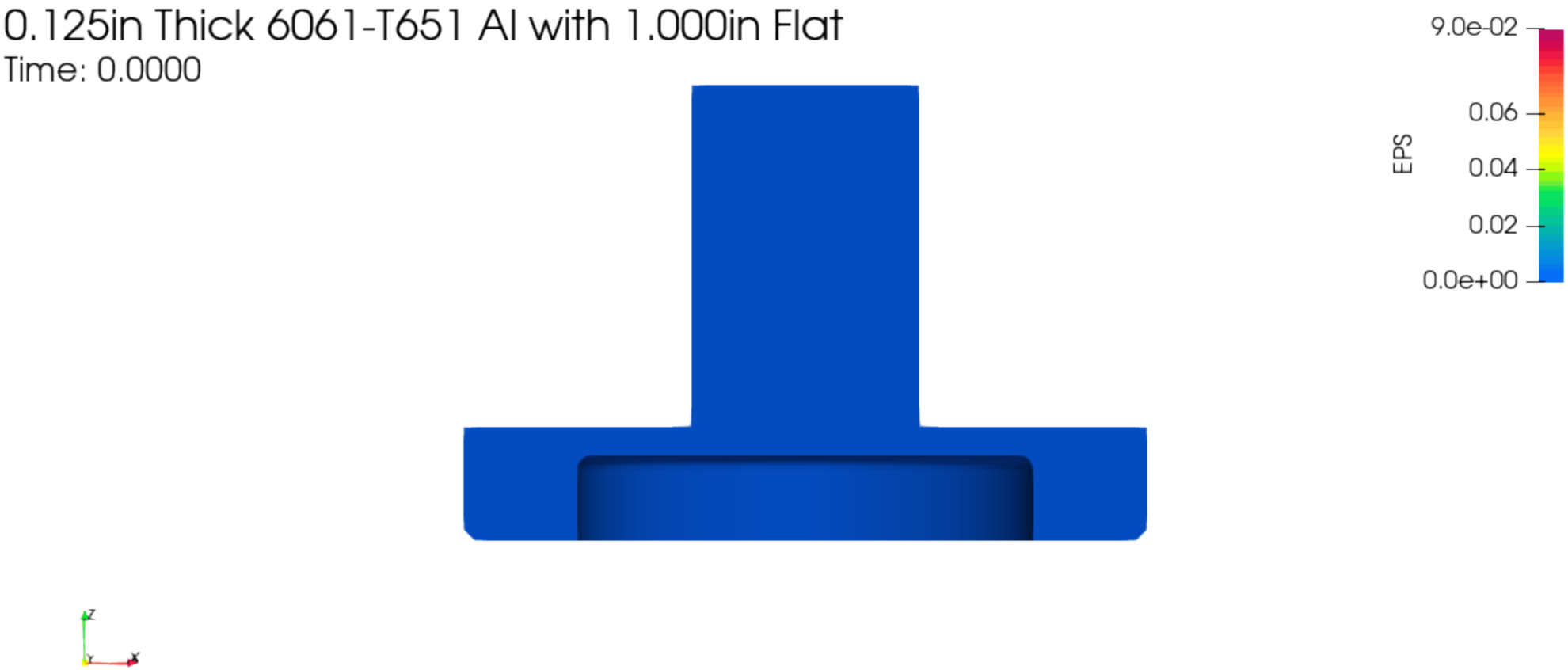

Probe Unique Aspects

- Flat : localizes stress at the circumference of the contact area
- Corner : acts like a wedge, cutting and spreading the coupon
- Hemispherical : the “smooth” probe shape induces the most plastic strain

Puncture Stages and Puncture Energy Determination

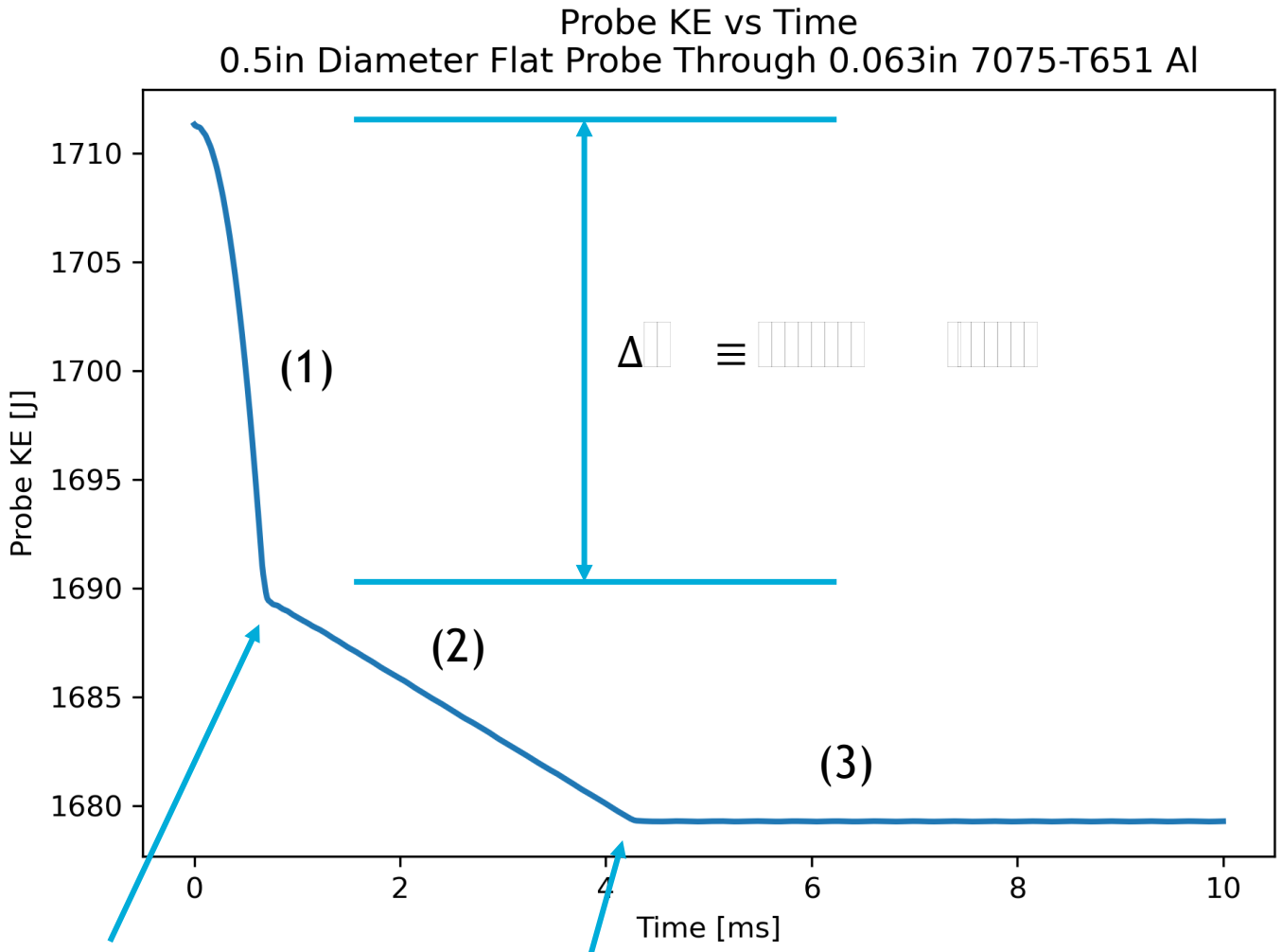

Stages of Puncture:

1. Probe contacts and deforms the coupon.
2. Probe scrapes the edge of the puncture hole.
3. Probe no longer in contact with the coupon.

Empirical Fit Equation by *Corona (2020)*

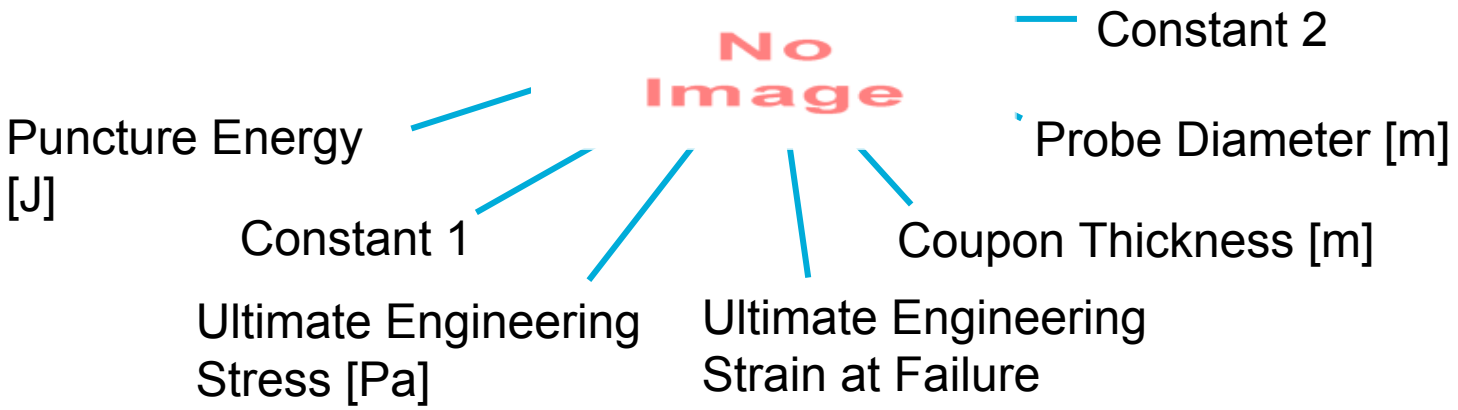

dimensionless energy = dimensionless geometry

Corona, E., “Empirical Formula for Puncture Energy of Flat Metal Plates by a Cylindrical Flat Punch,” Sandia National Laboratories, 6 November 2020.

Flat Probe Fit Using All Materials

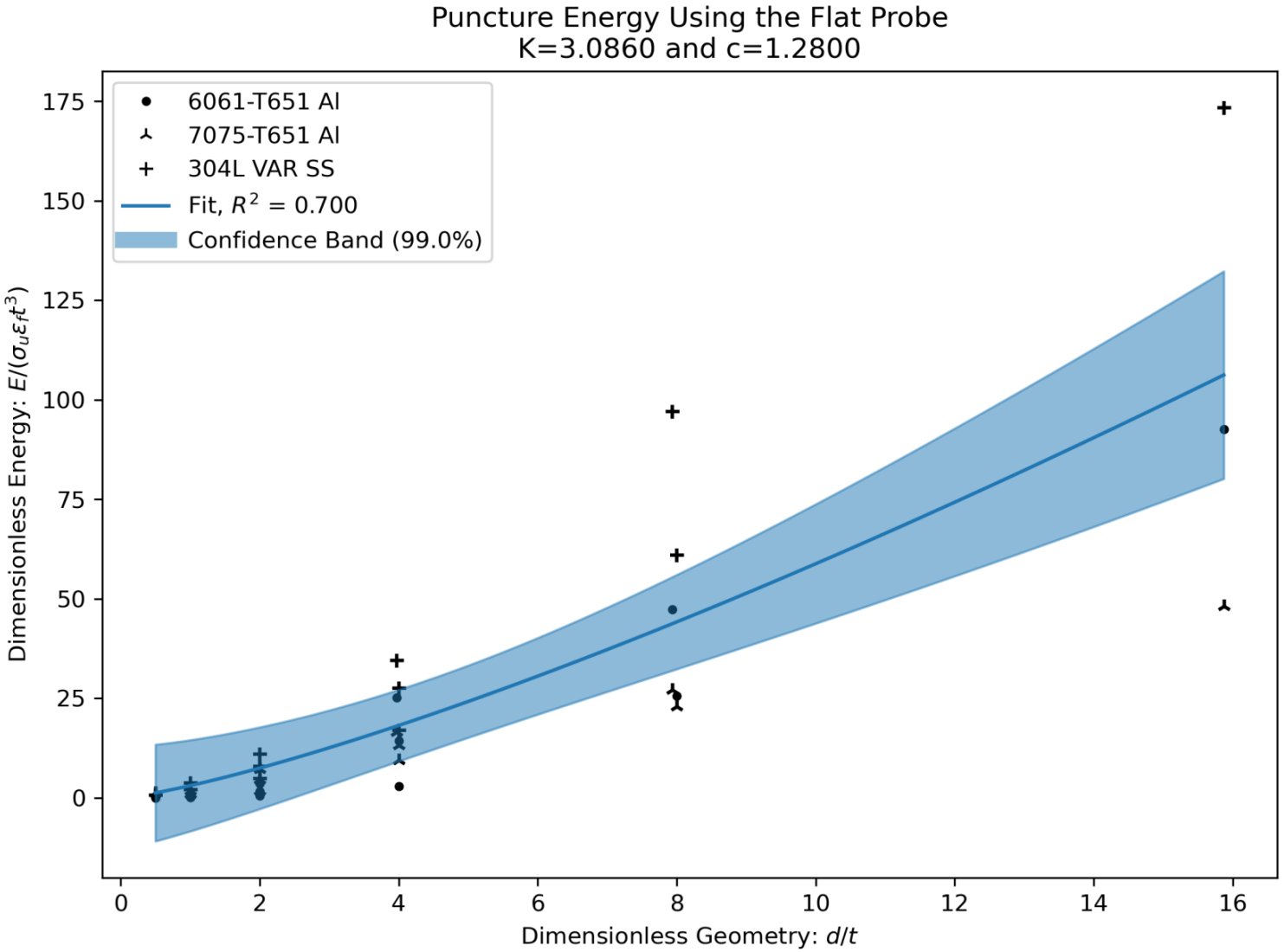

Flat Probe Fit Separating Materials

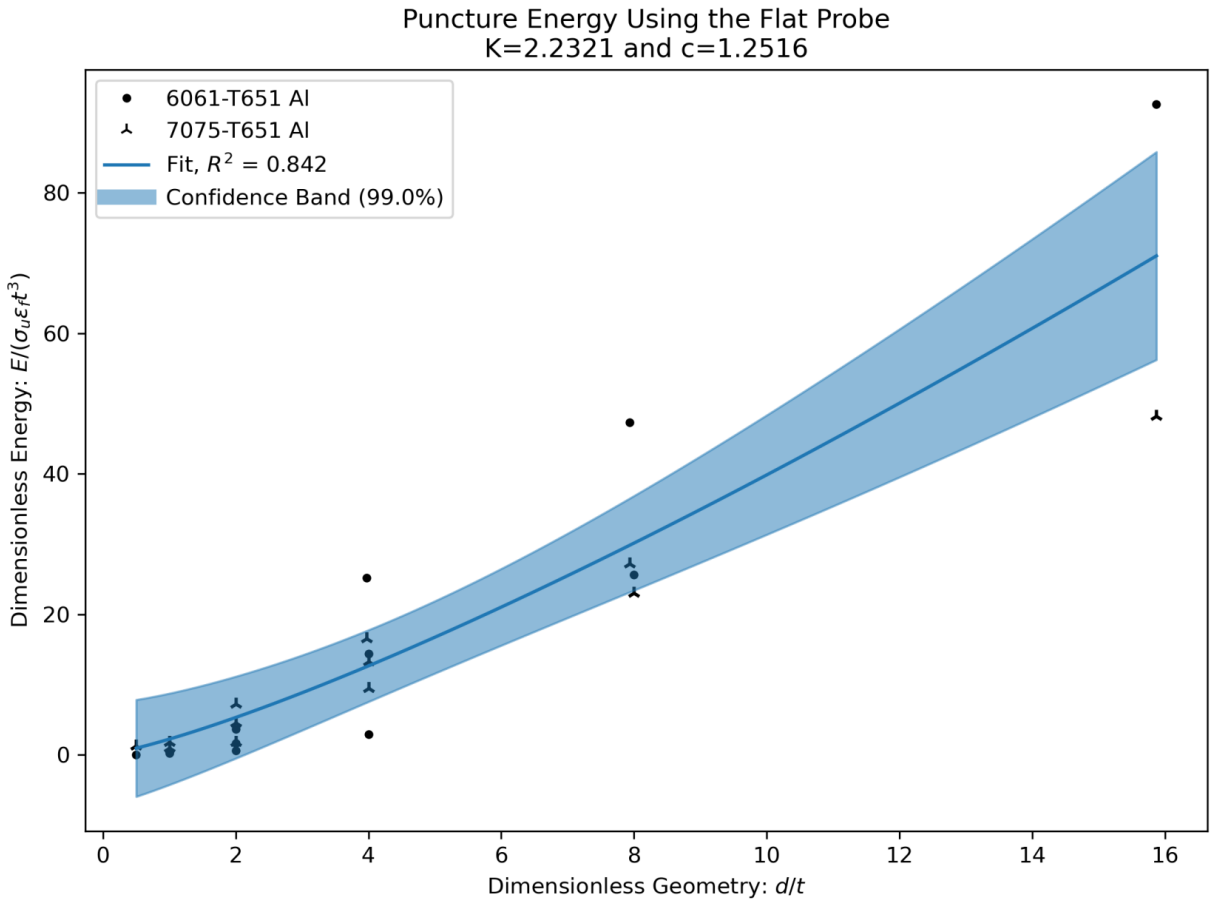

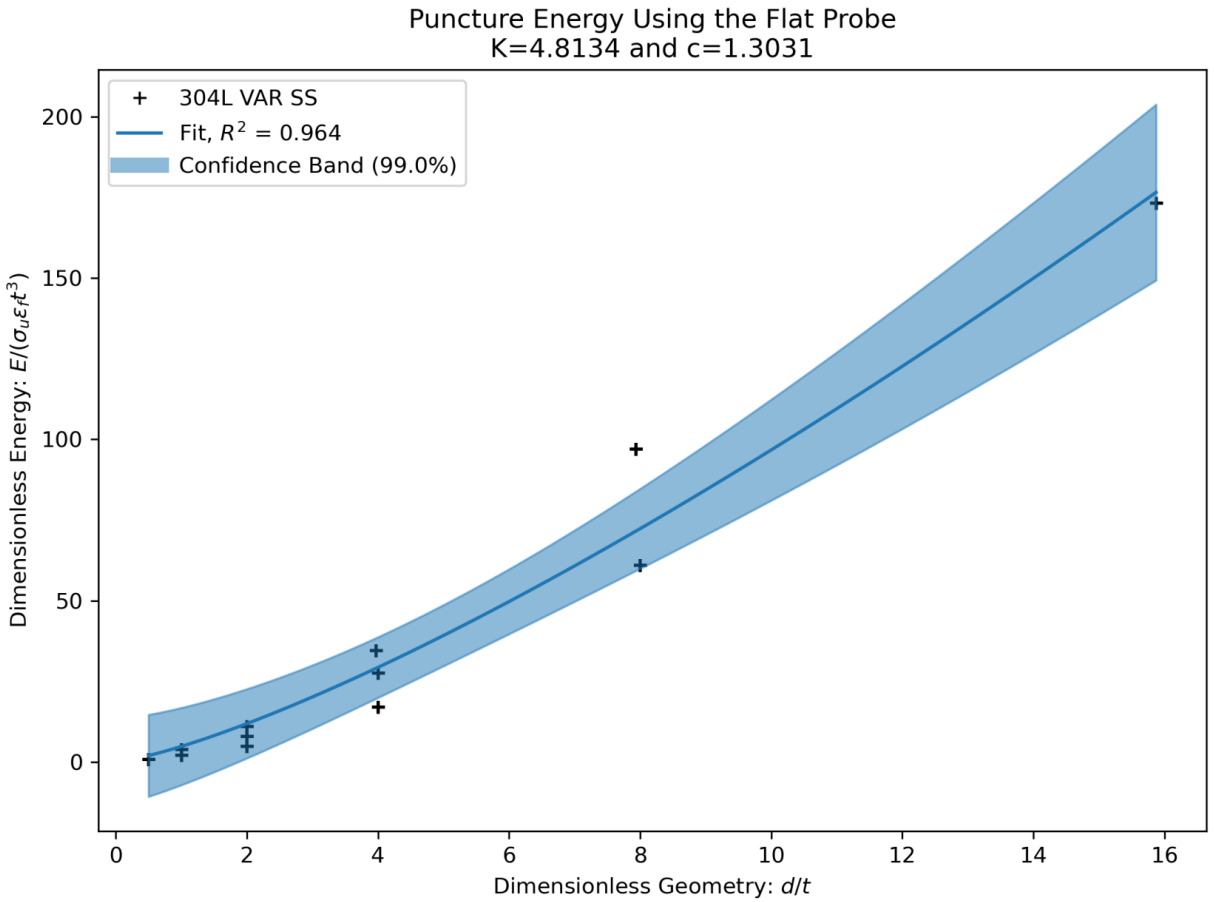

Corner Probe Fit Using All Materials

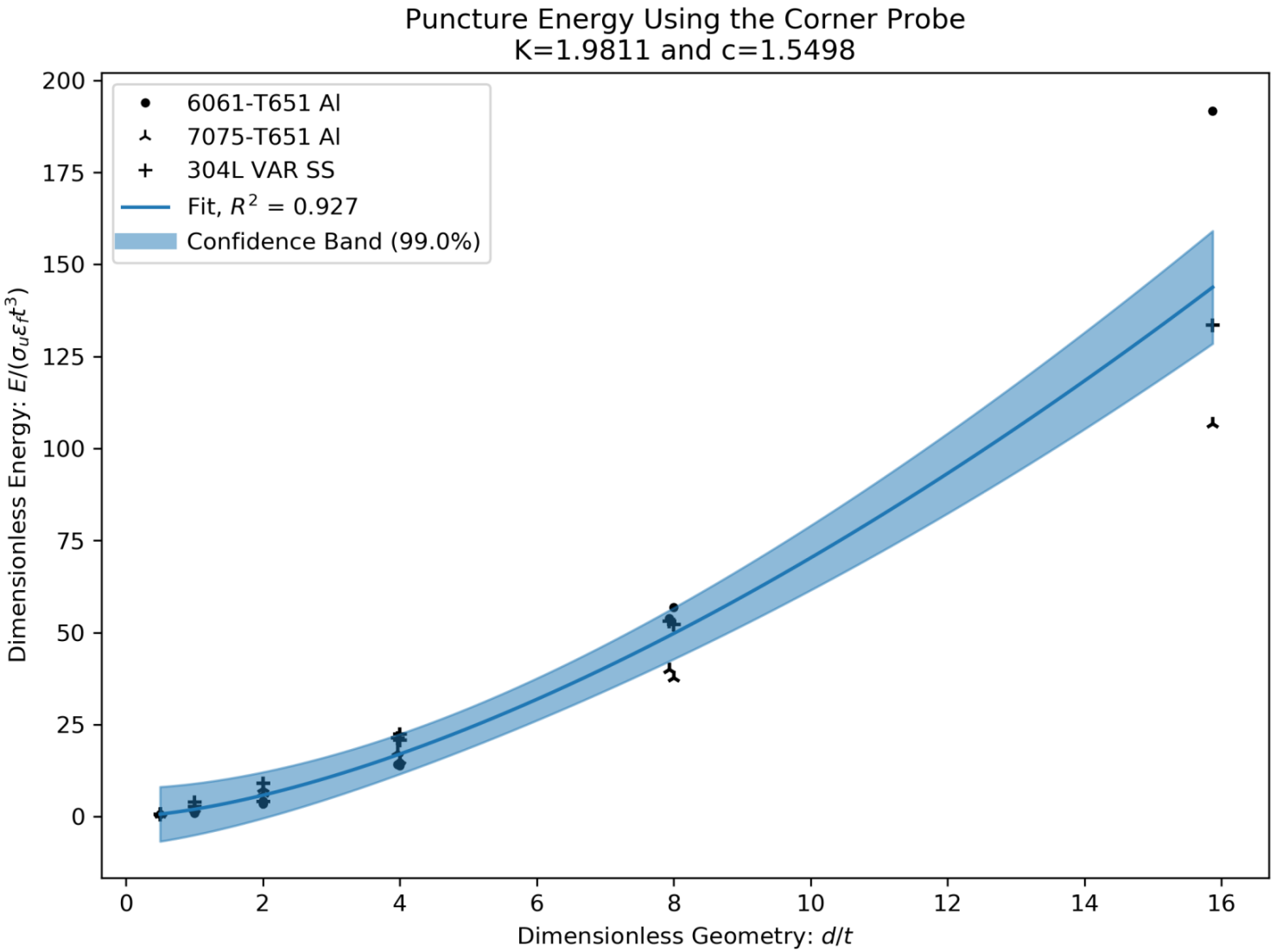

Corner Probe Fit Separating Materials

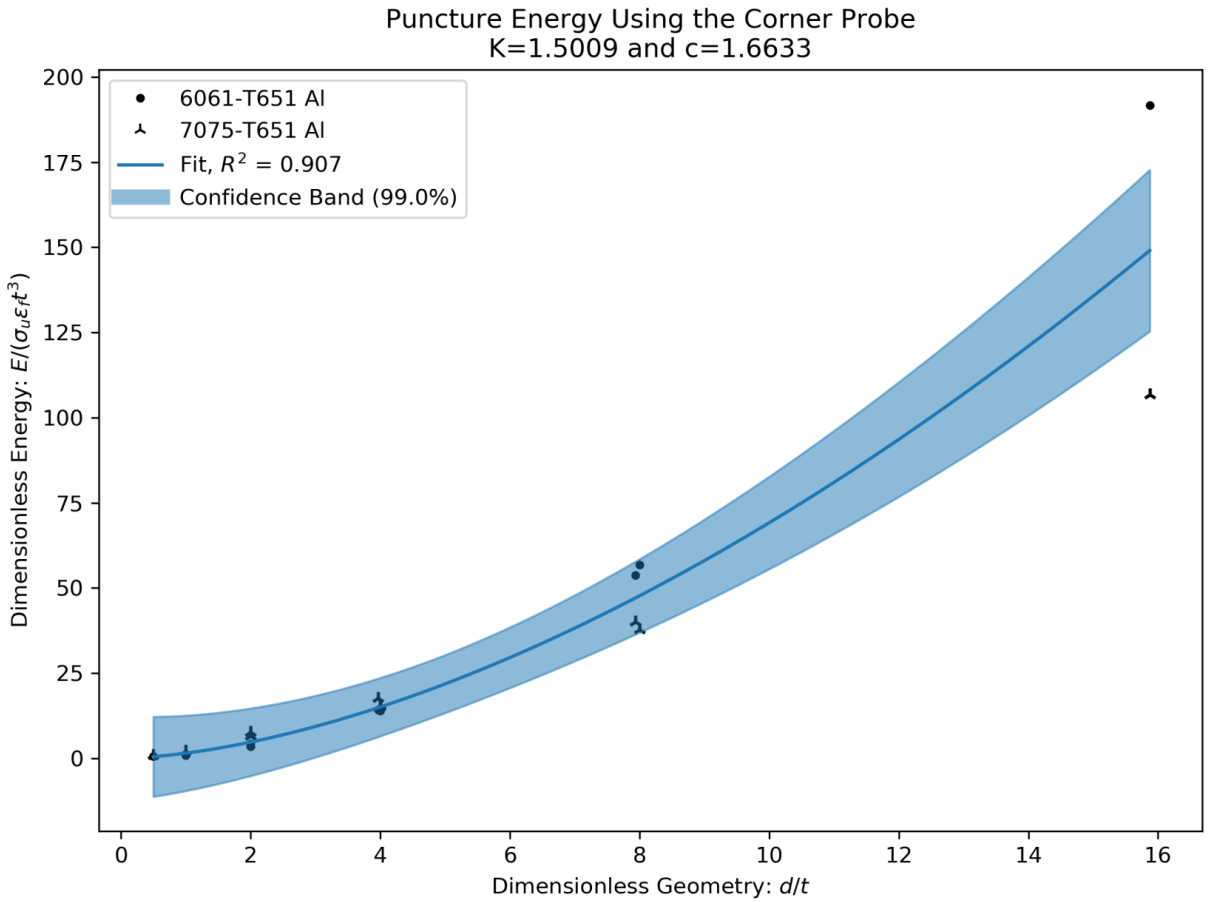

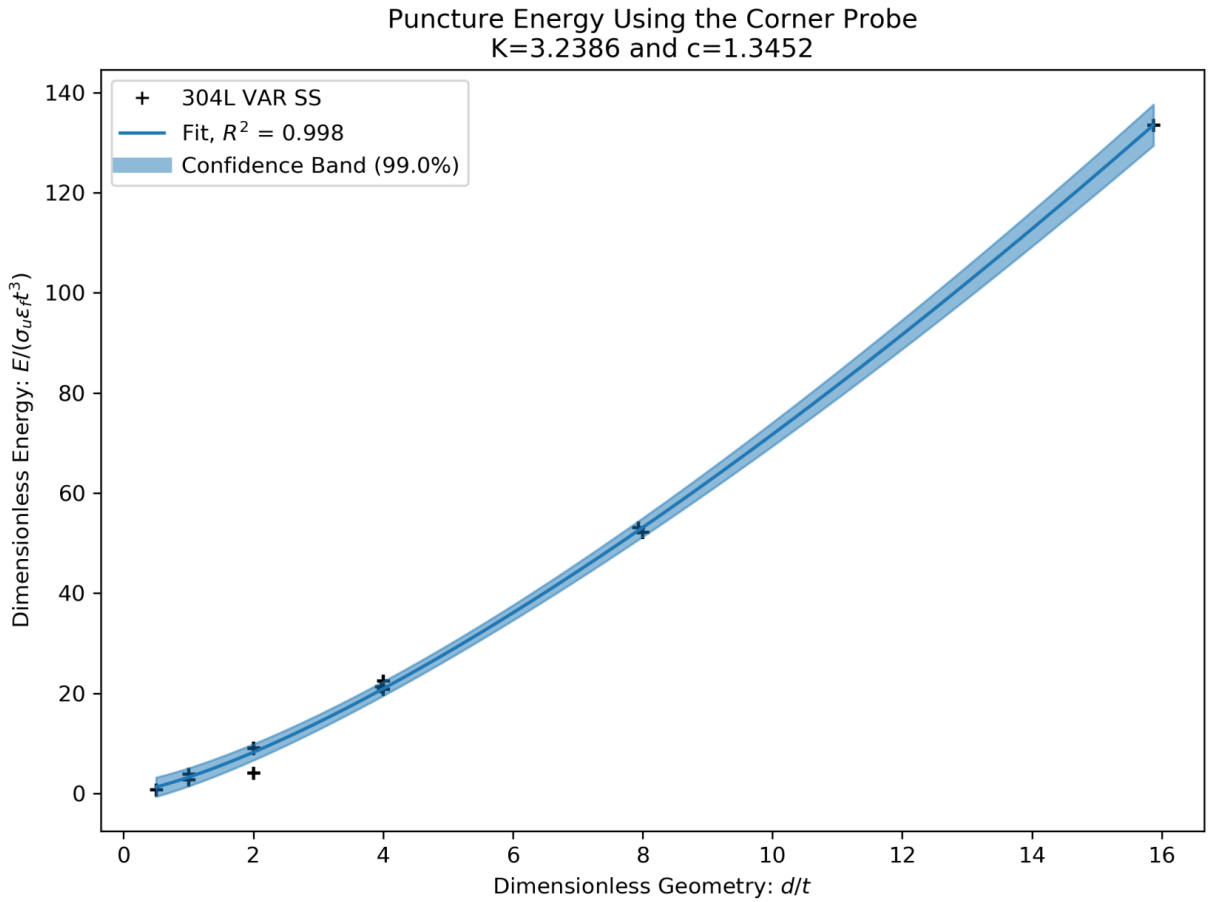

Hemisphere Probe Fit Using All Materials

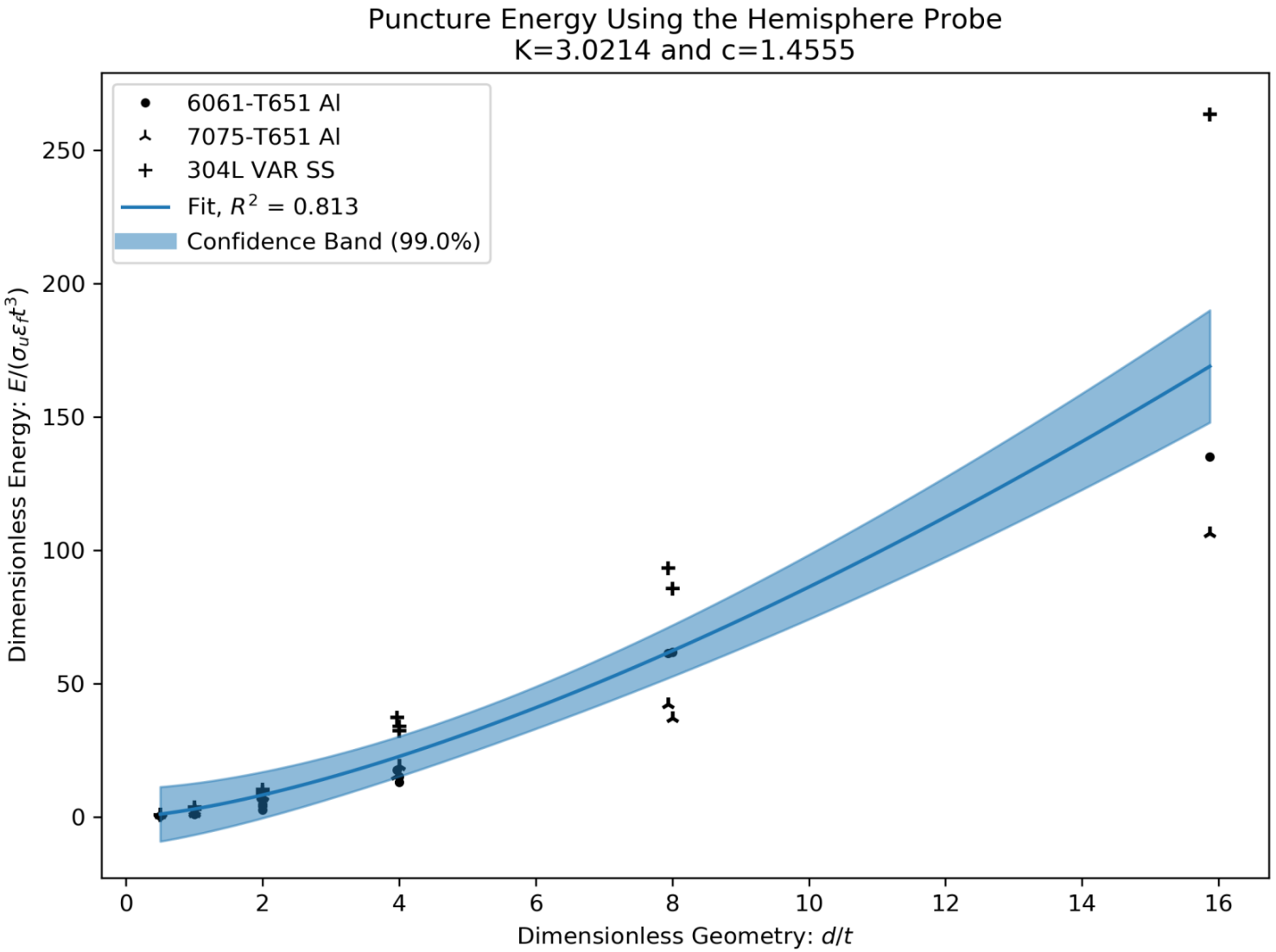

Hemisphere Probe Fit Separating Materials

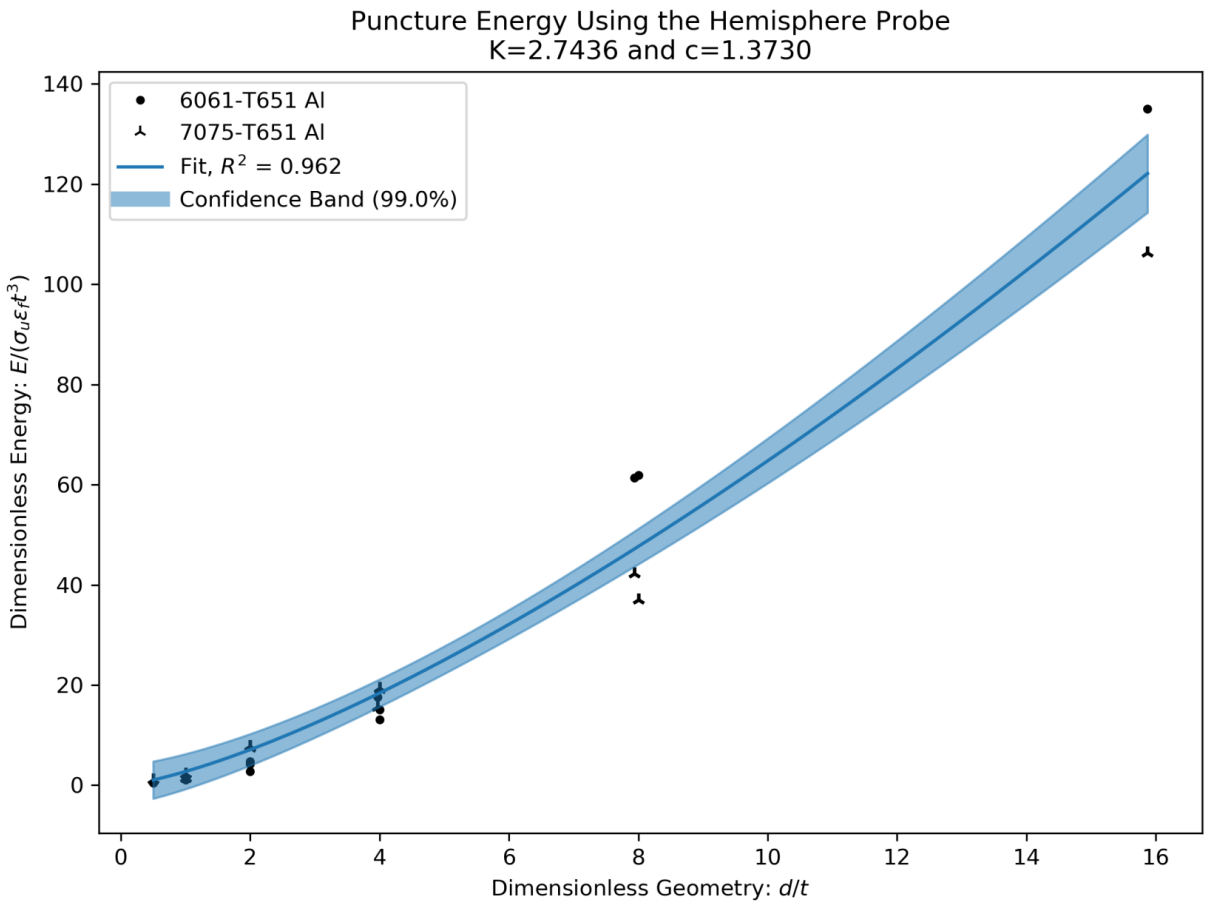

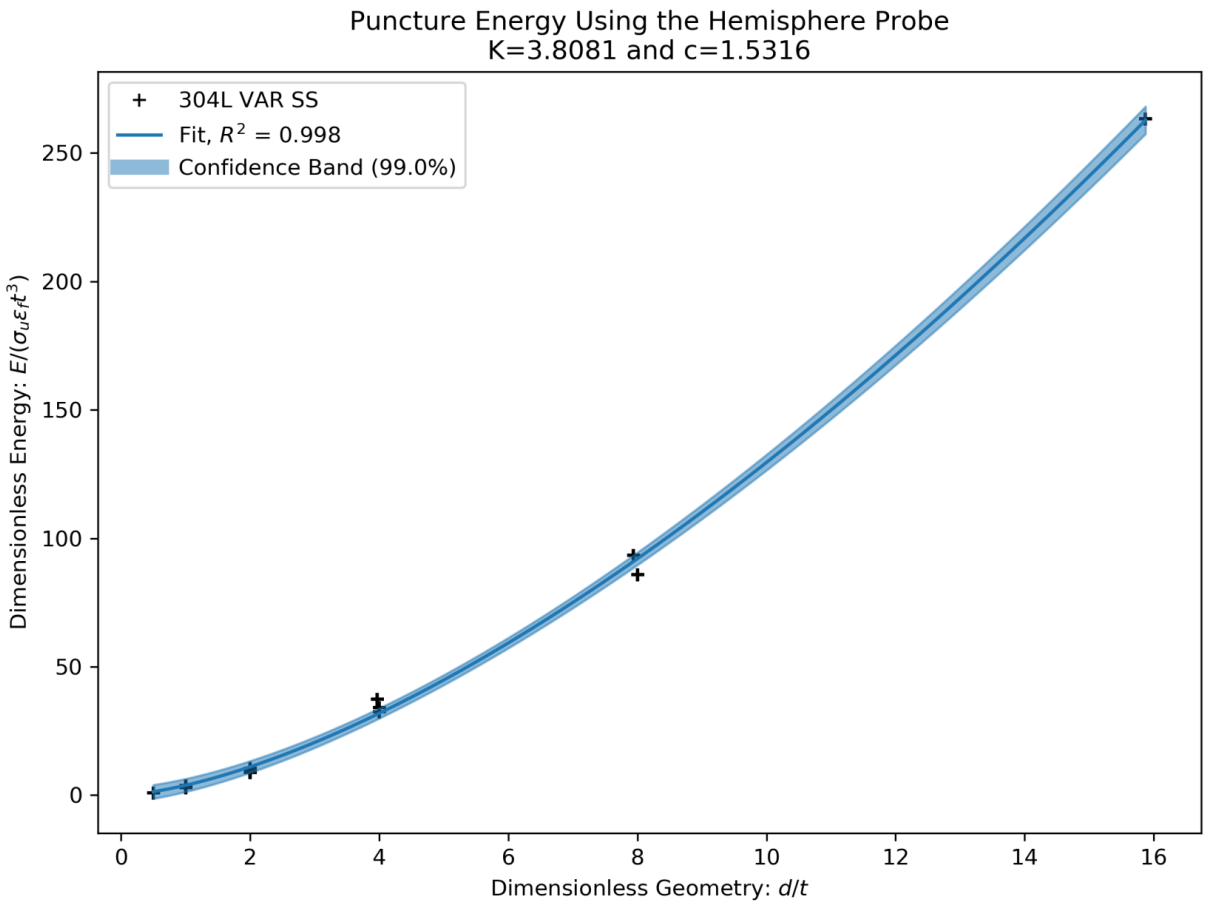

Conclusions

	Flat	Corner	Hemispherical
All data	0.700	0.927	0.813
Aluminum	0.842	0.907	0.962
Steel	0.964	0.998	0.998

The flat probe results were very scattered.

- Consequence: **lower quality fit** than the corner and hemisphere probes

Fits should be **separated by both material and probe shape**.

Conclusions (cont.)

	Flat	Corner	Hemispherical
All data	K = 3.086 c = 1.280	K = 1.981 c = 1.550	K = 3.021 c = 1.456
Aluminum	K = 2.232 c = 1.252	K = 1.501 c = 1.663	K = 2.744 c = 1.373
Steel	K = 4.813 c = 1.303	K = 3.239 c = 1.345	K = 3.808 c = 1.532

Observed trend: Higher K for steel than aluminum

Future Work

- **Simulate more alloys and dimensions** to ensure the fit stays statistically significant.
- Investigate the effects of **probe velocity**.
- Add **strain rate dependency** for all materials.
- **Increase the coupon puncture-area diameter** for thinner coupons.

Acknowledgements

Thank you to Neal Hubbard for teaching and guiding us through this project and answering all of our (many) questions. Thank you to Dr. Rob Kuether, Brooke Allensworth, Dr. Debby Fowler for organizing and running this summer research opportunity. Thank you to Dr. Tariq Kharishi (UNM) asking thoughtful questions to make us consider things more deeply. Thank you to Dr. Joe Bishop for checking in with us weekly and making sure we did not have any issues.

This research was conducted at the 2021 Nonlinear Mechanics and Dynamics Research Institute hosted by Sandia National Laboratories and the University of New Mexico.

Sandia National Laboratories is a multimission laboratory managed and operated by National Technology and Engineering Solutions of Sandia, LLC, a wholly owned subsidiary of Honeywell International, Inc., for the U.S. Department of Energy's National Nuclear Security Administration under contract DE-NA-0003525.

Appendix: Confidence Band Calculation

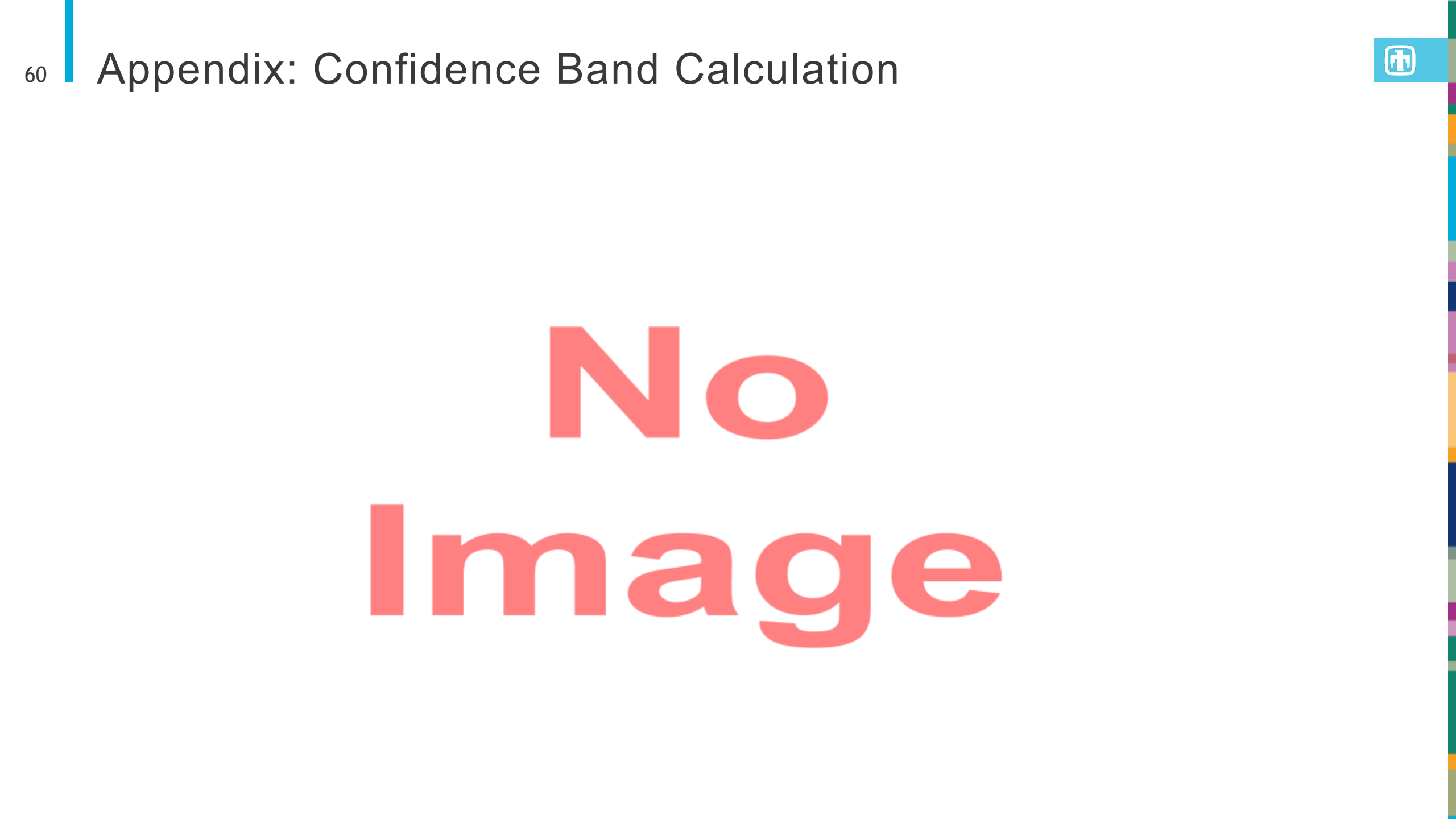

Mapping from Low Fidelity to High Fidelity Analysis for Failure Quantities of Interest

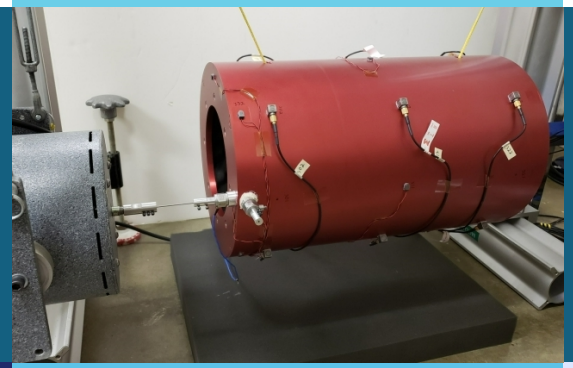

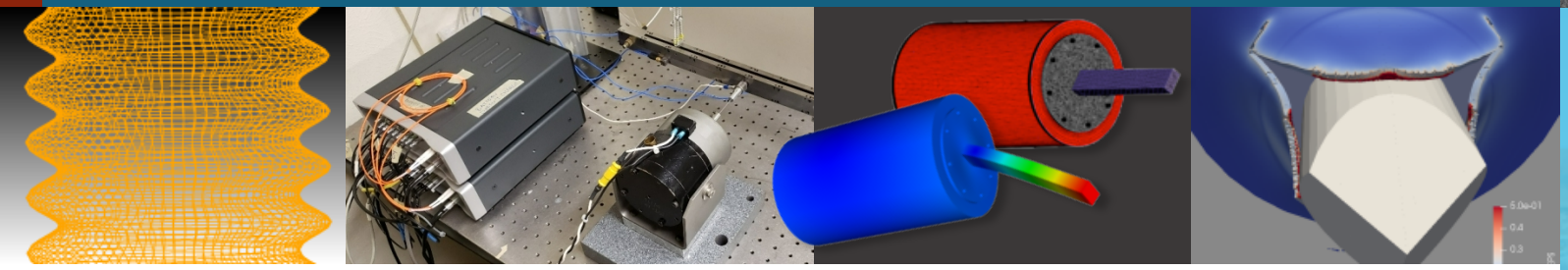

Mentors:

Mark Merewether, Edmundo Corona, Peter Grimmer, & Brendan Donohoe

Students:

Christopher Leonard, Joseph Redmond, & Leah Brinkman

Sandia National Laboratories is a multimission laboratory managed and operated by National Technology & Engineering Solutions of Sandia, LLC, a wholly owned subsidiary of Honeywell International Inc., for the U.S. Department of Energy's National Nuclear Security Administration under contract DE-NA0003525.

Motivation

Using a low fidelity model, can one predict failure seen in higher fidelity models?

Lower Fidelity

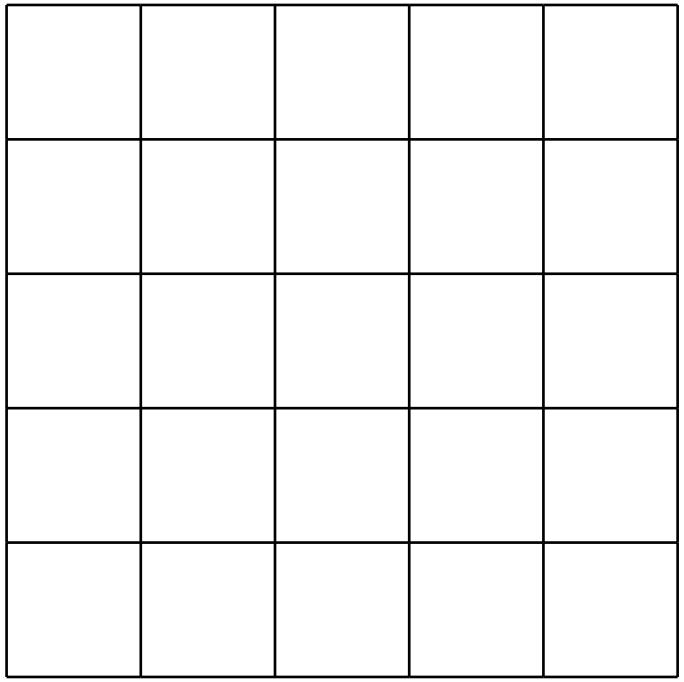

shell element models

element death failure models

Higher Fidelity

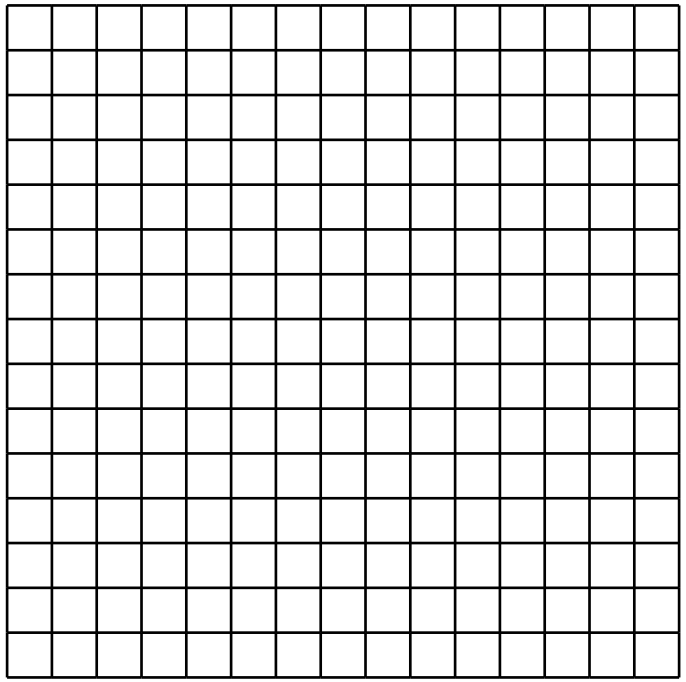

hexahedral element models

XFEM failure models

Outline

- Introduction
- Material Models
- Hexahedral (Hex) Model
- Shell Model
- Comparison of Hexahedral and Shell Models
- Neural Network
- Conclusions

Problem Setup

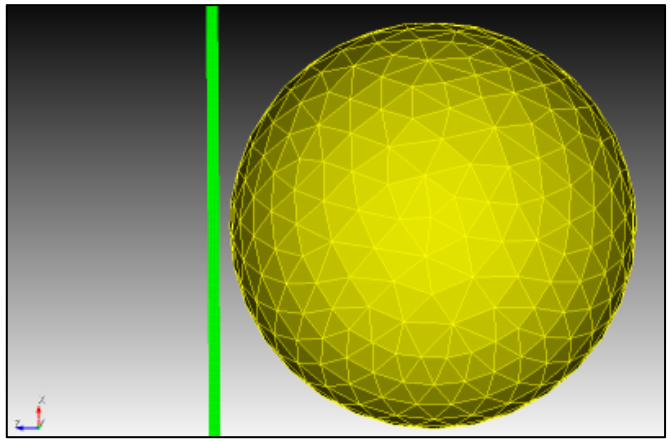

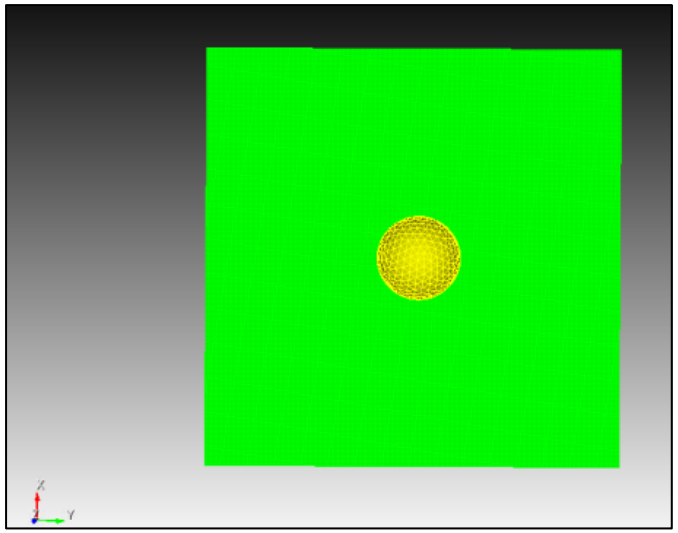

- Ball
  - 5” diameter
  - Made up of solid tetrahedral elements
  - Mesh size of 0.5”
  - 0.2” from plate in - z-direction
  - Initial velocity
- Plate
  - 25” x 25” x 0.12” square plate
  - Made up of either hexahedral (hex) or shell elements
  - Varying mesh sizes
  - Similar hex and shell models developed for comparison
  - Fixed on edges

Hexahedral and shell models developed at different levels of fidelity for comparison.

Relating Hexahedral & Shell Elements

Relating hexahedral and shell elements will be achieved by comparing the following:

- Breakthrough velocity magnitude
  - How fast must the ball travel to break through the plate?
- Kinetic energy change
  - What is the change in energy of the plate from the beginning time step to the end?
- Size of hole at ball speed of 5000 in/s
  - How much destruction is measured for each case?

Hexahedral vs. Shell Elements

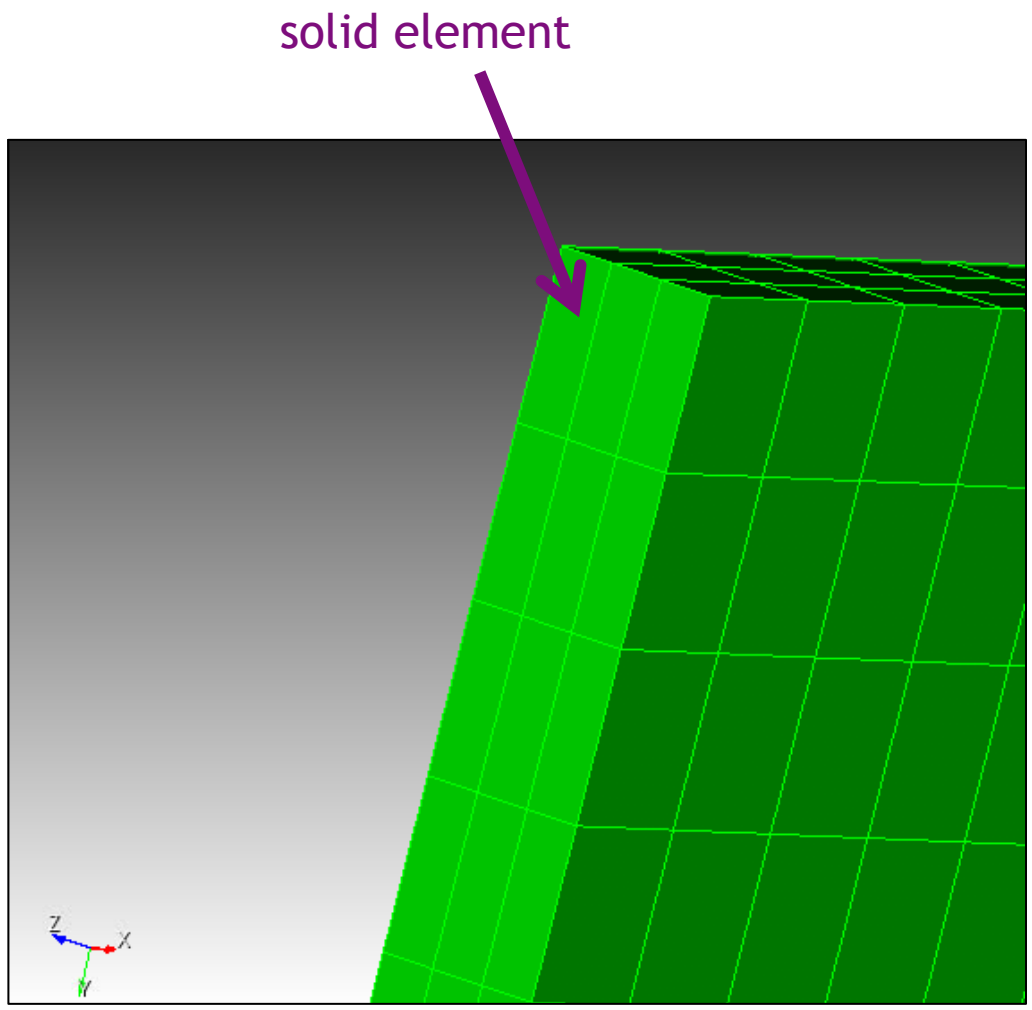

Hexahedral Plate

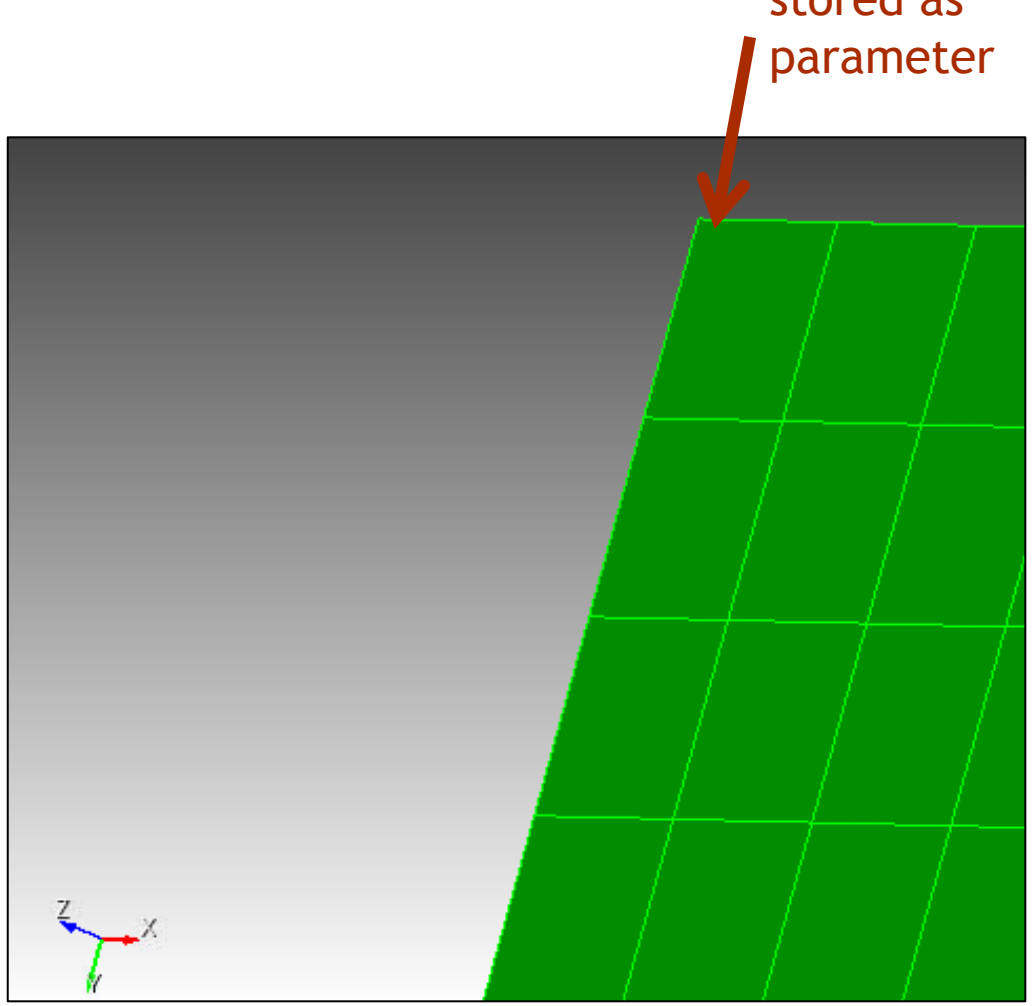

Shell Plate

Material Models

Plate: 6061-T651 Aluminum Alloy

Hex-Based Setup

J_2 Plasticity Model

Shell-Based Setup

Modular Plane Stress Plasticity Model

Ball: 304L Stainless Steel Alloy

All Setups

J_2 Plasticity Model

All components are set up with ductile failure models: J2 plasticity for solid elements and modular plane stress plasticity for shell elements.

J_2 Plasticity

Fixed Parameters

Aluminum

Parameter		E (psi)		
Value	2.5 x 10^{-4}	10.4 x 10^6	0.33	1.36 x 10^6

Steel

Parameter		E (psi)		
Value	7.49 x 10^{-4}	28 x 10^6	0.27	0.776 x 10^6

What is Calibrated: hardening function, failure model

Fixed parameters do not vary with plastic deformation and are used as constants during calibration.

Modular Plane Stress Plasticity

- A J_2 plane-stress model with modified forms for hardening
- Uses the same values from the J_2 plasticity model
- Developed for use with shell elements

Only the plane stress state is allowed in shell elements.

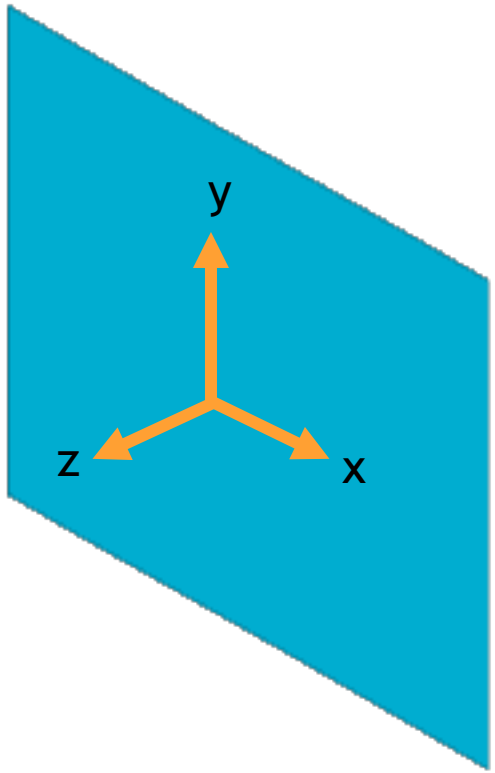

Death Criterion in Ductile Failure

- Element death will be defined using the damage variable D

- Factors of the damage variable
  - Calculated such that material failure occurs when damage ≥ 1
  - Accumulates with plastic deformation
  - Functional dependency chosen to be on the stress, equivalent plastic strain rate, and temperature histories

$$\text{팻} = \frac{1}{\text{폽}}$$

Element death occurs when the variable damage ≥ 1, which accumulates with plastic deformation.

Hexahedral Model Development

Plate Mesh Sizes Considered

Case Number	Element Side Length Across Face (in)	Number of Elements Through Thickness	Number of Nodes	Aspect Ratio
1	0.12	3	…	3
2	0.04	3	…	1
3	0.02	6	…	1

Varied number of elements through the thickness and across faces of plate.

Case 1

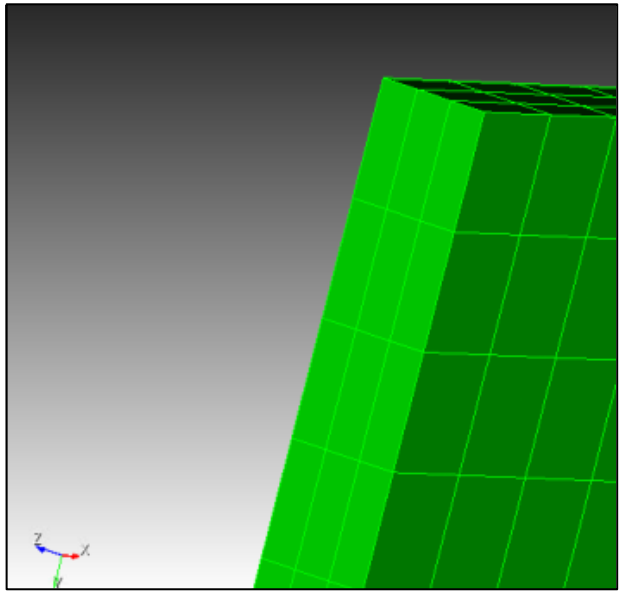

Case 2

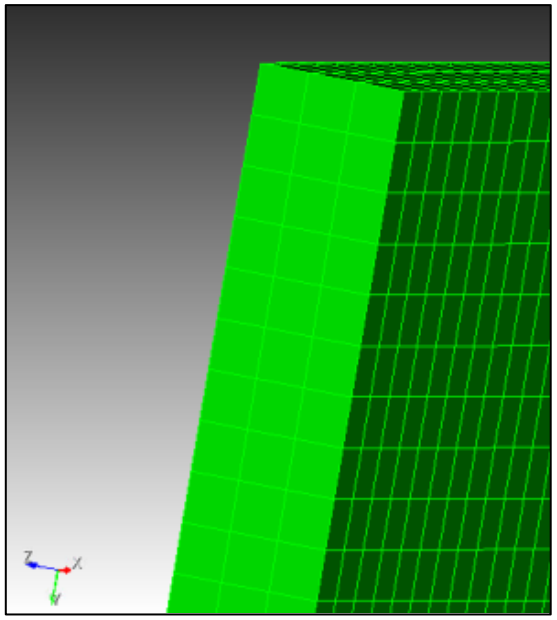

Case 3

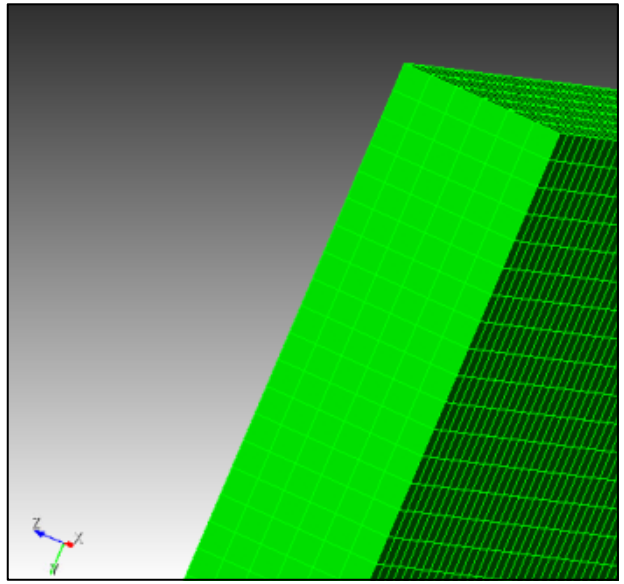

Hexahedral Fidelity Comparisons

Case 3 - Most Refined

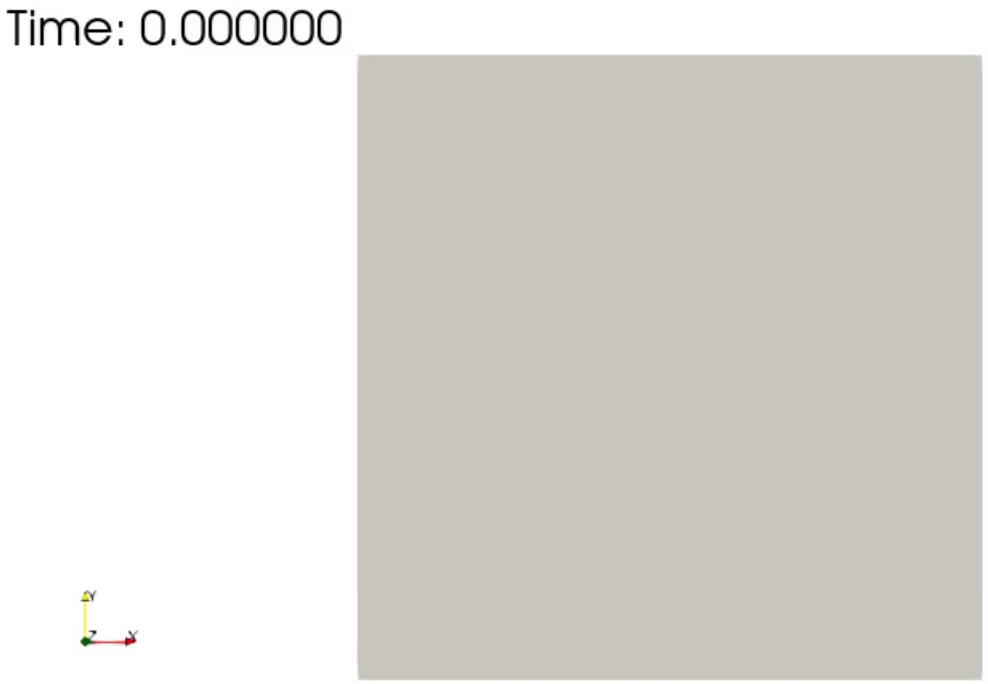

Case 1 - Least Refined

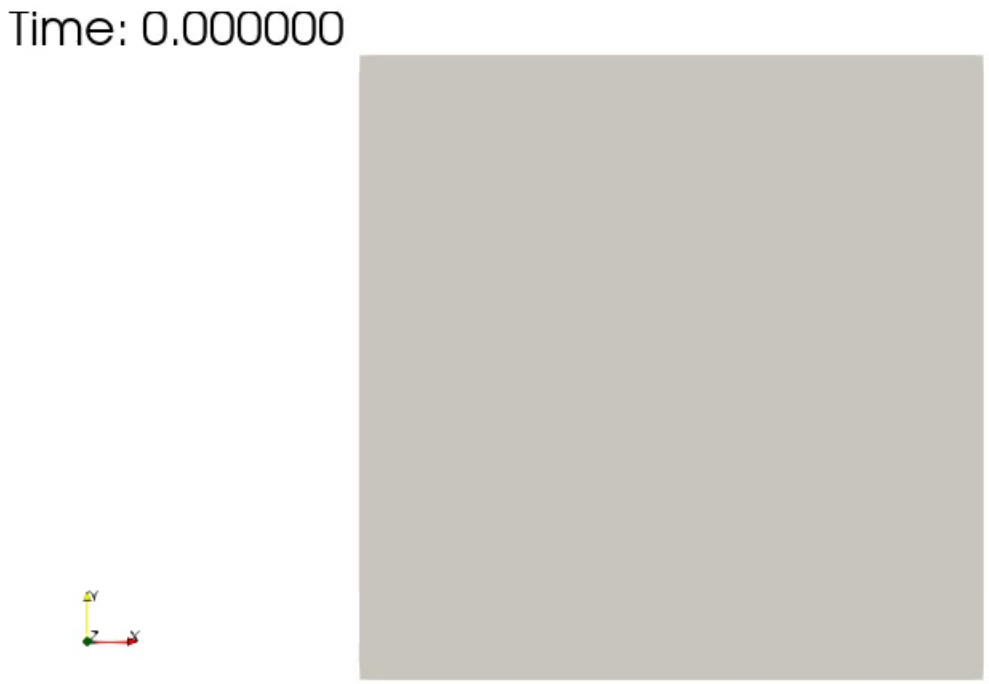

Hexahedral Velocity/Energy Threshold

Breakthrough Velocity and Change in Kinetic Energy

Case Number	Breakthrough Velocity (in/s)	Change in Kinetic Energy (J)
1	…	…
2	…	…
3	…	…

Shell Development

Case 1

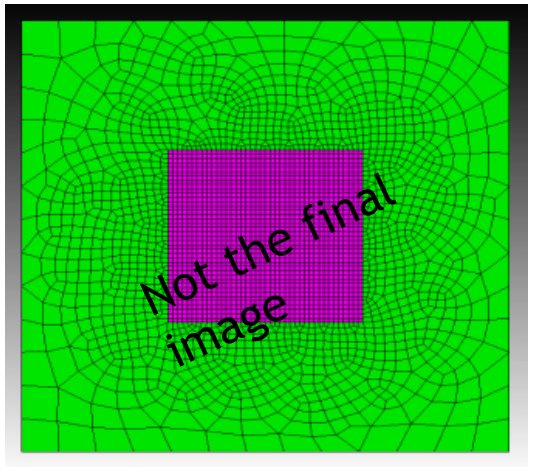

Case 3

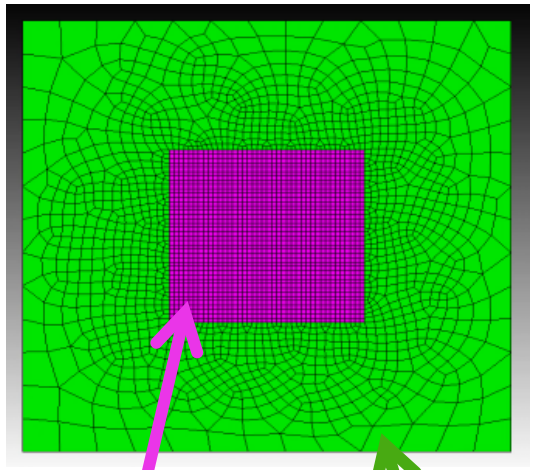

Case 5

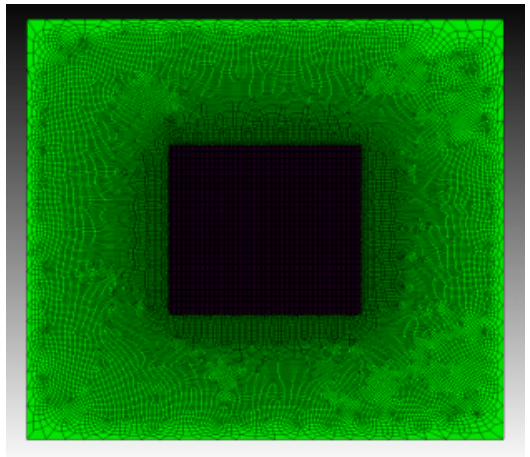

Fine Interval Mesh

Graded Pave Mesh

Shell Intervals Evaluated

Case	Element Interval (in)	Outer Interval Pave (in)	Total Number of Nodes
1	1	N/A	…
2	0.5	2	2,006
3	0.25	2	4,193
4	0.12	1	14,627
5	.04	1	110,920
6	.02	N/A	…

Shell Models have greater utility in lower fidelity schemes, as they can be localized, and do not have to adhere to aspect ratio limitations

Shell Fidelity Comparisons

Case 1 - 1” Mesh

Case 3 - 0.25” Mesh

Case 5 - 0.12” Mesh

Case 2 - 0.5” Mesh

Case 4 - 0.04” Mesh

Case 6 - 0.02” Mesh

Shell Velocity/Energy Threshold

Breakthrough Velocity and Change in Kinetic Energy

Mesh Size	Breakthrough Velocity (in/s)	Projectile Kinetic Energy Loss (J)
1	…	…
.5	844	…
.25	795	…
.12	765	…
.04	799	…

Shell – Varying Integration Point Thresholds

Number of Integration Points (IP) to Reach Death Criterion Before Element Killed

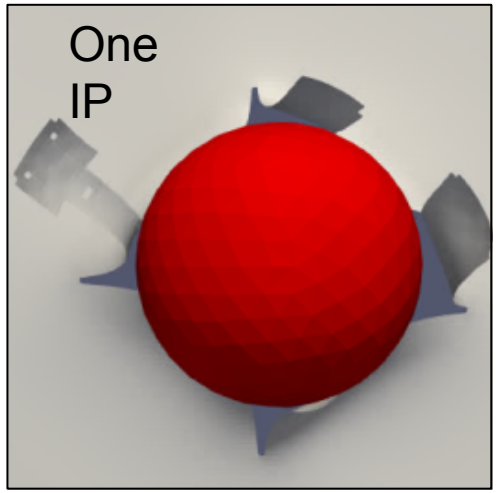

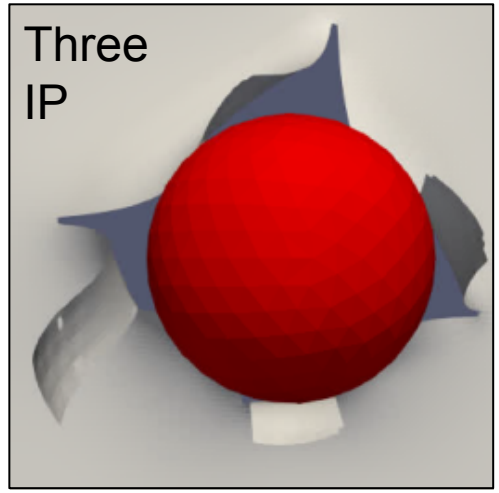

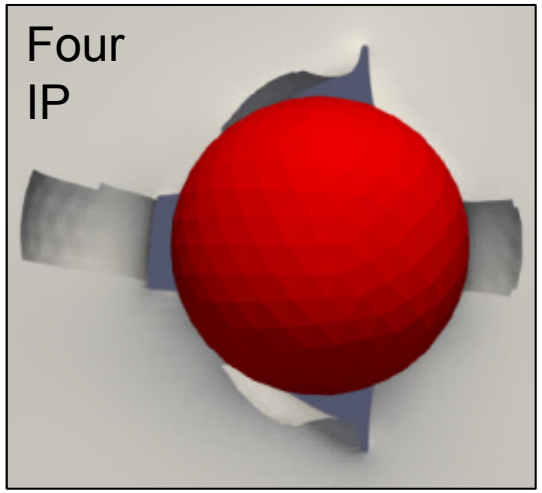

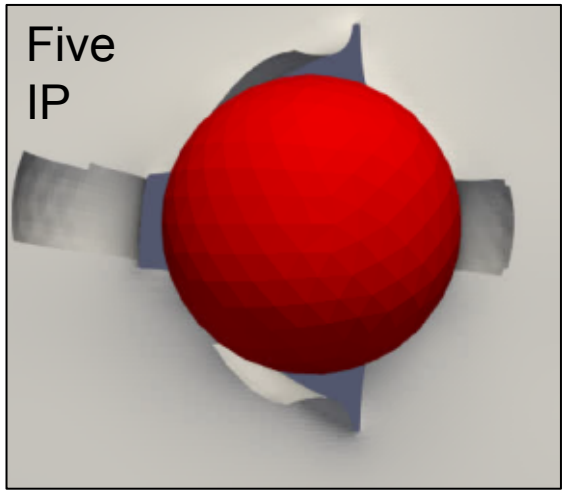

Shell – Varying Integration Point Thresholds

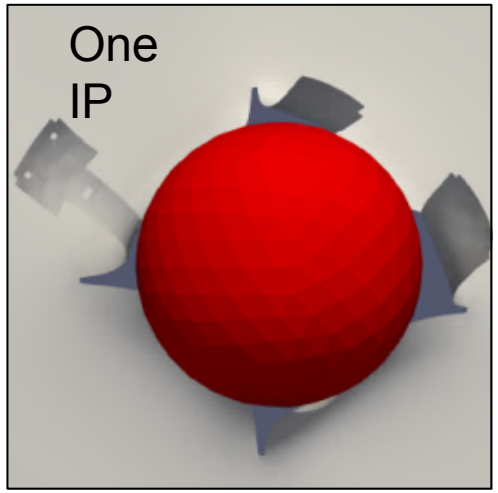

Number of Elements Killed

---num elems killed---

Number of Elements Killed

---num elems killed---

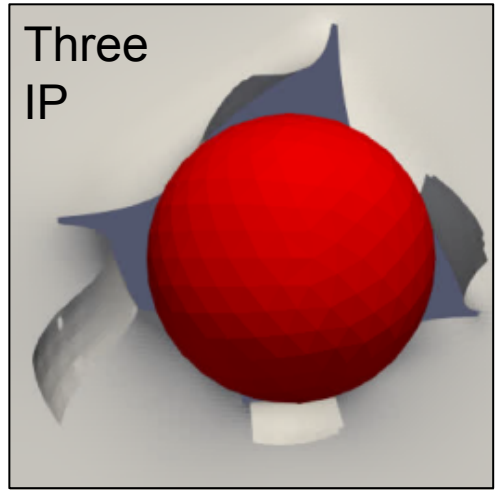

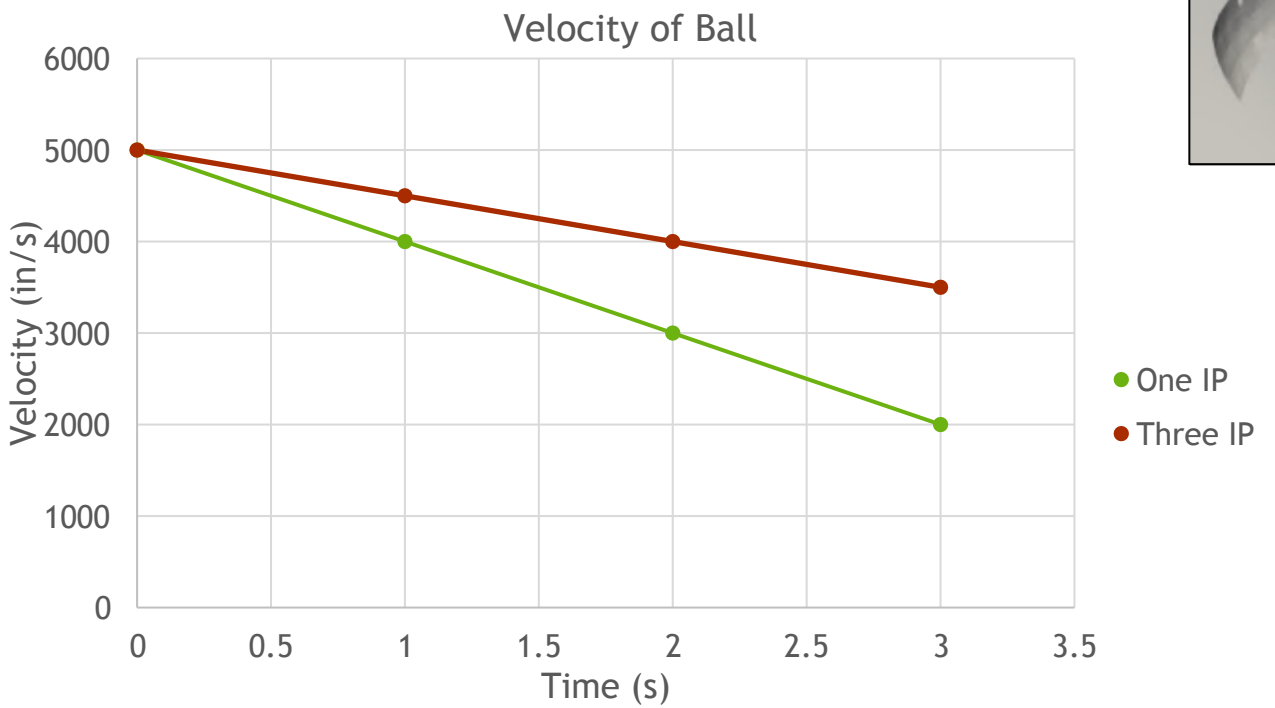

Comparison of Shell and Hex

	Hex Model (.04)	Shell (.04)	Shell (0.5)
Computation time	…	…	…
Projectile Kinetic Energy Loss	…	…	…

Hex Model (.04)

Shell Model (.04)

Shell model (0.5)

Comparison of Shell and Hex

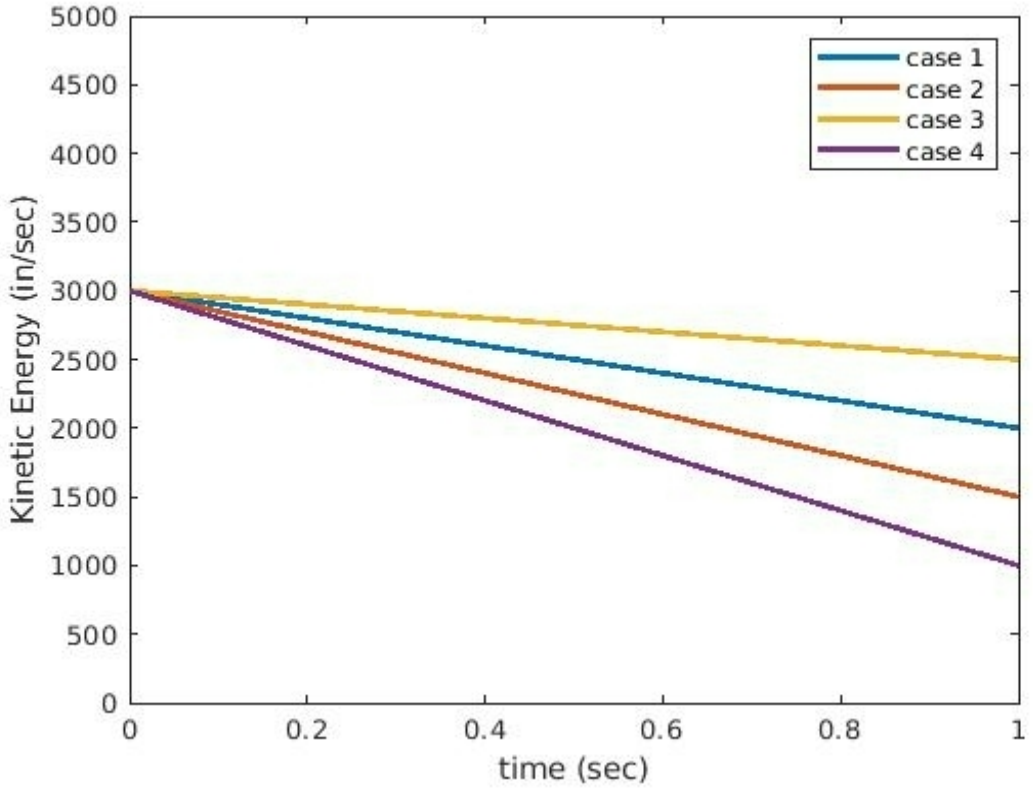

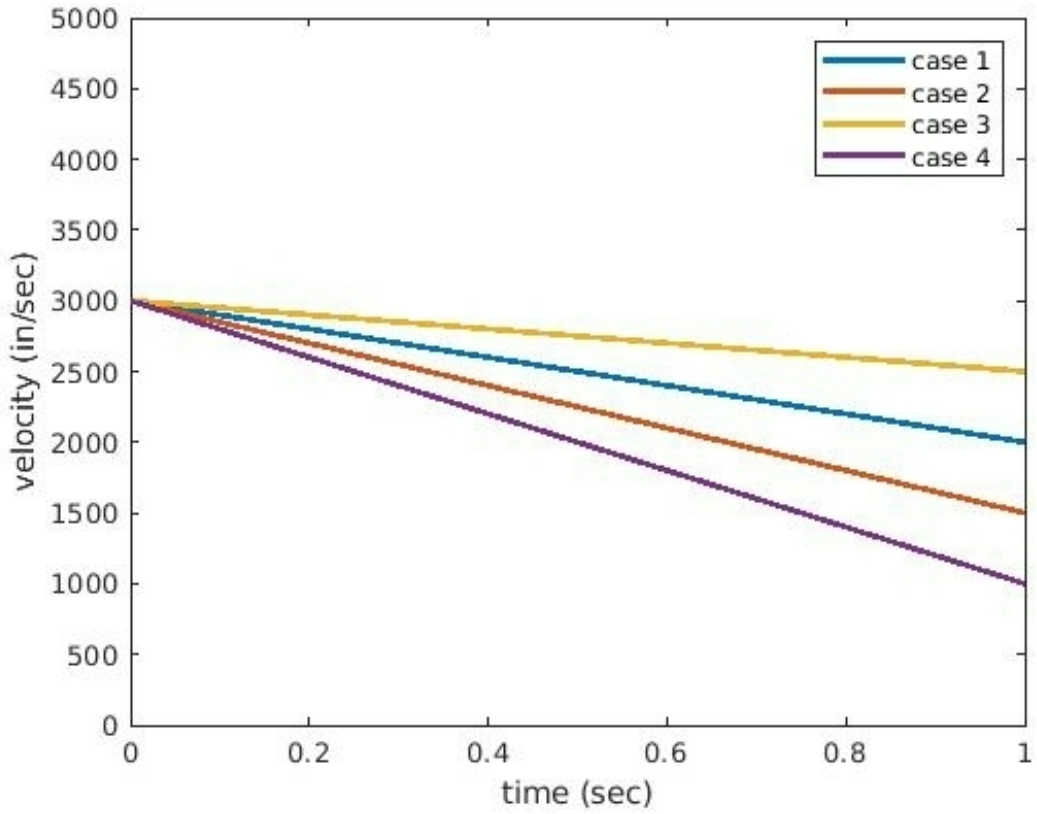

Kinetic Energy and Velocity of the ball for different models

Hexahedral Comparison of XFEM vs Element Death

Element Deactivation

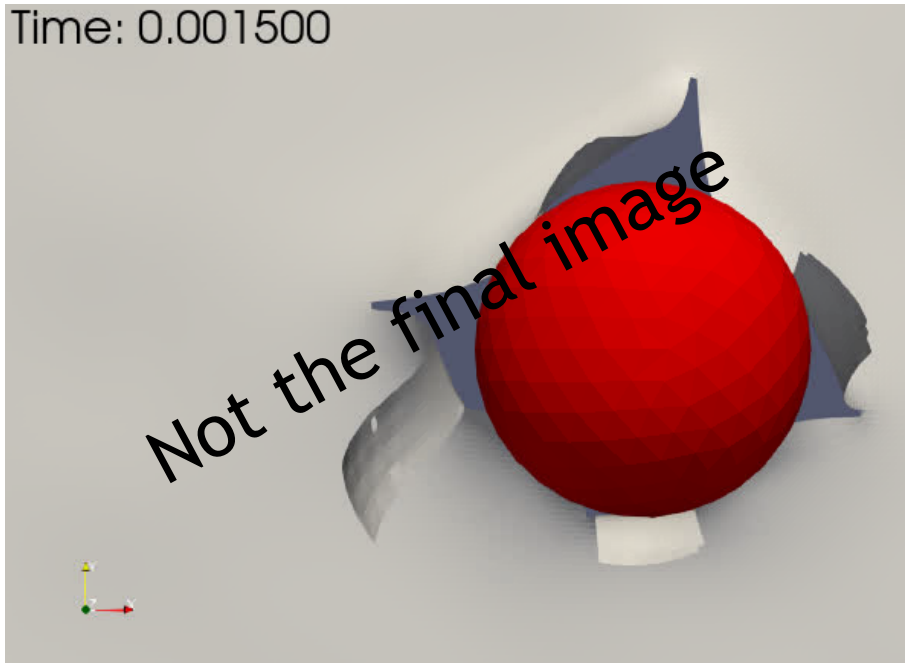

XFEM

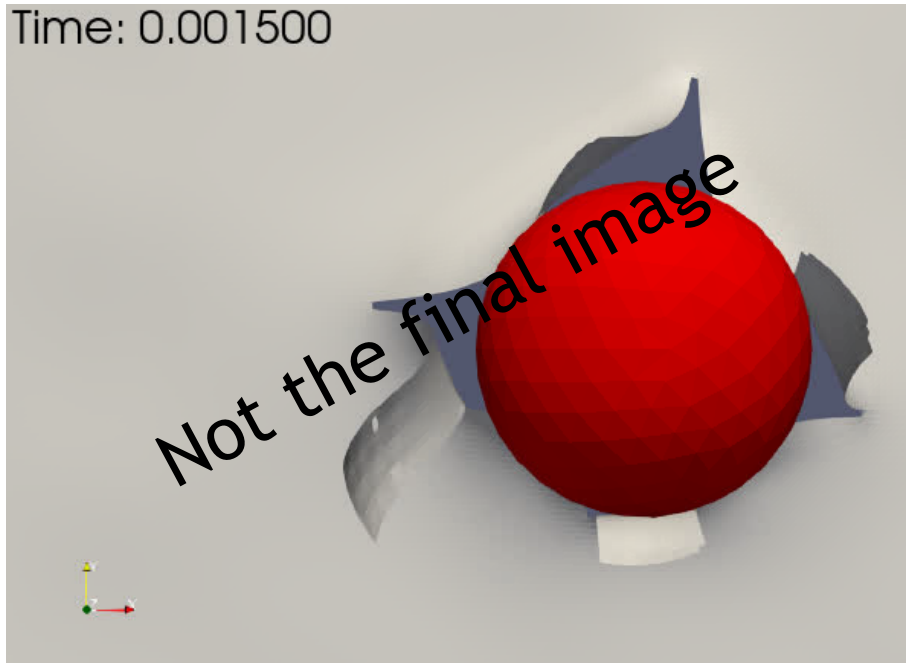

Crack patterns are similar/deviate from one another.

Hexahedral Comparison of XFEM vs Element Death (cont.)

Mass Lost

- XFEM – … lb
- Element Death (Element Deactivation) – … J

Kinetic Energy Change of Plate

- XFEM – … lb
- Element Death (Element Deactivation) – … J

Momentum Change of Plate

- XFEM – … lb
- Element Death (Element Deactivation) – … J

Neural Network problem

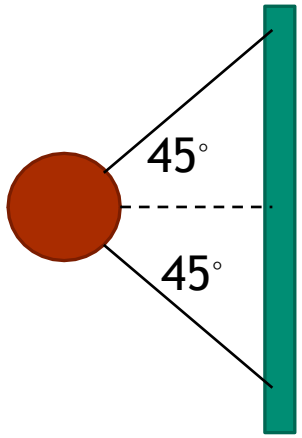

- A fully connected neural network was used to determine if there was a break in a plate given the initial velocity of the projectile.
- To train the neural network, highly accurate simulations with were used where the initial velocities magnitude and directions were varied. This simulation was then used to determine if there was a break in the plate or not.
- With this neural network, we can run simulations on a coarser grid and predict if there was break in the plate or not.

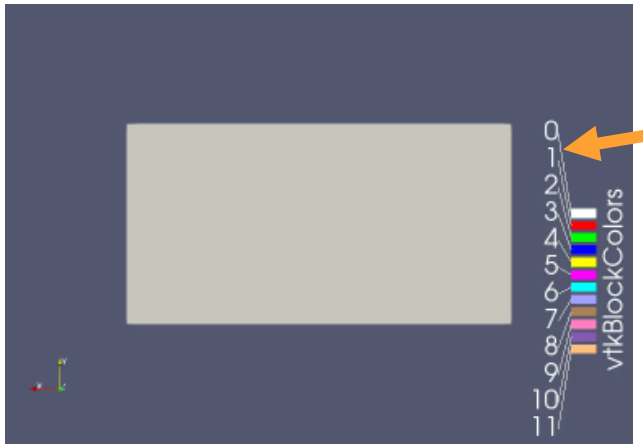

Left: Mesh size = .5
Runtime = 130 sec

Right: Mesh size = 2
Runtime = 21 sec

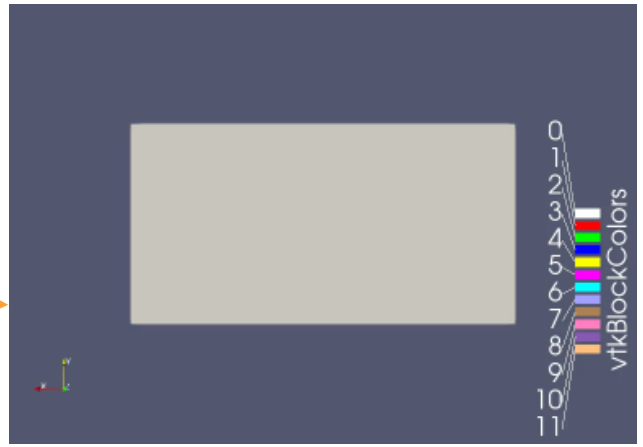

Fully Connected Neural Network

- For a fully connected neural network each connection between layers can be represented as

$$\varphi^i(A^i x^{i-1}+b^i)=x^i$$

- Here **i=1,2,…,n**, where **n-1** is the number of hidden layers.
- **A^i** and **b^i** are the weight matrix and bias vectors respectively..
- The vectors **x^{i-1}** are the inputs into the **i**th layer of the neural network.
- The function φ^i is a an element wise function known as the activation function. This is used to add nonlinearity to the neural network.

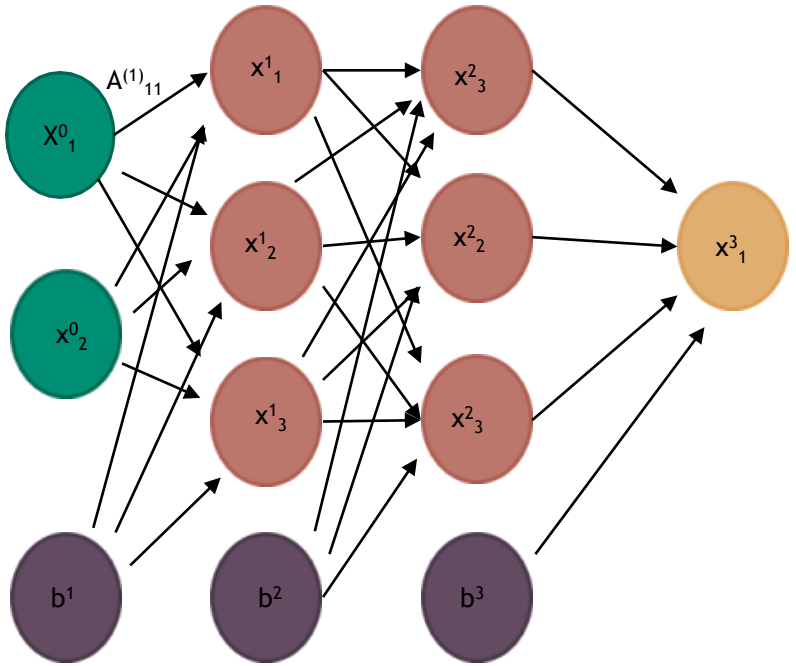

Neural Network Training

- Trained the network using 30 epochs.
- Use the adam optimization algorithm.
- Total training time approximately 20 secs.

Prediction Accuracy ≈ 99%

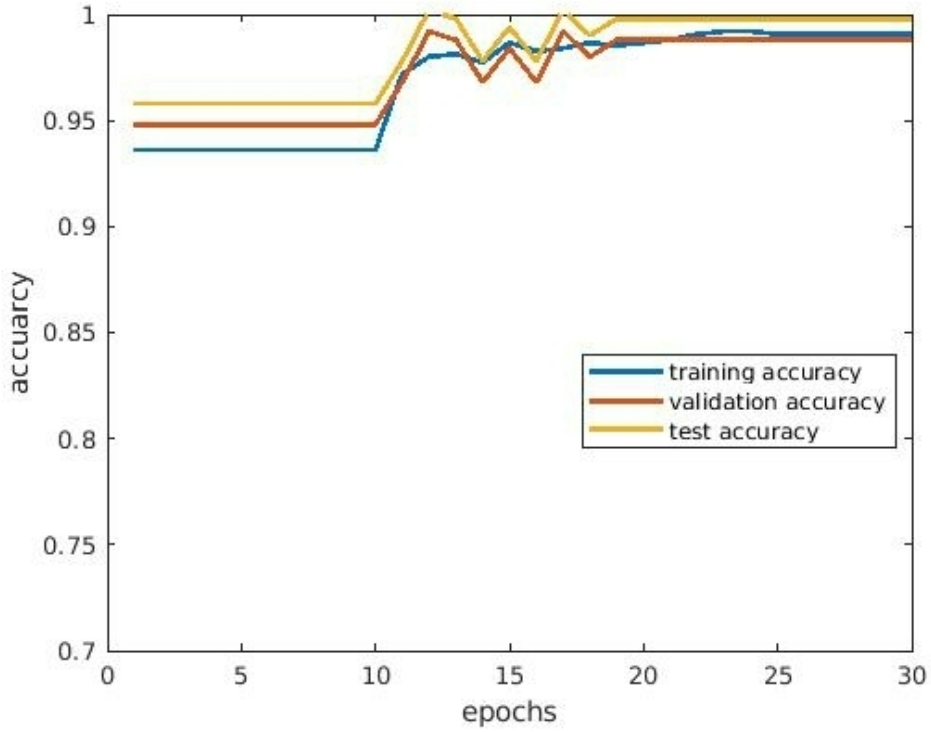

Impact Predictions

- Here, simulations are run to predict how large a tear there will be when there is element failure in the model.
- A fully connected neural network is used to make predictions on how wide the hole is and how many elements were destroyed (area of the hole).

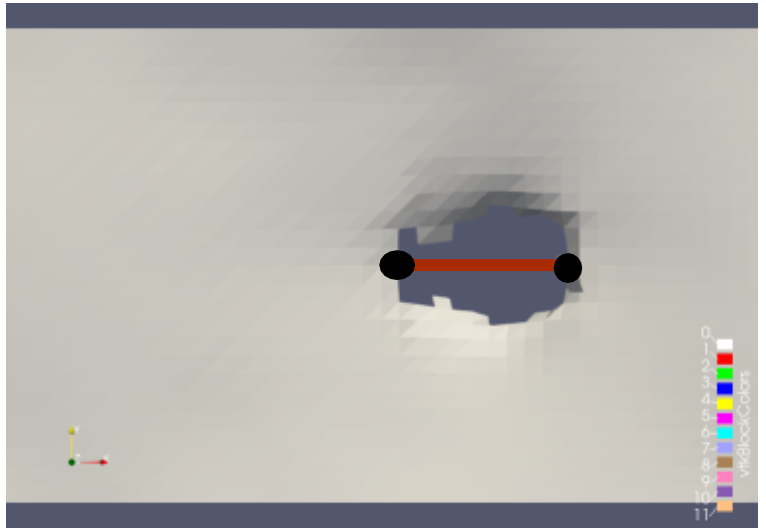

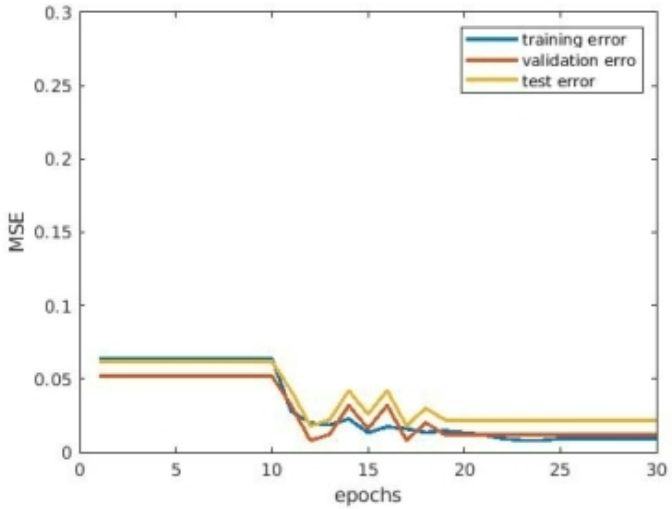

Mean Square error loss ≈ .05

Results

- Developed quantitative and qualitative comparison of shell and hex models
- Looked at the usefulness of XFEM in coarse shell models for crack propagation compared to a refined hex model
- Quantified disparity in model behavior dependent on mesh resolution
- Able to accurately predict if there will be a tear in the plate given the projectiles velocity

Looking into the Future

- Predictions of:
  - shape of the hole
  - Train neural networks with other inputs, such as stress, strain, contact force, etc.
  - amount of mass loss due to use of element deactivation vs. XFEM
  - change in kinetic energy from the beginning to ending time step

Acknowledgements

This research was conducted at the 2021 Nonlinear Mechanics and Dynamics Research Institute hosted by Sandia National Laboratories and the University of New Mexico.

Sandia National Laboratories is a multimission laboratory managed and operated by National Technology and Engineering Solutions of Sandia, LLC, a wholly owned subsidiary of Honeywell International, Inc., for the U.S. Department of Energy's National Nuclear Security Administration under contract DE-NA-0003525.

Project 4: Modeling Rate Dependent Interface Separation with Cohesive Zone Models and Bulk Viscoelasticity

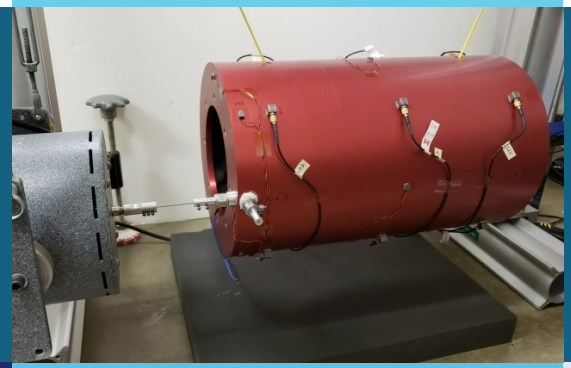

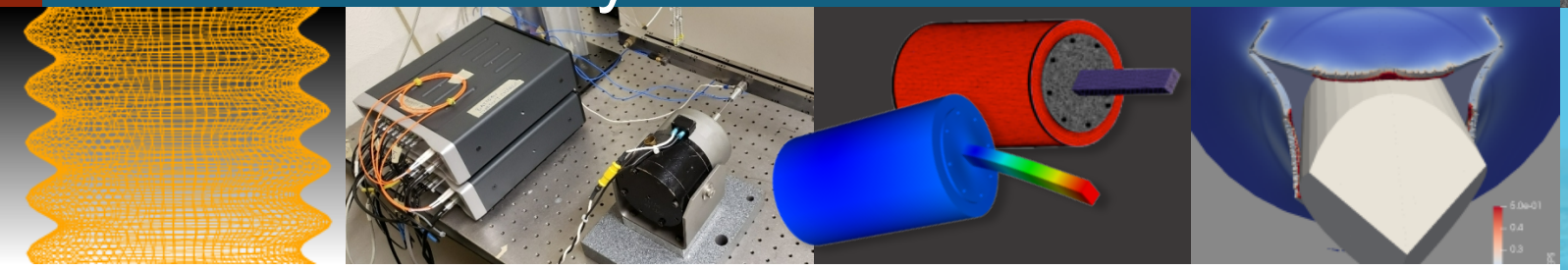

Students: Brandon Clarke, Chris Maiorana, Ryan Smith

Mentors: Scott Grutzik, Dave Reedy, Kevin Long, Jonel Ortiz, Frank DelRio, Yu-Lin Shen

Sandia National Laboratories is a multimission laboratory managed and operated by National Technology & Engineering Solutions of Sandia, LLC, a wholly owned subsidiary of Honeywell International Inc., for the U.S. Department of Energy's National Nuclear Security Administration under contract DE-NA0003525.

Motivation

- Components tend to fail at interfaces
- Accurate modeling of interface mechanics and failure is a critical aspect of modeling component behavior, reliability, and lifetime.
- While interfacial delamination shares many characteristics with traditional LEFM, there are a number of differences
  - A crack can become constrained to stay on a weak interface and forced to propagate under a mix of tensile and shear loading, interfacial toughness is strongly dependent on mode mixity
- Such cracks are often modeled using cohesive zone methods. Various experimental methods may be used to calibrate such models.
  - Asymmetric Double Cantilever Beam (ADCB)
  - Currently, to interpret ADCB data one must assume that all materials are linear elastic.
- Project Goal: explore the extent to which current Sandia capabilities (existing cohesive zone models and bulk viscoelasticity) can predict delamination at various rates and temperatures by comparing against measured data

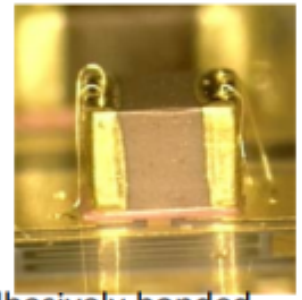

adhesively bonded electrical components

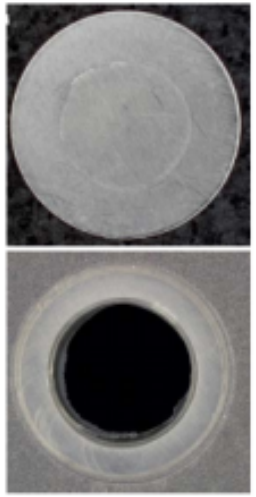

Adhesively bonded rupture disk

encapsulated components

Images courtesy of Dave Reedy

Background: Cohesive Zone Mod

Versatile fracture mechanics model
- Fracture resisted by “cohesive tractions”
- Must specify a traction-displacement relationship
- Crack confined to propagate along cohesive layer

Tvergaard-Hutchinson Model

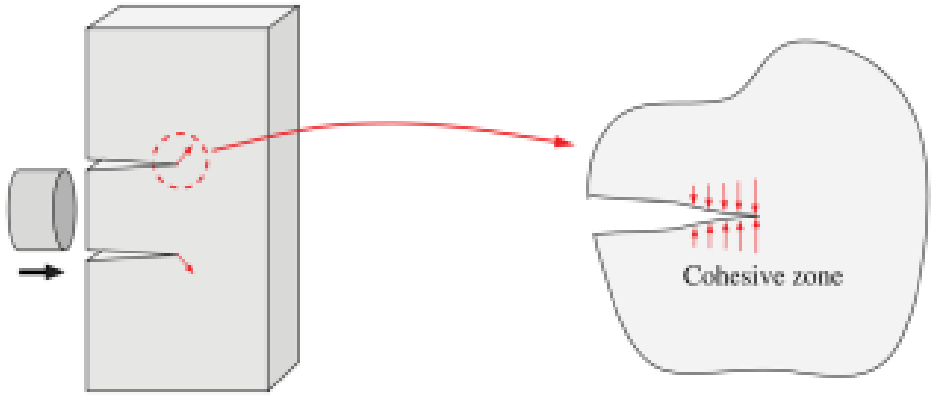

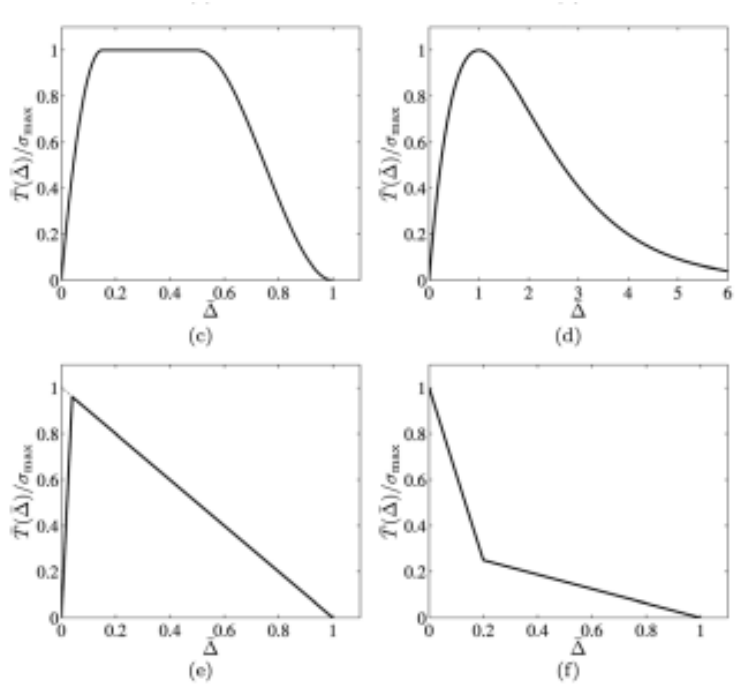

(Park and Paulino)

SINGLE ELEMENT MODEL

Viscoelastic Behavior of the Epoxy

- Often there is adhesive material or one of the bonded materials can exhibit inelastic effects.
  - An epoxy bonded interface may be used near or above its glass transition temperature or one of the bonded materials may be a soft metal like copper or gold.

- Single element of epoxy in tension, bottom is fixed, 1/8th symmetry

- Universal Polymer model based on Matthew's new 828/DEA cured fit

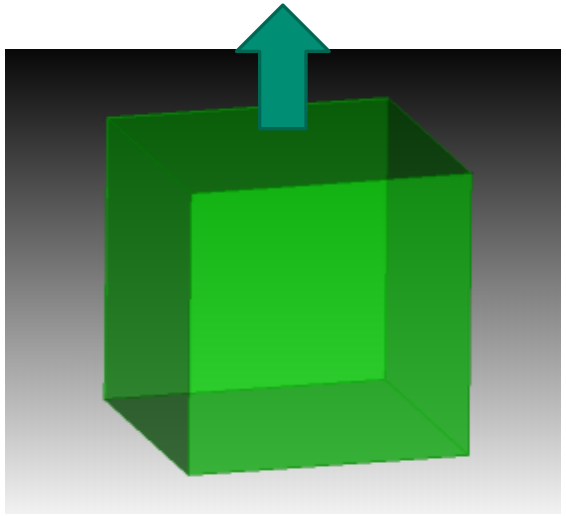

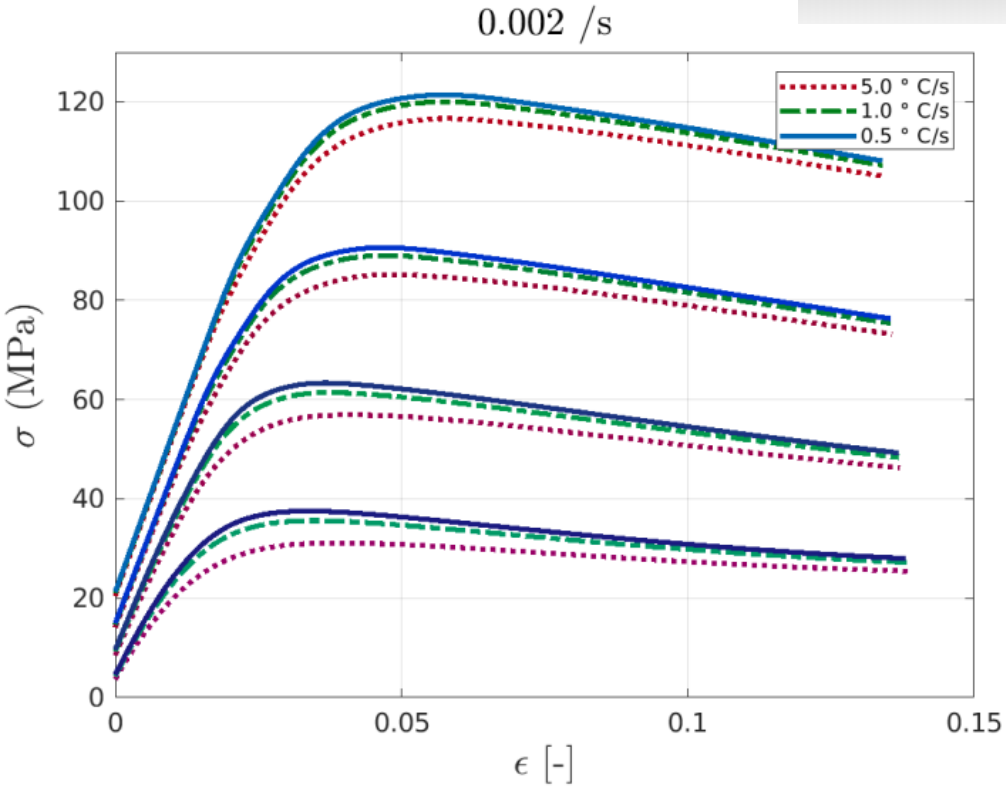

Yield vs Temperature

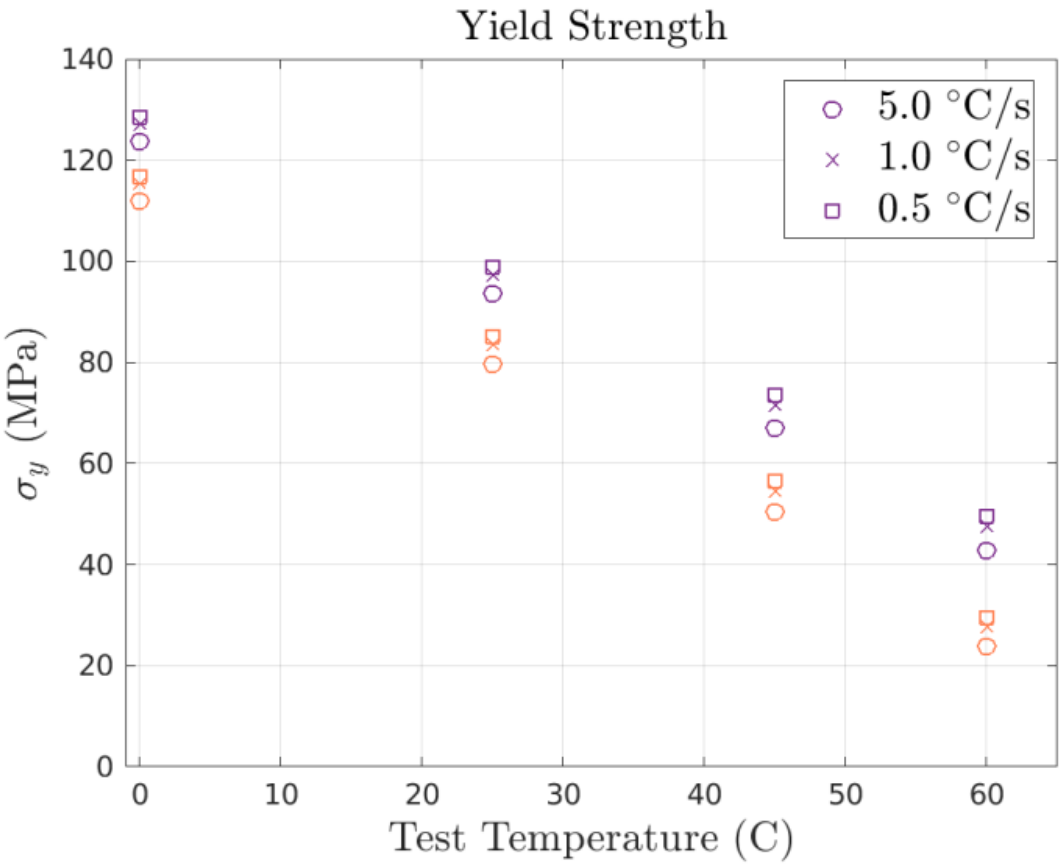

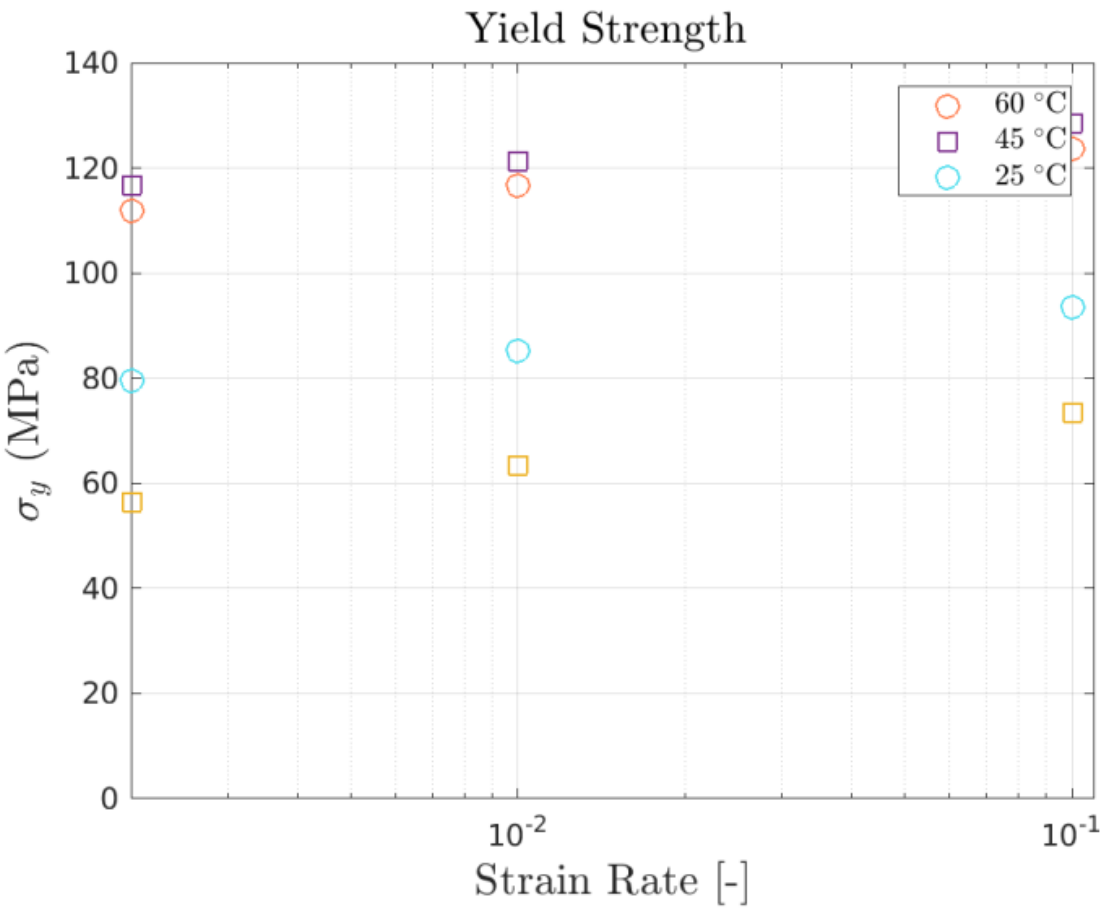

FULL ADCB MODEL – SET-UP

Model Layout

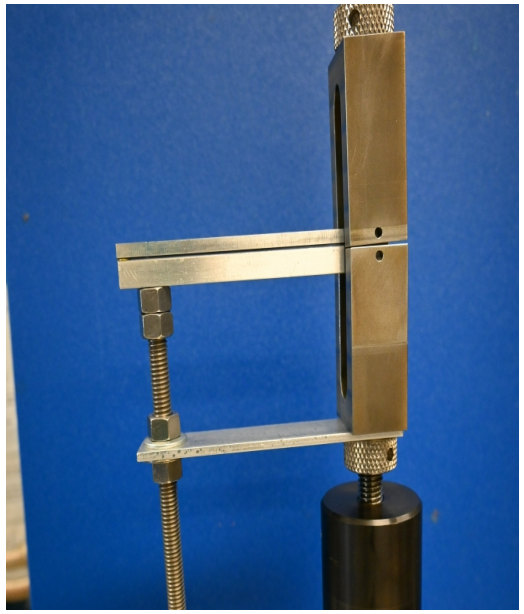

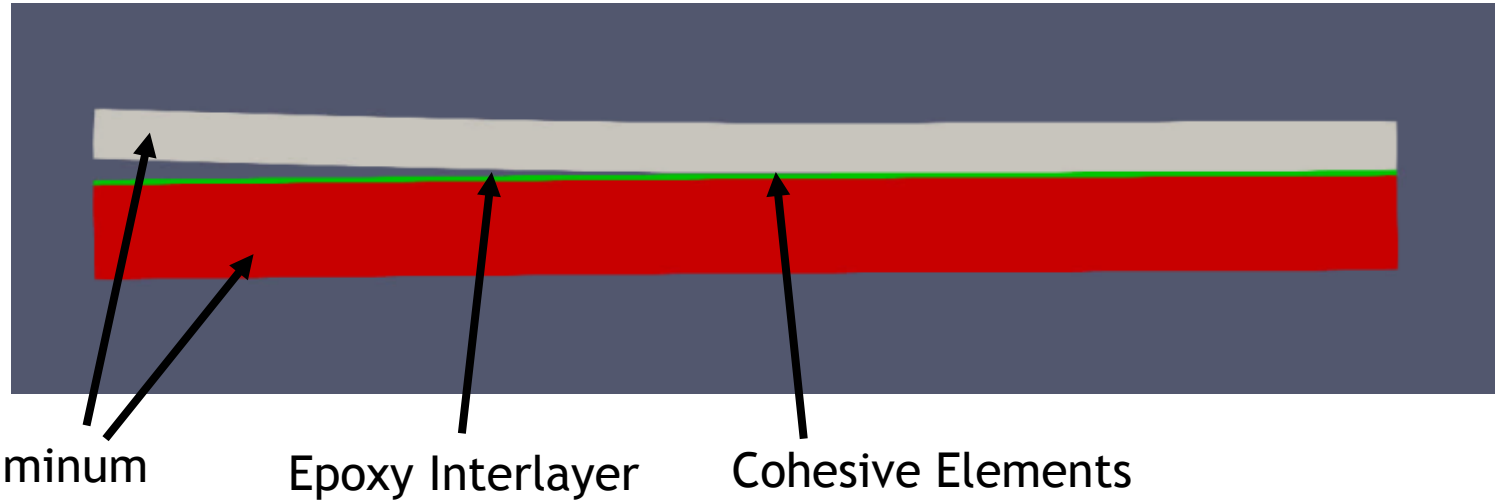

Simplify true geometry to single -thickness plane-strain model

Mesh And Boundary Conditions

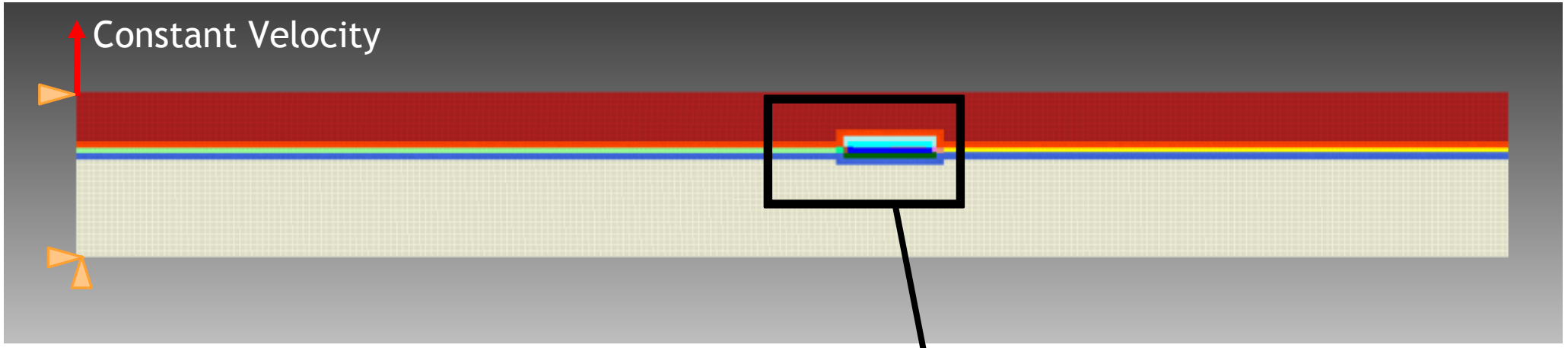

Fine Mesh around crack tip (~ 20 microns element edge length)

Transitions to Coarse Mesh

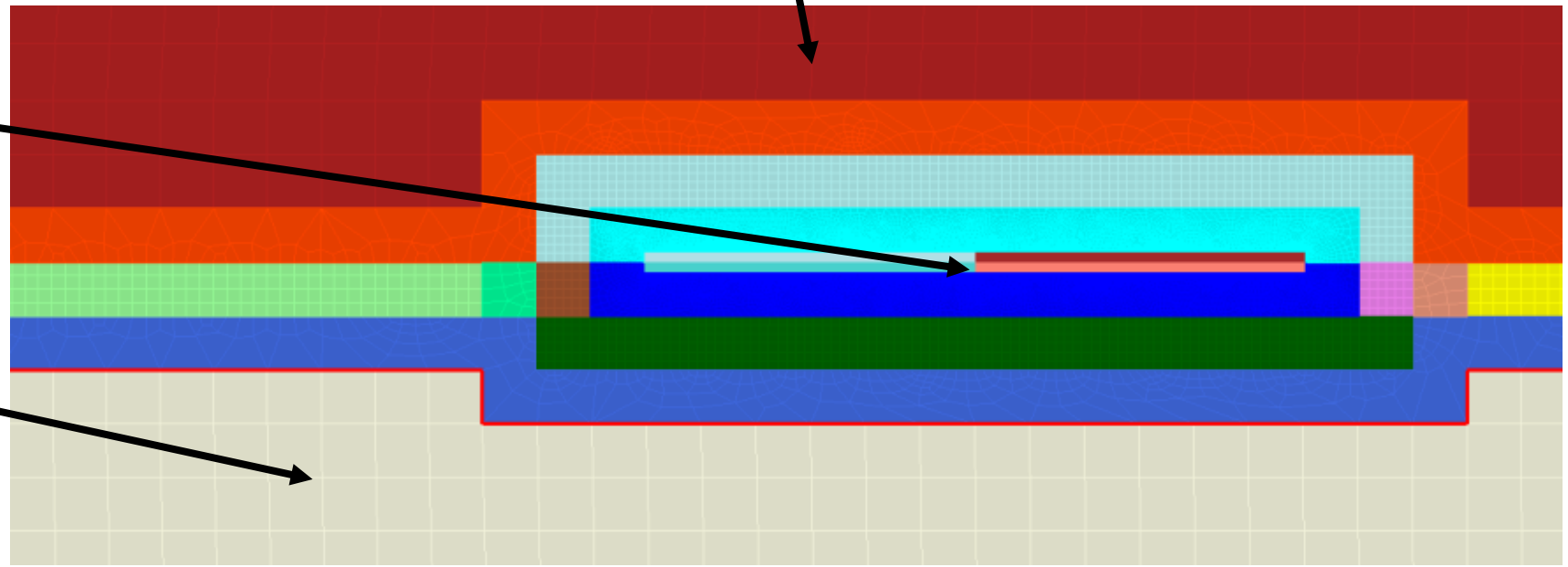

COHESIVE ZONE MODEL CONVERGENCE

CZM Convergence Evaluation without Viscoelasticity

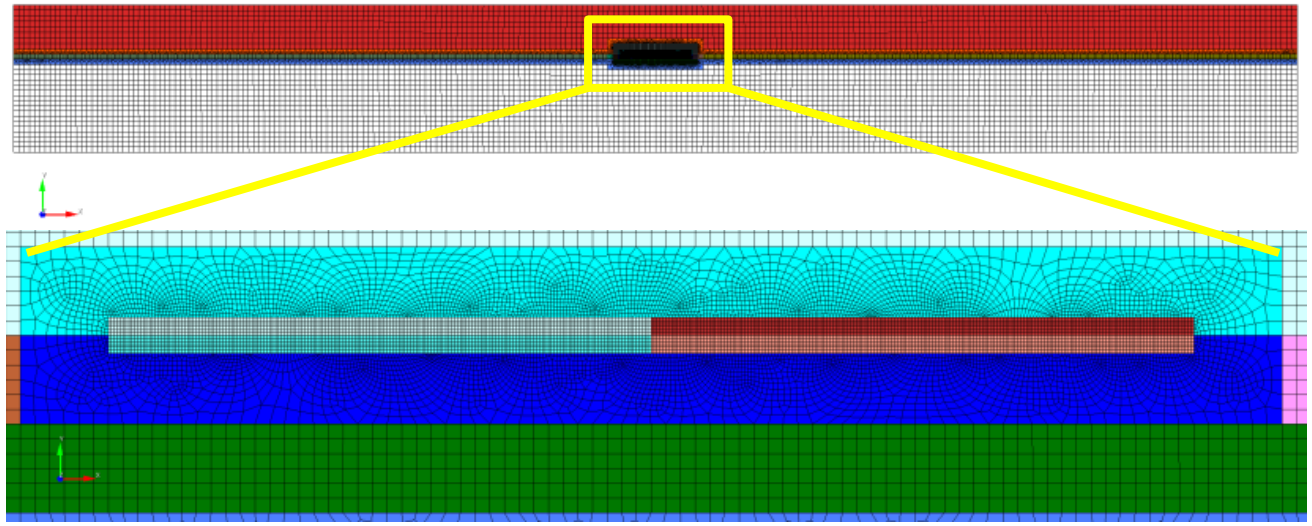

No Image

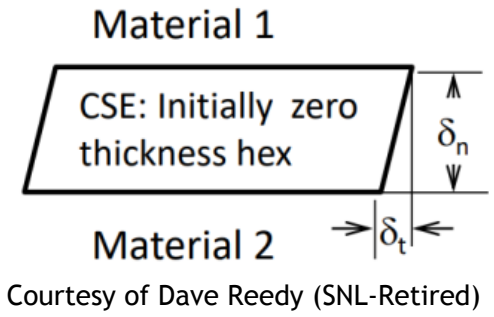

Courtesy of Dave Reedy (SNL-Retired)

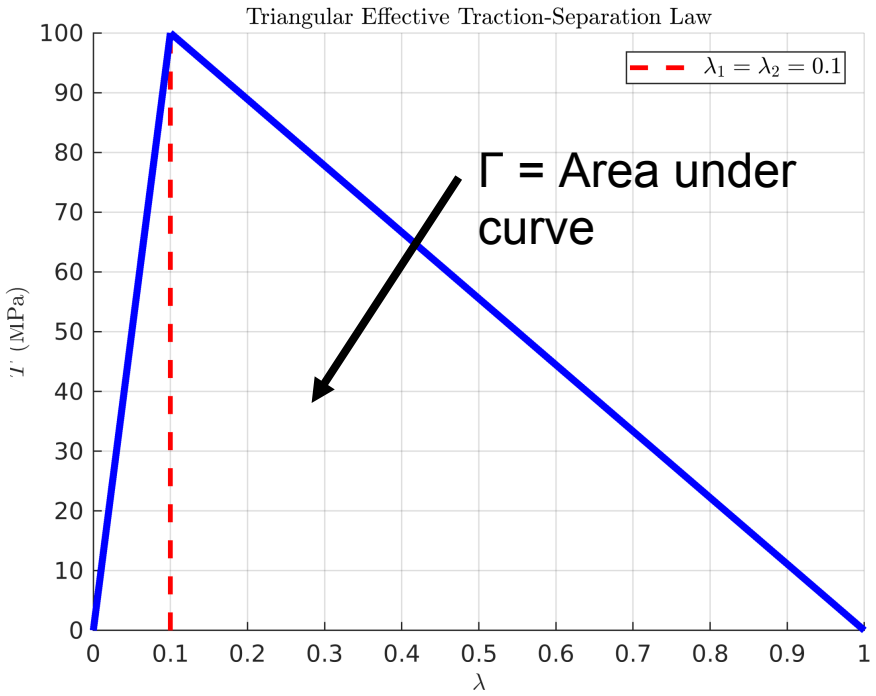

CZM Convergence Evaluation without Viscoelasticity

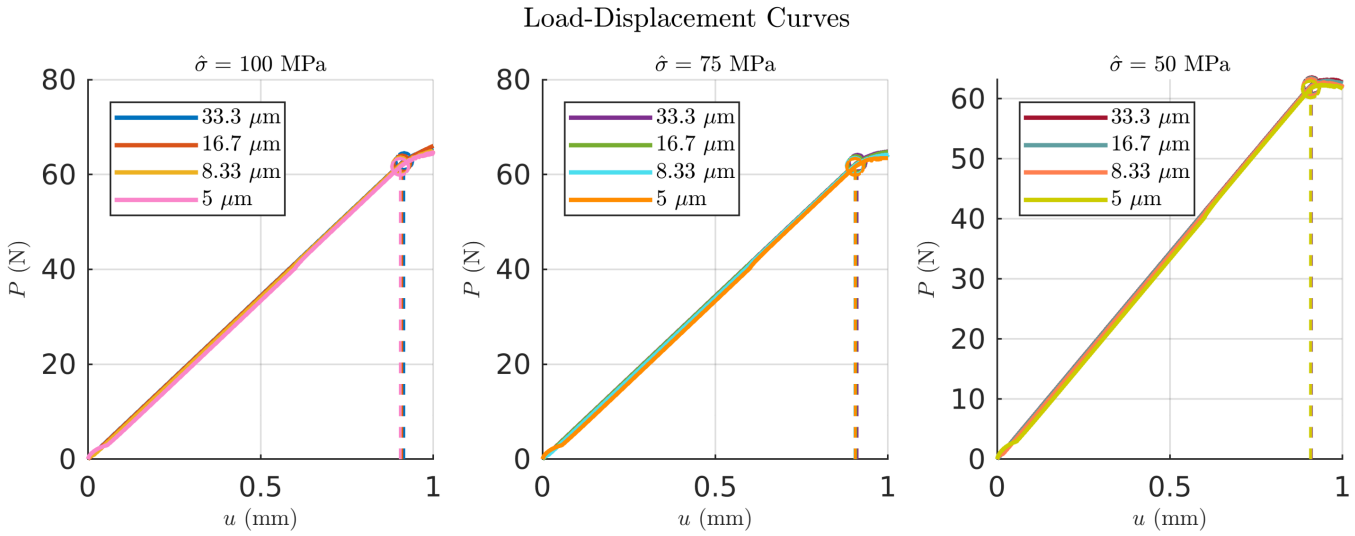

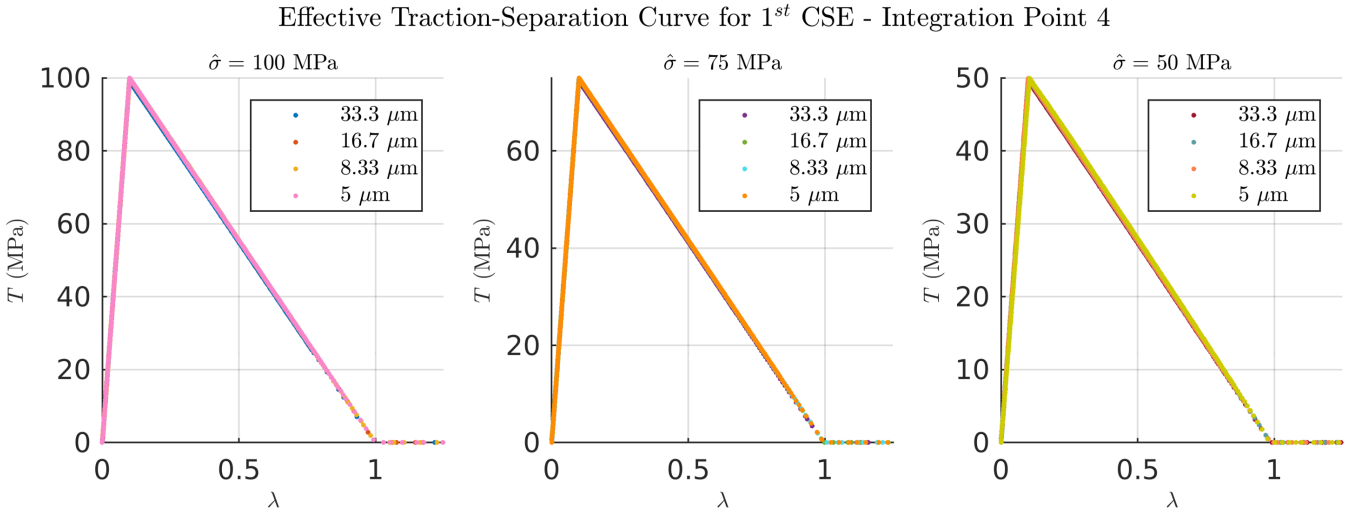

- Selected mesh size for CSE region: 16.7 μm
  - Excellent convergence – 0.5% relative error in Γ
  - Faster run times than smaller meshes

Appendix: Tabulated numerical results for toughness values

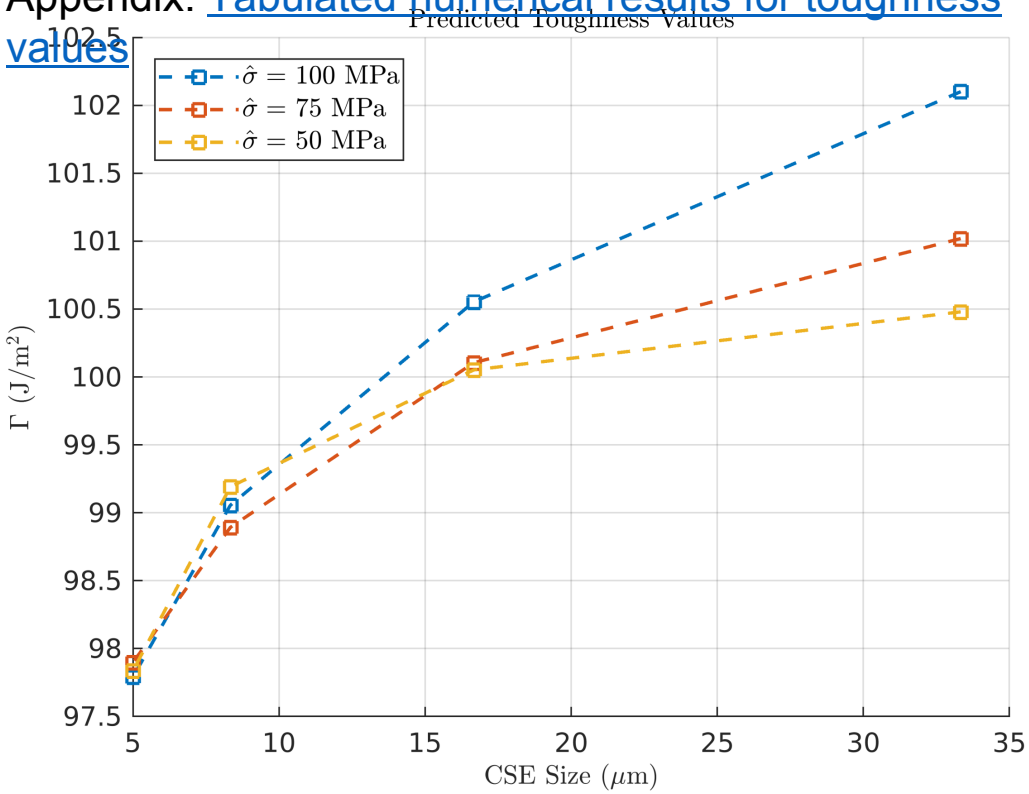

CZM Convergence Evaluation with Viscoelasticity

No Image

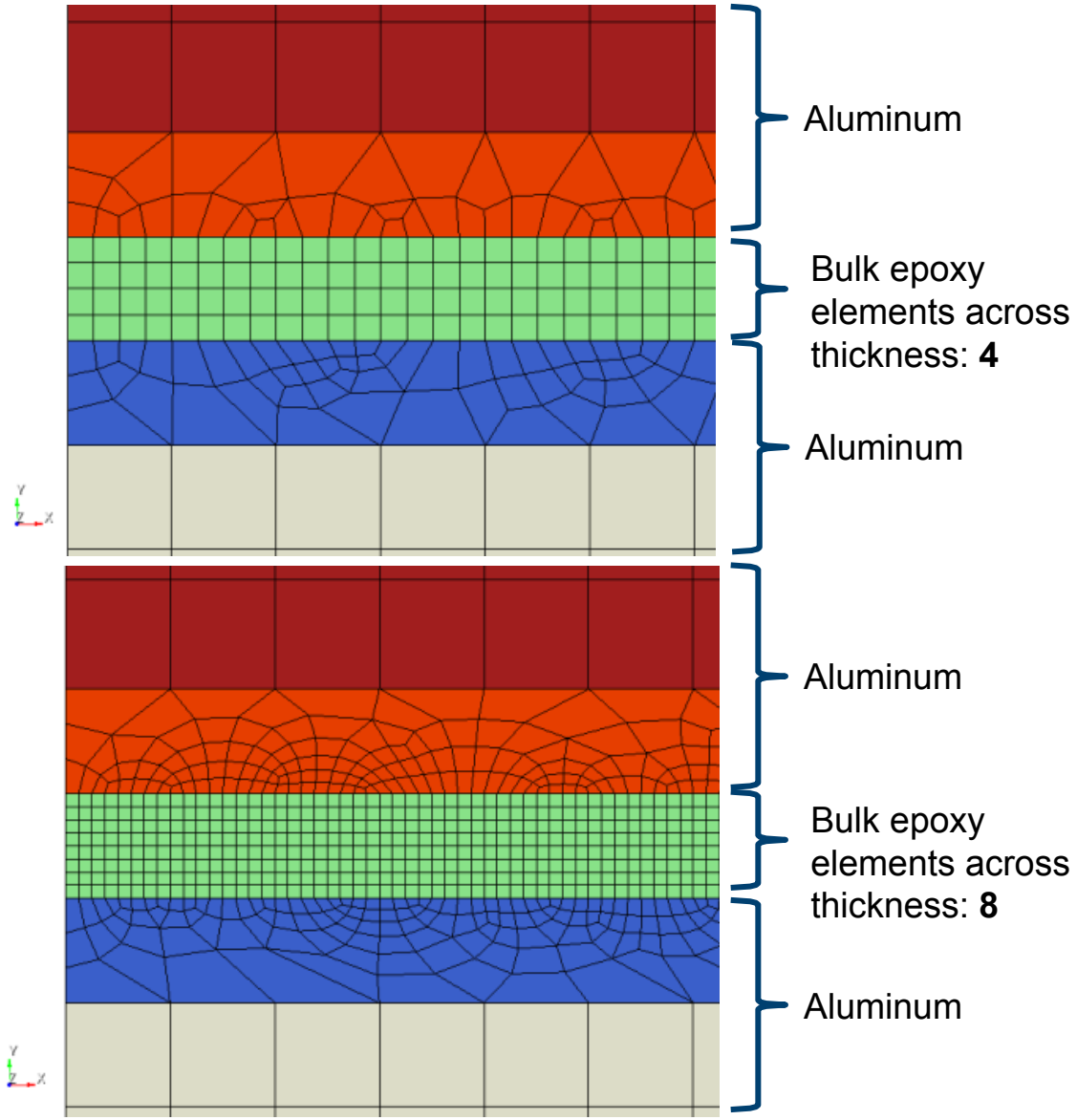

CZM Convergence Evaluation with Viscoelasticity

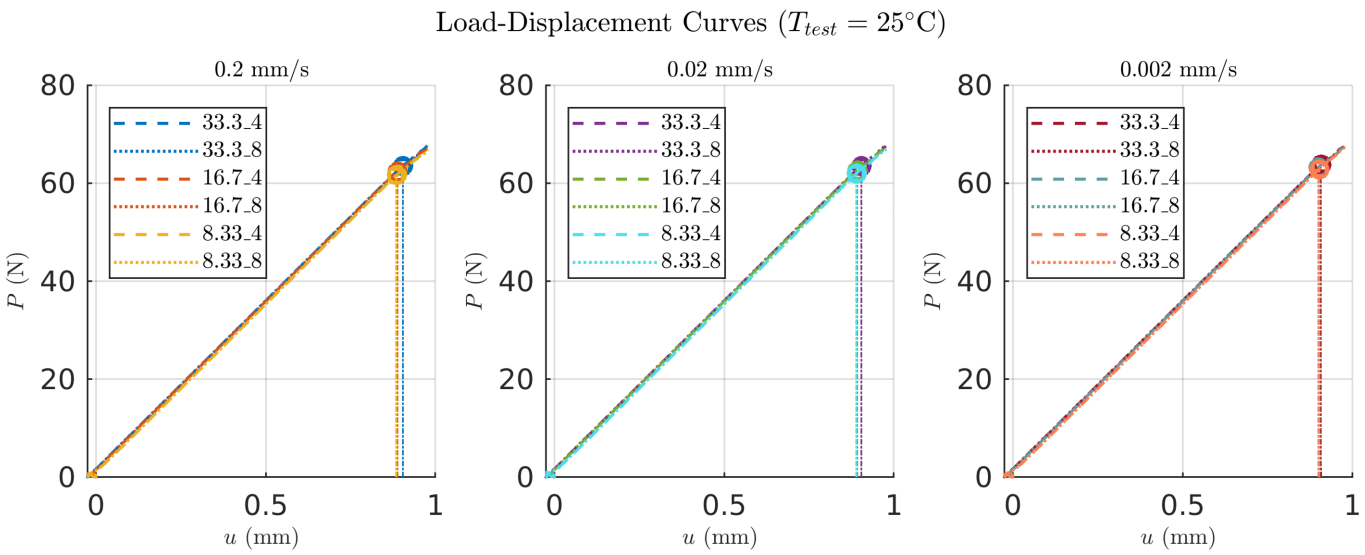

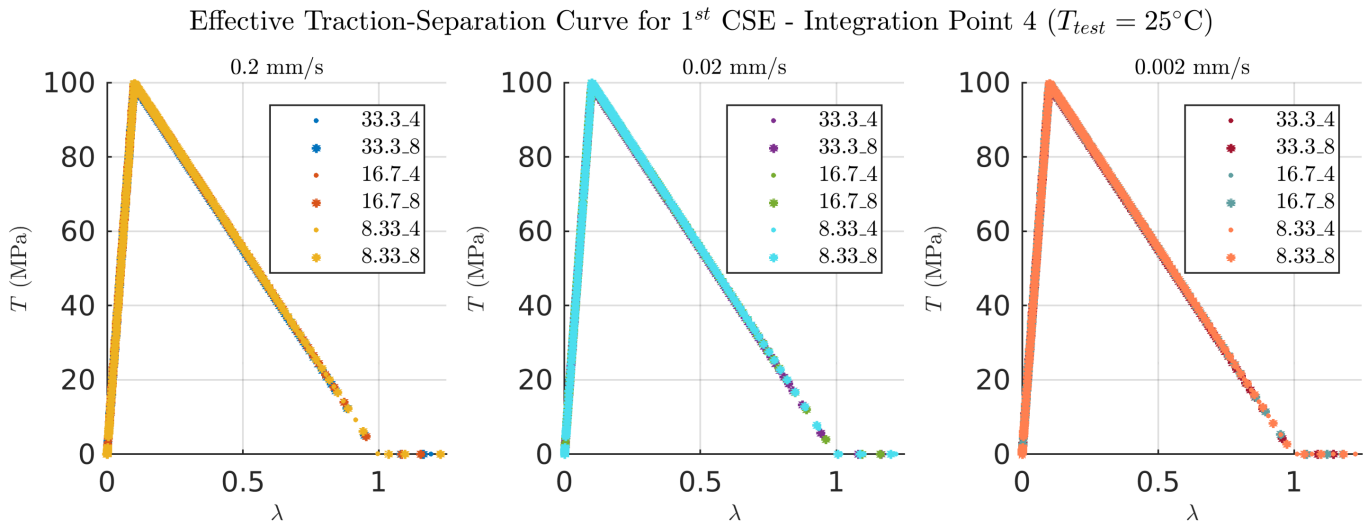

- Increased mesh sensitivity of predicted toughness values with viscoelastic epoxy behavior
- Effect likely to be more pronounced at higher test temperatures

Appendix: Tabulated numerical results for toughness values

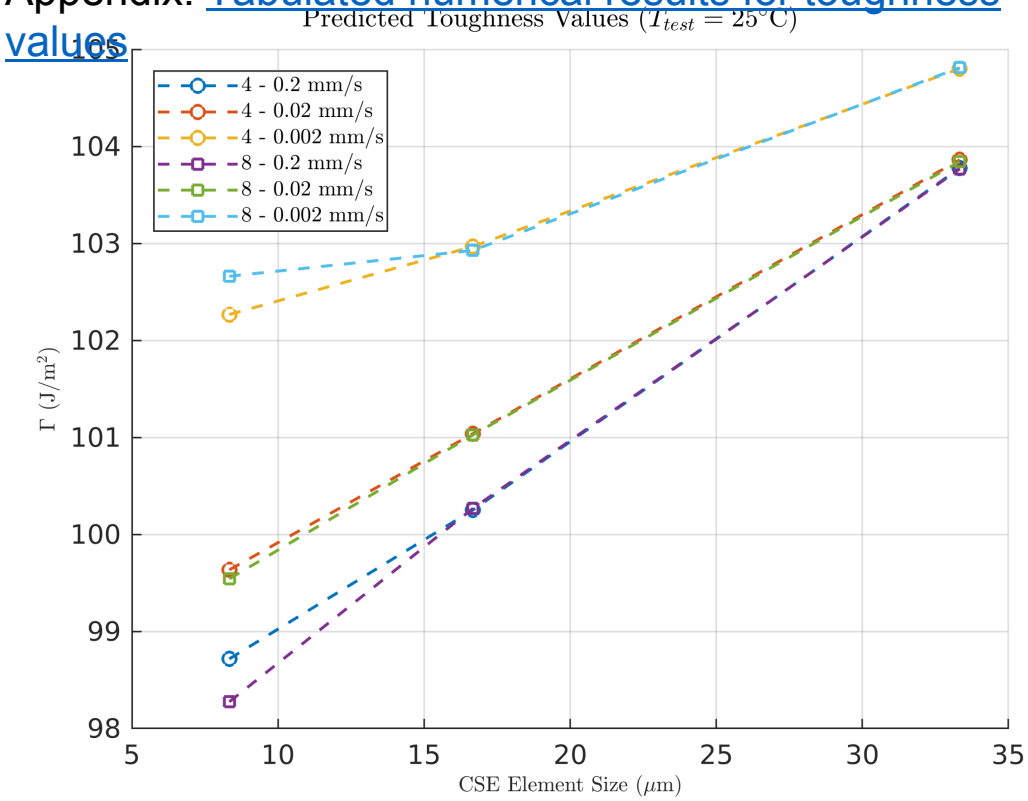

Convergence For Viscoelastic Without CSE elements

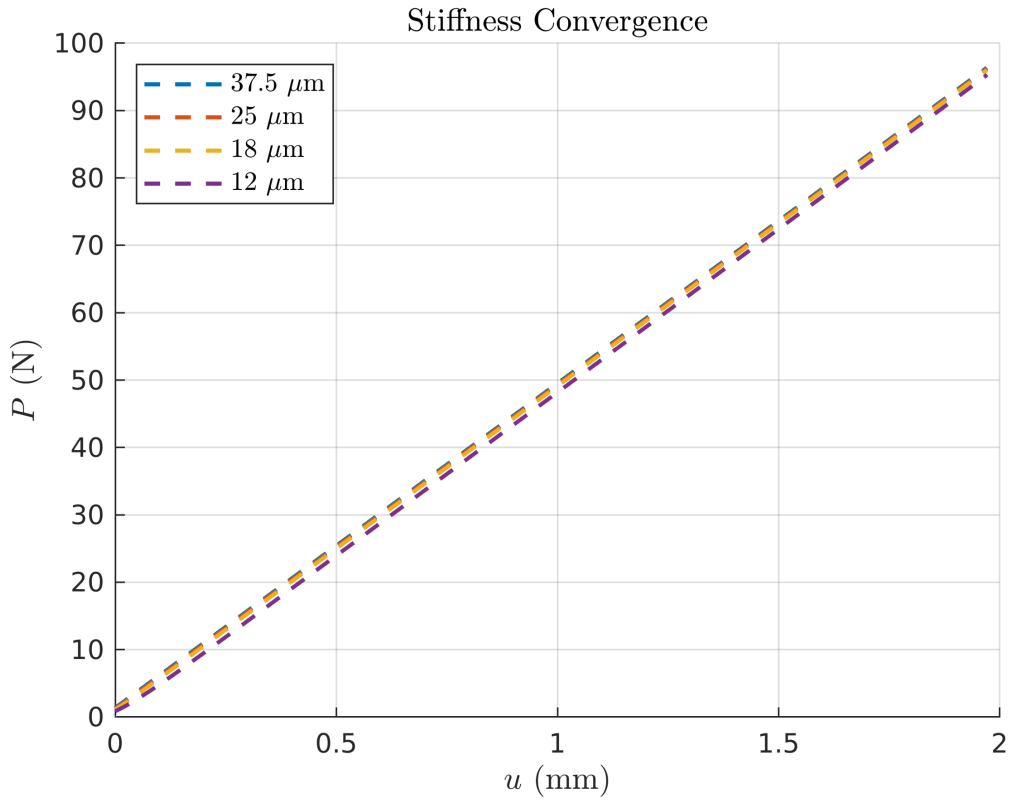

1% difference between stiffness of 37.5um and 12um mesh

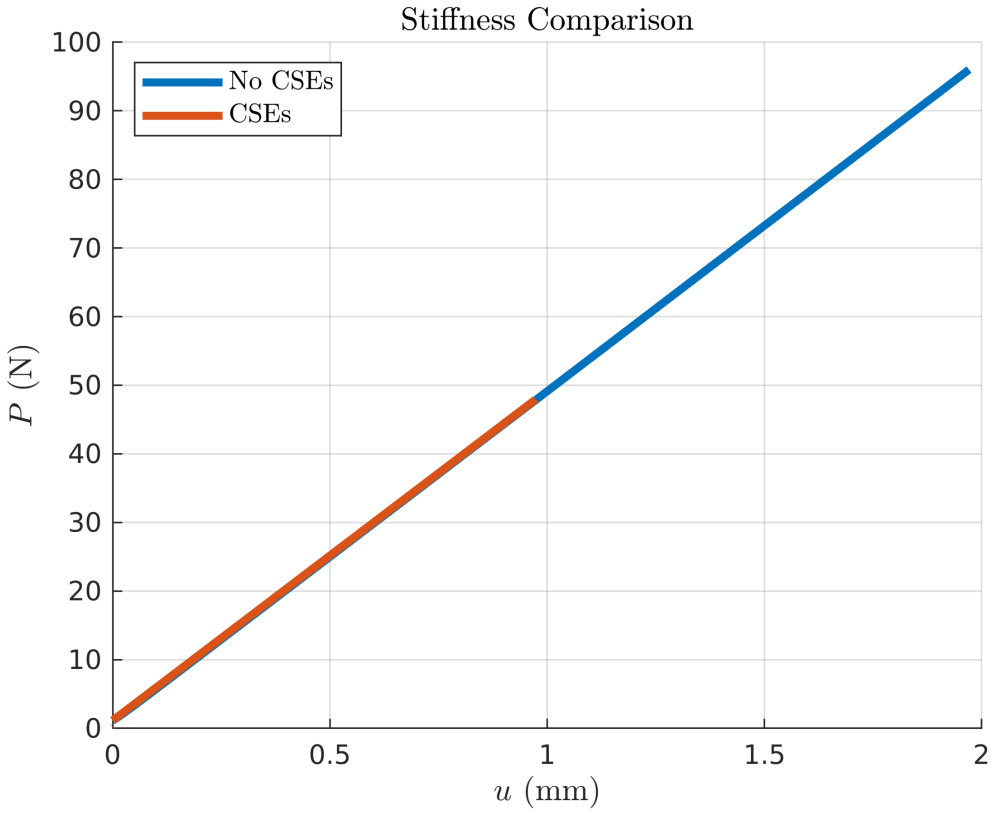

Good agreement on loading stiffness with and without cse elements

FULL SIMULATION

Full Simulation Results

No Image

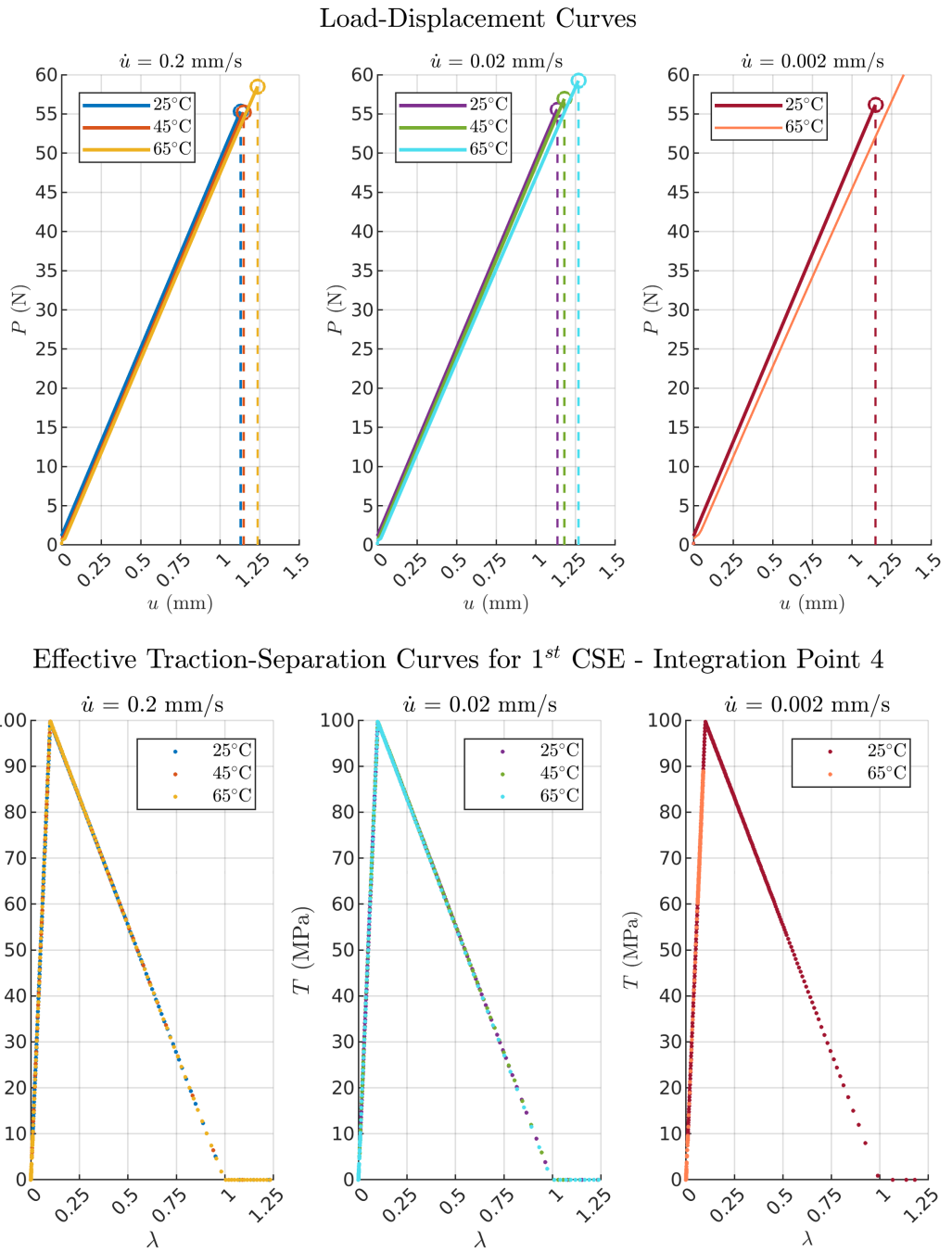

Full Simulation Results

No Image

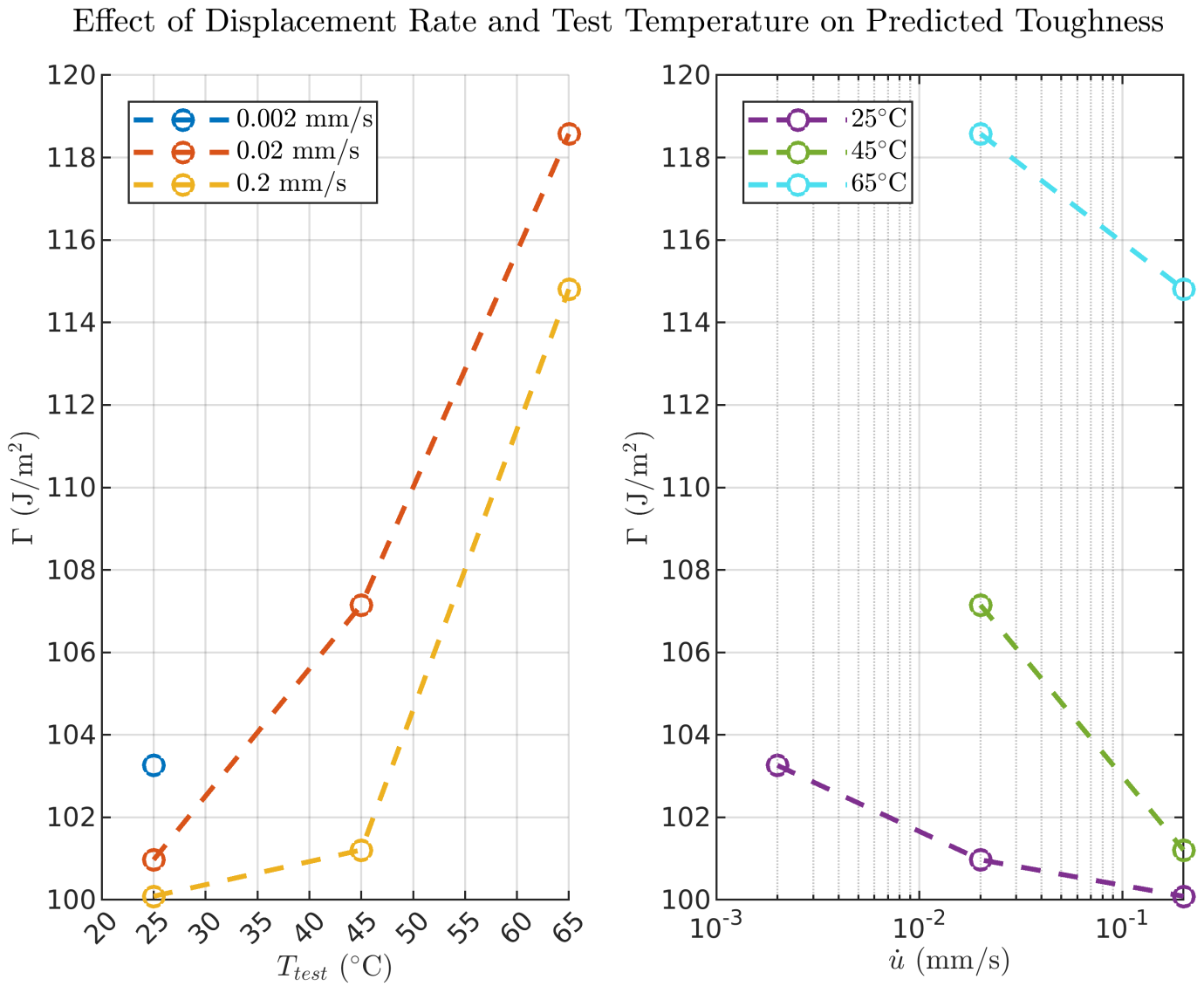

Appendix: Tabulated numerical results for toughness values

Comparison To Experimental Data

Loading Rate (mm/s)	True Crack Length	Actual Compliance (mm/N)	Predicted Compliance (70 mm crack)
0.2	70	1.99E-02	2.03E-02
0.02	70.5	2.03E-02	2.03E-02
0.002	70.1	2.00E-02	2.03E-02

Good agreement with compliance

Over predicts displacement at initiation

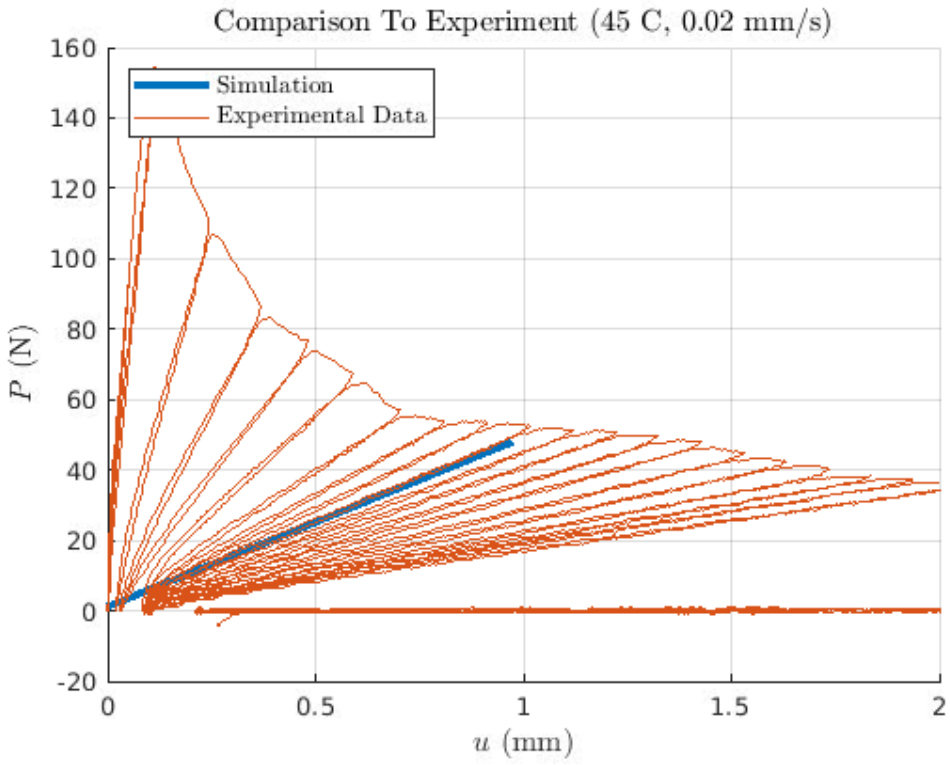

Varying Peak Traction at 65 C

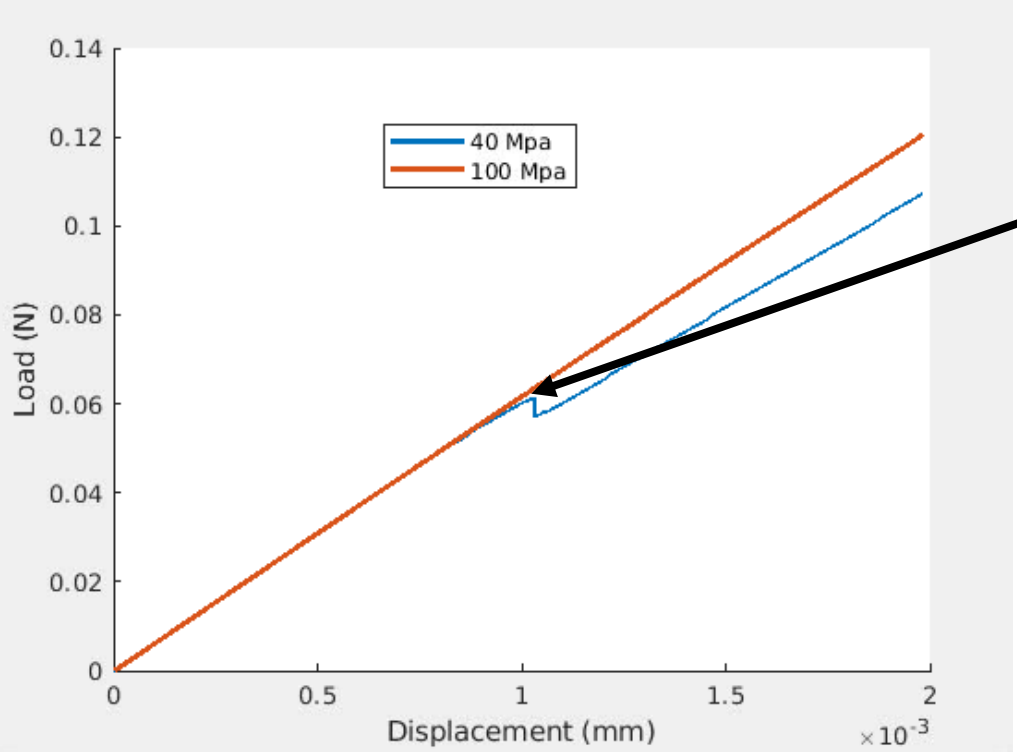

Fracture Initiation

Energy Release Rate For 40 Mpa Peak Traction: 80 J/um

Fracture does not occur with peak traction at 100 Mpa as this is far above yield at 65 C

Challenges and Next Steps

- Initially experienced stability issues in CSEs when using trapezoidal and rectangular traction -separation relationships
- Extreme localized deformation in epoxy at the crack tip observed during tests at 45 and 65 with 0.002 m/s displacement rate
- Determine appropriate cohesive zone model parameters for different temperatures and displacement rates to match future experimental data
- Expand quasi-plane stress model to full-width model

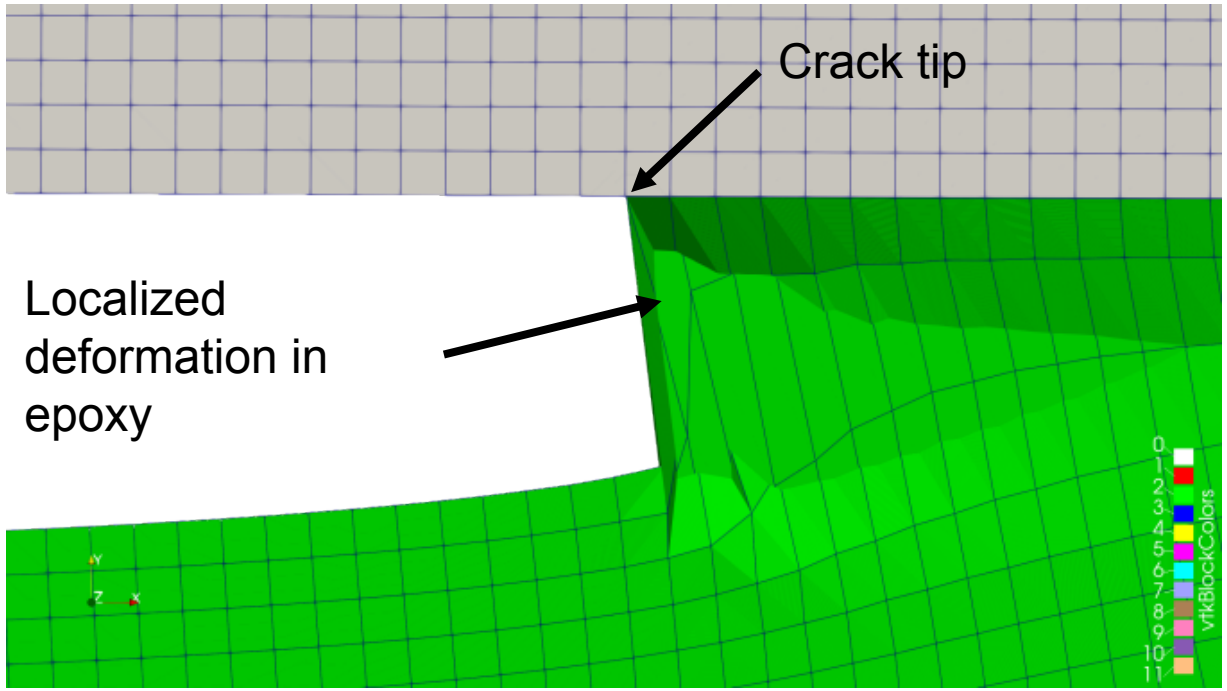

Acknowledgements

This research was conducted at the 2021 Nonlinear Mechanics and Dynamics Research Institute hosted by Sandia National Laboratories and the University of New Mexico.

Sandia National Laboratories is a multimission laboratory managed and operated by National Technology and Engineering Solutions of Sandia, LLC, a wholly owned subsidiary of Honeywell International, Inc., for the U.S. Department of Energy's National Nuclear Security Administration under contract DE-NA-0003525.

References

[1] K. Park and G. Paulino, “Cohesive Zone Models: A Critical Review of Traction-Separation Relationships Across Fracture Surfaces,” *Applied Mechanics Reviews*, vol. 64, no. 6, November, 2011.

APPENDIX

CZM Convergence without Viscoelasticity: Failure Conditions

33.3 µm, 100 MPa	0.915	62.854	102.101
16.7 µm, 100 MPa	0.909	62.338	100.553
8.33 µm, 100 MPa	0.905	61.952	99.055
5 µm, 100 MPa	0.904	61.925	97.790
33.3 µm, 75 MPa	0.911	62.473	101.019
16.7 µm, 75 MPa	0.907	62.184	100.105
8.33 µm, 75 MPa	0.904	61.886	98.892
5 µm, 75 MPa	0.905	61.941	97.897
33.3 µm, 50 MPa	0.910	62.261	100.479
16.7 µm, 50 MPa	0.0909	62.122	100.052
8.33 µm, 50 MPa	0.908	61.886	98.892
5 µm, 50 MPa	0.907	61.895	97.837

CZM Convergence with Viscoelasticity: Failure Conditions

33.3 µm, 0.2 mm/s, 4	0.903	63.521	103.776
16.7 µm, 0.2 mm/s, 4	0.888	62.386	100.251
8.33 µm, 0.2 mm/s, 4	0.885	61.705	98.717
33.3 µm, 0.02 mm/s, 4	0.903	63.547	103.862
16.7 µm, 0.02 mm/s, 4	0.892	62.623	101.038
8.33 µm, 0.02 mm/s, 4	0.889	61.990	99.635
33.3 µm, 0.002 mm/s, 4	0.907	63.829	104.801
16.7 µm, 0.002 mm/s, 4	0.900	63.214	102.968
8.33 µm, 0.002 mm/s, 4	0.901	62.803	102.267

33.3 µm, 0.2 mm/s, 8	0.903	63.520	103.767
16.7 µm, 0.2 mm/s, 8	0.887	62.392	100.268
8.33 µm, 0.2 mm/s, 8	0.883	61.566	98.275
33.3 µm, 0.02 mm/s, 8	0.903	63.542	103.843
16.7 µm, 0.02 mm/s, 8	0.891	62.625	101.026
8.33 µm, 0.02 mm/s, 8	0.888	61.962	99.542
33.3 µm, 0.002 mm/s, 8	0.907	63.834	104.812
16.7 µm, 0.002 mm/s, 8	0.899	63.208	102.928
8.33 µm, 0.002 mm/s, 8	0.903	62.923	102.662

Full Simulation: Failure Conditions

1.148	56.169	103.260
1.136	55.547	100.970
1.130	55.307	100.086
-	-	-
1.180	56.924	107.147
1.149	55.207	101.207
-	-	-
1.268	59.248	118.575
1.236	58.506	114.807

Investigating the Potential of Electrical Connection Chatter Induced by Structural Dynamics

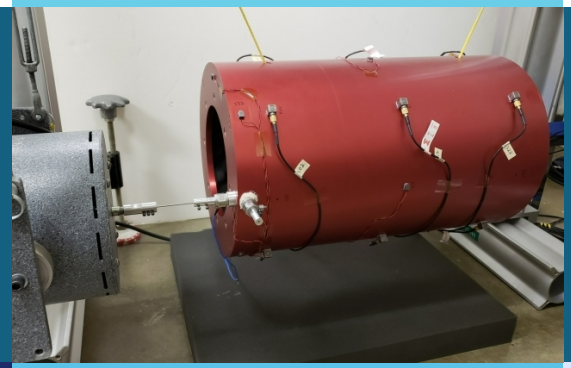

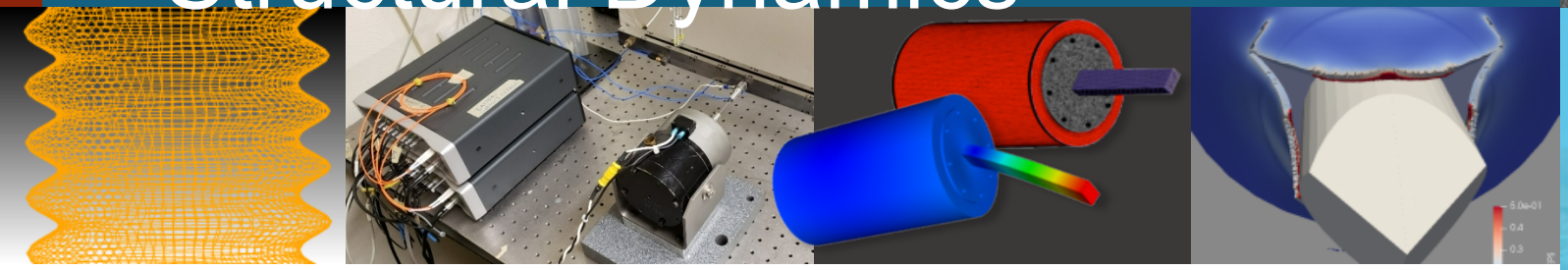

Students: Benjamin Dankesreiter, Manuel Serrano, Jonathan Zhang

Mentors: Benjamin R. Pacini, Karl Walczak, Kelsey Johnson, Robert Flicek, Benjamin Zastrow, Changdong Yeo (TTU)

Sandia National Laboratories is a multimission laboratory managed and operated by National Technology & Engineering Solutions of Sandia, LLC, a wholly owned subsidiary of Honeywell International Inc., for the U.S. Department of Energy's National Nuclear Security Administration under contract DE-NA0003525.

Agenda

Project Motivation

Summary of Previous Work

Goals for NOMAD 2021

Reality Check for NOMAD 2021

Pin-Receptacle Modelling

Future Work

Closing Remarks

Project Motivation

All modern systems rely on electrical components to function as designed.

Therefore, it is critical to ensure that electrical connections are **reliable** and **maintain electrical continuity** in **all operating environments**.

Under sufficiently large vibrations, the **resistance** between two components may rise such that **electrical signals can no longer be transferred.** This phenomenon is called **electrical chatter**.

Chatter is extremely **application specific** and it is defined differently depending on the system. A typical definition for chatter is when resistance exceeds 125 Ω for more than 25 ns.

Chatter is a complicated phenomenon whose root causes are **not well understood** and

Goal: Investigate the influences of structural dynamics on electrical chatter and develop/validate a reduced order model to accurately simulate chatter events.

Chatter is Complicated!

Several Engineering Disciplines

- Structural Dynamics
- Contact Mechanics
- Tribology
- Electrostatics

+

Wide Time Scale Range

- Short Duration Chatter Events (ns)
- Extended Duration Vibration Environments (s)

+

Wide Length Scale Range

- Surface Features (μm)
- Structural Length Scale (m)

=

Chatter

Previous Work

NOMAD 2019:

- Designed a test bed to measure electrical chatter
- Complicated test fixture which did not fully allow chatter to be isolated

Ben Zastrow et al. (1556):

- Developed and simulated a high-fidelity pin-receptacle in SIERRA/SM
- Simulation duration: **3-5 ms**
- Runtime on HPC's: **4 days**

Takeaway 1: A test fixture which does not influence the pin-receptacle structure is needed.

Takeaway 2: Although the high-fidelity model is powerful, it is too expensive to run. A simpler model which preserves accuracy is needed.

Goals for NOMAD 2021

Use a new test fixture design to excite a pin and receptacle, try to induce chatter.

- Modal hammer tests
- Shaker random vibration tests

Develop a Hurty/Craig-Bampton reduced-order model which can accurately simulate chatter events

- Validate the model against B. Zastrow's SM simulations and experimental data
- Test different contact formulations in the reduced-order model
- Significantly reduced computational cost

Determine an empirical relationship between contact force and electrical resistance with AFM measurements and incorporate this into the reduced-order model

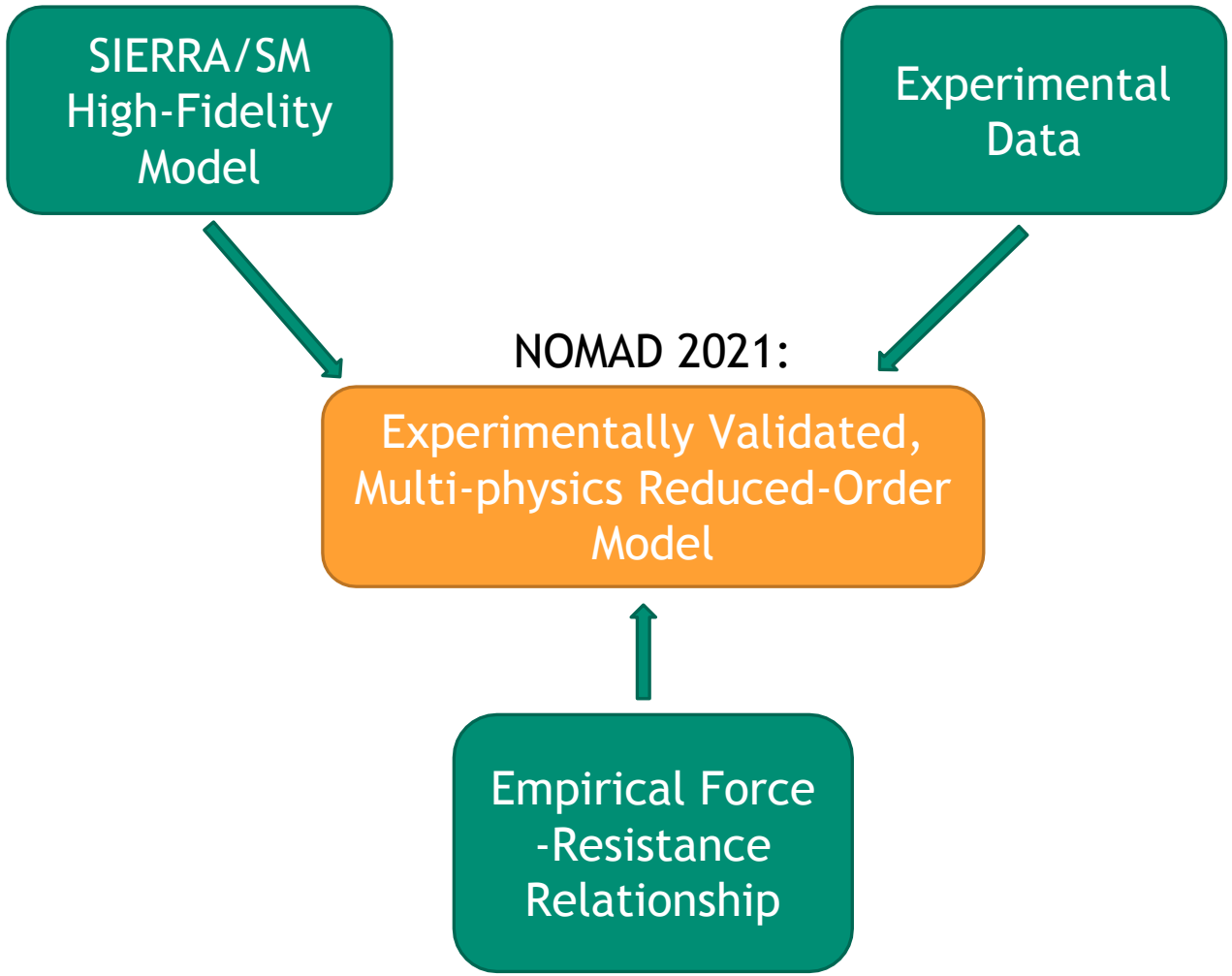

Reality Check for NOMAD 2021

Challenges associated with experimental setup – no data available.

- Resulted in a pivot to computational analysis only

Developed a Hurty/Craig-Bampton reduced-order model which can accurately simulate chatter events

- Validated the model against B. Zastrow's SM simulations
- Tested different contact formulations in the reduced-order model

Determined an empirical relationship between contact force and electrical resistance with AFM measurements, but did **not** incorporate this into the reduced-order model

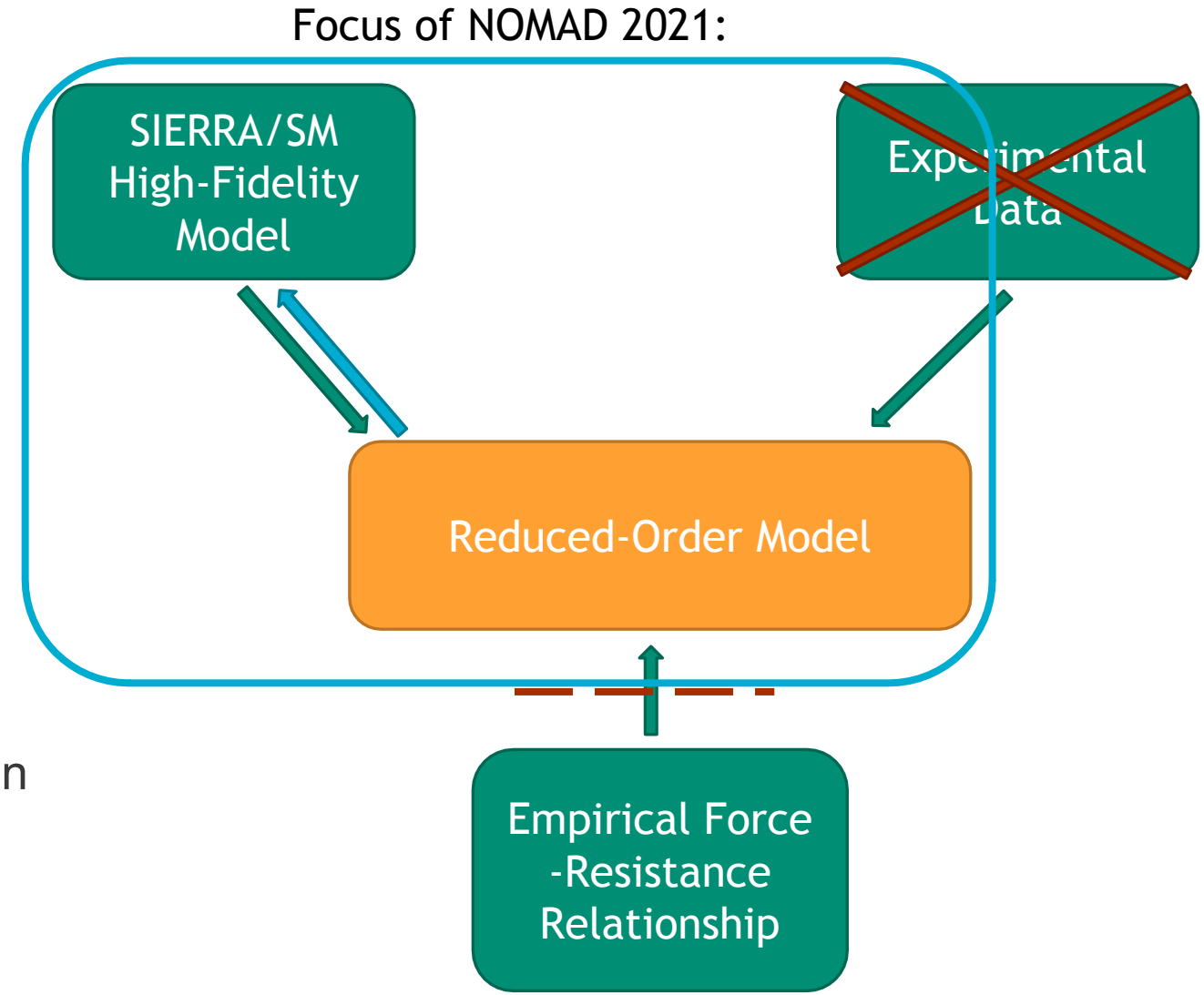

Measuring an Empirical Relationship between Contact Force and Electrical Resistance

Atomic Force Microscope and Optical Profiler Measurements

Goal: To measure surface features of the pin and receptacle and develop an empirical relationship between contact force and electrical resistance.

$$R_e = \frac{(V_2 - V_1)}{I} = \frac{(\rho_1 + \rho_2)}{Q}$$

$$\frac{dF}{dw} = MQ$$

$$C \equiv \frac{1}{R_e} = \frac{1}{M(\rho_1 + \rho_2)} \frac{dF}{dw}$$

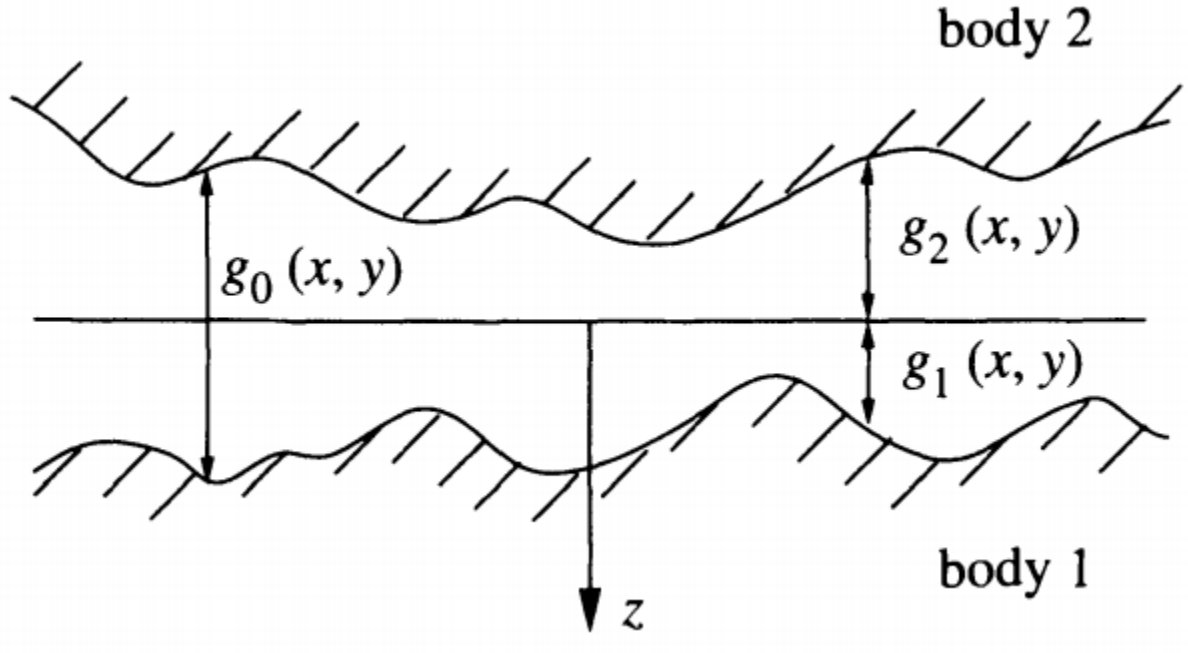

R_e = Resistance, V = Voltage, I = Current, Q = Total Flux, $\frac{dF}{dw}$ = Incremental Stiffness, M = Composite Modulus, C = Conductivity

But these calculations require the knowledge of how many asperities share the applied load in a given contact occurrence. Therefore, the roughness of the surfaces need to be found.

Barber, J. R. (2003). Bounds on the electrical resistance between contacting elastic rough bodies. Proceedings of the Royal Society of London. Series A: Mathematical, Physical and Engineering Sciences, 459(2029), 53–66. https://doi.org/10.1098/rspa.2002.1038

Atomic Force Microscope and Optical Profiler Measurements

Challenges:

Pin surface had rough machining marks from lathe, opted for profiler measurements

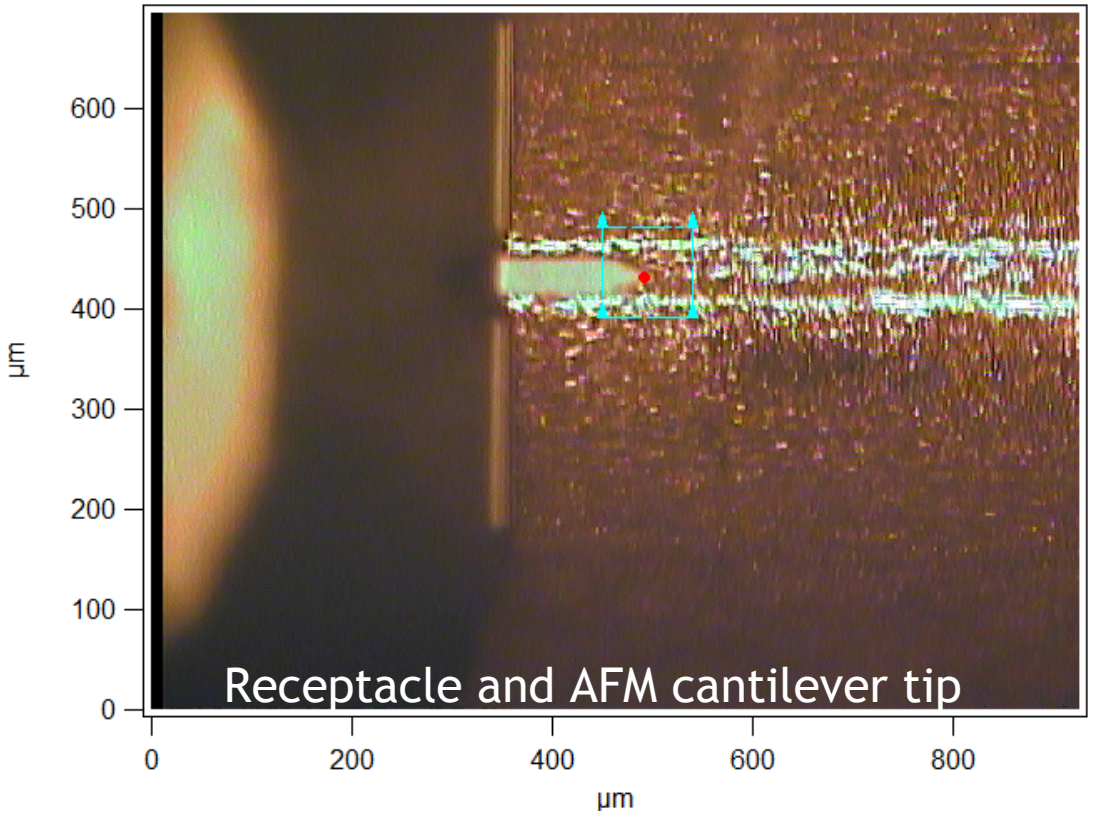

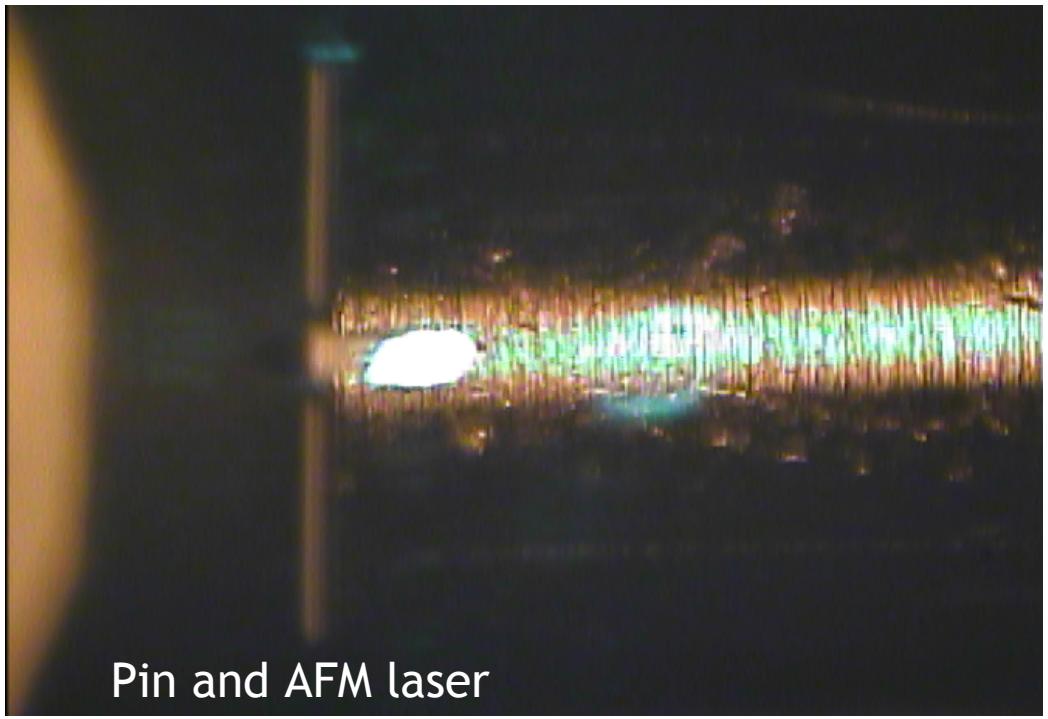

Additional Considerations: Oxidation, Temperature, Surface vs Bulk properties

Developing a Reduced Order Model for the Pin-Receptacle

Motivation → Previous Work → NOMAD Goals → Pin-Receptacle Modeling → Future Work

Pin-Receptacle Reduced Order Model

Goal: Develop a model which can be solved much faster while maintaining physical accuracy as much as possible.

Approach: Use the Hurty/Craig-Bampton reduction method, whose code is built into SIERRA/SD.

Basic Idea: Divide model into “interface set” and fixed-interface mode shapes.

$$\boldsymbol{u} \rightarrow \begin{Bmatrix} \boldsymbol{u}_{\text{interface}} \\ \boldsymbol{u}_{\text{leftover}} \end{Bmatrix} = \boldsymbol{\Phi}_{CB} \begin{Bmatrix} \boldsymbol{u}_{\text{interface}} \\ \underbrace{\boldsymbol{q}}_{\substack{\text{fixed-interface} \\ \text{mode shapes}}} \end{Bmatrix}$$

Can specify BC’s at the interface nodes as required

Significantly reduce size of model

Number of interface mode shapes is arbitrary, depending on quantities of interest in analysis

Pin-Receptacle Reduced Order Model

SIERRA/**SD** used to perform reduction. Outputs are the system mass and stiffness matrices.

After reduction, the system is propagated in time using MATLAB and a Newmark-Beta ODE solver

But, developing a reduced-order model is not as simple as typing “cbr” in the input file…

Critical questions for any reduced model:

1. How many **modes** do we need to include?
2. Which nodes should be placed in the **interface set**?
3. How do we model the **contact interaction** between the pin and receptacle?
4. What are the relevant **boundary conditions**?

Pin-Receptacle Reduced Order Model

Modes:
- First 20 modes of the structure are used

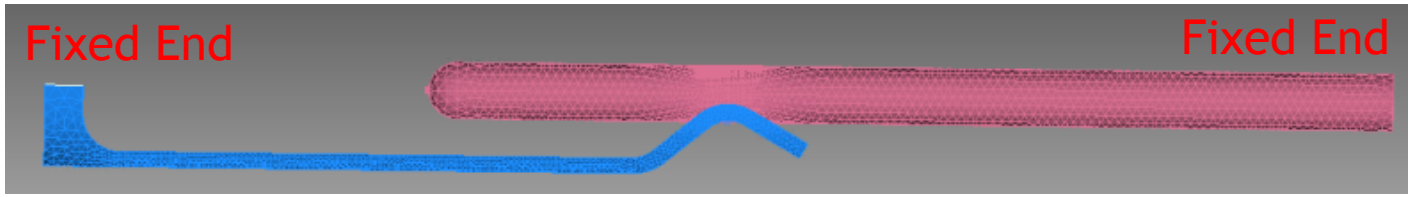

Interface Set:
- Seven nodes in the interface set, four are subjected to BC's, leaving three nodes (9 DOF)
- Physical significance of three interface nodes:
  - One node on the inner surface of the receptacle arm
  - One node on the outer surface of the pin
  - One node on the outer surface of the receptacle arm

Boundary Conditions:
- Fixed at the ends of the structure

Contact Formulation
- Initially a linear penalty spring
- More to come…

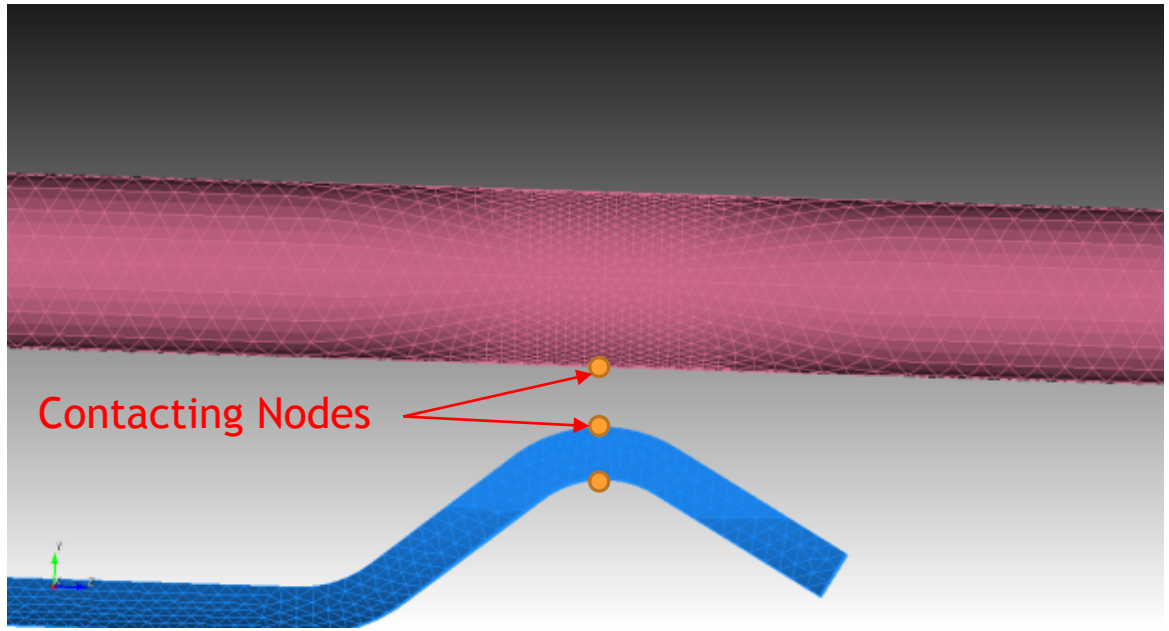

Pin-Receptacle Reduced Order Model

SIERRA/SM High-Fidelity Model:

215,773 Elements
Time to simulate: 4 days

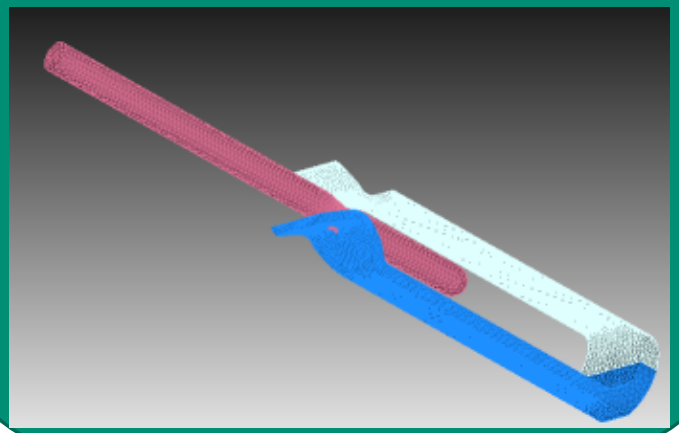

Reduces to:

MATLAB CB Model:

Number of Modes: 20
Number of Interface DOFs: 7

Total System Size: 29 x 29

$$M_{CB} = \begin{bmatrix} \cdots & \cdots \\ \cdots & \cdots \end{bmatrix}; \; K_{CB} = \begin{bmatrix} \cdots & \cdots \\ \cdots & \cdots \end{bmatrix}$$

Time to generate reduced matrices: 5 min
Time to simulate: 25 min

We go from 4 days on the HPC to 30 min on a basic workstation…**230x** reduction in computing time!

Contact Model Fitting

Goal: To most accurately model the contact force interaction between the pin and receptacle.

Approach: Using SM data, fit an expression for contact force, $F_c(x) = F_c(x)H(x)$ where x denotes the gap distance between nodes in contact and $H(x)$ is the Heaviside step function.

Several candidate forms for the contact interaction:

$F_c = Kx$

Linear:

$$F_c = K_0 + K_1 x + K_2 x^2 + \ldots + K_n x^n$$

Polynomial:

$$F_c = \frac{a_n x^n + a_{n-1} x^{n-1} + \ldots + a_2 x^2 + a_1 x + a_0}{b_m x^m + b_{m-1} x^{m-1} + \ldots + b_2 x^2 + b_1 x + b_0}$$

Rational:

$$F_c = \begin{cases} m_1 x + b_1 & x < a \\ m_2 x + b_2 & x \geq a \end{cases}$$

Piecewise Linear:

$$F_c = ax\exp(bx)$$

Exponential:

Contact Model Fitting

Polynomial:

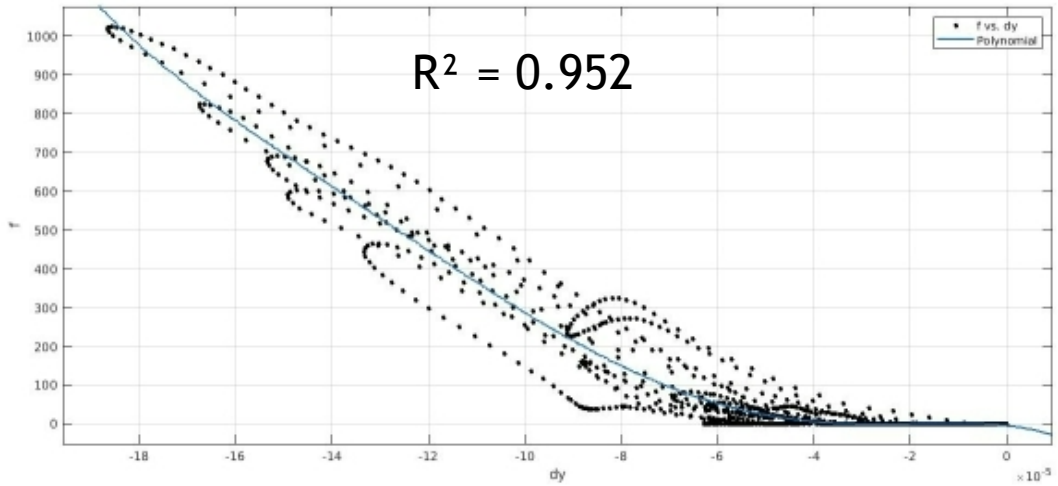

Rational:

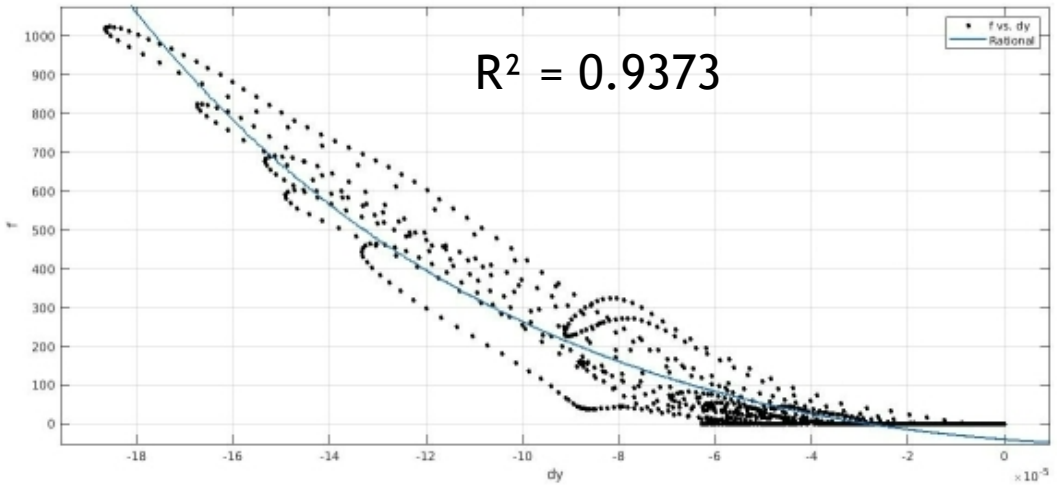

Piecewise Linear:

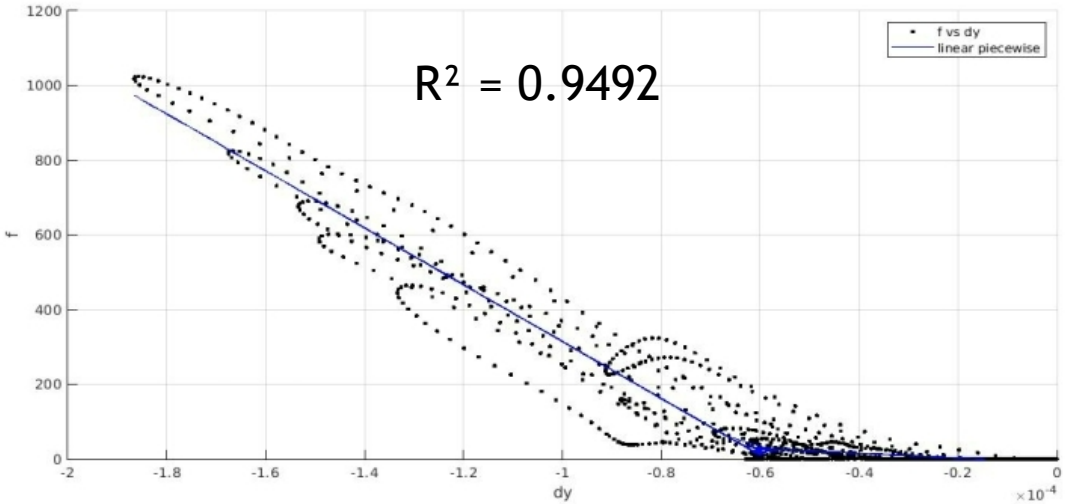

Exponential:

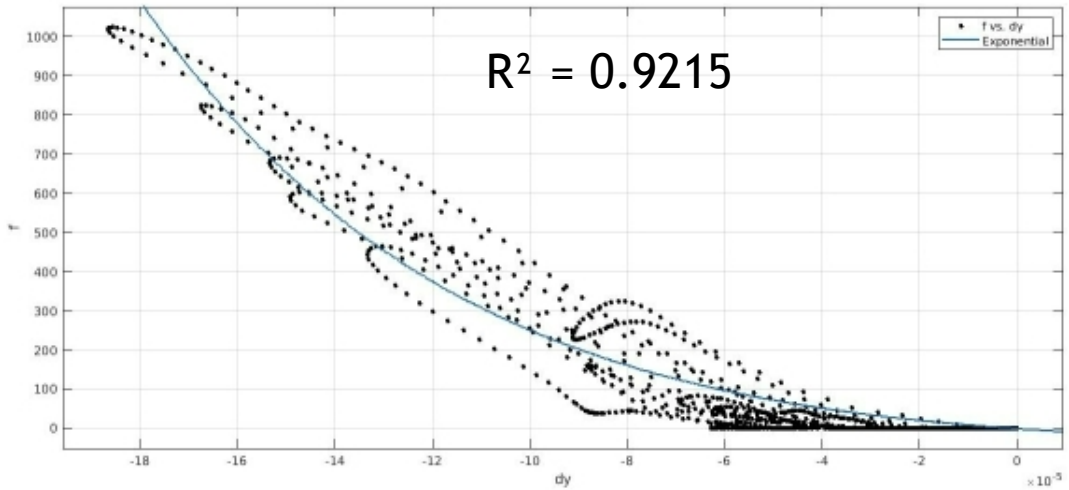

Contact Model Fitting

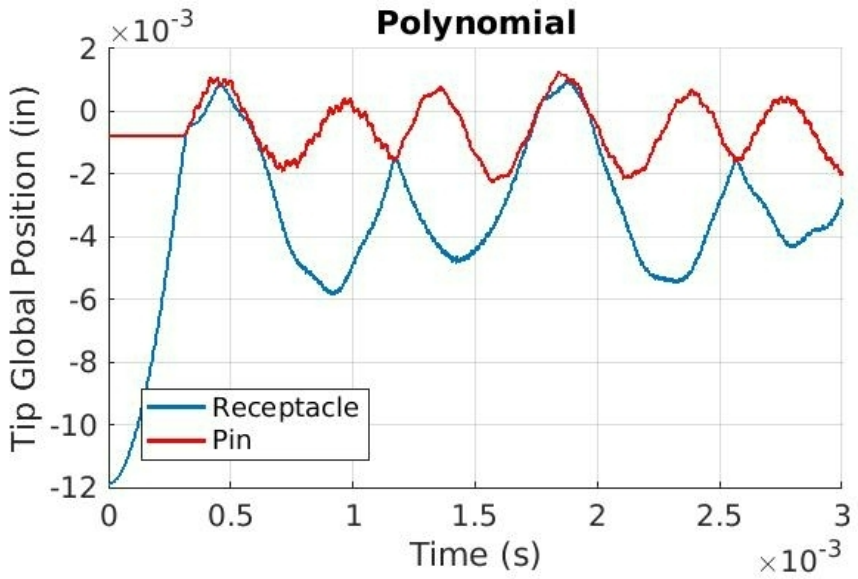

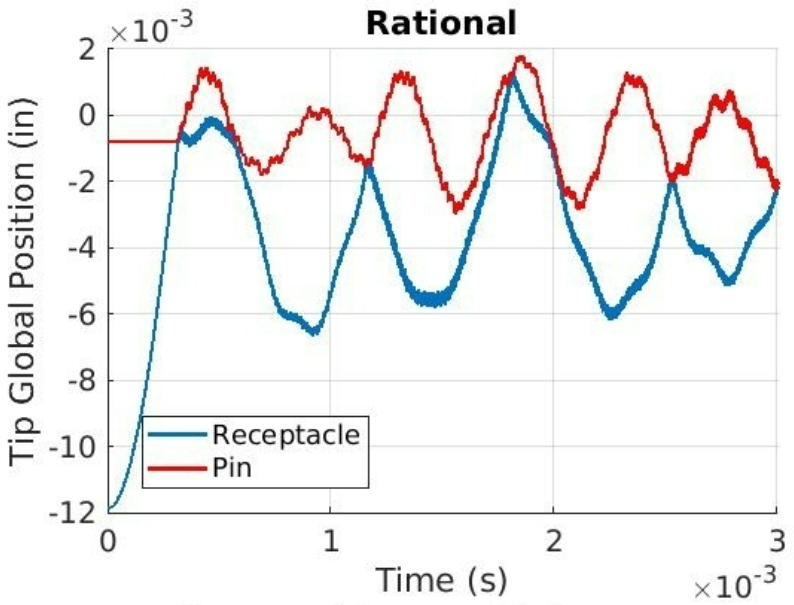

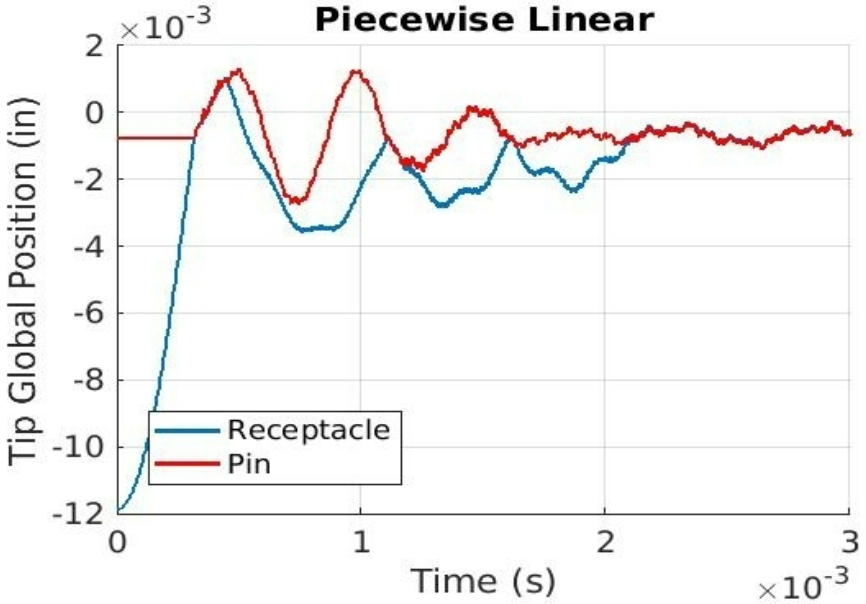

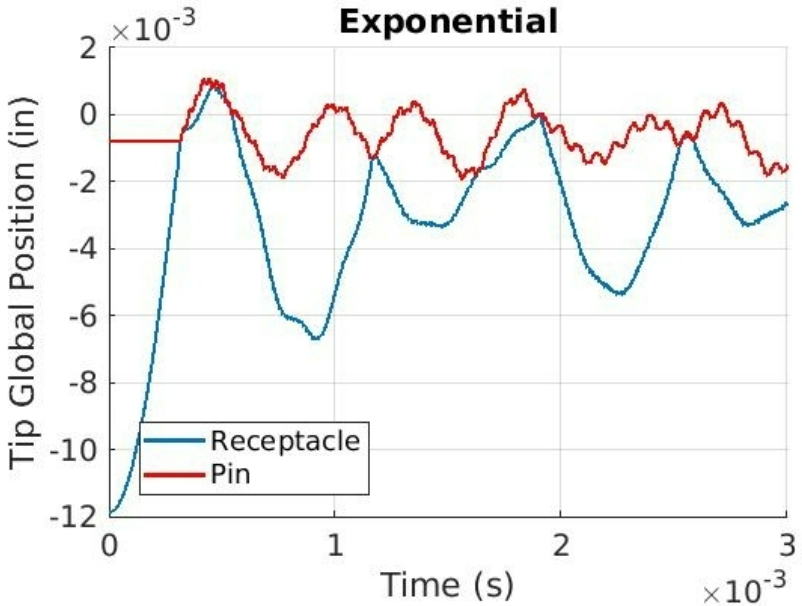

Validating the Reduced Order Model Against the High-Fidelity Model

Time Histories

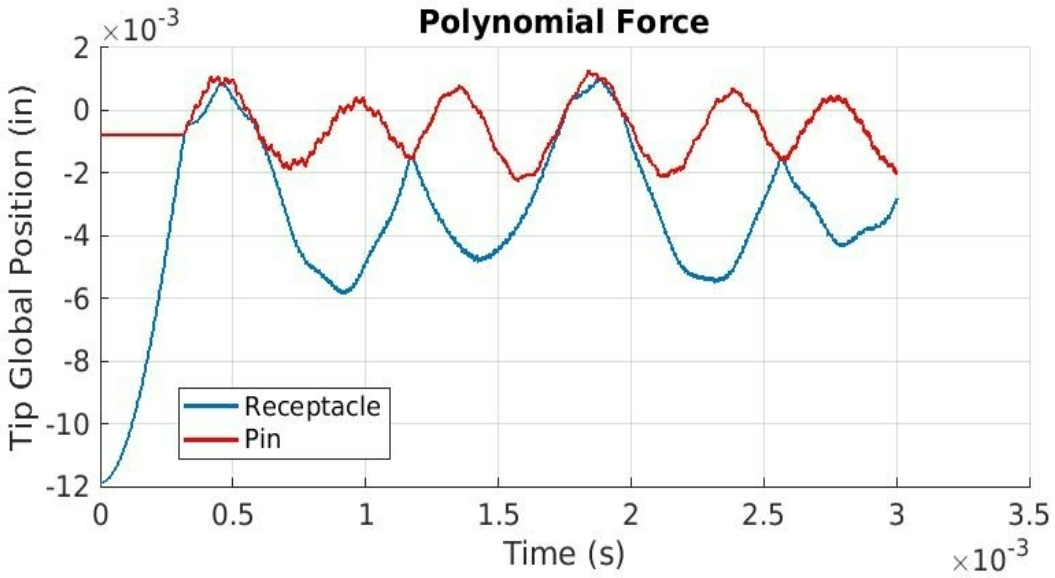

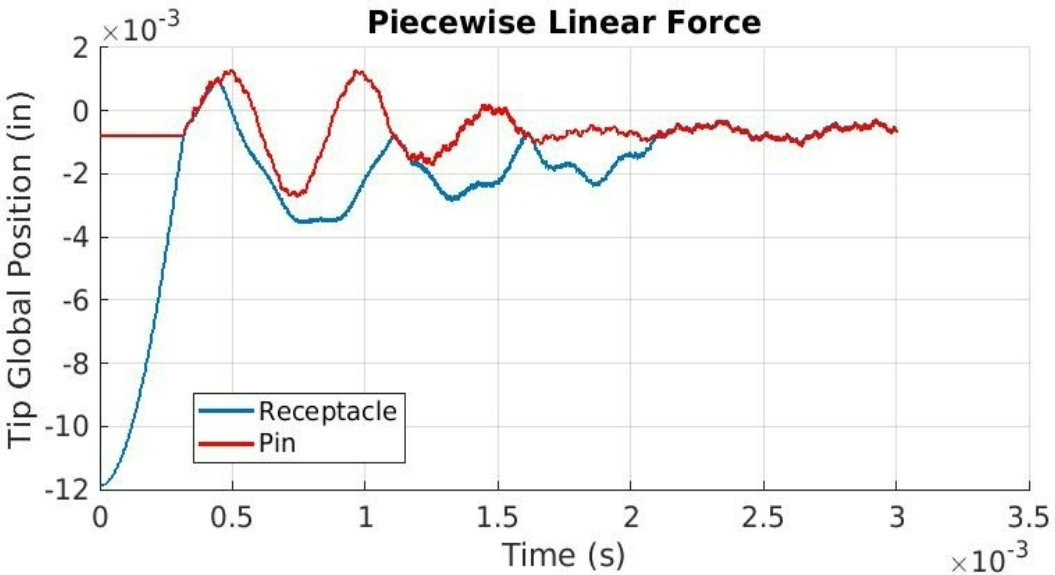

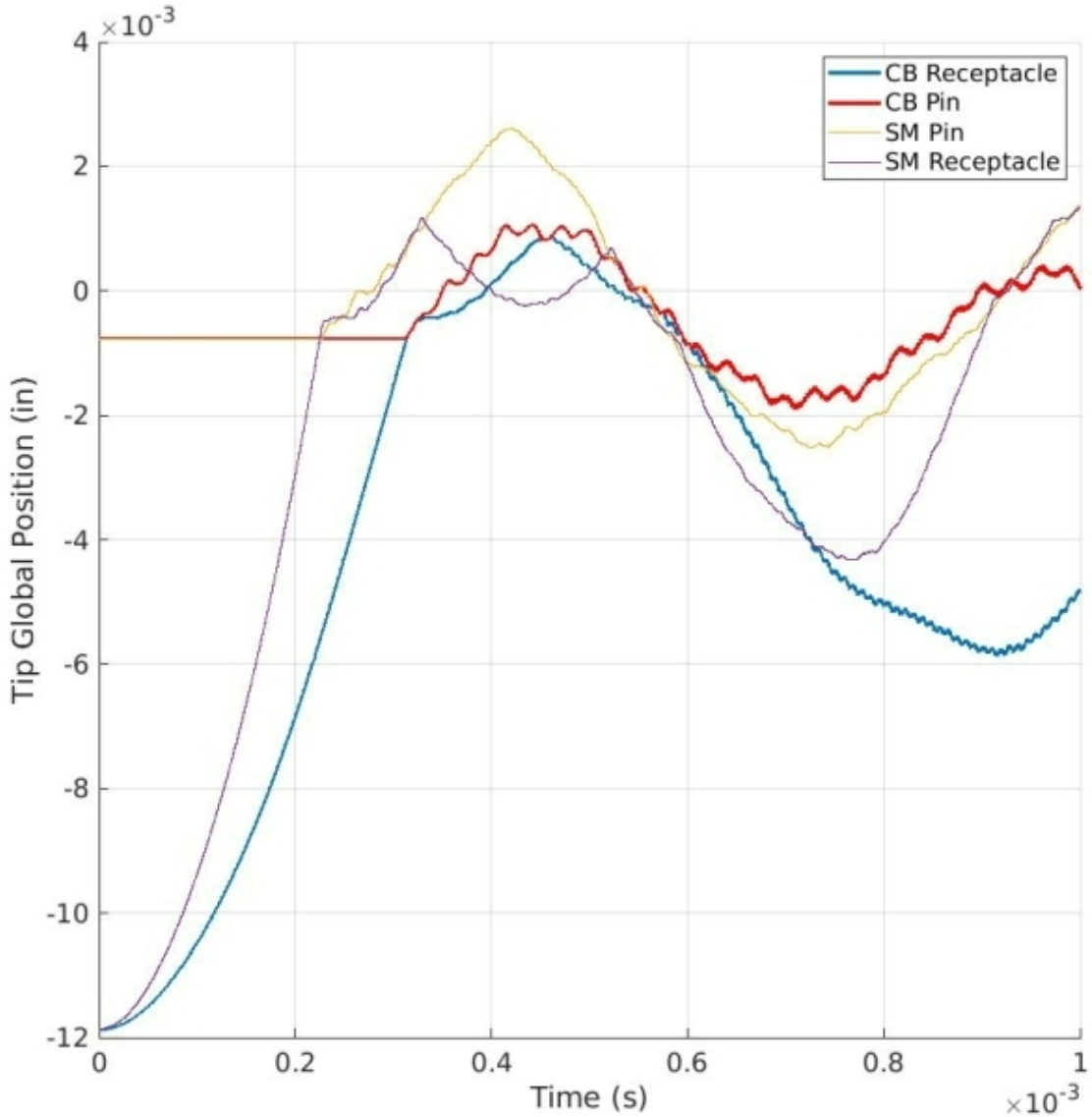

CB vs SM Wavelet transform

SM Model

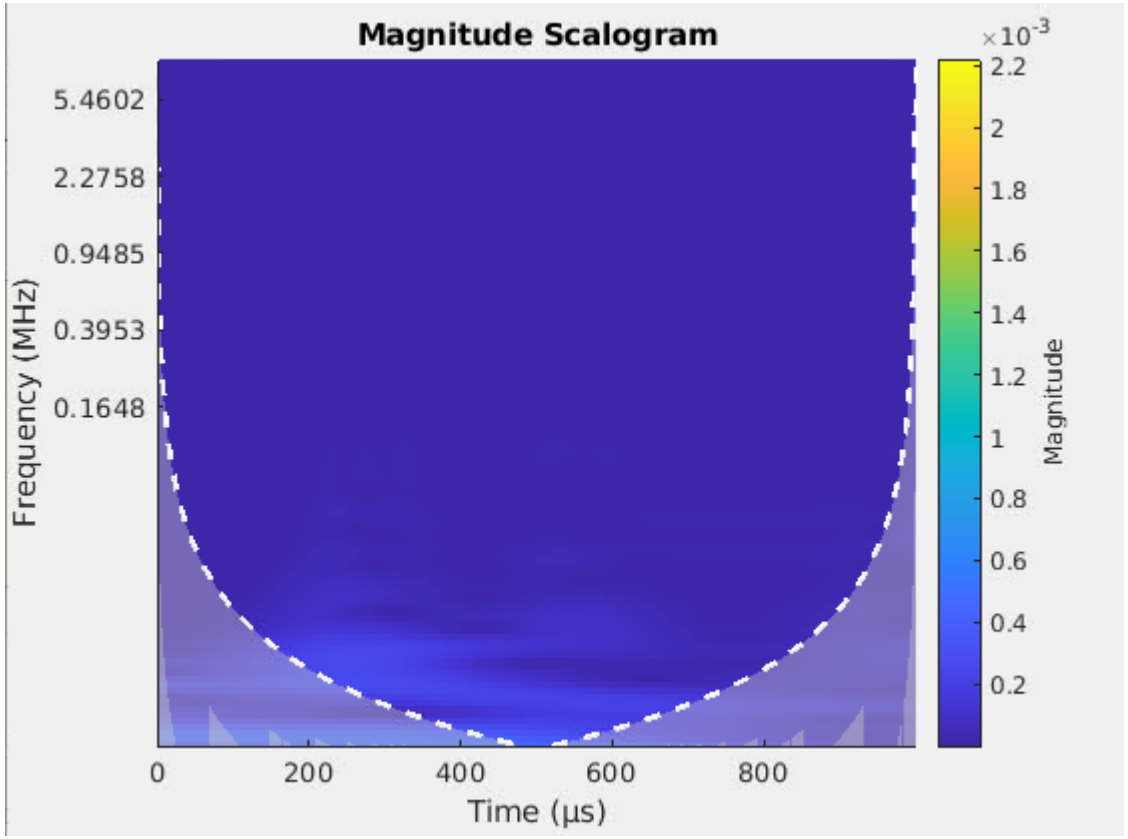

CB Model

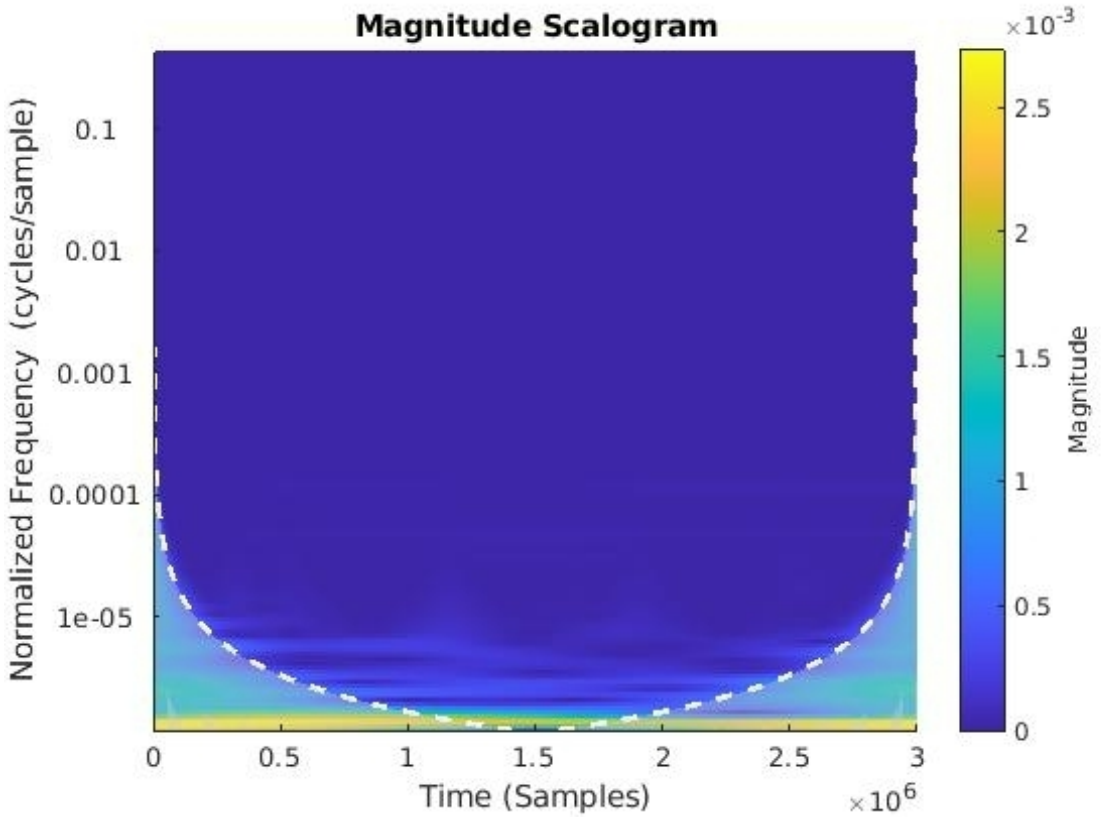

Future Work

Use experimental data to validate both the high-fidelity and reduced-order models.

Incorporate AFM measurement data into a mutli-physics model which directly predicts electrical contact resistance.

Work to parallelize solvers for reduced-order model, enabling even faster computation time.

Perform the same analysis on different types of electrical connections.

Closing Remarks

Chatter is complicated!

- Extremely difficult to isolate all variables and unknowns in the process.

Successfully developed a versatile Craig-Bampton model for the pin-receptacle configuration

- Extremely short runtime relative to high-fidelity model.
- Same codes can be used to analyze different electrical component geometries and contact algorithms.

Questions remain on the best way to directly/indirectly compare various chatter simulation results.

Acknowledgements

This research was conducted at the 2021 Nonlinear Mechanics and Dynamics Research Institute hosted by Sandia National Laboratories and the University of New Mexico.

Sandia National Laboratories is a multimission laboratory managed and operated by National Technology and Engineering Solutions of Sandia, LLC, a wholly owned subsidiary of Honeywell International, Inc., for the U.S. Department of Energy's National Nuclear Security Administration under contract DE-NA-0003525.

Additional Background Reading

B. Johnson, C. Schumann, R. Fadi, R. Flicek, K. Johnson, K. Walczak, C. Medina, D. Quinn, B. Zastrow and R. Kuether, "Investigation of Electrical Contact Chatter in Pin-Receptacle Contacts," Sandia National Laboratories, Albuquerque, New Mexico, 2019.

E. Robbins, T. Schreiber, A. Malla, B. R. Pacini, R. J. Kuether, S. Manzato, D. R. Roettgen and F. Moreu, "Pre-test Predictions of Next-Level Assembly Using Calibrated Nonlinear Subcomponent Model," in *Proceedings of the International Modal Analysis Conference*, Virtual, 2021.

P. Logan and P. Avitabile, "Impact reconstruction Using Modal Filters," in *The 36th International Modal Analysis Conference*, Orlando, FL, 2018.

P. Avitabile, "Experimental modal analysis (A simple non-mathematical presentation)," [Online]. Available: http://faculty.uml.edu/pavitabile/downloads/S&V_Jan2001_modal_analysis_MACLpdf.pdf. [Accessed 31 March 2020].

No contact

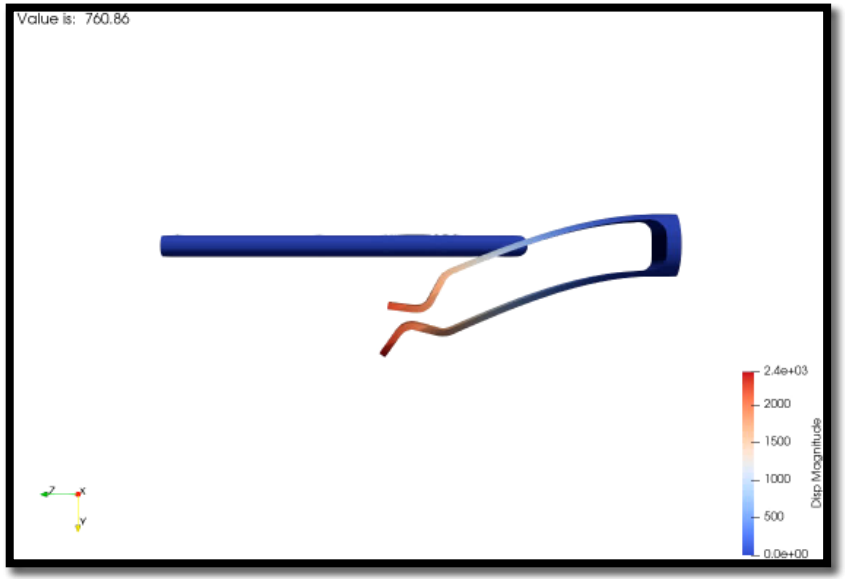

Mode 1

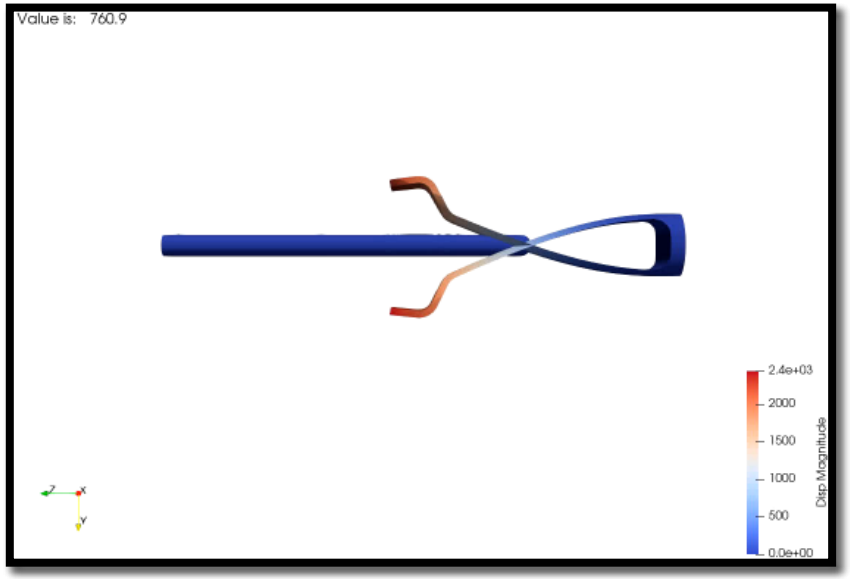

Mode 2

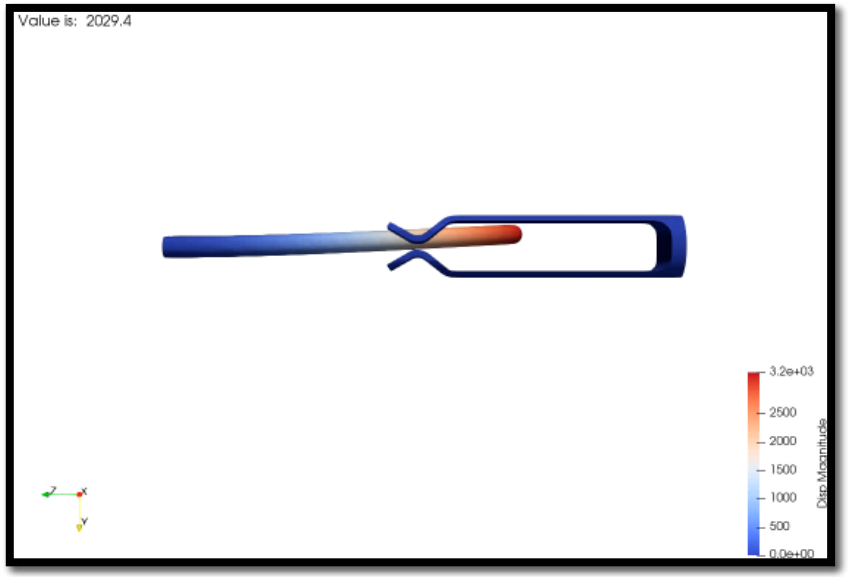

Mode 3

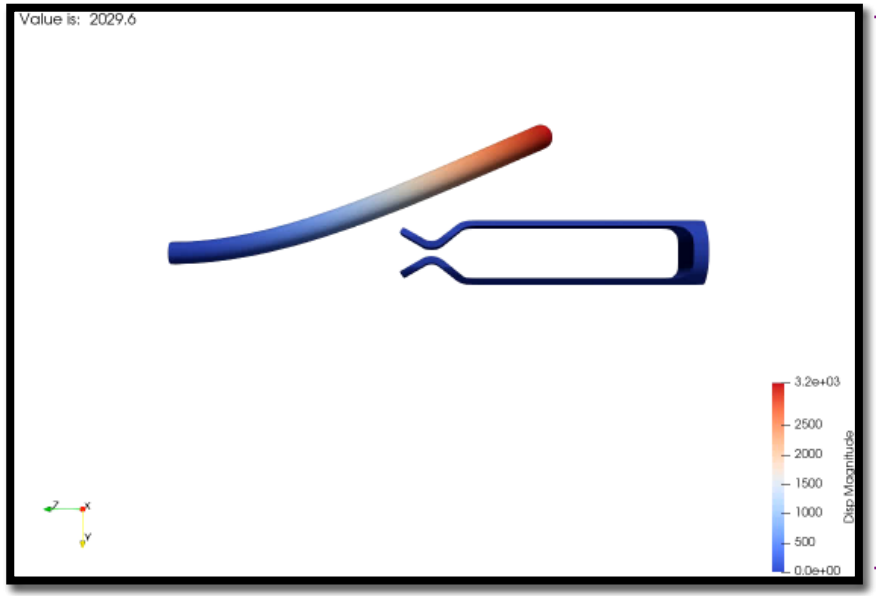

Mode 4

Full contact

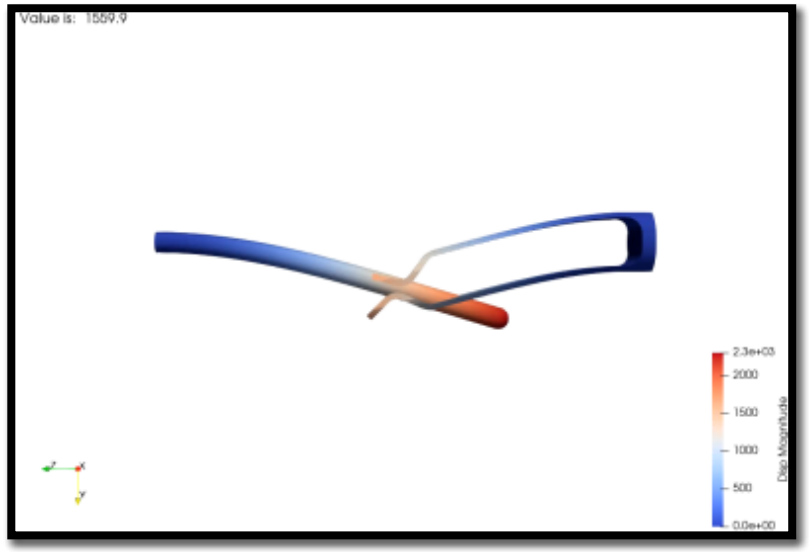

Mode 1

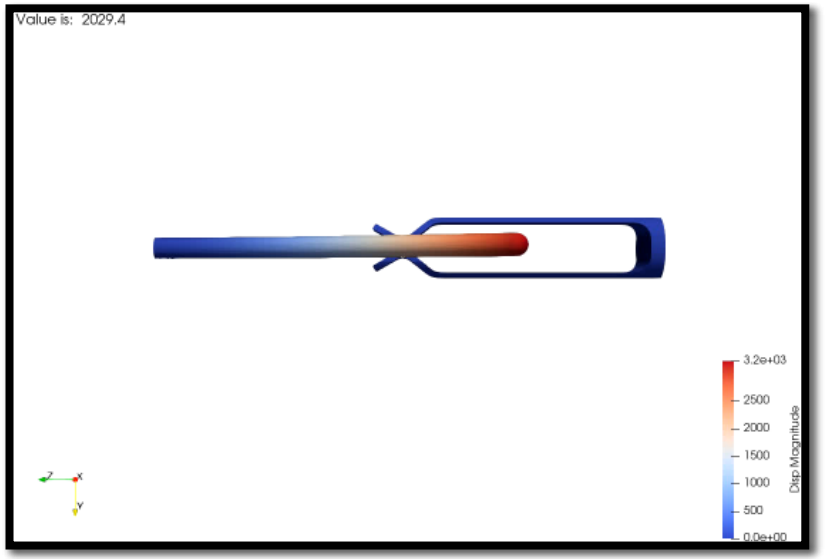

Mode 2

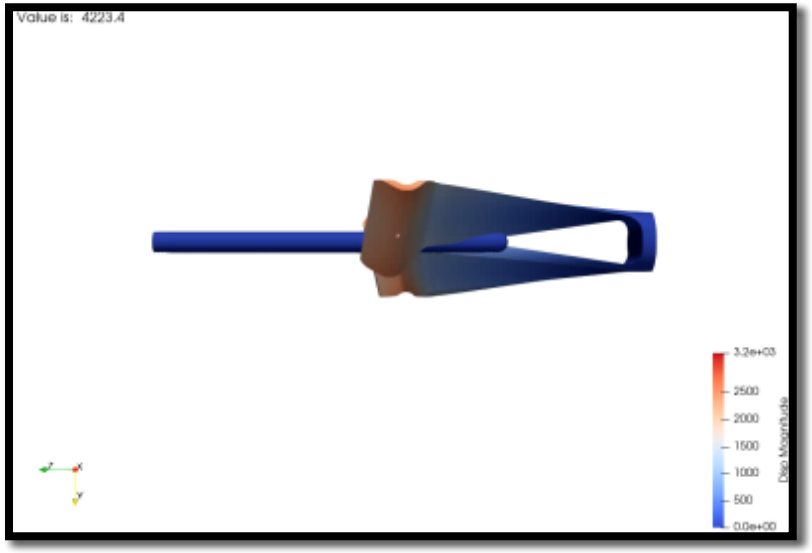

Mode 3

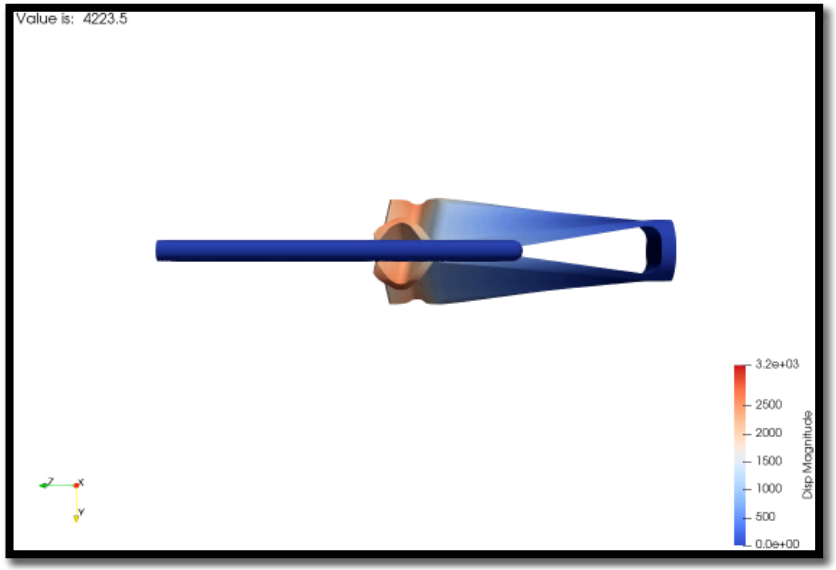

Mode 4

One arm contact

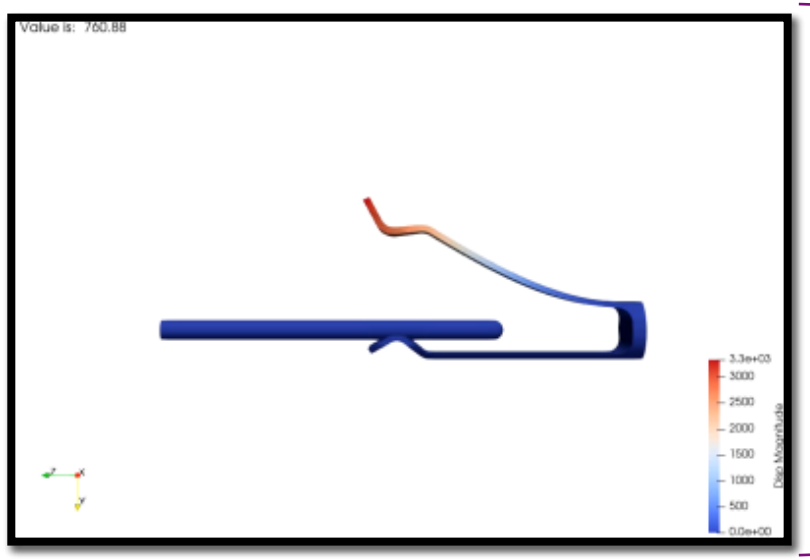

Mode 1

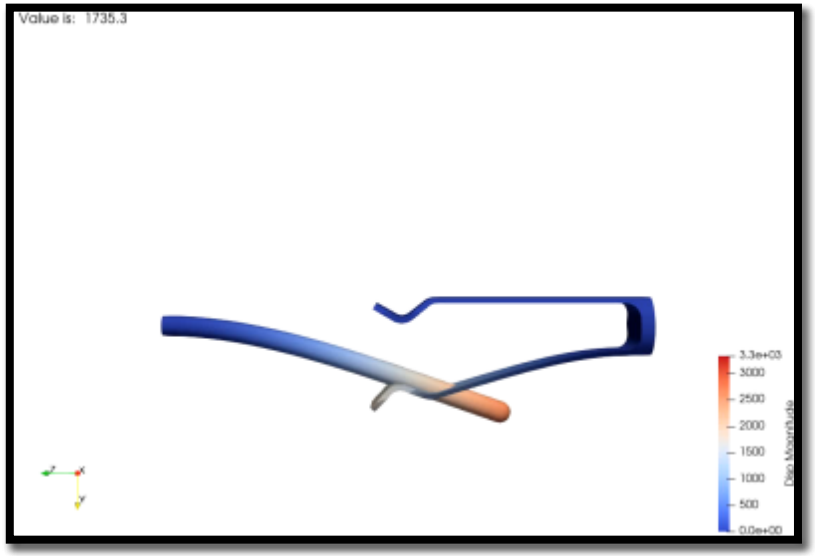

Mode 2

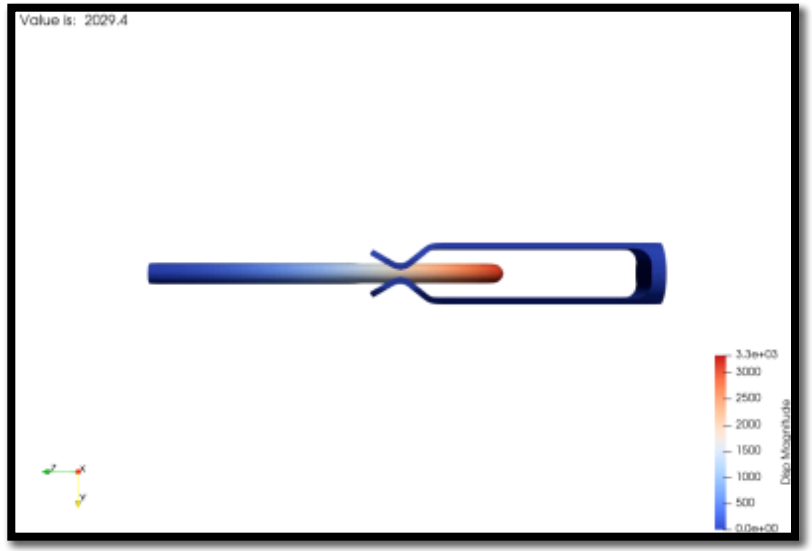

Mode 3

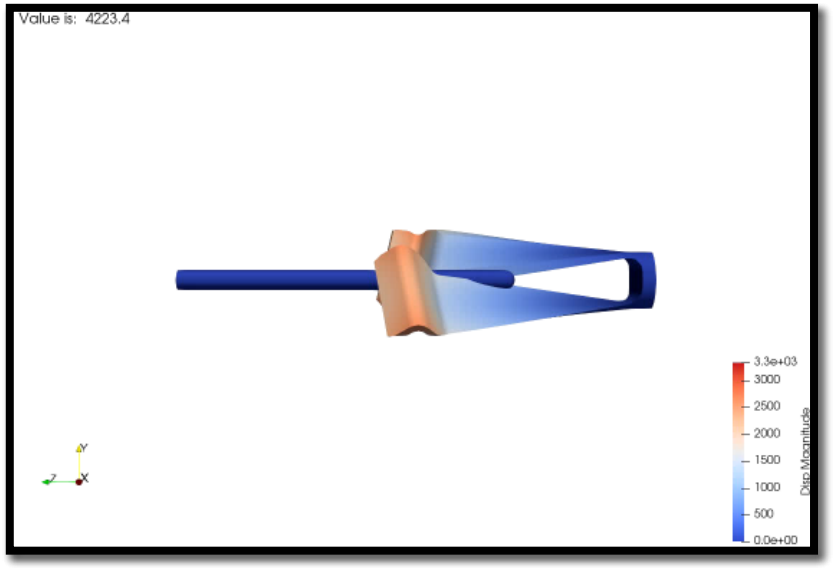

Mode 4

N=O=MAD Research Institute

Sandia National Laboratories

THE UNIVERSITY OF NEW MEXICO

Nonlinear Transient Response of Electromechanical Assemblies

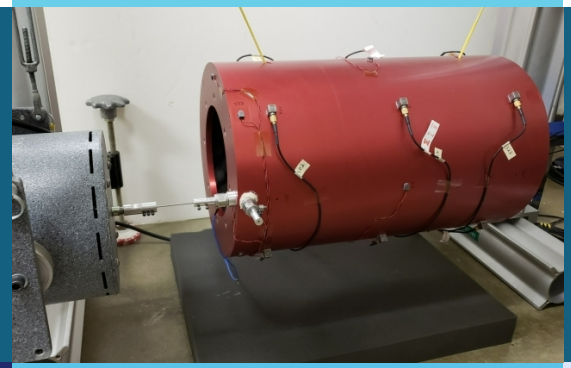

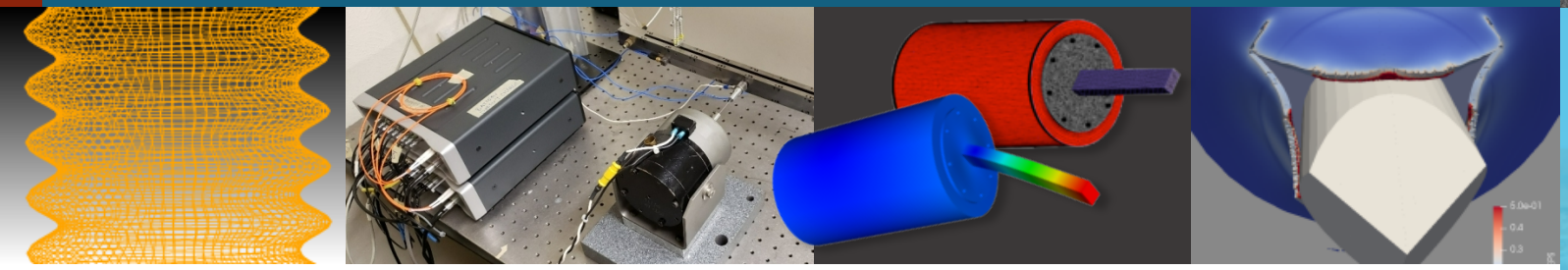

Students:

Sarah Demsky, Nathaniel Goldberg, Abdelrahman Youssef

Mentors:

Steven Carter, Deborah Fowler, Nathan Jackson, Robert Kuether, Andrew Steyer

U.S. DEPARTMENT OF ENERGY | NNSA National Nuclear Security Administration

Sandia National Laboratories is a multimission laboratory managed and operated by National Technology & Engineering Solutions of Sandia, LLC, a wholly owned subsidiary of Honeywell International Inc., for the U.S. Department of Energy's National Nuclear Security Administration under contract DE-NA0003525.

Introduction

Background

Low-amplitude vibrations

1. Long-duration random vibration
2. Linear responses produced
3. Classical modal analysis applicable

High-amplitude vibrations

1. Short-duration mechanical shock
2. Nonlinear responses produced
3. Classical modal analysis not applicable*

- Many electromechanical assemblies of interest to Sandia have sources of nonlinearity stemming from contact impacts
- This limits or invalidates the applicability of linear modal analysis techniques

Project Description & Goals

Description
Understand how contact-impacts due to bearing clearances lead to nonlinear coupling between elastic and rigid body modes in rotor-bearing assemblies

Method
Study an idealized system that will imitate the essential physics

Task 1 Analyze physical test model	**Task 2** Develop detailed Sierra model	**Task 3** Develop simplified FE model
Visualize the experimental linear modes	Create simplified geometry and generate a hexahedral mesh	Write implicit, transient finite element code in MATLAB
Validate the linear modes via modal assurance criterion (MAC)	Apply preload to the springs in Sierra SM	Correlate model parameters to experiment
Create a test plan to excite nonlinear modes	Transfer the preload and run modal analysis in Sierra SD	Replicate experimentally observed transient response
Generate spectrograms for the nonlinear responses	Replicate experimentally observed transient response	Contextualize transient response with NNM calculations

Physical Test Model

Test Set Up

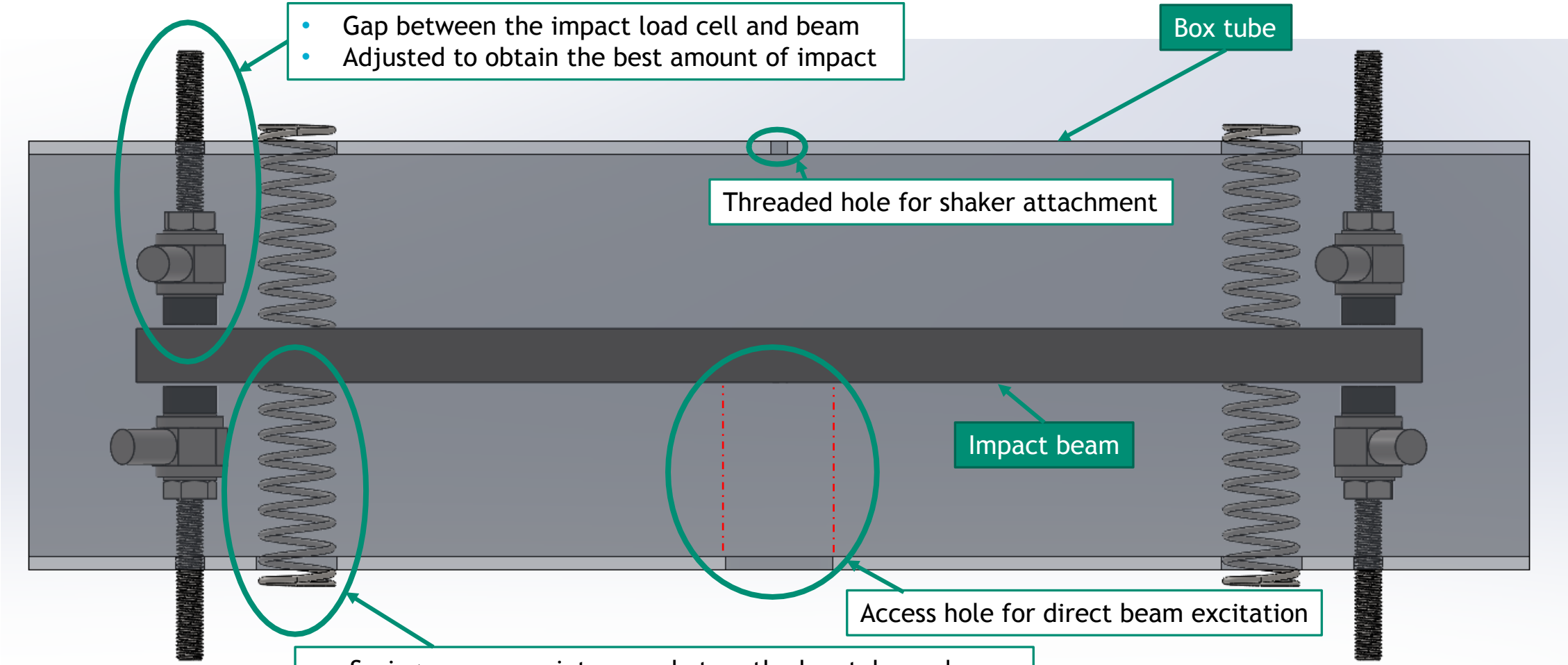
Gap between the impact load cell and beam
Adjusted to obtain the best amount of impact
Box tube
Threaded hole for shaker attachment
Impact beam
Access hole for direct beam excitation
Springs compress into a pocket on the box tube and are held in place via their own compressive force
Spring is epoxied into pockets in the impact beam
Spring rate is 11 lb/in (as reported by manufacturer)

Instrumentation & Test Plan

- 6 accelerometers were placed on the beam, 5 accelerometers on the box tube
- 4 impact load cells
- The system was excited with an impact hammer at a variety of locations on the box tube to excite the system in three orthogonal directions
- The system was tested in two configurations:
  - Impact gaps fully
  - Impact gaps fully closed – The preload is unknown, but it was sufficient to ensure that the tips were in contact with the beam for all ranges of excitation.

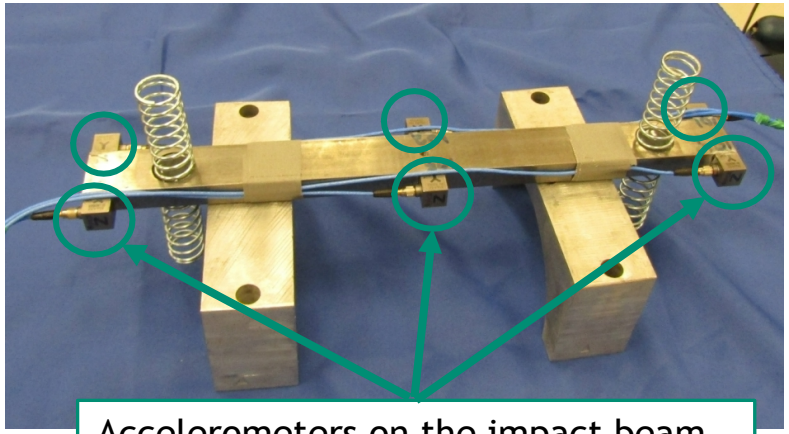

Accelerometers on the impact beam

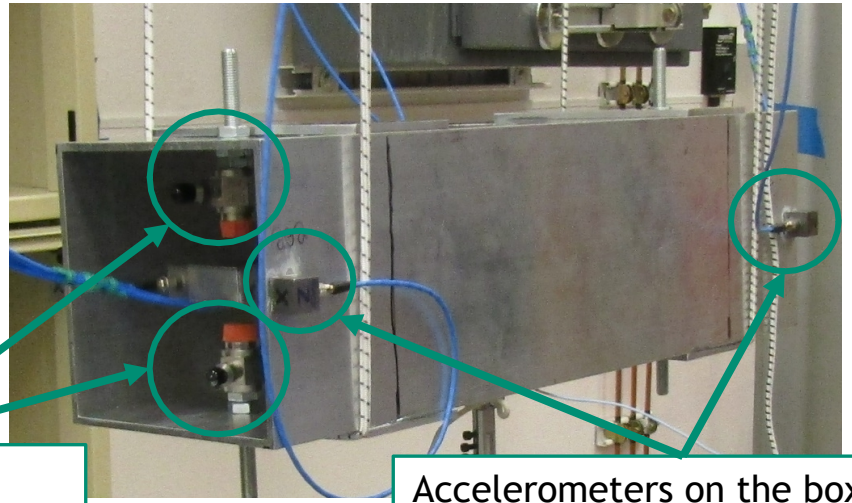

Impact load cells (mirrored on the other end)

Accelerometers on the box tube (mirrored on the opposite side)

Rigid Body Mode Shapes – Fully Open Case

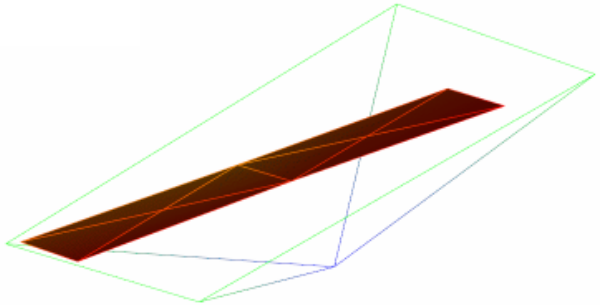

Longitudinal: 10.92 Hz

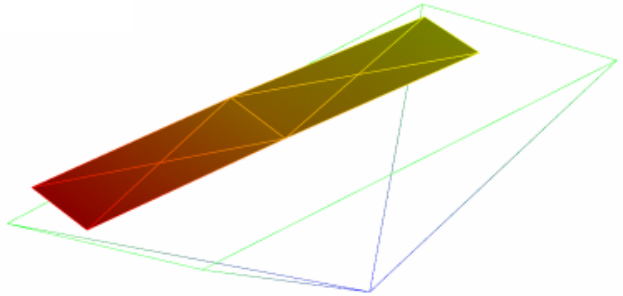

Lateral: 11.66 Hz

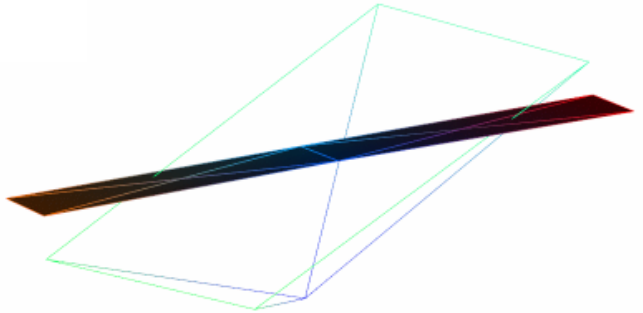

Yaw: 15.08 Hz

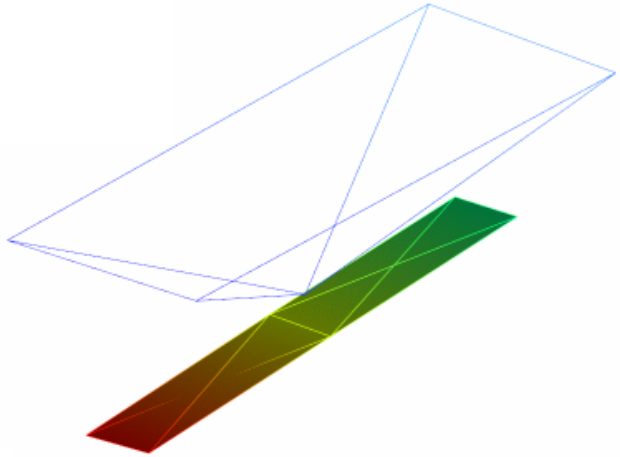

Bounce: 19.94 Hz

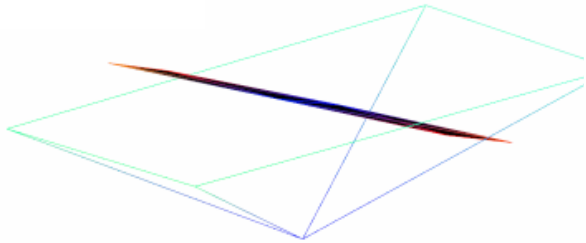

Pitch: 24.11 Hz

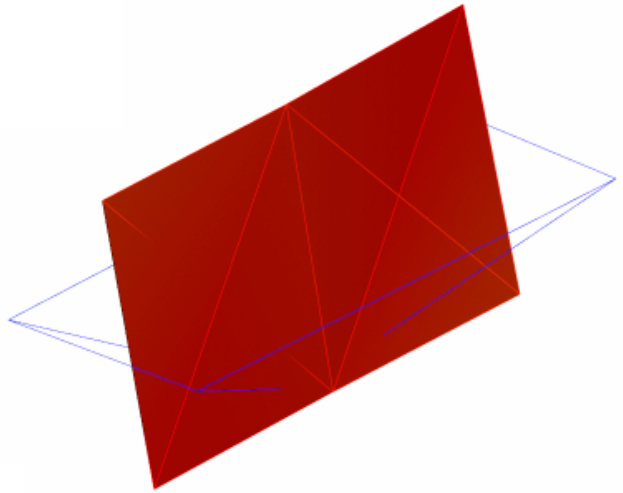

Roll: 33.69 Hz

Mode Shapes – Closed Gap Case

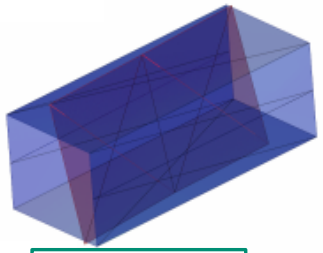
200.8 Hz

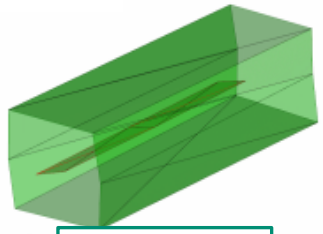
220.8 Hz

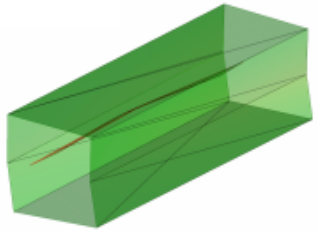
225.3 Hz

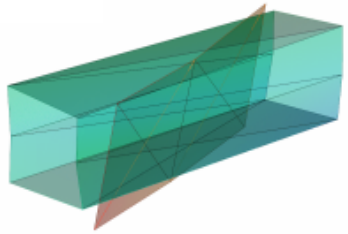
275.3 Hz

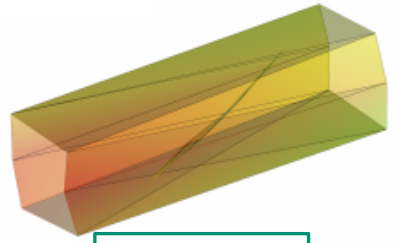
283.3 Hz

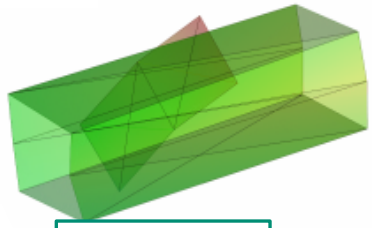
287.8 Hz

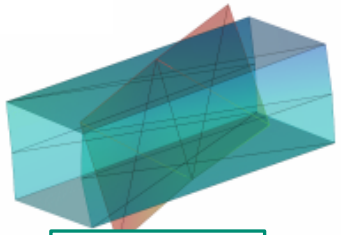
295.1 Hz

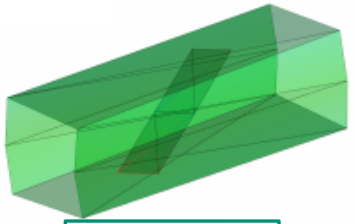
326.9 Hz

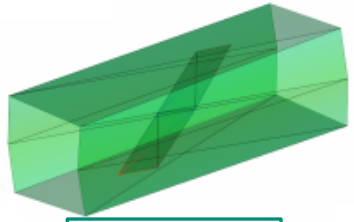
331.3 Hz

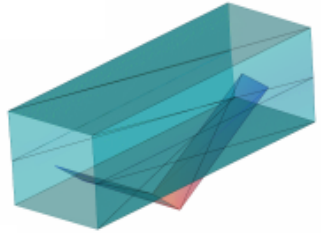
377.0 Hz

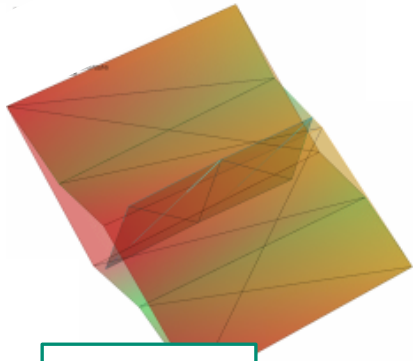
527.4 Hz

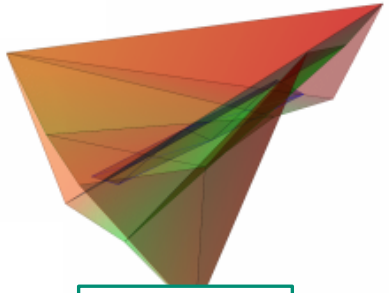
546.9 Hz

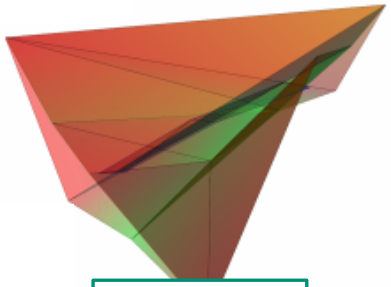
554.2 Hz

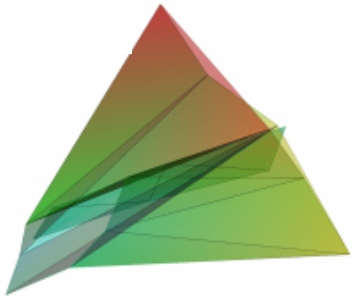
602.7 Hz

Preliminary Nonlinear Tests

- Experiments were performed to measure transient response with impacts
  - Gaps set to approximately 0.01”
  - Beam excited by impact hammer at midpoint
- Data show large amount of damping
  - Likely due to accelerometer cables
  - Questionable applicability of short-time Fourier transform

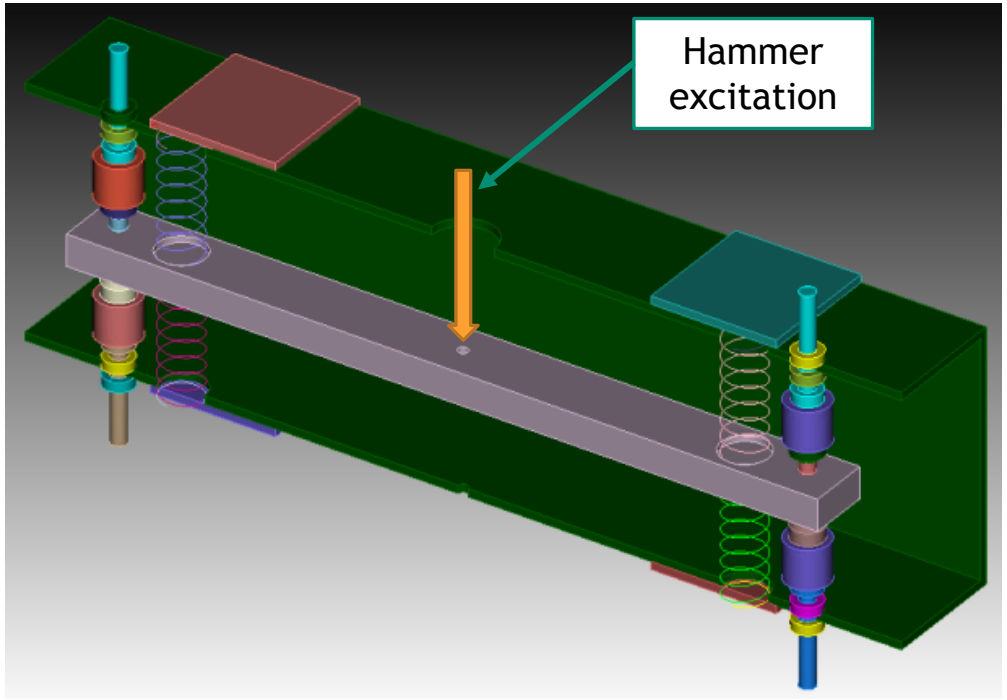

Simplified CAD model

Computational Capabilities

MATLAB Finite Element Code

No Image

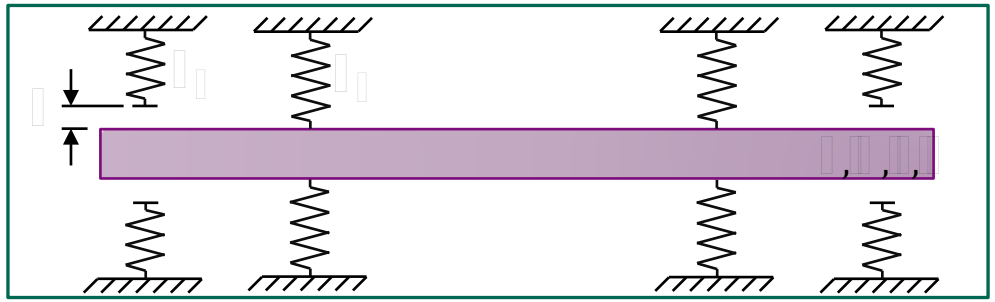

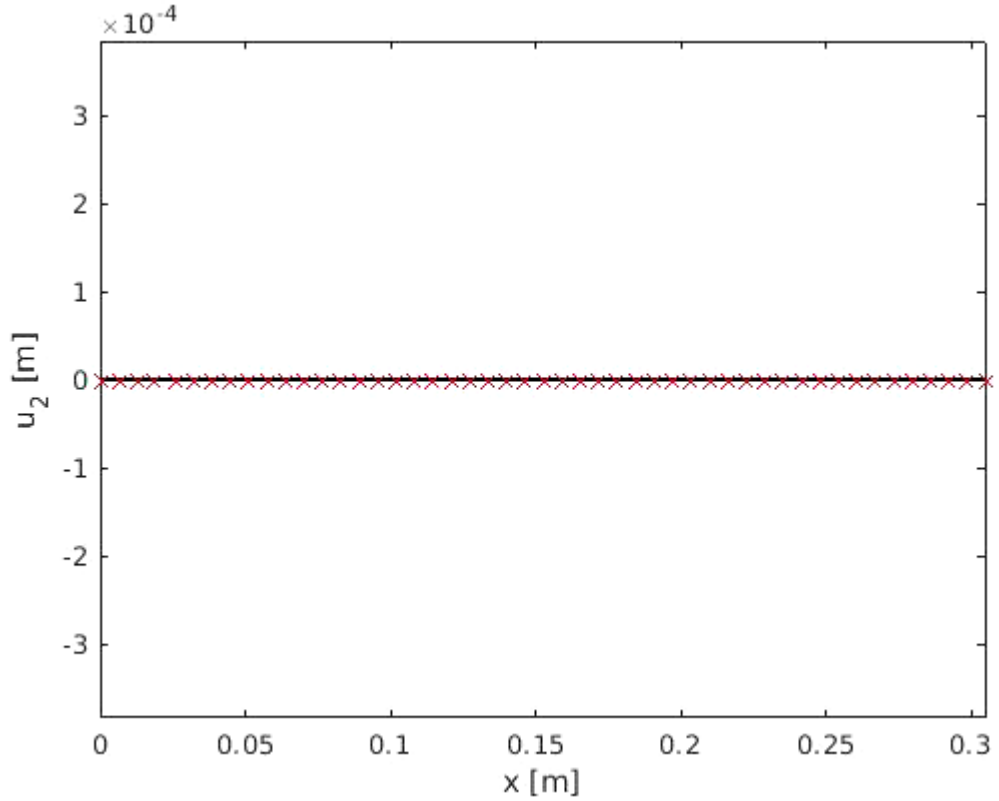

Automated Generation of Geometry and Mesh

- Created versatile CUBIT journal file
  - Input: various dimensions of parts
  - Output: CAD geometry and high-quality hex mesh
- Mesh is highly symmetric and regular
- Useful for future optimization studies

```
############################
###   MESH PARAMETERS    ###
############################
# Make this number bigger for a coarser mesh (1-10 range)
#{meshSizeFactor = 6}

# Unite all the volumes I webcut after mesh is created? (0 = no, 1 = yes)
# This operation can take some time, so be patient
#{uniteVols = 1}

# Unmerge backing plates from box tube, useful for doing preload in SM
#{unmergePlates = 0}

##############################
###   GEOMETRY PARAMETERS   ###
##############################
#{tol = 1e-5}

#{beamDepth = 1}
#{beamHeight = 0.5}
#{beamLength = 12}
#{beamCutoutRadius = 0.375}
#{beamCutoutDepth = 0.1}
#{beamDistFromCenterToCutout = 4.5}
#{beamCenterHoleRadius = 0.0795}

#{gap = 0.1}
#{distFromCenterToImpactPoint = 5.5}
#{impactTipRadius1 = 0.249}
#{impactTipRadius2 = 0.125}
#{impactTipRadius3 = 0.125}
##{impactTipRadius3 = 0.09375}
#{impactTipHeight1 = 0.2}
#{impactTipHeight2 = 0.1}
#{impactTipHeight3 = 0.16875}
#{impactTipHeight4 = 0.03125}
```

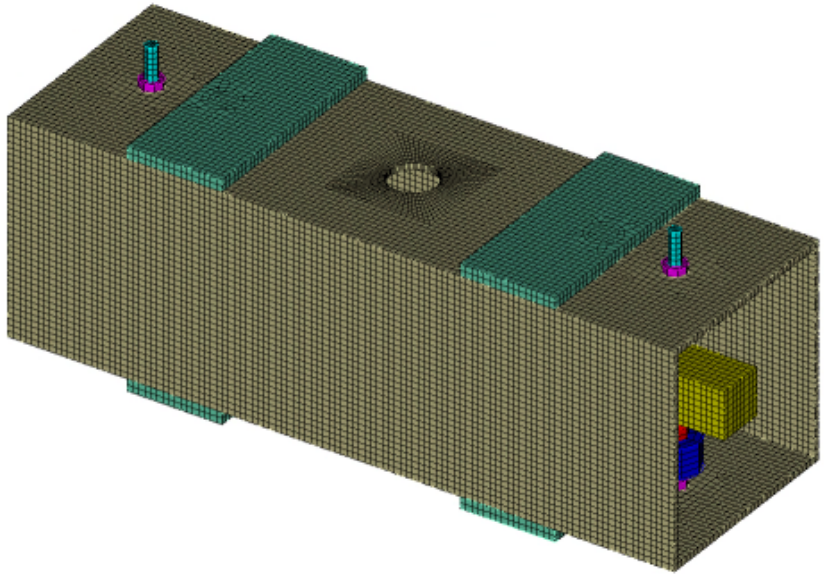

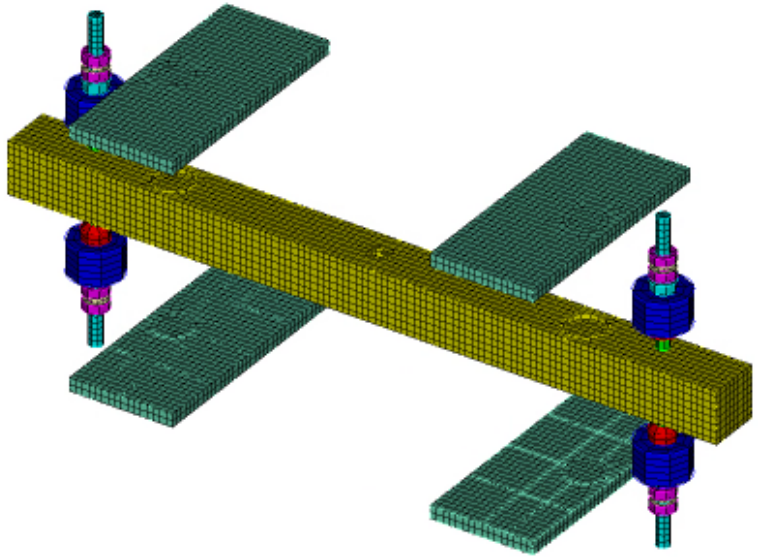

Automated Generation of Geometry and Mesh (cont'd)

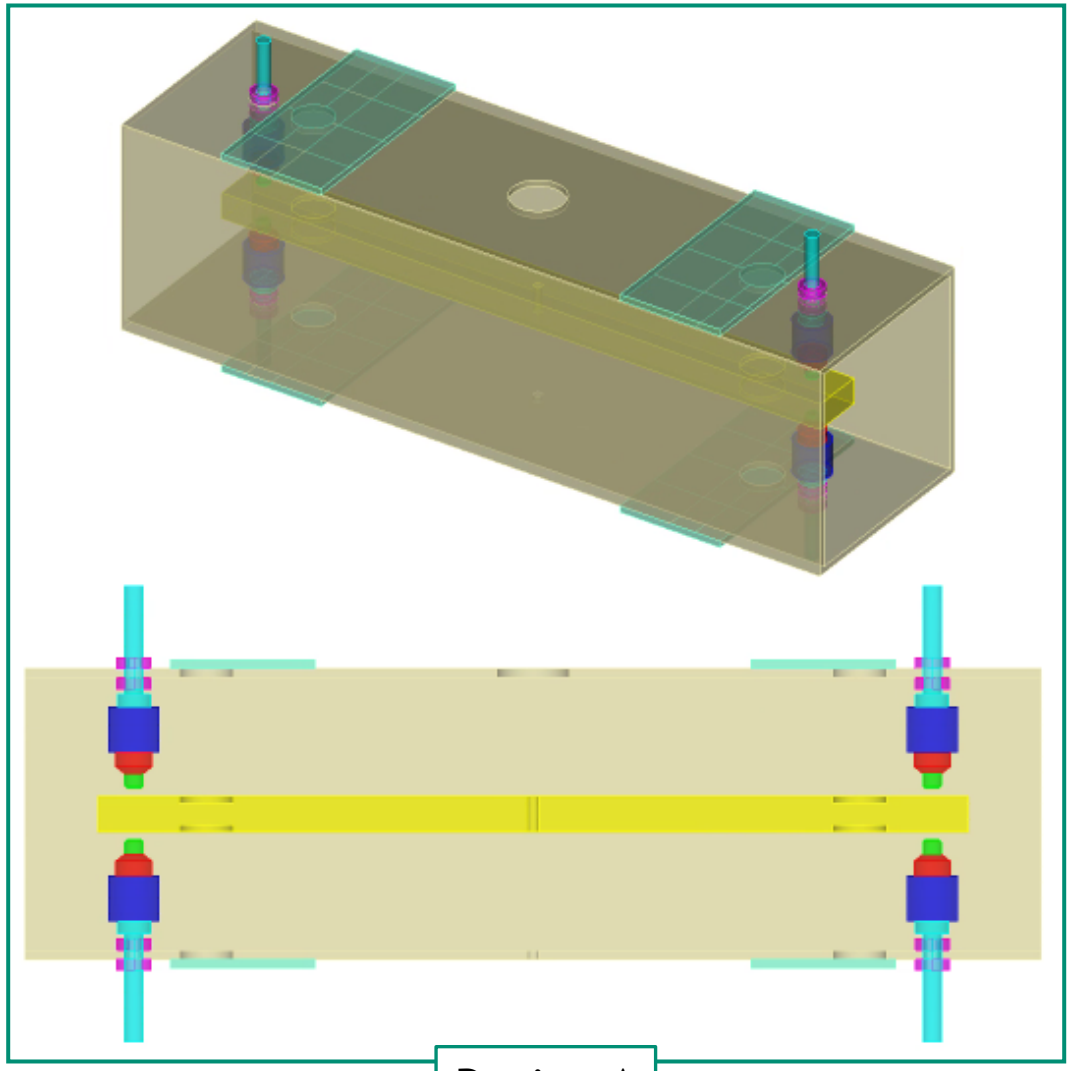

Design A

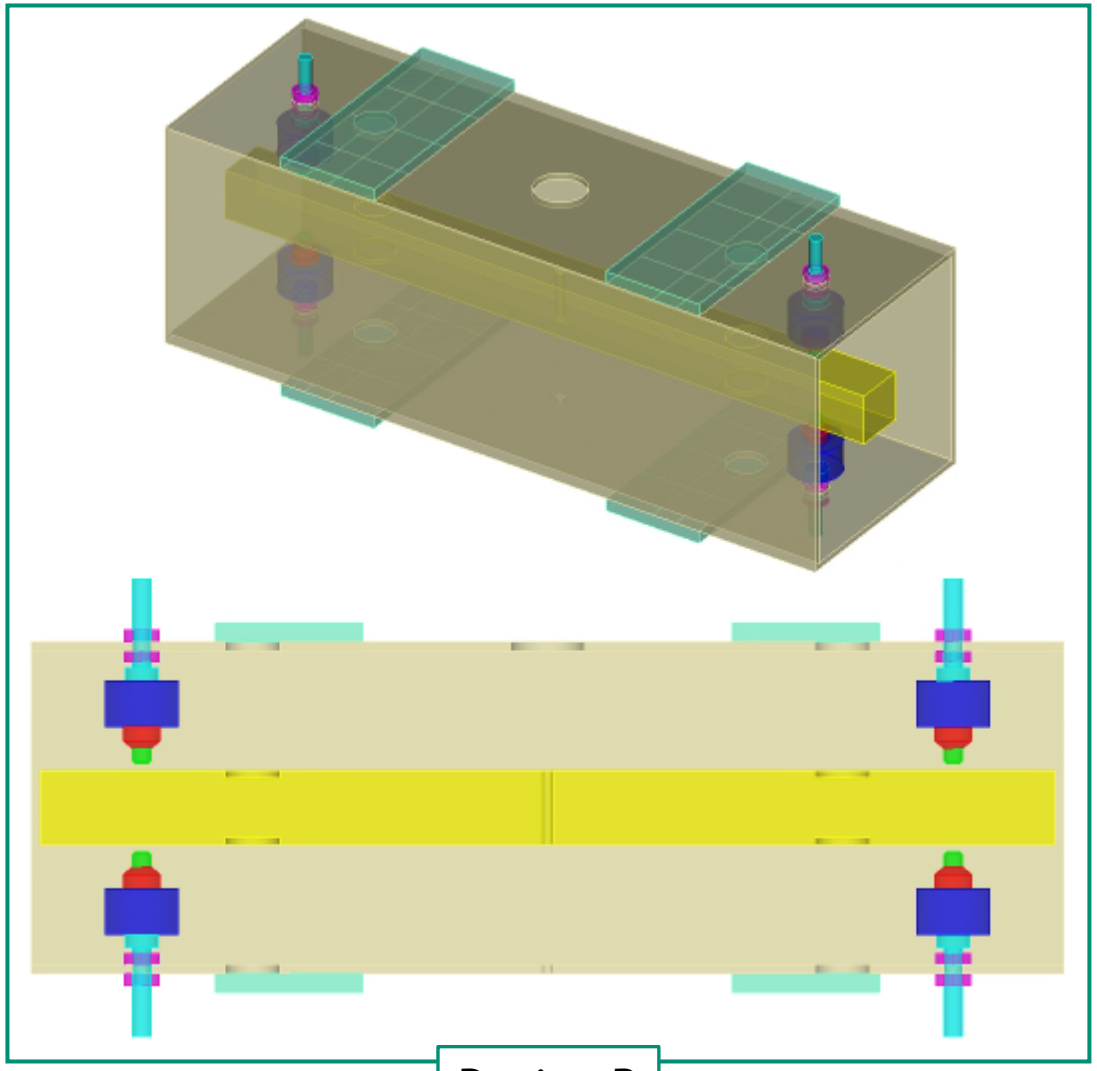

Design B

Spring Modeling

Parameters:

1. Meshing
2. Simulation
3. Fidelity

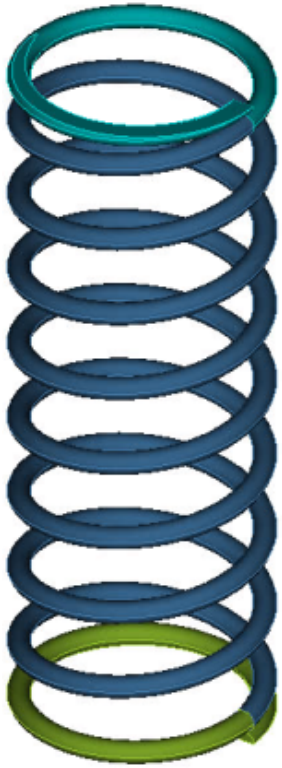

Solid elements (hex or tet)

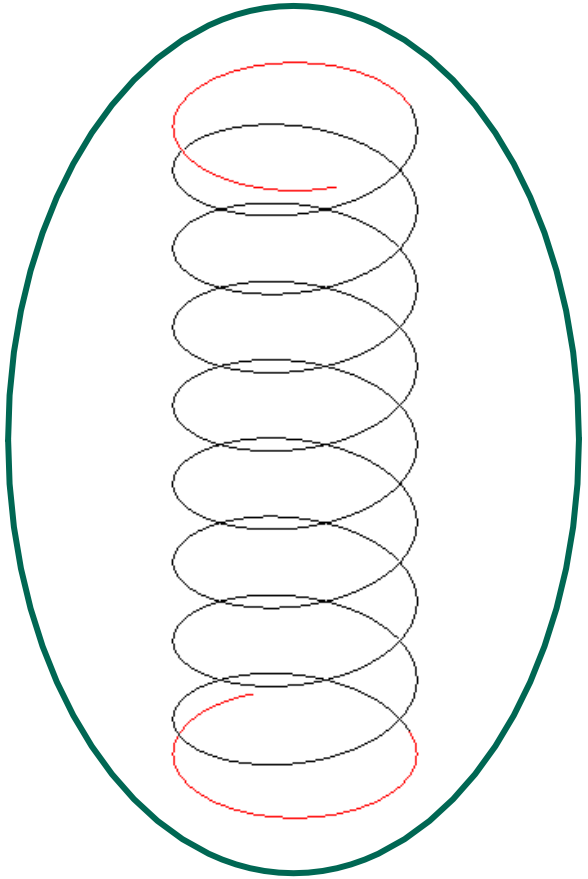

Beam elements

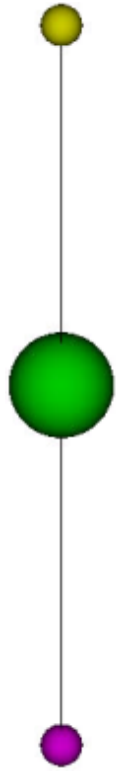

Spring elements w/ concentrated mass

Sierra Finite Element Model Workflow

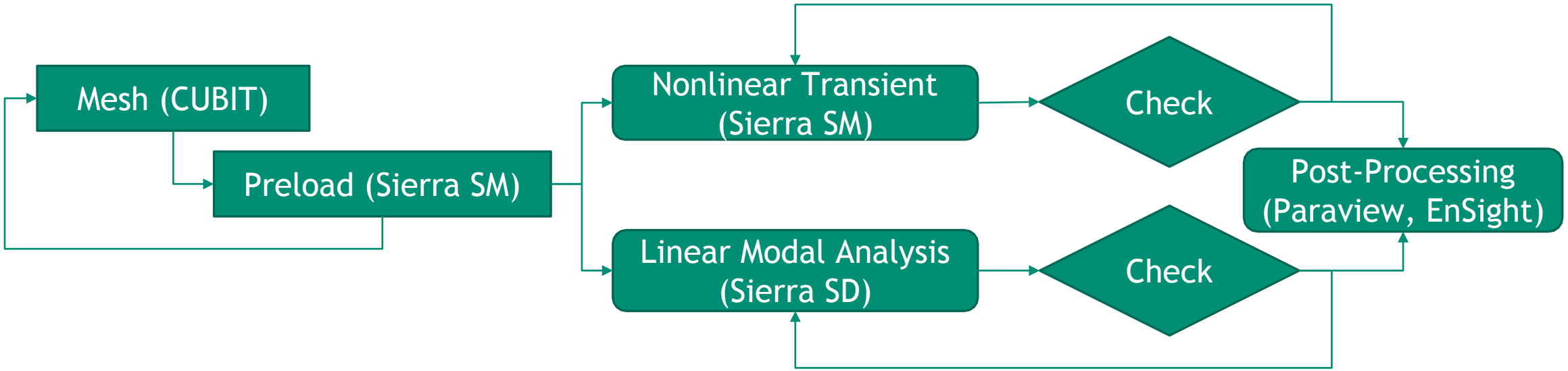

Sierra Model Workflow

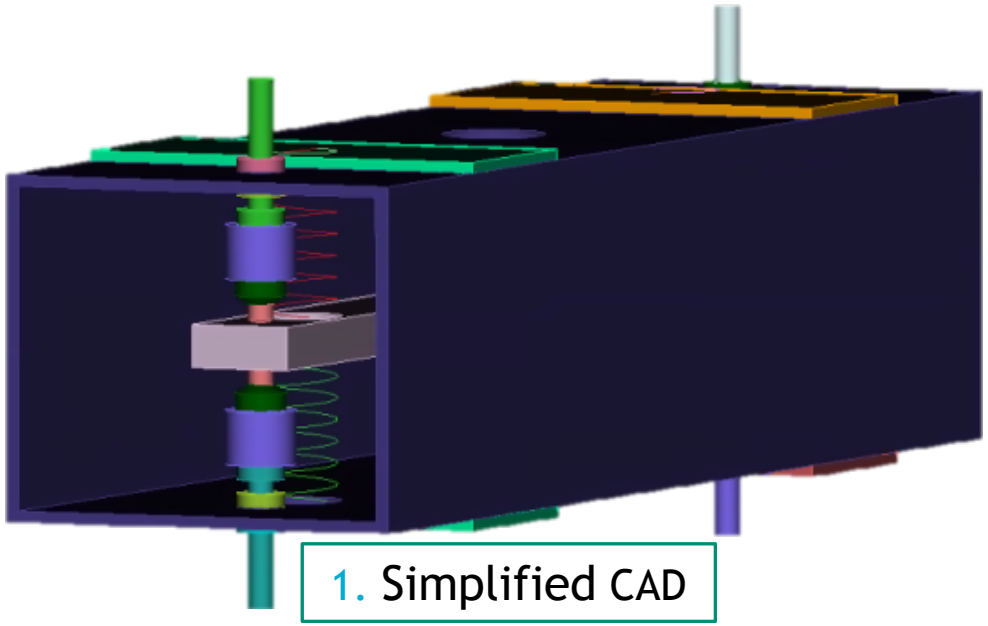

1. Simplified CAD

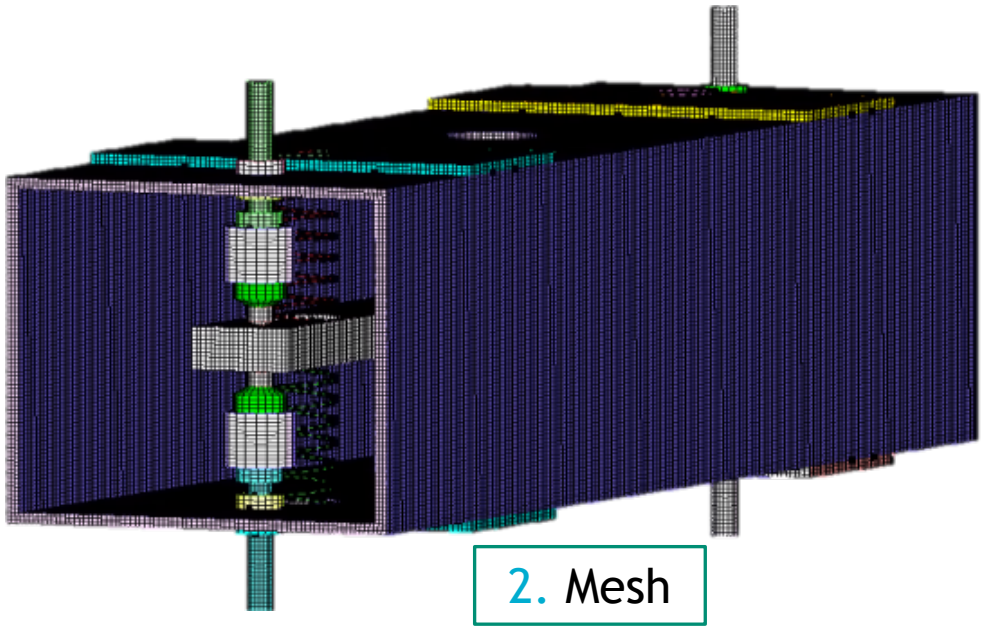

2. Mesh

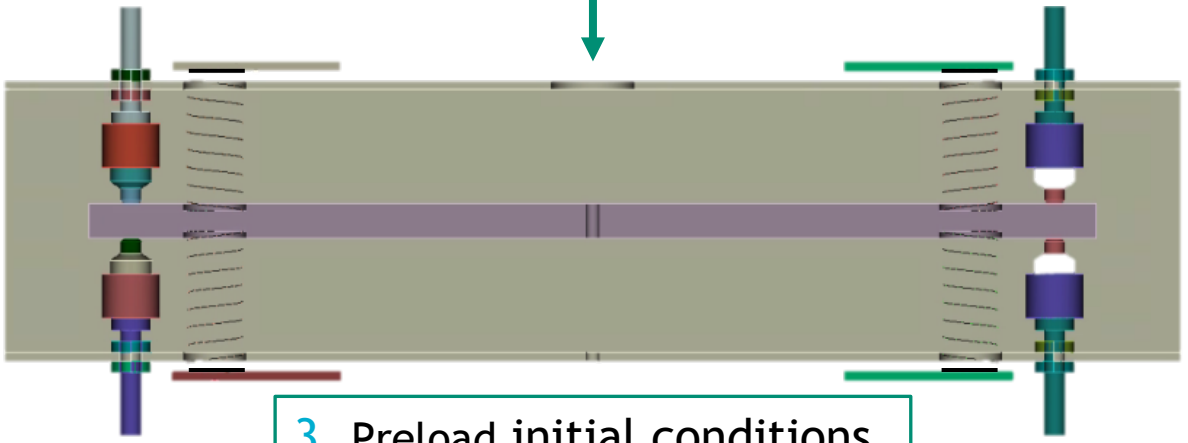

3. Preload initial conditions

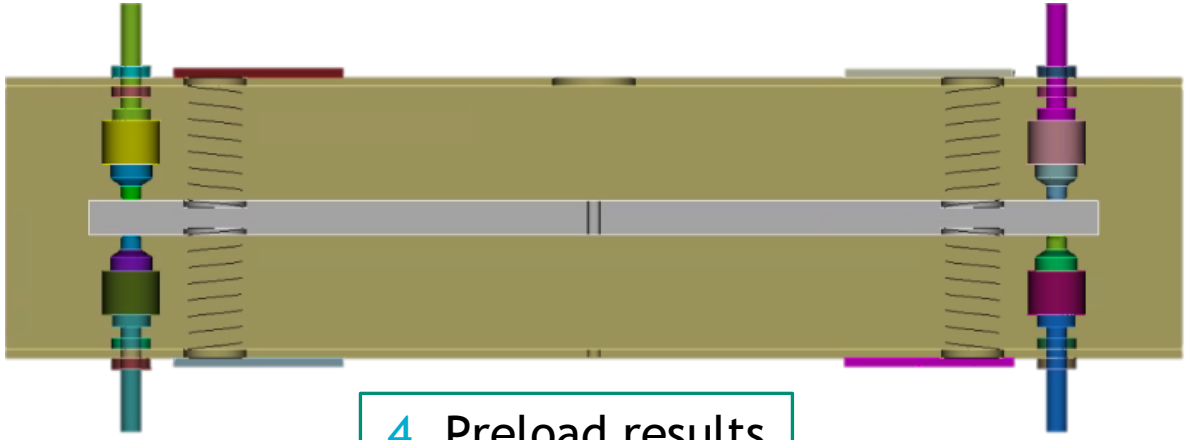

4. Preload results

Linear vs. Nonlinear Response

Linear Modal Analysis

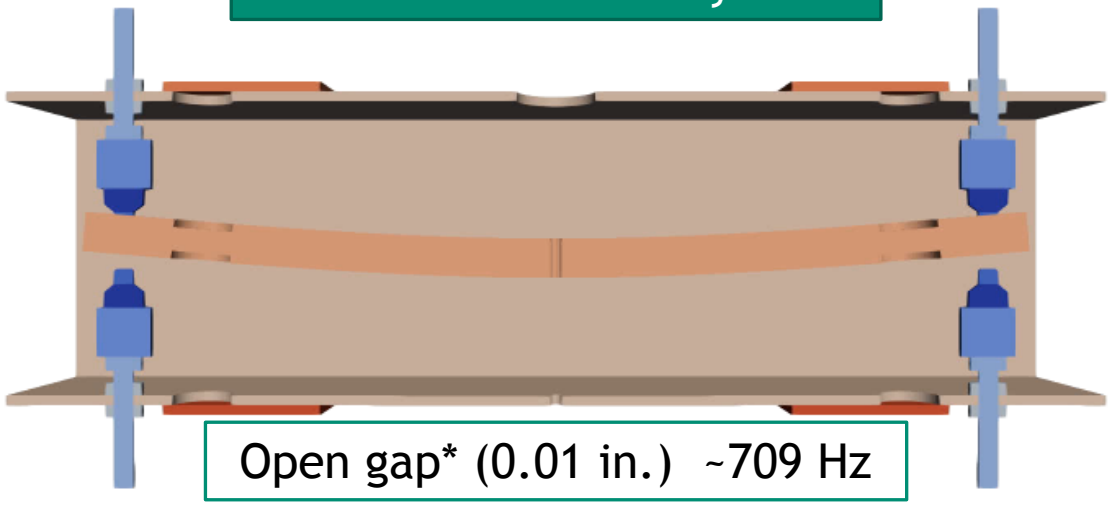

Open gap* (0.01 in.) ~709 Hz

*Springs not included in above animation

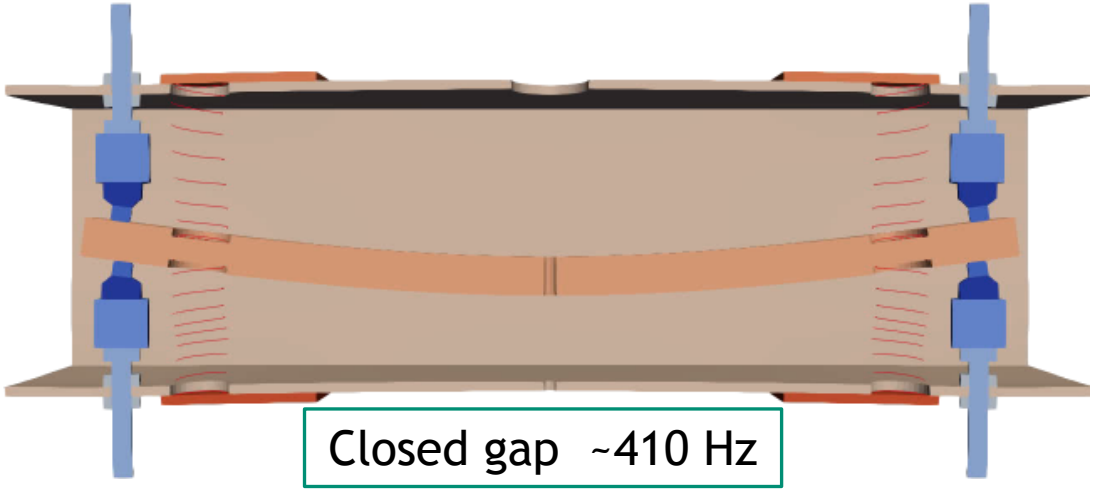

Closed gap ~410 Hz

Nonlinear Transient

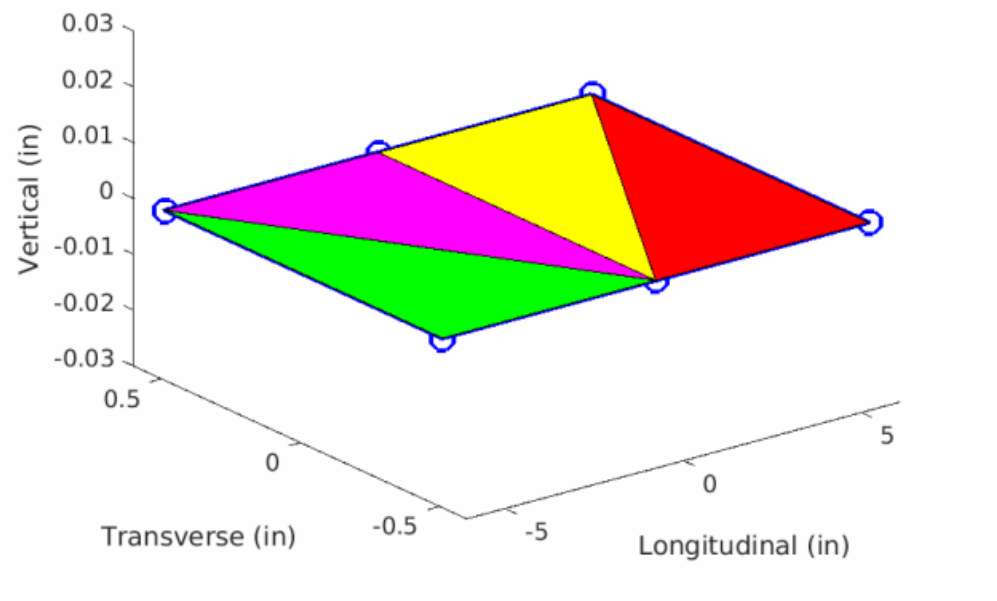

Open gap (0.01 in.)

Outcomes

Pseudo-Rigid Body Mode Shapes (Fully Open Case)

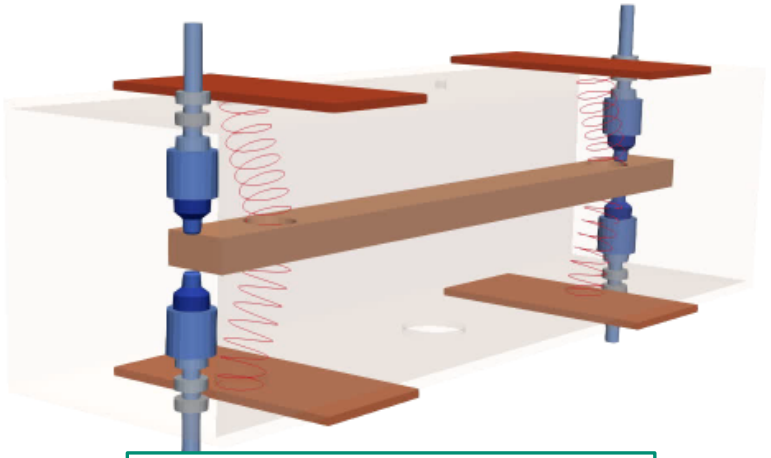

Longitudinal ~10.5 Hz

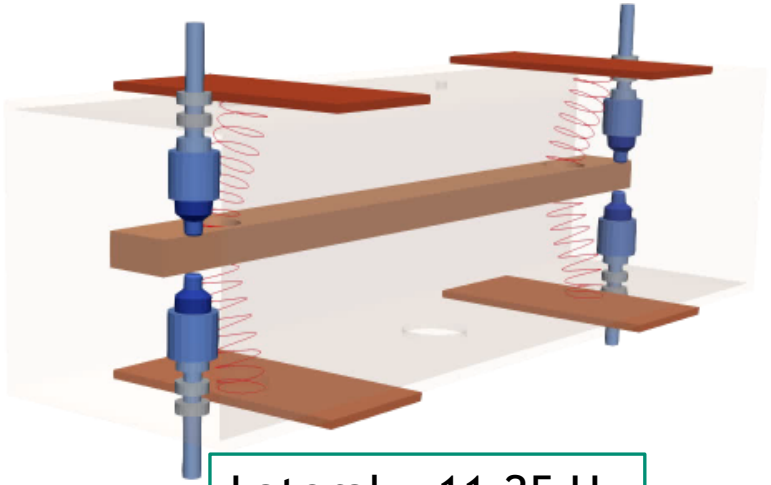

Lateral ~11.25 Hz

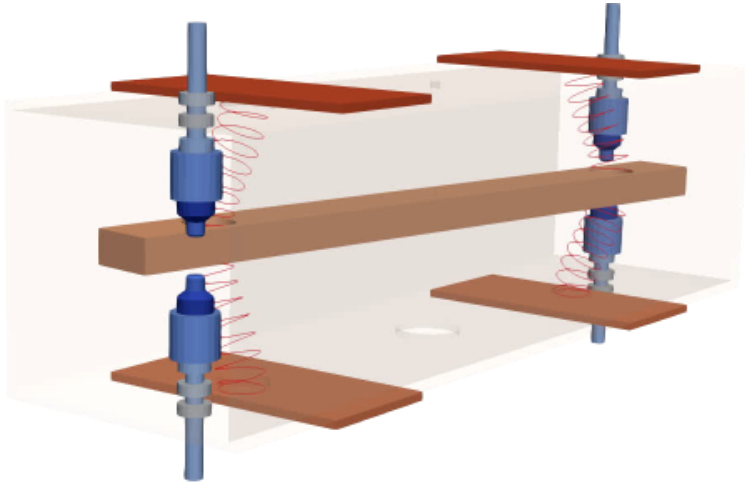

Yaw ~13.75 Hz

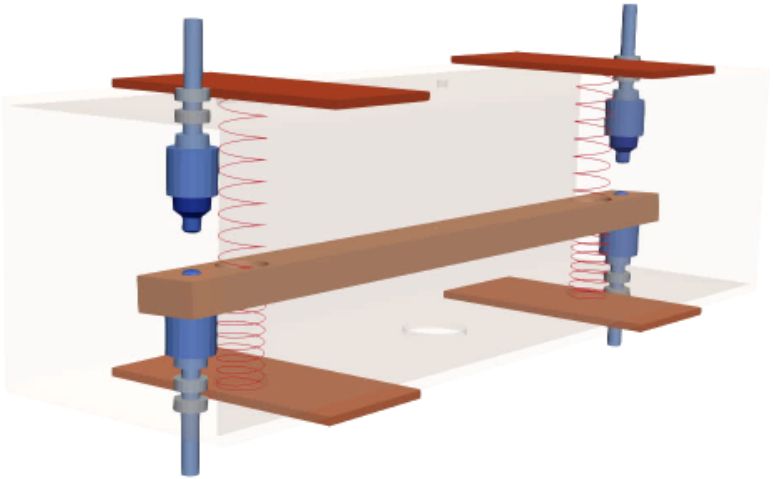

Bounce ~18.5 Hz

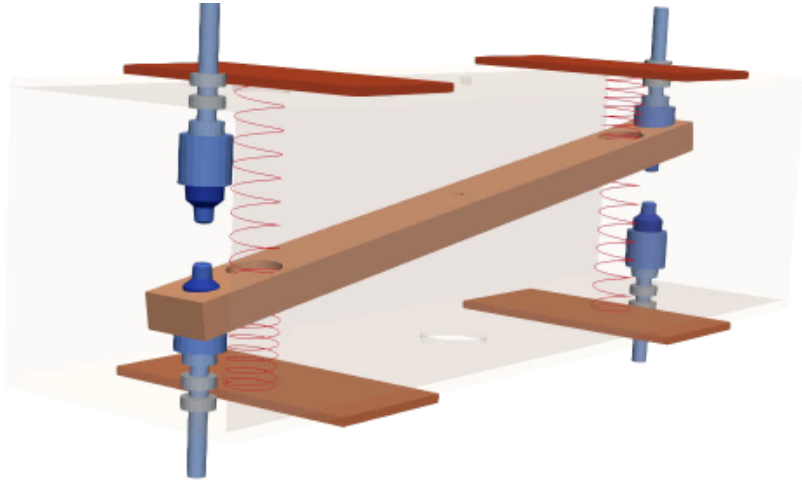

Pitch ~22.5 Hz

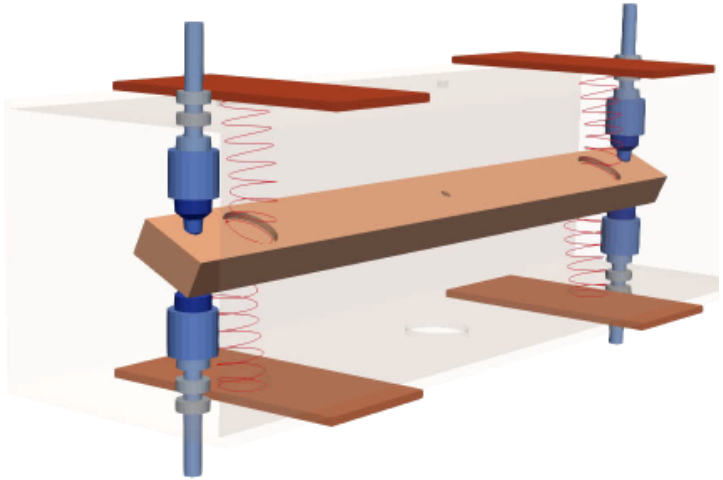

Roll ~34.75 Hz

Spring and Box Tube Mode Shapes

Spring Mode Shapes

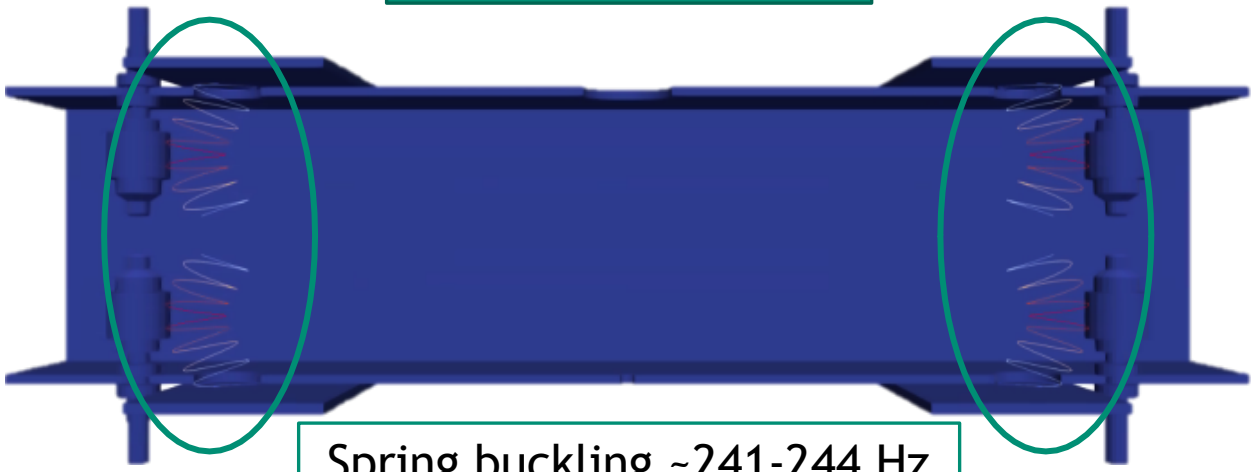

Spring buckling ~241-244 Hz

Spring barreling ~288 Hz

Box Tube Mode Shapes

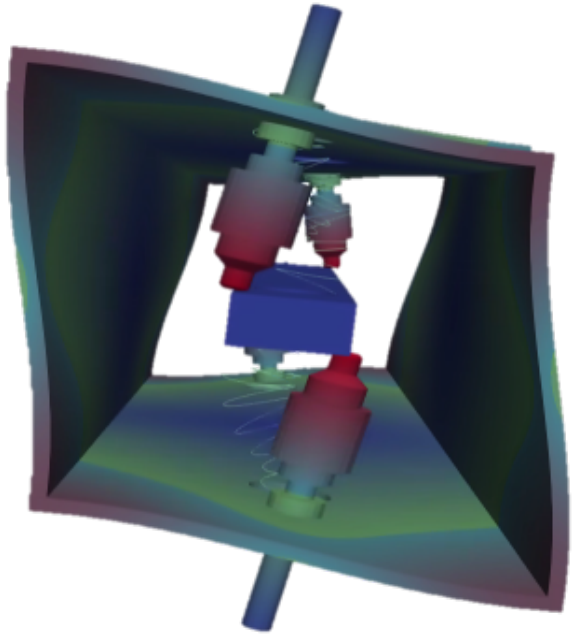

Matchboxing ~441-454 Hz

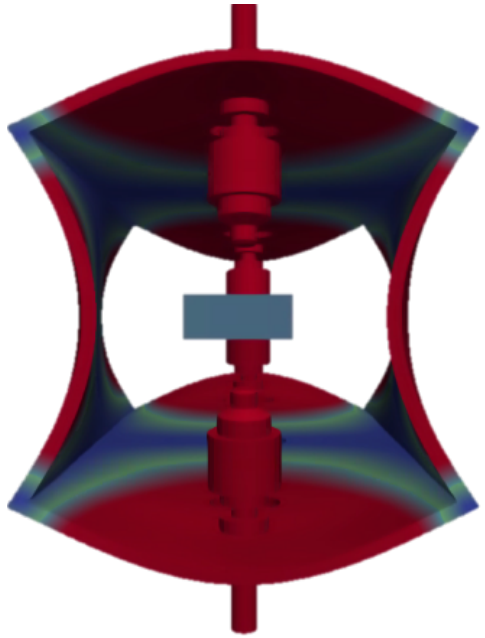

Buckling ~716 Hz

Coupling of Springs with Bending Modes

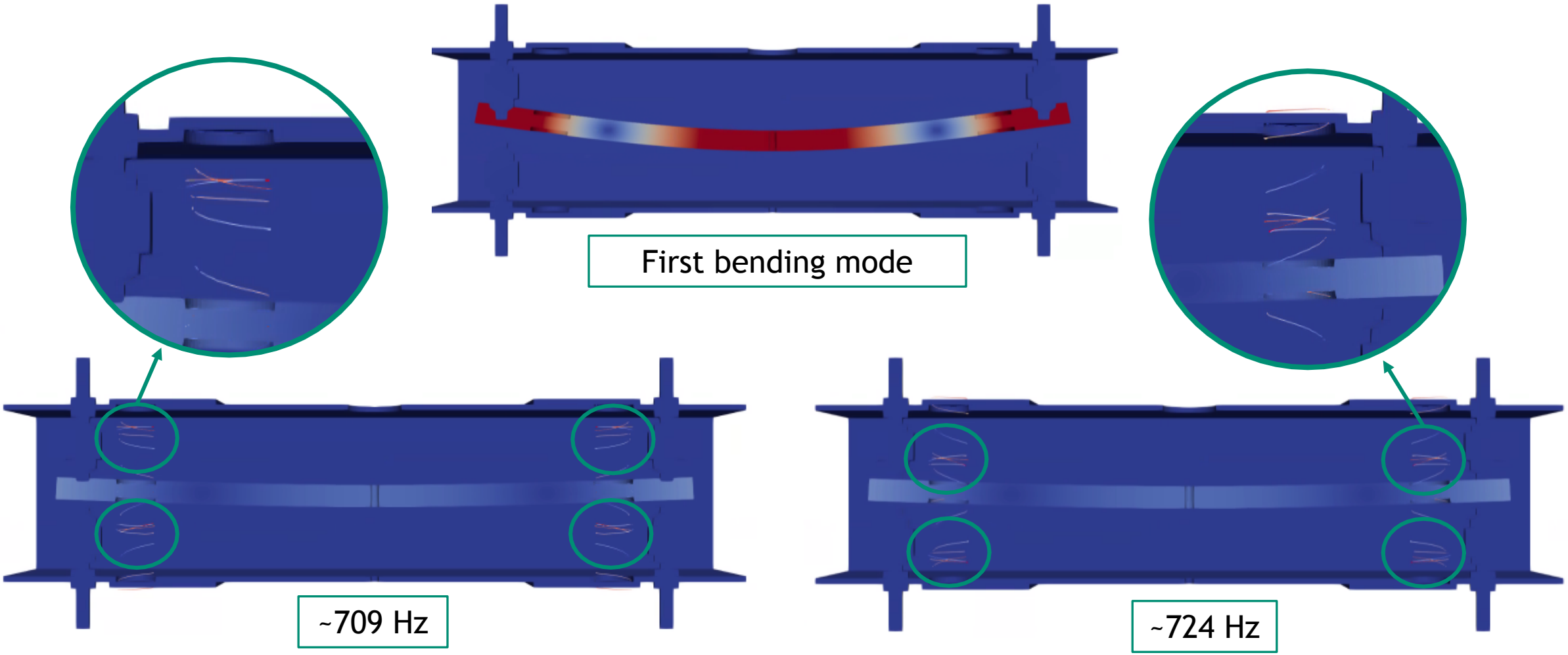

MAC for Linear Response of the Beam Only

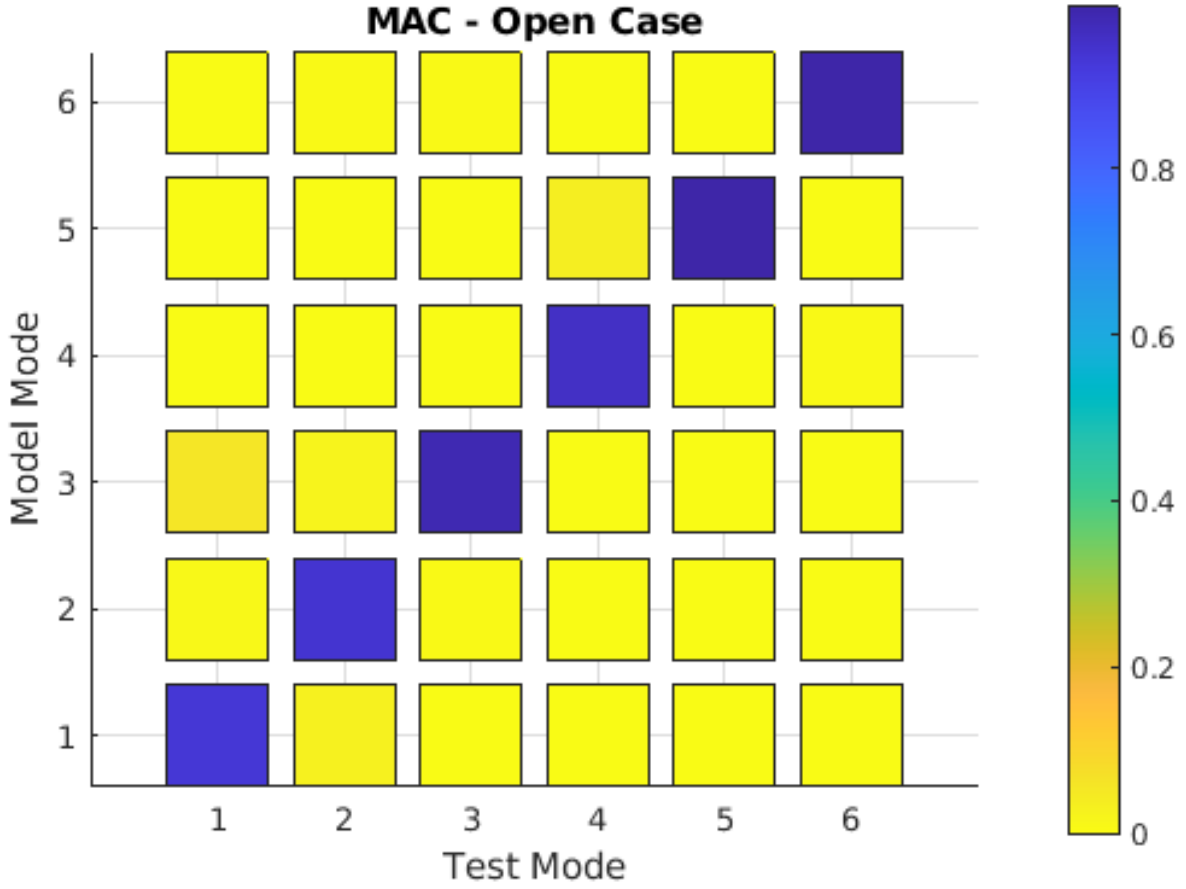

Mode Number	Mode Name	MAC Value
1	Longitudinal	0.9348
2	Lateral	0.9414
3	Yaw	0.9834
4	Bounce	0.9567
5	Pitch	0.9943
6	Roll	0.9974

MAC for Linear Response of the Beam and Box

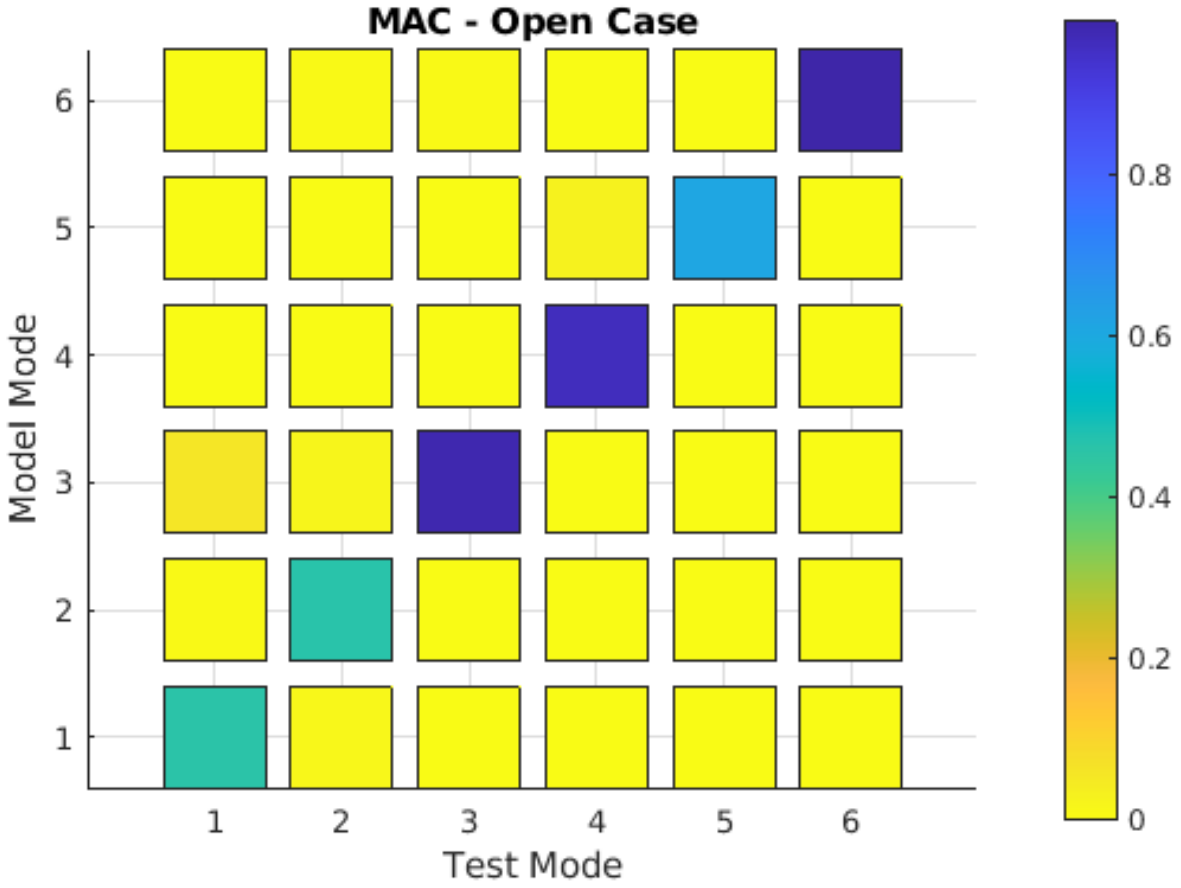

Mode Number	Mode Name	MAC Value
1	Longitudinal	0.4598
2	Lateral	0.4625
3	Yaw	0.9821
4	Bounce	0.9607
5	Pitch	0.6086
6	Roll	0.9913

Transient Response - Experimental

- Hit beam with impact hammer at mid-span
- Gap size 0.01”
- Several hammer hits with varying force
- Data is preliminary (damping due to cables, malfunctioning load cell, etc.)

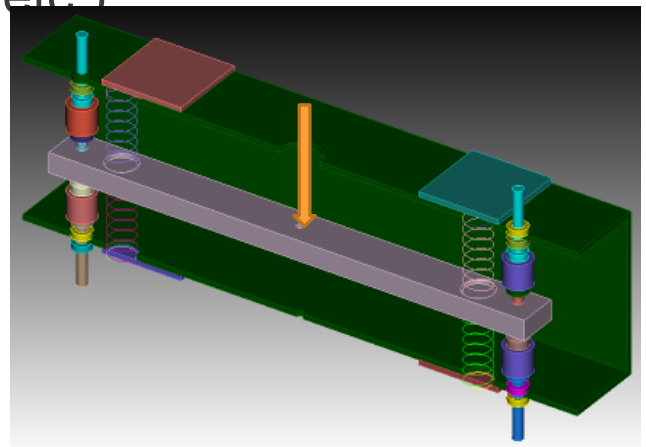

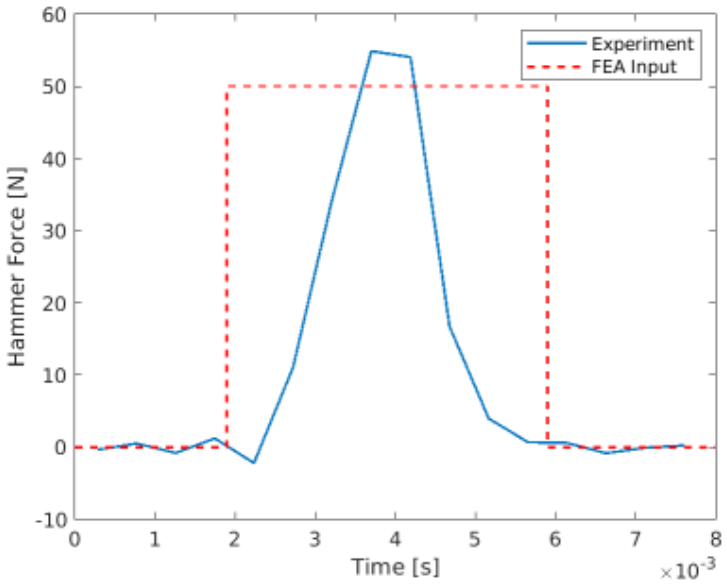

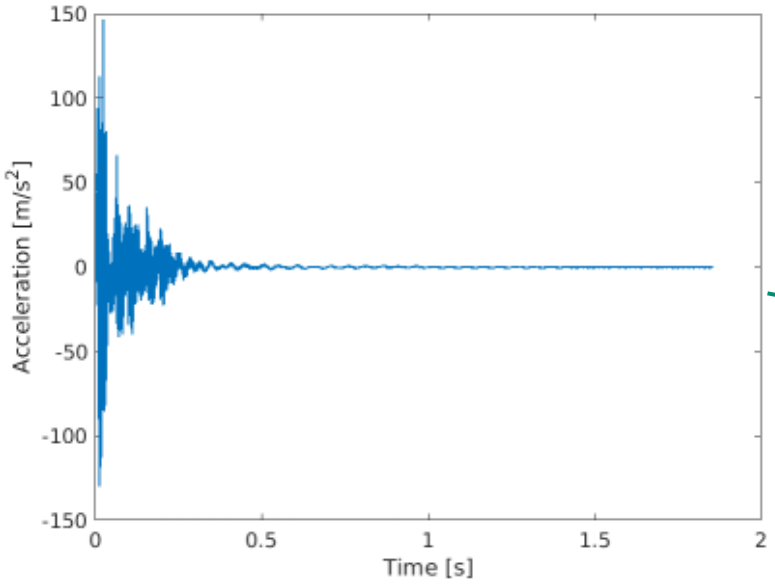

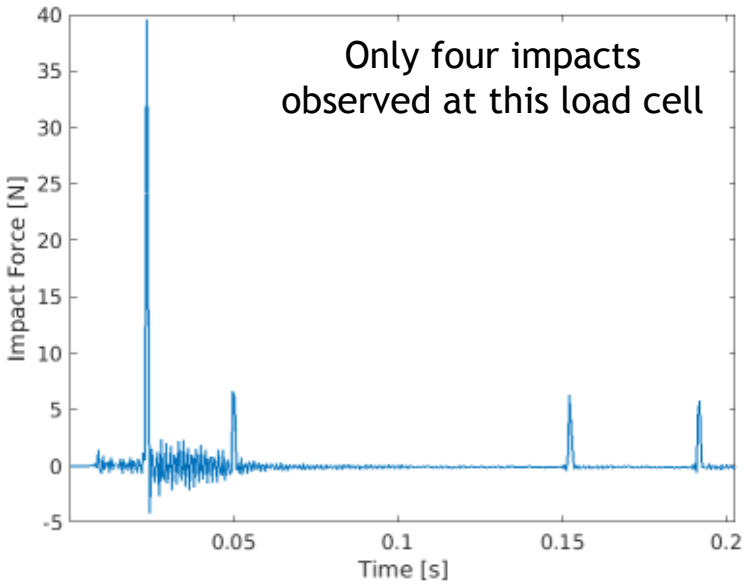

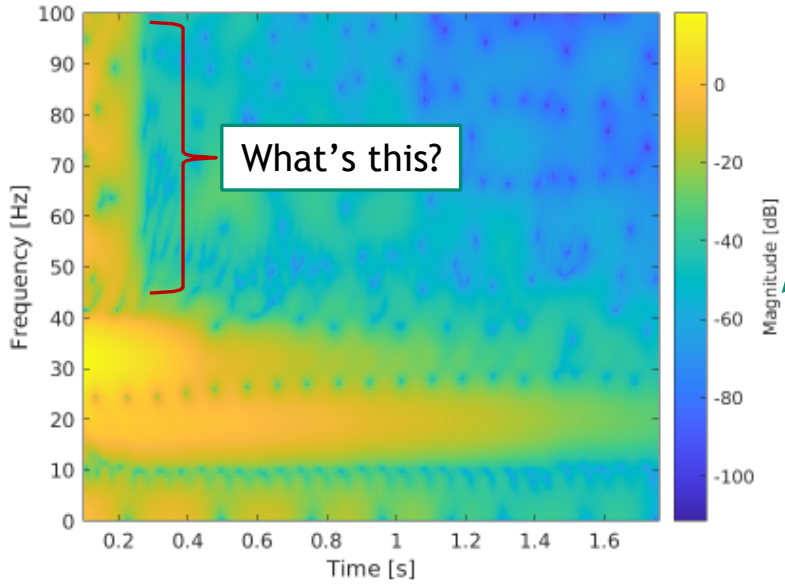

Transient Response - Linear Regime

- Emulate weak excitation with hammer
  - 5-N pulse for 4 ms at middle node
  - Best estimate of model parameters
  - Light Rayleigh damping

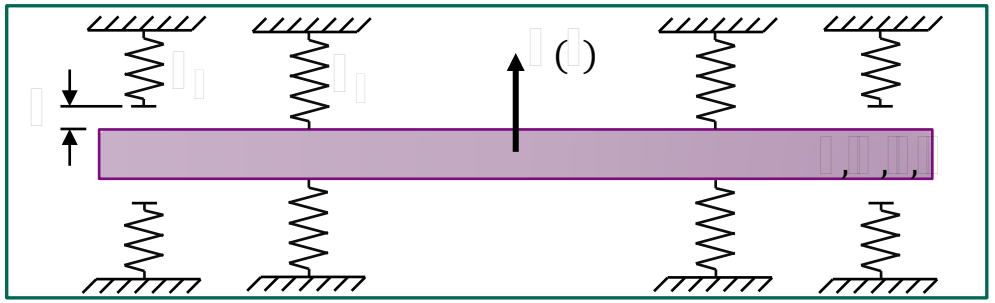

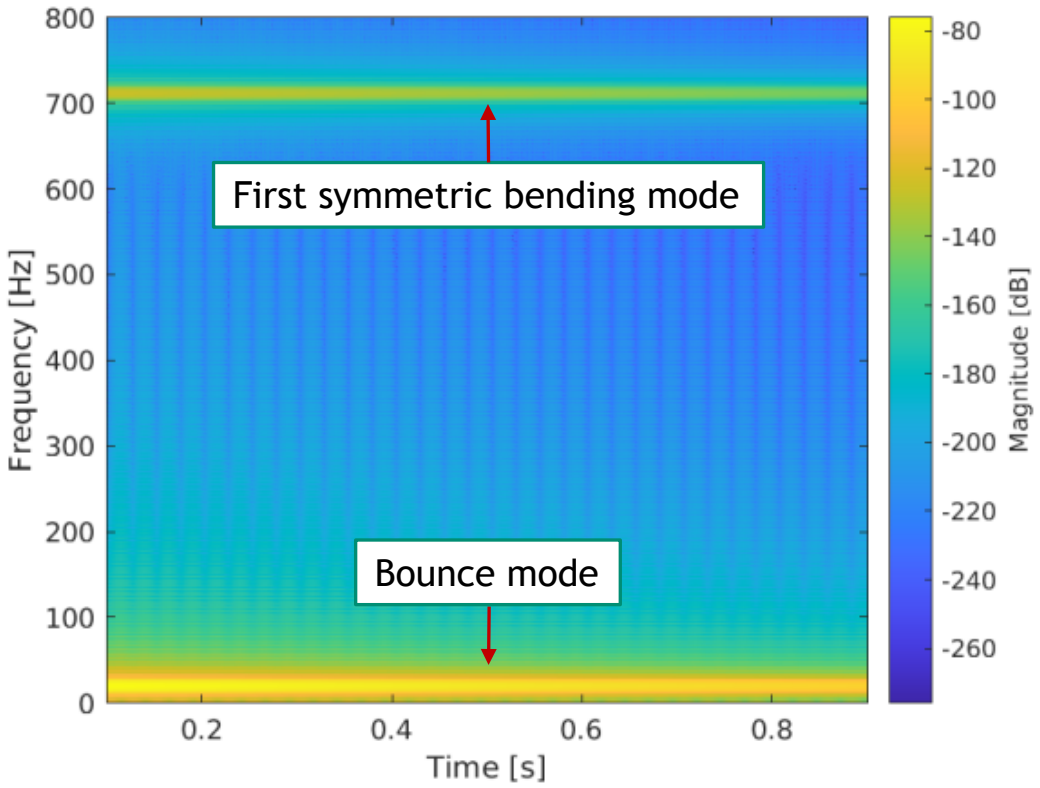

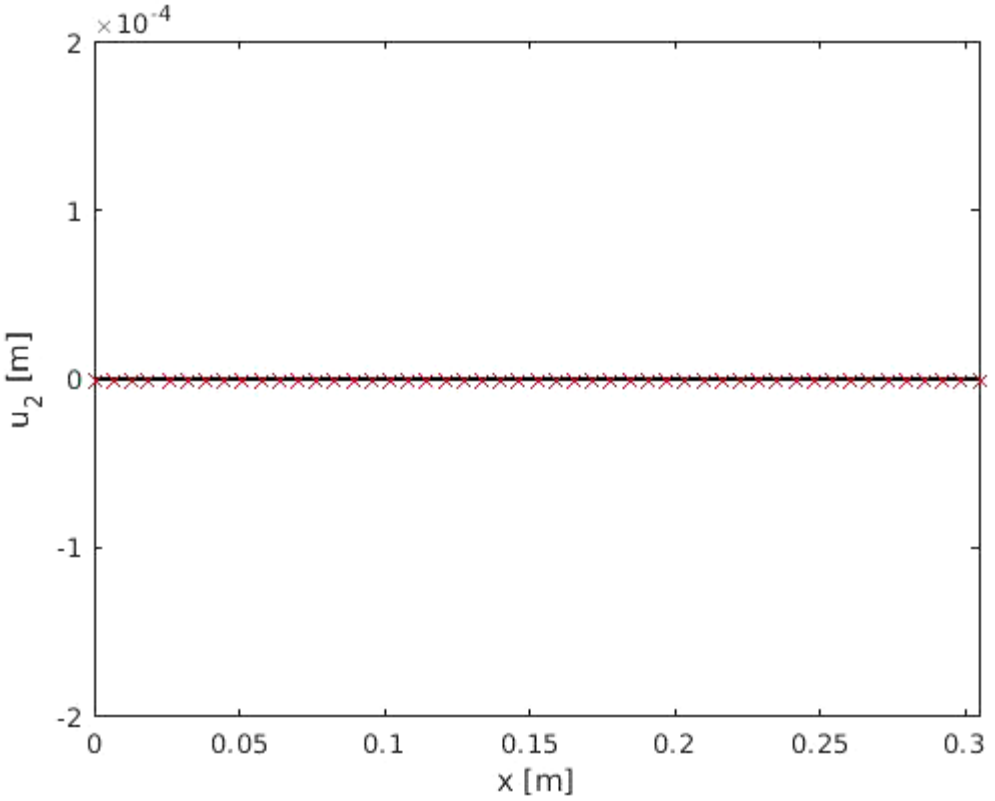

Transient Response - Nonlinear Regime

- Emulate strong excitation with hammer
  - 50-N pulse for 4 ms at middle node
  - Best estimate of model parameters
  - Light Rayleigh damping

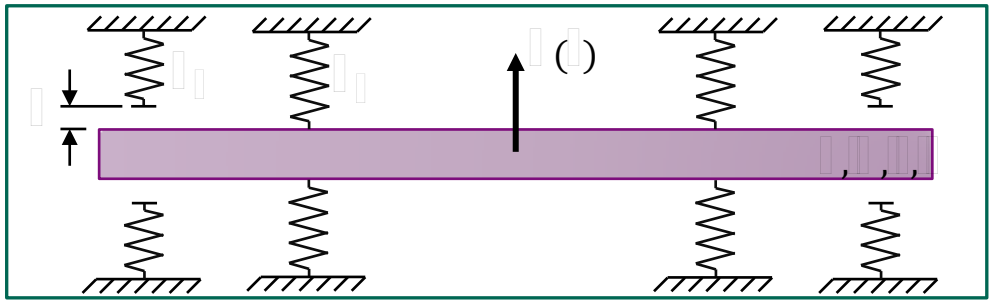

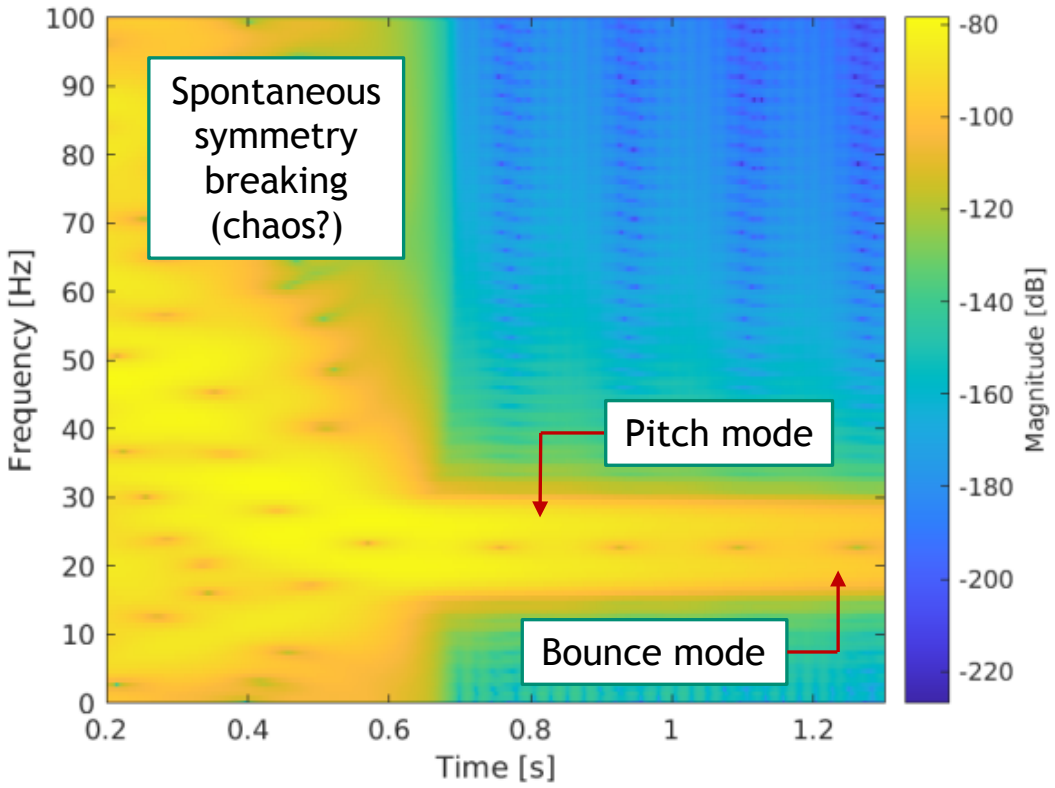

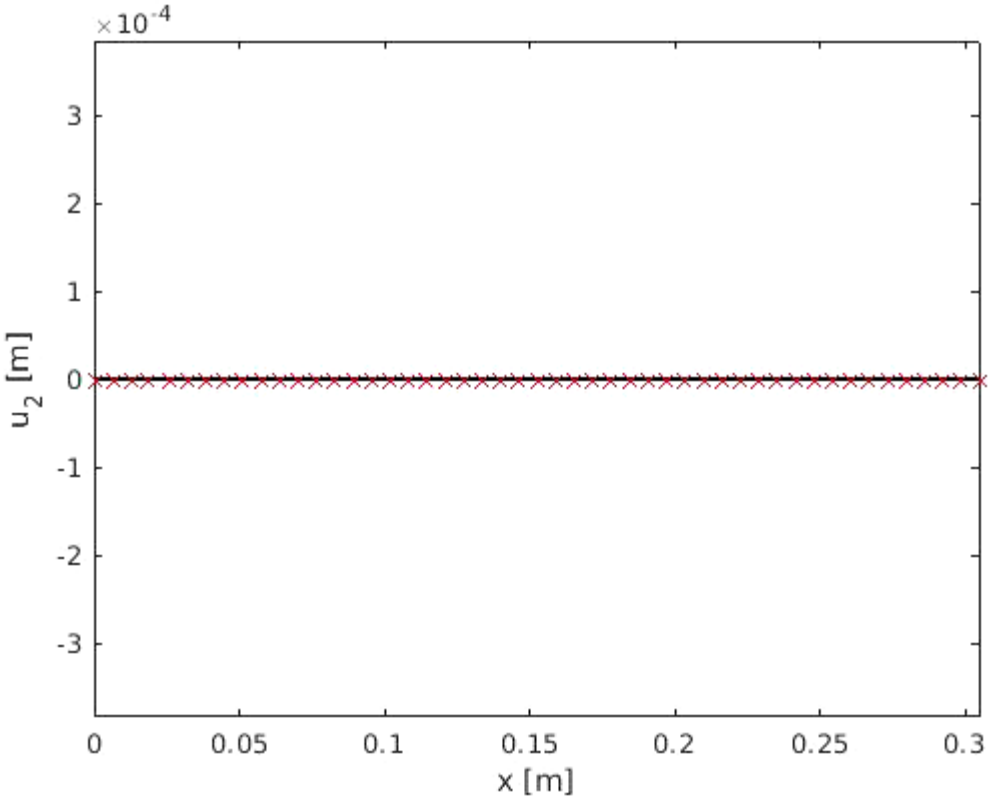

Outcomes

- Computational capabilities developed
  - Transient finite element code for simplified model
  - Multi-harmonic balance input files for nonlinear periodic response (free and forced)*
  - CUBIT input files for parametric CAD and hexahedral mesh generation
  - Sierra SD linear modal analysis input files
  - Sierra SM nonlinear transient input files
- Key conclusions
  - Linear modal testing and modal analysis techniques can successfully characterize the system when no impacts occur
  - Modal coupling may be difficult to observe due to instabilities and/or chaos
  - Highly discontinuous nature of contact complicates both modeling and experimentation

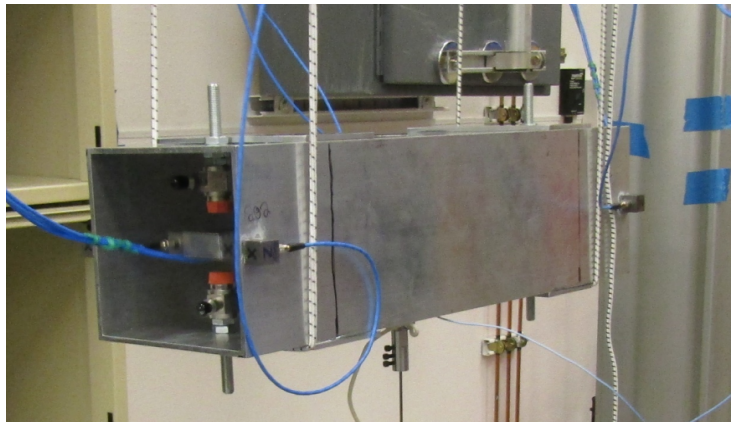

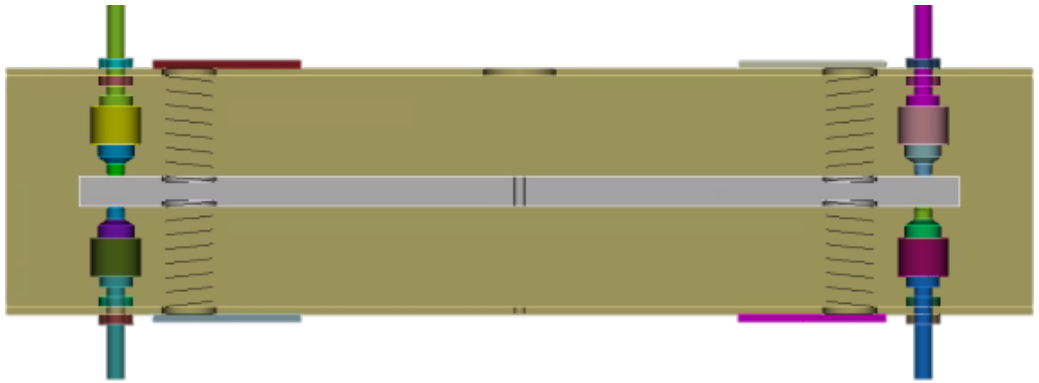

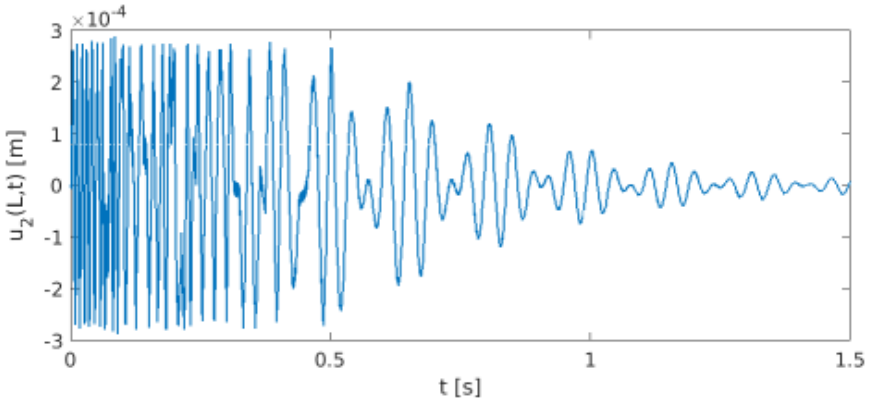

Future Work

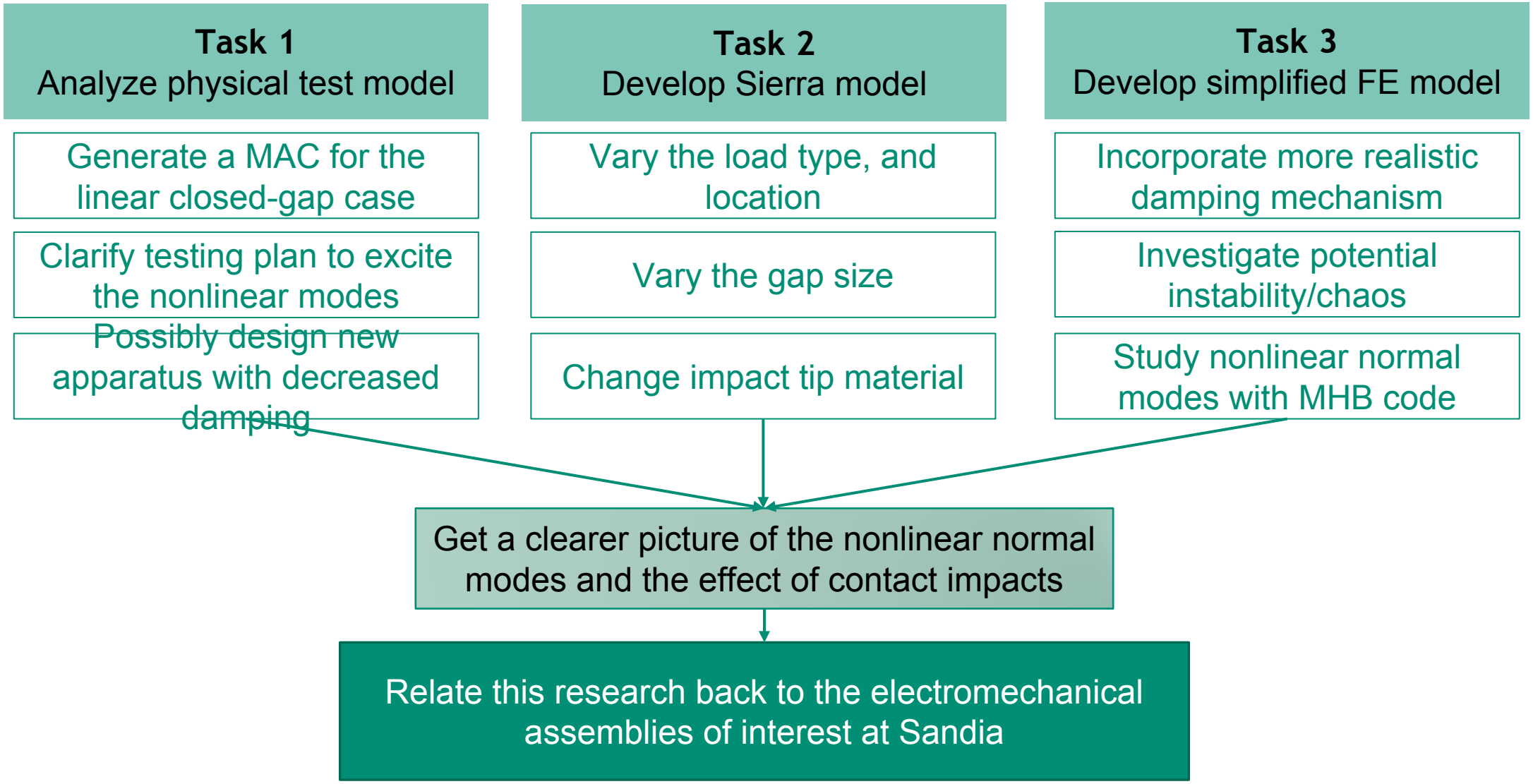
Task 1
Analyze physical test model
Task 2
Develop Sierra model
Task 3
Develop simplified FE model
Generate a MAC for the linear closed-gap case
Clarify testing plan to excite the nonlinear modes
Possibly design new apparatus with decreased damping
Vary the load type, and location
Vary the gap size
Change impact tip material
Incorporate more realistic damping mechanism
Investigate potential instability/chaos
Study nonlinear normal modes with MHB code
Get a clearer picture of the nonlinear normal modes and the effect of contact impacts
Relate this research back to the electromechanical assemblies of interest at Sandia

Acknowledgements

This research was conducted at the 2021 Nonlinear Mechanics and Dynamics Research Institute hosted by Sandia National Laboratories and the University of New Mexico.

Sandia National Laboratories is a multimission laboratory managed and operated by National Technology and Engineering Solutions of Sandia, LLC, a wholly owned subsidiary of Honeywell International, Inc., for the U.S. Department of Energy’s National Nuclear Security Administration under contract DE-NA-0003525.

Backup Slides

Mesh Generation